Performance of nanofillers embedded polymer for HVDC applications

Thesis submitted for the degree of

Doctor of Philosophy

in

Department of Electronic & Electrical Engineering

University of Strathclyde

by

Xiaosi Lin

2022

Declaration of Authorship

The thesis is the result of the author's original research. It has been composed by the author and has not been previously submitted for examination, which has led to the award of a degree.

Signed: 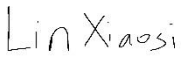

Date: 24/05/2022

Acknowledgement

I would like to give my first appreciation to my supervisors Prof. W. H. Siew, Prof. John Liggat and Dr. Martin J. Given, for their continued support and guidance throughout the course of this research. Thanks for their kindness to provide me with the opportunity to pursue a Ph.D. degree in the University of Strathclyde and moreover always being supportive and patient in supervision of my study.

I would also like to acknowledge my host supervisors Prof. Jinliang He and Prof. Qi Li in Tsinghua University, where I carried out part of my research. I appreciate a lot for the kindness of Prof. He in providing the relevant laboratory facilities, which allowed me to carry on my research under their supervision.

My deep appreciation too to my colleagues, Dr. Jiajia Liu and Mr. Xuhui Duan at the University of Strathclyde for giving me encouragement and useful knowledge for my research project. Thanks also to Mr. Francis Cox for his kind support. Thanks to my colleagues in the High Voltage Technologies Group for providing a convivial working environment.

Many thanks to all colleagues at Tsinghua University for their kindness and assistance in my project.

Thanks a lot to my wife for her company and patience.

Finally, thanks to my family, especially my parents for their support in my Ph.D. study.

Abstract

Nowadays the crossing-linked polyethylene (XLPE) has been widely used as the cable insulation materials in the high voltage direct current (HVDC) application. It has some disadvantages including non-recyclable properties, pollutants in the crosslinking process and bad mechanical properties under high temperature. Therefore, it is a main research direction to develop the new generation of polymeric insulation materials with excellent electrical properties, recyclability and environmental-friendly characteristics for the HVDC cable insulation. Polypropylene (PP) is one of commercial thermoplastic polymers which can be recycled and used as a high voltage insulator under high temperatures. Additionally, the electrical performance of PP is better than XLPE in terms of breakdown strength, conductivity, and space charge characteristic. Based on the nanodielectrics theorem, the excellent electrical performance of polymers can be achieved through the nanocomposite process. Therefore, nanocomposites based on PP can have much higher electrical properties and higher thermal stability than XLPE, which provides a new idea for the development of new HVDC cable insulation technology. Over the past few decades, significant attention was paid to the traditional inorganic nanofillers, especially to nano-MgO and nano-Al_2O_3, in order to modify the properties of PP. However, there is not sufficient research information available in the literature on the effect of POSS on the properties of PP .

The main aim of this PhD project is to develop new PP's nanocomposites with high DC electrical performance for HVDC underground power cable insulation. Firstly, nano-MgO, nano-Al_2O_3, octavinyl-POSS (OvPOSS) and octaphenyl-POSS (OpPOSS) are selected as nanofillers to manufacture the nanocomposites of PP by the solution method. Then, the electrical properties of PP and its nanocomposites were measured and the mechanism about the nanofiller effect on the electrical performance was explored though the micro-observation and macro-tests of PP's nanocomposites, especially for OvPOSS and OpPOSS. The formulation and preparation of PP's nanocomposites were optimized through the comparison between the effect of different

nanofillers on the electrical performance of PP. The result of electrical measurements shows the electrical performance of POSS/PP nanocomposites is better than MgO/PP and Al_2O_3/PP nanocomposites under the temperature of 30 ℃, which means that POSS/PP nanocomposites have higher potential to be the next generation of polymeric cable insulation materials with the compare of traditional PP's nanocomposites, including MgO/PP and Al_2O_3/PP nanocomposites.

Secondly, the electrical properties of OvPOSS/PP and OpPOSS/PP nanocomposites at higher temperatures, including 50, 70 and 90℃, have been measured. Then, the electrical measurement revealed that the effect of temperatures changes on the breakdown strength, DC conductivity and space charge characteristics. The relationship between the conductive current and space charge suppression of PP nanocomposites under different temperatures was still discussed to show the mechanism about how the effect of POSS addition can affect the electrical performance of PP under high temperatures.

Finally, OpPOSS/PP nanocomposites are selected to explore the electrical and mechanical properties of aged samples through the thermal-oxidation aging (TA) and the electro-thermal aging (ETA) processes at the temperature of 110℃. Through the comparison between OpPOSS/PP and pure PP, the OpPOSS can still improve the electrical performance of PP, but it cannot suppress the aging process occurring in pure PP. Under the operation of HVDC cable, the addition of OpPOSS can reduce the electrical damage in the bulk of PP then enhance the lifespan of PP under the HVDC conditions.

In this PhD research project the effects of OvPOSS and OpPOSS on the electrical properties of PP have been investigated and the potential of OvPOSS/PP and OpPOSS/PP nanocomposites for the HVDC cable insulation has been analysed. Compared with the traditional nanocomposites, this thesis showed that OvPOSS/PP and OpPOSS/PP nanocomposites have higher electrical properties at the temperature of

30 ℃, this thesis also analyses the reason why addition of OvPOSS and OpPOSS into PP can result in its higher electrical performance . By testing the electrical properties of OvPOSS/PP and OpPOSS/PP nanocomposites at high temperatures, the changes of the electrical properties of these nanocomposites at different temperatures were revealed. Based on the TSDC test results, the influence of nanocomposites on the high temperature electrical properties of PP was demonstrated, the physical mechanism and method of regulating the space charge accumulation in the bulk of PP under the action of electric field at elevated temperature were proposed and the concentrations of nanofillers were optimized. Finally, the experimental platforms for thermal-oxidation aging and electro-thermal aging processes were designed to carry out aging experiments on PP and its nanocomposites. Under different aging times, the effects of OpPOSS on the mechanical and electrical properties of PP were analysed by FTIR spectroscopy. Finally, at 110 ℃ and 60 kV/mm, the breakdown time of PP and OpPOSS/PP was measured, and the lifespan of PP and OpPOSS/PP nanocomposite insulation layer in the actual operation of HVDC cable was theoretically predicted, which indicated the potential of OpPOSS/PP nanocomposites to be the next generation of HVDC cable insulation materials with environmental-friendly properties.

Key words: ***Polypropylene, nanocomposites, electrical properties, thermal-oxidation aging, electro-thermal aging***

List of abbreviations

UK	United Kingdom
EC	European Commission
PP	Polypropylene
iPP	Isotactic Polypropylene
sPP	Syndiotactic Polypropylene
aPP	Atactic Polypropylene
XLPE	Crosslink polyethylene
PE	Polyethylene
LDPE	Low Density Polyethylene
HDPE	High Density Polyethylene
PI	Polyimide
EPDM	Ethylene-Propylene-Diene Monomer
PVDF	Polyvinylidene Fluoride
PP-g-MAH	Grafted PP with Maleic Anhydride
HVDC	High Voltage Direct Current
HVAC	High Voltage Alternative Current
POSS	Polyhedral Oligomeric Silsesquioxane
OvPOSS	Octavinyl Polyhedral Oligomeric Silsesquioxane
OpPOSS	Octaphenyl Polyhedral Oligomeric Silsesquioxane
C60	Fullerene Derivatives

DCTH	2,6-dicyclohexylterephthalamide
DCP	Dicumyl Peroxide
wt %	Weight percentage %
KH570	γ-methacryloxypropyltrimethoxysilane
C8	Octyltrimethoxysilane
C18	Octadecyltrimethoxysilane
MAH	Maleic Anhydride
POM	Polarized Optical Microscopy
FE-SEM	Field- Emission Scanning Electron Microscope
TGA	Thermogravimetric Analysis
FTIR	Fourier Transform Infrared Spectroscopy
DS	Dielectric Spectroscopy
DSC	Differential Scanning Calorimetry
TSDC	Thermal Stimulated Depolarized Current
PEA	Pulse Electro-Acoustic
DFT	Density Function Theorem
QM	Quantum Mechanics
DOS	Density of State
TF	Trap-Filled Limited Region
SCLC	Space Charge-Limited Current
TA	Thermal-oxidation aging

ETA	Electro-thermal aging

List of Figures

List of Tables

List of Publications

[1] X. Lin., WH Siew, J. Liggat, M. Given and J. He.: Octavinyl polyhedral oligomeric silsesquioxane on tailoring the DC electrical characteristics of polypropylene. *High Voltage.* 1–11 (2021). doi: 10.1049/hve2.12146

[2] X. Lin., WH Siew, J. Liggat, M. Given and J. He.: "Influence of Octavinyl-Polyhedral Oligomeric Silsesquioxane on the Electric Treeing Resistance of Polypropylene," *2021 International Conference on Electrical Materials and Power Equipment (ICEMPE)*, 2021, pp. 1-4, doi: 10.1109/ICEMPE51623.2021.9509166

[3] X. Lin., WH Siew, J. Liggat, M. Given and J. He.: "Nanocomposites Based on Magnesium-oxide/ Aluminum-Nitride/Polypropylene for HVDC Cable insulation," *2020 IEEE International Conference on High Voltage Engineering and Application (ICHVE)*, 2020, pp. 1-4, doi: 10.1109/ICHVE49031.2020.927971

Table of Contents

1. Introduction

1.1 The research backgrounds

Since the greenhouse effect is becoming more and more serious, the development of clean energy has become more and more important in order to reduce the greenhouse gas emissions especially CO_2 [1]. It is a tendency that human beings have been using the clean energy to replace fossil energy gradually. While the increasing demand for clean and sustainable energy may cause the instability of power generation, which may lead to the collapse of the power grid. In this case, the high voltage direct current (HVDC) power system is the most suitable choice to solve this problem [2-3]. HVDC power transmission can be sorted into two categories including the over-head transmission line and submarine/underground power cable system. Compared with over-head transmission line system, the power transmission cable has many advantages, including no need to occupy surface corridors, less impact by the changes of climate and environment, high operation, reliability, less maintenance workload and flexible laying, simpler electromagnetic environment. Therefore, the installation of power transmission cable is the more suitable choice in modern power system and now it has been widely used in the fields of transmission, distribution and power consumption, such as outgoing lines of power stations, cross-river and cross-sea transmission, internal power supply of industrial and mining enterprises and urban power supply [4-5].

Now the installation of HVDC cable system is believed that it can make the power grid smarter by providing flexibility, availability and sustainability through the connection with Renewable Energy Sources which usually located in remote locations from large consumer areas [6-7]. In fact, the search for a large number of clean energy has promoted the power generation to remote areas, such as the deep sea and the ocean with rich wind energy and "blue" energy banks, as well as the desert with huge solar

energy, high and wide mountains have a large number of solar and hydraulic resources. In the past two decades, this has led to the increasing growth of HVDC cable systems in global services, but also made the working conditions of HVDC cables harsher [8-10].

The UK has one of best locations for the wind power generation in the world [11]. The power generated by wind farm reached 24.8 % of total electricity supplied by the UK in 2020 and the power generation from coal was less than wind farm [12-13]. Also, the offshore wind farm capacity has increased to 10.4 gigawatt which has occupied 43.0 % of wind power generation in the UK in 2021 [14]. Therefore, the continued development of offshore wind resources is an important support to ensure the healthy development of British economy and society and the power supply of the island and the offshore platforms will increasingly rely on the HVDC cable system.

1.2 Overview of power transmission cables

Since the 1950s, with the increasing power demand and the increasing long-distance and high-capacity transmission, the High Voltage Alternative Current (HVAC) transmission has met some problems, especially the limitation from the stability of synchronous operation [3]. In long-distance transmission, complex and huge compensation system is required for synchronous adjustment [15]. However, with the development of semiconductor technology and the advent of DC converter, high-voltage, long-distance and high-power DC transmission can be achieved [16]. In some cases, DC transmission is more reliable and has more superior operation characteristics than the HVAC transmission, especially for the renewable power transmission.

The European Union has paid significant attention to the development of HVDC power system. In 2018, the European Commission (EC) announced its long-term strategy "a clean earth for all" [17], which identified marine renewable energy as a key source of clean energy. The transition and EC funded "promotion" project described the advantages of HVDC, focusing on offshore power technology, so as to integrate

large-scale renewable energy into the energy system through the cables, then ensure that the future affordable power grid is reliable and sustainable. Compared with the HVAC power system, the HVDC power system has many advantages, including [18-19]:

1. AC systems on both sides do not need to operate synchronously during DC power transmission therefore DC power transmission is more stable.
2. There is no capacitive current in the DC power transmission, therefore the power loss is reduced.
3. DC power transmission can achieve large transmission capacity, and the power transmission can be quickly controlled.
4. DC power transmission does not need the reactive power compensation.

Therefore, without the need of synchronization operation, HVDC power system is a suitable strategy to overcome the instability of power generation during the connection with renewable power generation.

1.3 Basic requirements for insulation characteristics of HVDC power cables

The requirements of HVDC cable insulation are different from HVAC insulation. In HVDC system, the insulation layer should meet specific requirements and characteristics which have been listed below [20]:

a. The DC conductivity should be low enough in order to reduce the hot electron production which is defined as the electron with high kinetic energy, these electrons and cause degradation of insulation materials leading to the DC electrical breakdown.
b. Space charge accumulation should be minimized. There is a space charge injection problem in DC cable. Space charge would cause the distortion of the

electric field and reduces the breakdown strength of the cable. Especially during the polarity reverses in the VSC HVDC system, the current direction of the cable remains unchanged, while the voltage polarity changes. This is because the electric field of applied voltage and the electric field distortion caused by the space charge accumulation have a superposition effect, resulting in further reduction of breakdown strength. Therefore, there is a need to suppress the space charge accumulation and ensure that it will not cause serious electric field distortion and withstand the high electric field caused by polarity reversal.

c. The conductivity should be as stable as possible, which means that the conductivity is insensitive to the changes of temperature and electric field during the operation. Under HVDC conditions, the insulation conductivity coefficient of cable changes exponentially with temperature and the applied voltage. Conductor heating causes a large temperature gradient in cable insulation from inside to outside and the temperature gradient will greatly change the electric field distribution in the bulk of cable. The high conductivity temperature coefficient will cause serious non-uniform electric field gradient and greatly increase the breakdown probability. The electric field distribution in the insulation layer of DC cable is much more complex than that of AC cable, and even the polarity reversal of electric field occurs.

d. The insulation layer should have high DC breakdown strength, especially in the environment of superimposed pulses, and insensitive to temperature rise and polarity reversal. DC cable insulation has high breakdown strength, which can appropriately reduce the cable insulation thickness, increase the cable insulation thermal conductivity and improve the cable transmission capacity.

e. The insulation layer should have higher thermal conductivity which can make the temperature gradient smoother. Therefore, the electric field distribution would be more uniform in the bulk of cable insulation.

1.4 The different kinds of cable insulations

At present, the HVDC cables used in industrial applications can be classified as adhesive impregnated paper cable, oil-filled cable and extruded polymeric insulation cable.

Adhesive impregnated paper cable: It is composed of paper insulation impregnated with high viscosity compound, and the working voltage strength can only reach about 25 kV/mm. In 1954, the world's first submarine DC viscous impregnated paper cable with voltage grade of ± 100 kV and cable length of 98 km was laid between Gotland island and the mainland of Sweden. At present, the working voltage for this cable type has reached 500 kV and the cross-section area of conductor has reached 2500 mm^2. It is suitable for long-distance submarine laying. The good cooling effect of seawater can avoid the leakage of impregnant, but it is not suitable for large drop laying. The typical diameter is 110 ~ 140 mm and the typical weight is 30 ~ 60 kg/m.

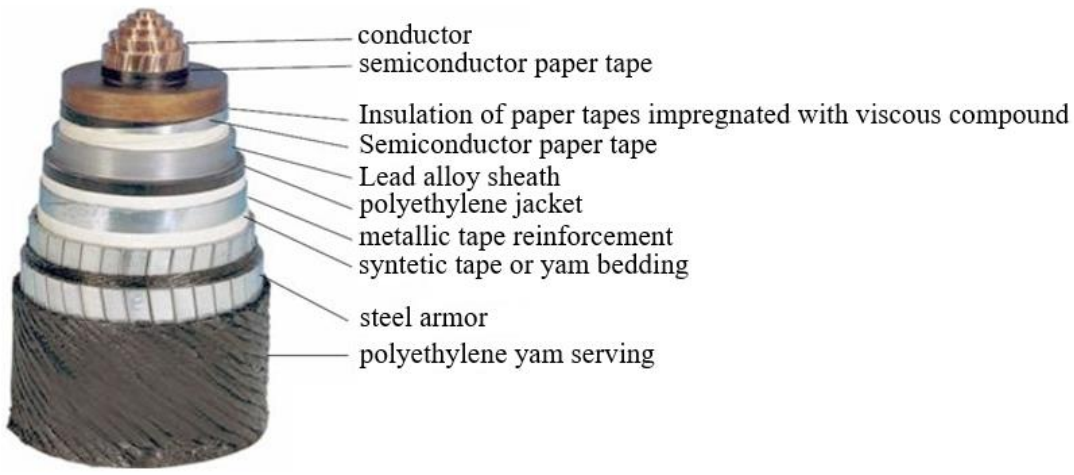

Figure 1.1 The structure of adhesive impregnated paper cable [21]

Oil-filled cable: Special paper impregnated with low viscosity insulating oil is used for insulation. In 1976, a submarine DC oil filled cable with voltage grade of ± 300 kV was laid in Vancouver, Canada. At present, the voltage of this type of cable has reached 600 kV and the cross-sectional area of the conductor has reached 3000 mm^2. It is widely used when the rated voltage of the line exceeds 250 kV. In addition to being widely

used on land, it is also used as submarine cable. The typical diameter is 110 ~ 160 mm and the typical weight is 40 ~ 80 kg/m .

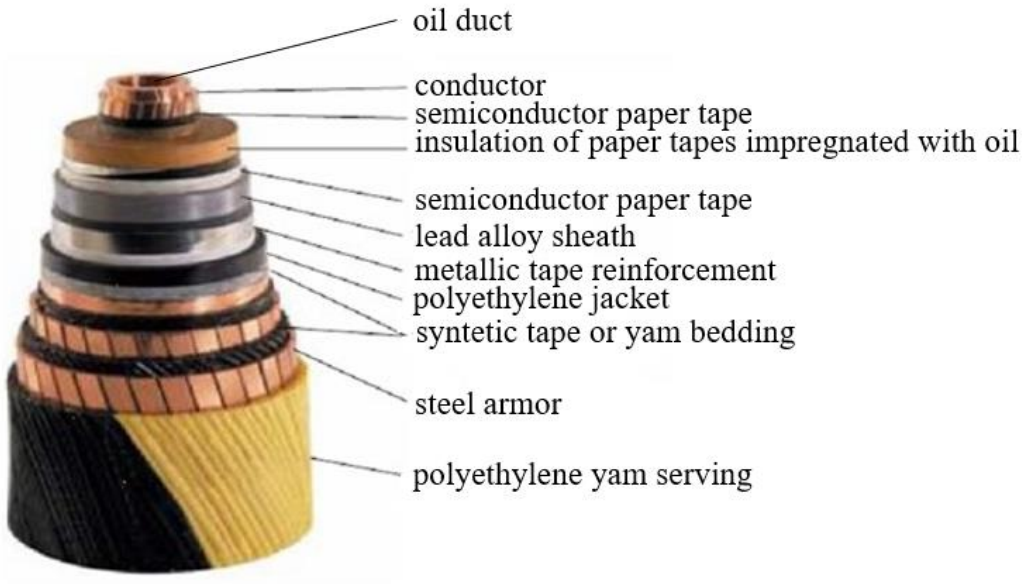

Figure 1.2 The structure of oil-filled cable [22]

Extruded polymeric insulation cable: It is extruded from XLPE insulating material. It has simple and firm structure and is suitable for submarine cable. In 1999, the world's first commercial XLPE extruded DC cable was applied in Gotland Island phase II project in Sweden. The cable voltage grade is ± 80 kV, the transmission power is 50 MW, and the cable length is 140 km. The typical diameter of 200 kV cables is 90 ~ 120 mm and the typical weight is 20 ~ 35 kg/m. With the development of XLPE insulation, the voltage level of XLPE DC cable is gradually improved, and the transmission power is also greatly increased. At present, the maximum voltage level of XLPE insulated high-voltage DC cable that has been put into operation at home and abroad is ± 500 kV, and the working voltage of AC cable has reached 500 kV. The electrical, mechanical and thermal properties of XLPE formed by physical or chemical crosslinking of polyethylene materials are improved. The use of XLPE DC cable gradually exceeds that of viscous impregnated paper and oil filled DC cable and maintains a continuous growth momentum. It has become the mainstream of cable insulation at present.

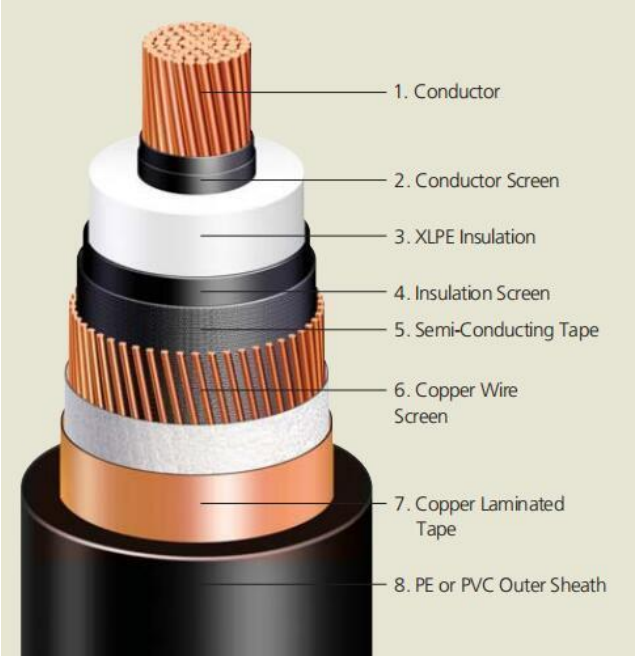

Figure 1.3 Extruded polymeric insulation cable [23]

The oil-filled cable and adhesive impregnated paper cable were widely used in the early stage of HVDC transmission. However, both of them may have the leakage of liquid and pollute the environment during the long-term operation. Additionally, the liquid in both of the cables could flow from the high to low gravity potential energy, which would reduce the breakdown strength of cable insulation. Therefore, the maintenance costs of these cables are very high, and the installations are very complicated.

The extruded polymeric insulation cable has some advantages, including simpler manufacturing process, lower maintenance cost and high-power capacity. Since 1999, XLPE extruded cable have been widely spread in the HVDC transmission project shown in Table 1.1. [24-32]

Table 1.1 European extruded XLPE DC cable transmission project

Time	Project	Location	Voltage (kV)	Capacity (MW)

2013	East-West Interconnector	UK---Ireland	±200	500
2013	HelWin 1	Germany	±250	576
2013	DolWin 1	Germany	±320	800
2013	Borwin2	Germany	±300	800
2014	SounthWest Link	Sweden	±300	720
2015	SylWin 1	Germany	±320	864
2019	NEMO Link	UK--- Belgium	±400	1000
2020	IFA 2	UK---France	±320	1000

At current stage, the extruded XLPE DC cable can reach the maximum voltage level of ±400 kV and the maximum transmission capacity have increased to 1000 MW. However, even though the XLPE has high electrical performance under HVDC conditions, the XLPE still has some disadvantages. Firstly, due to the thermoset properties, XLPE could not be recycled after the end of service life. Secondly, the crosslinking process is very complicated, and some pollutants would be produced in the manufacture of XLPE. Finally, the byproducts of the crosslinking process may cause the degradation of XLPE, which will increase the space charge accumulation and reduce the lifespan of extruded XLPE DC cable [33]. Therefore, there is a need to develop the new generation of environmental-friendly polymeric insulation material for the HVDC cable insulation. This kind of polymer should be thermoplastic so that there is non-crosslinking process in the manufacturing process, and it can be recycled after the end of its lifespan. Compared with XLPE, the preparation cost of thermoplastic insulation material can be reduced by 14 %, the manufacturing cost of cable can be reduced by 17 %, and the carbon emission of production can be reduced to 80 % of

extruded XLPE insulation cable [34]. Therefore, taking into account to the environmental aspects and recyclability, the extruded thermoplastic polymeric insulation cable is suitable for HVDC applications.

1.5 Widely-used commercial thermoplastic polymers

The current strategy is to use thermoplastic polymeric insulation materials with high heat resistance as the new generation of cable insulation. At present, there are two kinds of polymers which can be used in the cable insulation. One is polyethylene and another is polypropylene. However, it is difficult for the pure polymers to satisfy the requirements of HVDC cable insulation, including high temperature mechanical strength and electrical performance. For DC cable insulation materials, it is also required to enhance the electrical performance and inhibit the accumulation of space charge.

1.5.1 Polyethylene

Polyethylene (PE) is a kind of thermoplastic polymer which is polymerized with propylene monomer shown in Figure 1.4. Due to the different chemical structures including branching degree, molecular weight and molecular weight distribution, PE can be classified as low-density polyethylene (LDPE) and high-density polyethylene (HDPE). Figure 1.5 shows that LDPE has a higher branching degree. Because the side chains or branched chains reduce the molecular regularity, the crystallinity, density and rigidity of PE containing a large number of branched chains are low. HDPE has a lower branching degree, so it has high crystallization and good properties such as higher electrical performance.

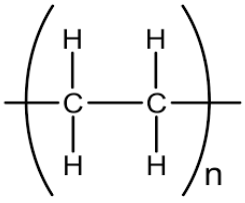

Figure 1.4 The chemical structure of PE

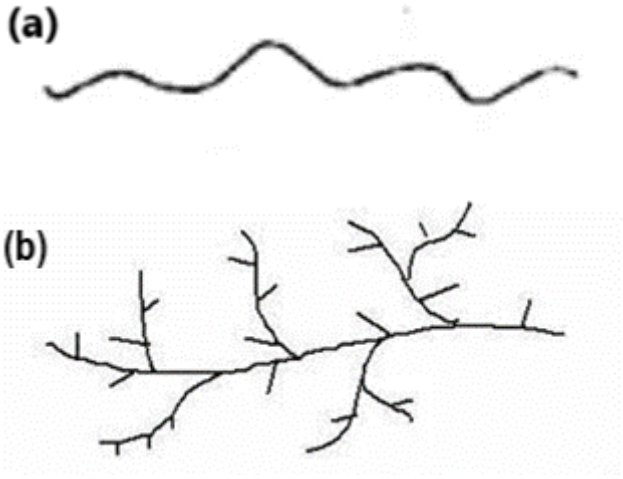

Figure 1.5 The shape of molecular chain (a) HDPE (b) LDPE [35]

1.5.2 Polypropylene

It is well-known that PP has better thermal properties than polyethylene, which means that it has a higher melting point. The structure of PP is shown in the Figure 1.6.

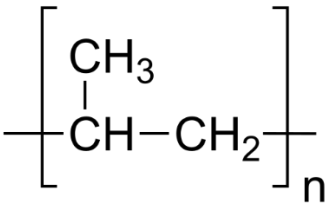

Figure 1.6 The chemical structure of PP [36]

PP is a polymer polymerized with propylene monomer, due to the spatial configuration of methyl group. PP can be classified as isotactic polypropylene (iPP), syndiotactic polypropylene (sPP) and atactic polypropylene (aPP), shown in Figure 1.7. The Methyl groups are arranged on the same side of the main molecular chain and periodically on the main molecular chain in iPP and sPP respectively. While the methyl groups are arranged irregularly on the main molecular chain in aPP.

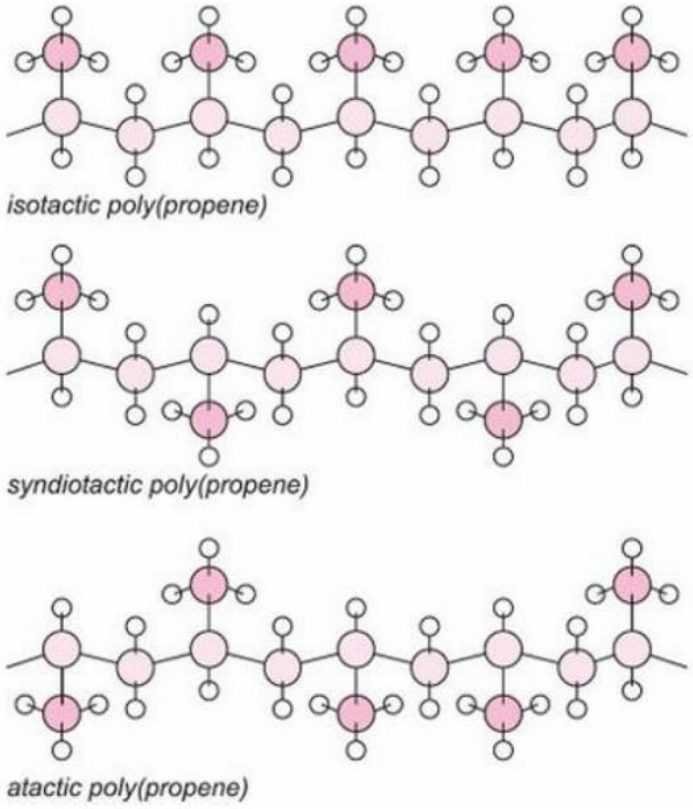

Figure 1.7 The different spatial configuration of PP. iPP, sPP and aPP [37]

The insulation performances of different PP are strongly affected by the spatial configuration. iPP is a kind of semi-crystalline polymer with high melting temperature of 165℃, which can satisfy the requirement of HVDC cable insulation. While the melting point of sPP is only 135℃, the mechanical performance is better than iPP. In the past few decades, S. Kohalmy et al. believed that sPP have the potential to be a new thermoplastic polymeric insulation material with a good electrical properties. However, the price of sPP is higher than iPP because of the complex arrangement of methyl group on the main chain. The crystallinity of aPP is too low so that the electrical properties are very poor. Therefore, in this group, iPP is the best one to be the cable insulation materials.

Table 1.2 demonstrates the electrical properties of LDPE, HDPE and iPP. Compared with other thermoplastic polymers, iPP has the high breakdown strength and the highest

melting point. Hence, iPP should be suitable for the large capacity HVDC cable transmission.

Table 1.2 The electrical properties of thermoplastic polymers [38-39]

Parameters	LDPE	HDPE	iPP
DC volume resistivity	$0.94 \times 10^{15}\Omega$·m	$2.2 \times 10^{15}\Omega$·m	$2.2 \times 10^{15}\Omega$·m
DC breakdown strength	345 kV/mm	450 kV/mm	440 kV/mm
Melting Point	100 ℃	132 ℃	165 ℃

1.6 Methodologies for improving electrical properties of polymers

In recent years, PP has been used as the matrix materials to develop the new thermoplastic polymeric insulation materials. There are two kinds of methodologies adopted to increase the electrical properties of polymers including the chemical grafting modification, the polymeric morphology modification, and the nanocomposites modification.

1.6.1 Chemical grafting modification

The introduction of polar groups on non-polar polymers by chemical grafting modification could improve the microstructure and charge transport process of polymers to improve the electrical properties of polymers. In the past few decades, many researchers improved the electrical properties of LDPE, XLPE and PP by the chemical grafting modification. They found that the maleic anhydride (MAH) group can suppress the space charge accumulation by 50-70 % in XLPE under high level of DC voltage and some other polar groups, including carbonyl group, nitro group, cyano group and aromatic ring group could obviously reduce the conductivity of PE and LDPE [40-42]. The mechanism by which chemical grafting modifies the electrical

properties of a polymer is that the polar group introduces the deep traps to capture the electron, so that the mobility of electrons could be reduced, and the space charge injection could be suppressed. Therefore, the breakdown strength, space charge characteristics and volume resistivity of polymers could be greatly enhanced.

In recent years, some research groups have started the research on the chemical grafting modification of PP. Y. Zhou, et al. proposed that 3.0 wt % maleic anhydride groups containing carbonyl groups were grafted onto PP to increase the DC breakdown strength of PP by 13.5 % and raise the threshold electric field of space charge injection from 33.5 kV/mm to 46.7 kV/mm shown in Figure 1.8, which is caused by the introduction of deep traps about 0.7~1.0 eV shown by the thermal stimulated depolarized current (TSDC) measurement in Figure 1.9 [43].

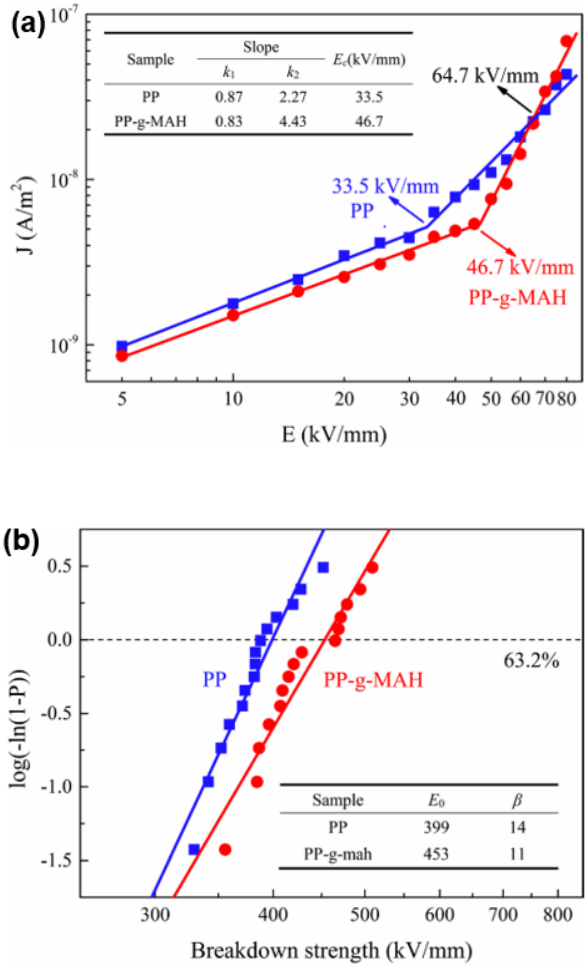

Figure 1.8. (a) the conductivity current of PP and PP-g-MAH with the increase of electric field (b) DC breakdown strength of PP and PP-g-MAH [43]

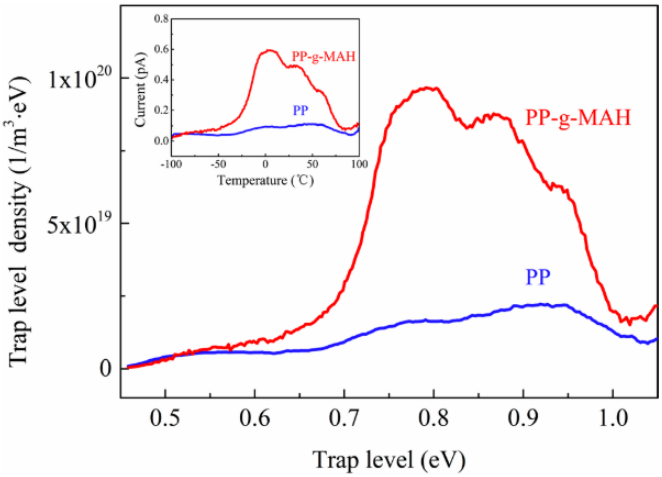

Figure 1.9 The trapping characteristics of PP and PP-g-MAH from the TSDC results Figure from [43]

J. Zha, et al. have studied the effects of different grafting amounts of maleic anhydride on the microstructure and electrical properties of PP [44]. They indicated that firstly, the chemical grafting modification by maleic anhydride will change the aggregation structure of the molecular chain of PP and reduce the diameter of crystal spherulites. Secondly, the introduction of MAH can improve the trapping level distribution to reduce the space charge accumulation. When the grafting content of MAH is 2.0 %, the volume resistivity of PP-g-MAH was more stable with the change of temperature.

The basic principle of chemical grafting modification is that the initiator such as dicumyl peroxide (DCP) and benzoyl peroxide is thermally decomposed into primary free radicals. Then, the primary free radicals seize the hydrogen atoms on the molecular chain of PP to form active points and free radicals on the molecular chain of PP. After that, the groups grow on these active points to form grafted side chains. Finally, the PP grafted with MAH can be produced and the structure shown in Figure 1.10. Because the grafting process of PP is carried out by melt extrusion reaction under the action of

the initiator, the degradation of PP molecular chain, the residuals of grafting group and initiator would still reduce the electrical performance of PP in the long-term operation. Therefore, there is still a need to improve the manufacturing process of the chemical grafted modification of PP [43].

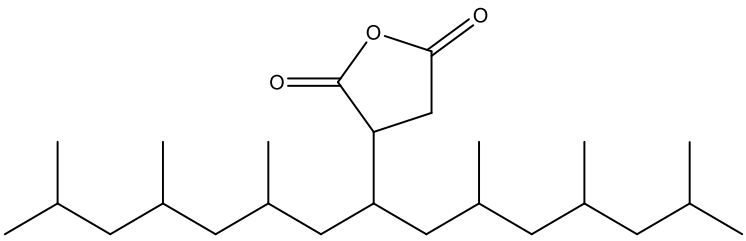

Figure 1.10 The chemical grafted PP with MAH (PP-g-MAH)

1.6.2 The modification of polymeric morphology

PP is a kind of semi-crystalline polymers with crystalline and amorphous regions. The amorphous region is usually distributed between the interface between spherulites and spherulites, and its DC breakdown strength is significantly lower than that in the crystalline region [45]. Therefore, it is easier for the breakdown process inside PP to develop across the interface between spherulites than the spherulites. With the increase of spherulite size, the interface between spherulites becomes clearer, the free path of charge would become shorter, and the breakdown strength of PP would be lower. Many researchers found that the morphology of polymers has an important influence on the electrical properties of polymers, therefore, many scholars regulated the crystallization behavior of polymers by blending modification and adding nucleating agents [46-48].

There are three common crystal forms of PP, including α, β and γ. Different crystal forms have great differences in density, melting point and electrical properties. PP usually behaves as α crystal form. With the addition of some nucleating agents, the crystal form of PP can be transformed into β crystal form. As Figure 1.11 shown, Y. Wu, et al. introduced nucleating agent, 2,6-dicyclohexylterephthalamide (DCTH) to PP to increase the content of β crystal form in PP and greatly reduce the carrier injection at the electrodes. The results showed that the crystal form can introduce deep traps,

reduce the charge carrier mobility (electrons), and inhibit the space charge accumulation in the bulk of PP, to improve the electrical properties of PP [49].

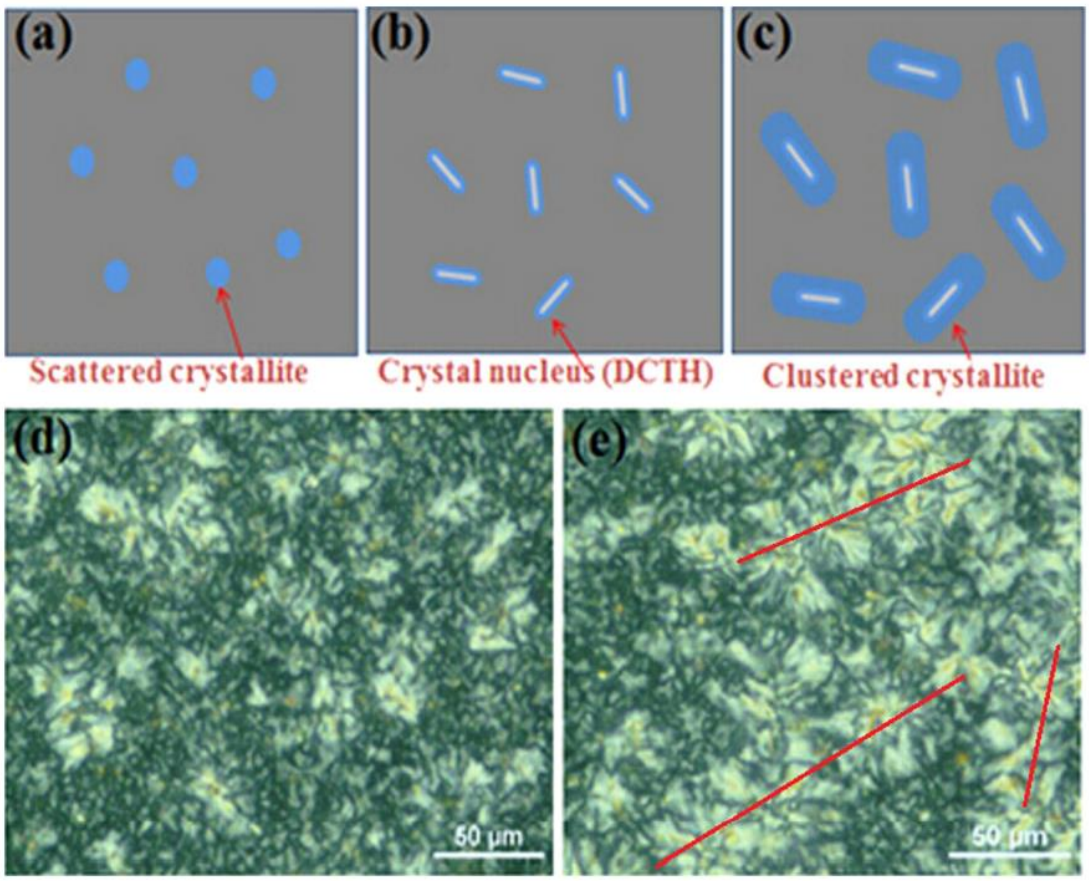

Figure 1.11 Schematic illustration of formation of crystal morphology in iPP (a) status of α crystal (b) DCTH act as β-nucleating agent (c) process of clustered β-crystal formation; (d) scattered α and (e) clustered β crystal from POM Figure from [49]

1.6.3 The nanocomposites modification

As a new generation of insulating materials, nanocomposite dielectrics show the great advantages in improving the electrical properties of polymer insulation [50-58]. Some characteristics of based polymers, including the breakdown strength, volume resistivity, corona aging resistance, space charge accumulation, partial discharge, dielectric loss and electrical tree aging could be greatly improved, especially for LDPE, XLPE, epoxy resin, silicon rubber and ethylene-propylene-diene monomer (EPDM) [50-55]. Now with the increasing need of thermoplastic polymeric insulation materials, PP has become one of the most popular matrix to manufacture the polymeric nanocomposites insulation materials.

However, the electrical properties of nanocomposites are closely related to the dispersion of nanoparticles in a polymeric matrix. Generally, inorganic nanoparticles and organic polymers are incompatible which would cause the agglomerate of inorganic nanoparticles in the polymers and reduction in their electrical strenght. Therefore, the surface of nanoparticles needs to be modified to increase the interfacial compatibility between PP and inorganic nanoparticles [56]. X. Duan, et al. studied the effect of different silane coupling agent on the electrical properties of Al_2O_3/LDPE nanocomposites and indicates that the interface structure formed by different silane coupling agents has an important influence on the dispersion of nanoparticles and the electrical properties of nanocomposites, then better dispersion of nano-Al_2O_3 has higher breakdown strength [56]. S. Hu, et al. explored the effects of coupling agents, including octyltrimethoxysilane (C8) and octadecyltrimethoxysilane (C18) on the electrical properties of MgO/PP under the temperatures of 30 ℃ and 90 ℃ [57]. The structures of those two silane coupling agents have been shown in Figure 1.12. The results showed that MgO/PP nanocomposites treated by C18 has higher DC breakdown strength under 30 ℃ and the MgO/PP nanocomposites treated by C8 has higher DC breakdown strength under 90℃, which means that the longer molecular chain of silane coupling

agent can have better improvements of electrical properties of PP while coupling agent with longer molecular chain would have the worse chemical stability under the high temperature so that the electrical properties could be decreased by the degradation of silane agent.

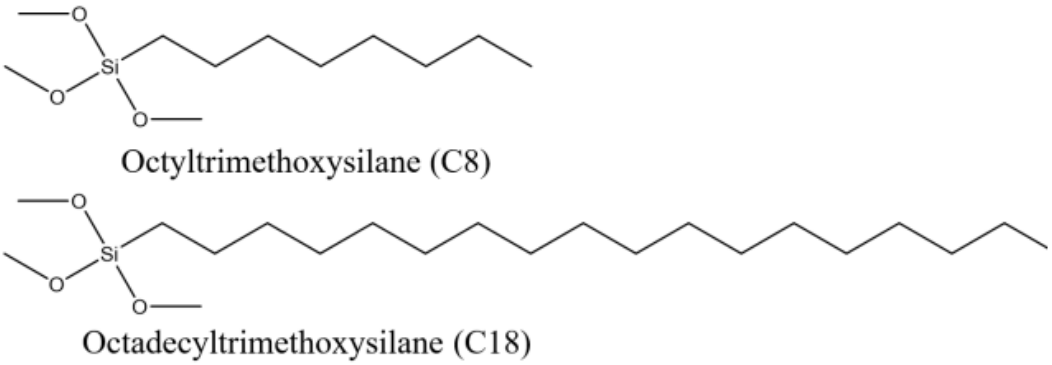

Figure 1.12 Molecular structure of silane coupling agents [57]

In addition to inorganic nanofillers like MgO, SiO_2, TiO2, $BaTiO_3$, Al_2O_3, etc., there are some new kinds of nanofillers such as polyhedral oligomeric silsesquioxane (POSS) and fullerene derivatives (C60). B, Du, et al. found that the addition of 3.0 wt% OvPOSS could introduce deep traps into EPDM and the electric treeing growth of EPDM could be significantly reduced [55]. B. Dang, et al. also used the pulse electro-acoustic (PEA) method to find that 1.0 wt% C60 can greatly suppress the space charge accumulation and reduce the DC electric field distortion of PP from 10.3 % to 2.8 % and achieve 21.1 % breakdown strength improvements of PP [58].

In our research group, octavinyl polyhedral oligomeric silsesquioxane (OvPOSS) was used to modify the characteristics of iPP and it is found that the OvPOSS nanofiller can introduce the deep traps into the surface between OvPOSS and PP so that the homocharges injection near electrodes could be suppressed. 1.0 phr OvPOSS nanofiller can achieve the best DC breakdown strength of OvPOSS/PP nanocomposites and the breakdown strength of 1.0 phr OvPOSS/PP nanocomposites is 31% higher than pure PP, which means that nanofiller introduction can greatly enhance the electrical performance of PP and shows the nanocomposite dielectrics of PP has great potential

to be the next environmental-friendly polymeric insulation materials [38]. In the thesis, our research group optimized the type and content of nanofillers for PP's nanocomposites.

However, most work was carried out under the room temperature and on the unaged polymers. Therefore, it is necessary to deeply discuss the effects of various improved methods and the properties of modified PP at high temperature, which is the main work of this thesis.

1.7 Research aims and objectives

To investigate the effect of the different nanofillers introduction on the electrical performance and tensile strength of PP in order to propose a new methodology and develop a new generation of environmental-friendly polymeric insulation materials due to its thermoplastic properties.

To achieve this aim:

i. Nanocomposite samples of PP containing different kinds and contents of nanofillers are manufactured. The effects of the types and contents of nanofillers on the microstructure, crystallinity behaviors and electrical properties of PP are analyzed, and the correlation between the microstructure and macro electrical properties of nanocomposite dielectrics is studied by comparing the dielectric properties, DC volume resistivity, space charge characteristics and DC breakdown strength of PP's nanocomposites with different types and contents of nanofillers. Then, combined with the changes of crystal morphology and charge trapping characteristics, the mechanism of the effect of nanofillers on the electrical properties of PP at room temperature is explained. By comprehensively considering the electrical performance parameters of nanocomposite dielectrics at room temperature, the types and contents of nanofillers are optimized and analyzed.

ii. Based on the optimized PP's nanocomposites insulation materials, its electrical properties such as dielectric properties, conductivity, space charge and DC breakdown strength are tested at different temperatures, and the influence of temperature on the electrical properties of PP's nanocomposites insulation materials is obtained. Through the discussion and analysis of the conductivity characteristics of PP and its nanocomposites insulation materials at 30, 50, 70 and 90 ℃ and different point fields, the carrier migration characteristics and conductivity mechanism in nanocomposites at different temperatures are confirmed. The space charge accumulation characteristics and corresponding electric field distortion of PP nanocomposite dielectric at different temperatures are studied and the generation, transport, and accumulation process of space charge in nanocomposite dielectric is clarified.

iii. The thermal-oxidation aging and electro-thermal aging properties of PP and its nanocomposite dielectrics are studied. In the process of thermal aging and electro-thermal aging, the DC breakdown strength, space charge accumulation, mechanical properties, carrier mobility and trap energy level before and after aging are compared. Finally, combined with the changes of physical and chemical properties, the aging mechanism of insulating materials is analyzed, and finally the influence of nanofillers on its insulation aging characteristics is evaluated.

1.8 Outline of the thesis

The thesis consists of 10 Chapters which are listed below:

i. Chapter 1:

This part briefly introduces the basic characteristics of HVDC transmission, HVDC cable insulation, the advantages and disadvantages of different cables, and why to develop thermoplastic polymer insulation materials. The methods of

improving the electrical properties of polymer materials are listed. Finally, the research aim and objectives of this paper are described.

ii. Chapter 2:

This part describes the current research progress of nanocomposite insulating materials and a series of problems, including the electric field distortion caused by space charge accumulation in polymeric insulating materials and aging process of insulating layer during long-term use of cables. At present, only a few studies have used POSS to improve the electrical properties of polymers. Therefore, the thesis will specifically discuss the modification of PP by the addition of OvPOSS and OpPOSS in the following chapters.

iii. Chapter 3:

This part mainly introduces the test methods and experimental design of micro and macro properties of polymer insulating materials, including Field- Emission Scanning Electron Microscope (FE-SEM), Polarized Optical Microscopy (POM), Thermogravimetric Analysis (TGA), Dielectric Spectroscopy Measurement (DS), Fourier Transform Infrared Spectroscopy (FTIR), Differential Scanning Calorimetry (DSC), TSDC Measurement, DC conductivity Measurement, DC Breakdown Test, Pulse Electro-Acoustic Measurement (PEA) and Tensile Strength Test. These test methods are very important to show the influence of nanofillers on the electrical properties of PP

iv. Chapter 4:

This part describes the polymer insulating materials used in this study and the nanofillers used. The preparation process, the characterization of physical properties and the changes of microstructural properties of the samples were introduced. In the manufacture of DC cable, the mechanical properties of insulating materials also need to meet specific conditions. For example, the

elongation at break should not be too low, so it is necessary to conduct mechanical tests on PP and its nanocomposites. These physical measurements on nanocomposites could show that how the distribution of nanofillers in PP can affect the crystallization behavior of PP and further affect its electrical properties.

v. Chapter 5:

This part introduces the measuring results of electrical properties of PP's nanocomposites under 30 ℃, including dielectric spectrum, trapping characteristics, conductivity characteristics, breakdown performance and space charge detection. All electrical measurements in this chapter were carried out at 30 ℃, showing the influence of nanofillers addition on the electrical performance of PP. The electrical test results are discussed in combination with the results of physical measurements in Chapter 4, revealing the regulation mechanism of the nanofillers addition on the electrical performance of PP. Finally, the nanocomposites of PP are optimized.

vi. Chapter 6:

This part describes the electrical properties of nanocomposites of PP optimized in chapter 5 at different temperatures and determines the characteristics of charge transport at different temperatures. The electrical tests in Chapter 6 were conducted at higher temperatures to explore the impact of high temperatures on the electrical properties of PP and its optimized nanocomposites, and to assess suitability of PP nanocomposites for cable insulation under high temperatures. Additionally, higher cable operating temperature also means higher power transmission capacity and efficiency. By comparing the electrical properties of PP nanocomposites corresponding to OvPOSS and OpPOSS, the nanocomposites of PP were further optimized.

vii. Chapter 7:

This part describes the experimental design of the thermal-oxidation aging of further optimized PP's nanocomposites in chapter 7 and measures the performance changes at different times, analyzes its aging mechanism, and judges the influence of the addition of nanofillers on its performance. In Chapter 7, the thermal-oxidation aging process of PP and its nanocomposites was carried out in an extreme way. The effect of aging time on the mechanical and electrical properties of nanocomposites could be observed, and then the long-term regulation law of nanofillers addition on the electrical properties of PP could be obtained.

viii. Chapter 8:

This part describes the electrical and mechanical performance of optimized PP's nanocomposites with different contents under electrothermal aging process and states the effects of preferred nanofillers with different contents on the electrical properties of the aged samples. Then the effect of the addition of nanofillers on the aging process was judged. In Chapter 8, electro-thermal aging process of PP and its nanocomposites in an extreme way can simulate the practical aging conditions of PP and its nanocomposites during HVDC cable operation. By observing the effect of electro-thermal aging process on the mechanical and electrical properties of PP and its nanocomposites, it was demonstrated that the addition of OpPOSS could enhanced the service life of PP. From the perspective of long-term operation of HVDC cable insulation, it was established that OpPOSS/PP nanocomposites are more suitable for long-term use at higher temperatures than XLPE and pure PP.

ix. Chapter 9:

This part discusses the presented test result of PP's nanocomposites to give the main conclusion of this thesis. Finally, the future work of this research field will be identified and proposed.

2. Literature review

2.1 Nanodielectrics theorem

2.1.1 The development of nanodielectrics theorem

Since T. J. Lewis proposed the first concept of nanodielectric and nanocomposites application in high voltage electrical insulations in 1994 and indicated that the interfacial effect between nanofillers and polymeric insulation materials performance an important roles in the electrical improvement of polymers [59], lots of attention had been attracted by the field of nanodielectrics with the gradual deepening of the research on nanodielectrics by J. K. Nelson, L. A. Dissado and J. C. Fothergill [60-62], a large number of nanocomposite dielectrics with different polymer matrices were manufactured and investigated for different industrial applications. Many researchers believe that the existence of interface has a significant impact on the macro behavior of nanocomposites. Around 1997, DuPont has developed a sandwich structure film based on the mixing of nano-Al_2O_3 and polyimide (PI), which has increased the strong corona resistance of PI by 500 times and showed the great potential of polymeric nanocomposites materials [63]. Then, nanocomposite dielectrics have attracted extensive attention in industry and academia because of their excellent thermal, mechanical and electrical properties.

From 2000, the progress in preparation and characterization technology of nanocomposites has accelerated the development of nanodielectrics [64]. The size and morphology of nanoparticles [particles, one-dimensional fibers, and two-dimensional platelets] and the spatial distribution of nanofillers in the polymer matrix can be controlled. Adjusting the different properties of corresponding nanofillers is conducive to the realization of the ideal properties of nanocomposites. The interface region is formed by two different materials (nanofillers and polymer matrix). When the size of fillers decreases to nanoscale, the interface region will increase sharply. Generally, in terms of material design and application, nanotechnology provides flexibility to adjust

the dielectric properties of composites by adjusting the microstructure and nanofillers distribution in the polymer matrix. Nanocomposites technology can benefit many dielectric properties, including space charge suppression [65], high energy density storage [66-67], partial discharge (PD) resistance [68], nonlinear field classification [69] and high thermal conductivity [70]. The polymer matrix in the study of nanocomposite dielectrics has been extended to various commonly used polymeric insulation materials such as LDPE, XLPE, epoxy resin, silicone rubber, and PI. Nanocomposites show excellent properties in many aspects including electrical tree aging resistance, breakdown strength, volume resistivity, space charge characteristics, partial discharge and dielectric loss, and has become an important research direction in the development of polymeric insulating materials with high-performance [71-74].

2.1.2 Nanocomposites and space charge suppression

Different from HVAC conditions, the space charge accumulation in the insulation layer of DC extruded polymeric cable will lead to DC extruded polymeric cable failure under HVDC conditions, which is the main factor to cause the degradation of cable insulation performance and the key problem restricting the development of DC extruded polymeric cable to higher voltage level. The local accumulation of space charge in the insulation layer will cause the local electric field to be much higher than the average electric field of the cable, leading to the local breakdown of the insulating layer (electric treeing phenomenon), and then lead to the final breakdown of the overall insulating layer [75]. The accumulation of space charge leads to the distortion of local electric field, produces more hot electrons to cause electrical damage to the polymeric insulating layer, and accelerates the aging of the polymeric insulating layer [76]. Therefore, the suppression of space charge accumulation in the bulk of polymeric insulating layer plays a significant role in improving the performance and enhancing the long-term use of extruded polymeric cable under HVDC conditions.

The introduction of nanofillers into polymeric insulation materials shows the obvious improvements of electrical properties of polymers, especially for the space charge suppression. In recent decades, many scholars have done a lot of research on space charge suppression of nanocomposites. J. Yoshida, et al. studied the space charge characteristics of nano-MgO/LDPE nanocomposites at different temperatures and different electric field. He found that 1.0 phr MgO nanoparticles can always suppress the space charge packet phenomenon of LDPE at high electric field and high temperatures, reduce the charge mobility and inhibit the injection of space charge at the electrodes [77]. By studying the space charge behavior of MgO/LDPE nanocomposites under high temperature, T. Tanaka, et al. pointed out that the reason why MgO nanoparticles inhibit space charge is that MgO produces dipoles and captures injected charges through the induction effect [78]. Q. Zhong, et al. studied the effect of 1.0 phr nano-MgO addition with different particle sizes on the space charge behavior of LDPE and found that the inhibition effect of space charge accumulation was inversely proportional to the particle size of nanoparticles [79]. Through the influence of nanoparticle surface treatment on the space charge of MgO/LDPE nanocomposites, S. Peng, et al. found that nano-MgO could suppress the space charge accumulation in the bulk of LDPE, and the appropriate surface treatment of nano-MgO could improve the compatibility between nanoparticles and LDPE matrix to promote the dispersion of nanoparticles in LDPE, so as to obtain better space charge characteristics [80]. Y. Zhou, et al. used γ-methacryloxypropyltrimethoxysilane (KH570) silane coupling agent to treat the surface of different nanoparticles, studied the effects of different nanoparticles on tuning the electrical properties of PP and found that different nanoparticles could play different roles in the modification of PP. They believed that the modification of trapping characteristics by the addition of nanoparticles is one of key point for tuning the electrical properties of PP and deep traps can enhance the electrical properties of polymers [81].

In sum, the problems of nanocomposite dielectric materials and space charge still need to be deeply studied in the following aspects:

i. It is necessary to analyze the generation, migration, accumulation and dissipation of space charge in polymers, so as to obtain the action mechanism of adding nanofillers to inhibit space charge.

ii. It is necessary to explain the role of nanofillers from the micro morphology and interface characteristics of nanocomposites.

iii. It is necessary to pay attention to the influence of temperature on space charge characteristics and measure the space charge accumulation of nanocomposites at different temperatures, so as to understand the transport mechanism of space charge in polymers, especially for the electrical performance of PP at high temperatures.

iv. There is a need to focus on the induction effect produced by chemical groups and the influence of the hybridization mode of electronic orbits on the trapping characteristics of polymeric matrix and explore the correlation between conductivity characteristics and space charge characteristics, so as to further obtain the mechanism of nanofillers on the modification of polymer electrical properties.

2.1.3 The interface between nanofillers and polymers

The properties of polymeric nanocomposites are greatly improved compared with pure polymers, so many studies have been carried out on nano dielectrics. The general consensus is that the coupling of electrical, mechanical, chemical potential field and entropy gradient at the interface between nanofillers and polymers give nanocomposites excellent properties [82-84]. Compared with micron fillers, the direct benefit of nanofillers is that the interface area increases significantly with the decrease of particle size. In other words, for nanocomposites, the interface region

will occupy a large volume of the material, and it will mainly affect the macro properties of nanocomposites.

Due to the complexity of the interface between nanofillers and polymers and the spatial dimensions with nanoscale, it is difficult to observe and evaluate the performance of the interface area. Therefore, so far, only from the phenomenon, some theoretical models have been developed to describe the interface of nanocomposites and explain some experimental phenomena. As two representative researchers, Lewis and Tanaka have developed different models to thoroughly study the physical and chemical interactions in the interface region. Those models include the Stern layer and Gouy–Chapman diffuse double layer model, the multi-core model and the potential well model.

i. Stern layer and Gouy–Chapman diffuse double layer model [85]:

The first model is the Stern layer and Gouy–Chapman diffuse double layer which was proposed by T. J. Lewis in 2004 and shown in Figure 2.1. Under the action of external electric field, space charges will accumulate on the surface of the nanofillers, and different charges will accumulate around the nanofiller due to the induction effect. The charged particles in the matrix materials will begin to migrate and diffuse under the action of Coulomb force, and finally form a diffuse double layer structure around the nanoparticles. There is a low resistance part in the diffuse double layer, so when the diffuse double layers of adjacent nanofillers overlap, a low resistance path like Figure 2.2 will be formed to accelerate charge transport.

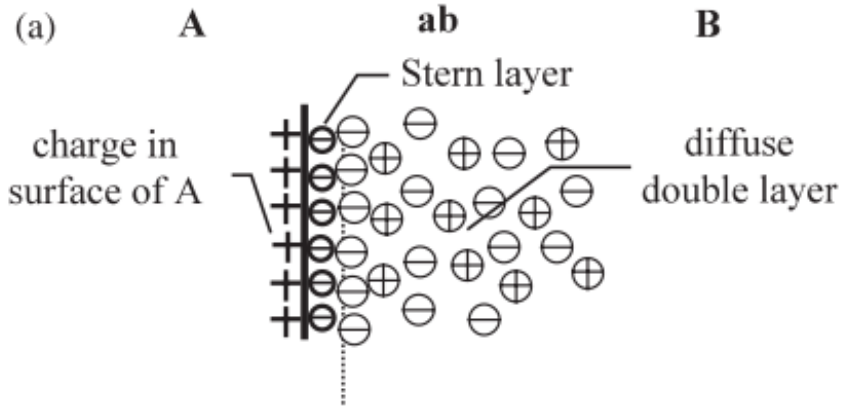

Figure 2.1 The Stern layer and Gouy–Chapman diffuse double layer around the nanofillers under the action of external electric field [85]

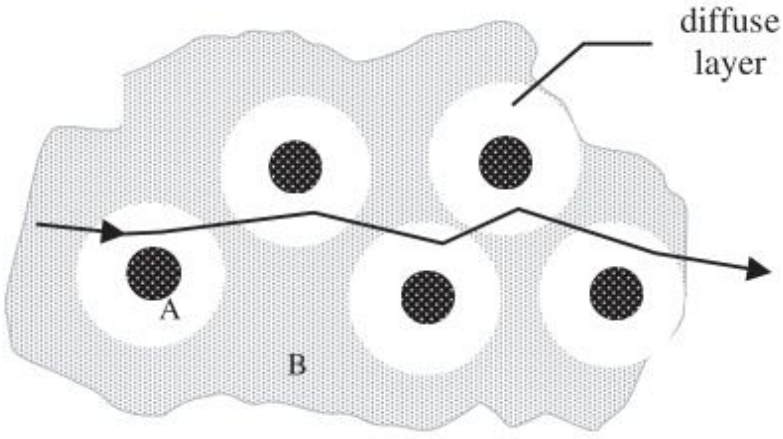

Figure 2.2 A low resistance path formed by the overlap of diffuse double layers of adjacent nanofillers [85]

ii. The multi-core model:

T. Tanaka defined the multi-core model to describe the nanofiller effect on the modification of the interface between nanofillers and polymers and he believed that there is a three-layer structure at the interface composed of nanofillers and polymers [86]. From Figure 2.3, the surface of nanofillers to the outside, there are bond layer, bound layer and loose layer in order. The first layer corresponds to a transition layer tightly bonded to nanofillers and polymers by a coupling agent. The second layer, defined as bound layer, is the interface region, which is composed of a layer of polymer

chain closely combined or interacting with the first layer and the surface of nanofillers. Finally, the third layer is loose layer, which is a region loosely coupled and interacted with the second layer. It is generally believed that the chain conformation, chain fluidity, and free volume or crystallinity in loose layer is different from the polymeric matrix, bound layer and bond layer. Therefore, it is easier to build a low resistance path for hopping electrons in the overlap of loose layer, which could introduce the shallow traps into the polymers. Therefore, it is easier to build a low resistance path for hopping electrons in the overlap of loose layer, which could introduce the shallow traps into the polymers, while the deep traps would be introduced by the bound layer and bond layer due to their dense structure. In the research paper [87], T. Tanaka has described and explained the multi-core models in terms of dielectric constant, dielectric loss, conductivity, space charge characteristics, breakdown strength and partial discharge properties of polymeric nanocomposites [86, 88].

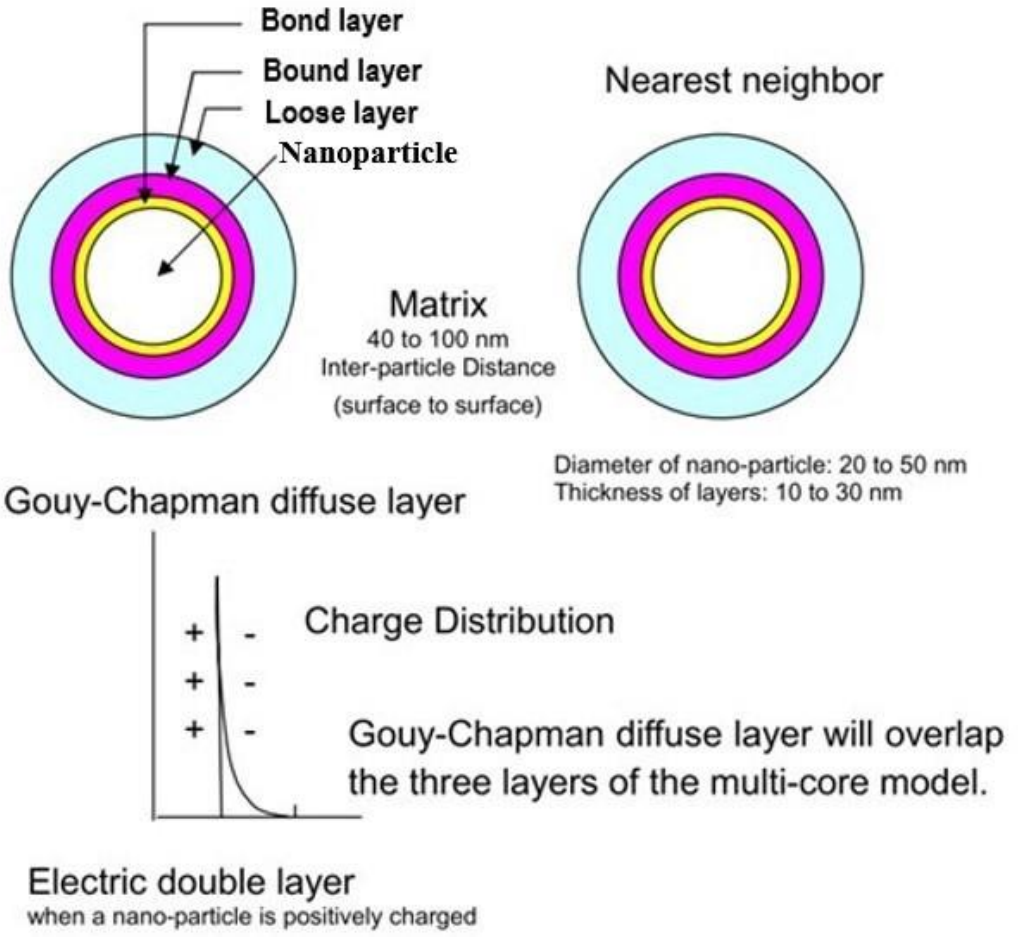

Figure 2.3 The Multi-core model for nanofillers – polymers interfaces [86]

iii. The potential well model:

The potential well model was proposed by T. Tanaka in 2008 and consists of an induced dipole by a high-permittivity dielectric nanofillers [89]. T. Tanaka pointed out that both the permanent dipole moment of chemical defects and the induced dipole moment of nanoparticles with high dielectric constant under high electric field can produce charge traps. Due to the density function theorem (DFT), the permanent dipole moment of chemical defects in LDPE can produce the traps with the trapping level of 0.45 eV, which is not enough to capture the electron injected from electrodes. Therefore, it is easy for space charge to accumulate in the bulk of LDPE under high DC electric field. After the addition of nano-MgO, the induced dipole moment of

nano-MgO can produce many deep traps with the trapping level of 1.5-5.0 eV, which is much higher than the traps in pure LDPE. Hence, those deep traps can capture the mobile electron and reduce the charge injection from electrodes. According to this model, the introduction of deep traps will be increased with the increase of nanofillers' size so that the electrical performance of nanocomposites will be better. However, the electrical performance of nanocomposites will be degraded with the increasing size of nanofillers.

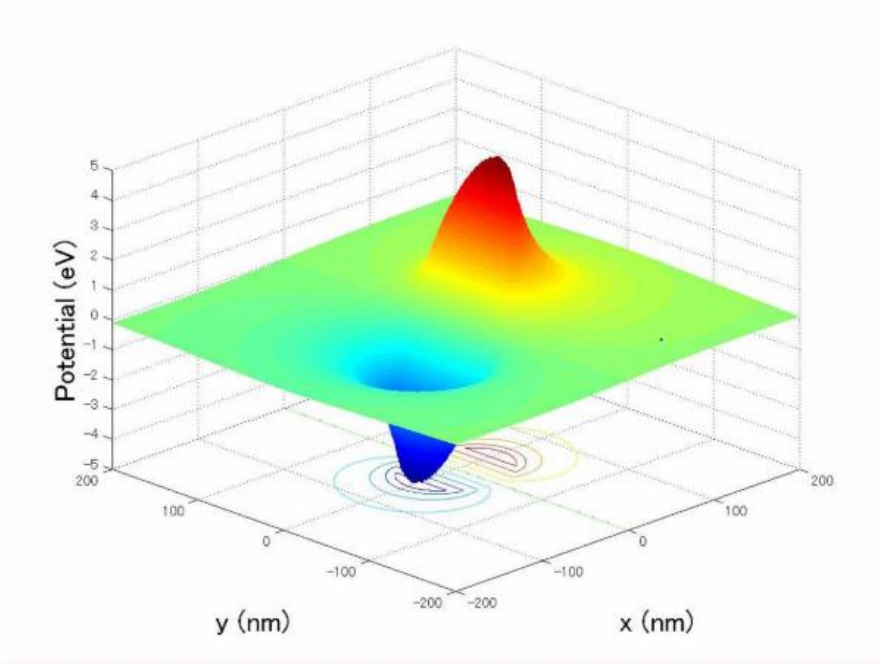

Figure 2.4. Electric potential distribution produced by an induced surface charge of a spherical conductor (diameter: 2a=100 nm) subjected to the electric field E0=100 kV/mm [89]

The above model can explain the changes of electrical properties of nanocomposites to a certain extent, but due to the lack of intuitive test methods for the interface generated by nanofillers and polymers, it is difficult to fundamentally demonstrate the correctness of the model. Most existing studies on interface or surface treatment of nanofillers explained the influence of the structure and electrical properties of nanocomposites from the perspective of improving the dispersion of nanoparticles. However, the effect of nanofillers on the electrical properties of

polymers is the result of many factors, not only in the interface and compatibility between nanoparticles and polymers, but also in the influence of the introduction of polar chemical groups on the electrical properties of polymers.

2.2 The limitation of extruded HVDC polymeric insulating materials

2.2.1 The electric field distortion due to space charge in materials

Space charge accumulation greatly limits the development and safe operation of polymer HVDC cables. The space charge would be injected from the electrodes under the external electric field. The region of polymer can be divided into 2 parts, shown as figure 2.5. For A, the homocharges are injected from the cathode, which would reduce the electric field of A region. For B, the injected electrons are the heterocharges which would increase the positive charge accumulated on the anode and cause the electric field distortion of B region [90]. This phenomenon will cause the electric field in region B be higher than the average electric field in the polymer. Even if the applied electric field does not reach the breakdown strength of polymer, the breakdown would more easily occur in the region B by the heterocharges injection.

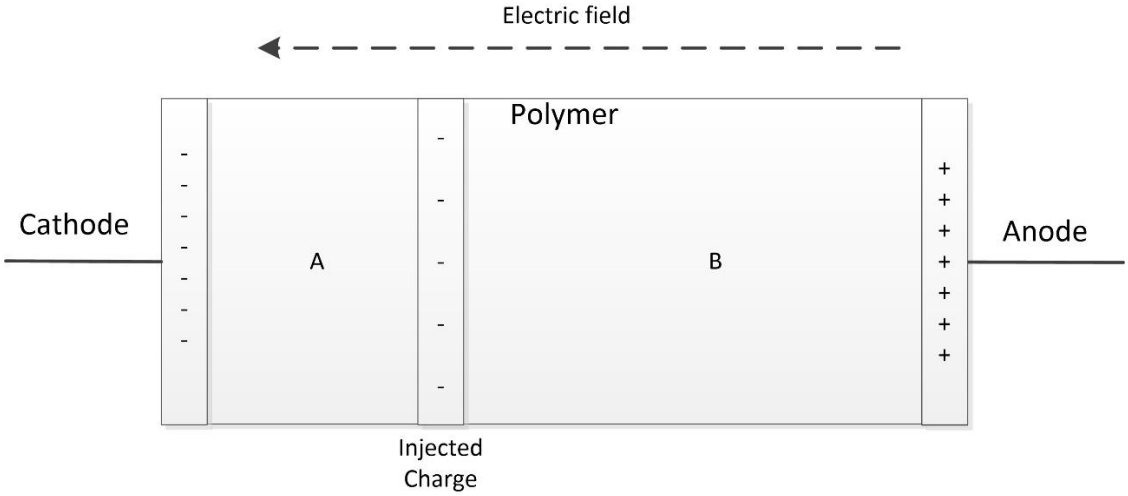

Figure 2.5 The simple diagram to explain the space charge accumulation in the polymer

In polymer HVDC cable insulation materials, space charge behavior is affected by conductivity, thermal conductivity, charge trap distribution and electric field. The electric field distribution is also affected by space charge accumulation. Hence, the nonlinear relationship between these parameters and external excitation (temperature and electric field) makes the causal relationship between material properties, electric field distribution, temperature distribution and space charge distribution coupled with each other. Therefore, how to achieve the coordination between the physical properties of insulating materials and external excitation is very important for the design of polymer HVDC cables.

2.2.2 The aging process occurs during the cable operation

The main form of long-term aging of insulating materials is electrochemical aging, also known as electrical aging. It is a process in which the molecular chain of materials is gradually degraded, and the mechanical and insulation properties are slowly reduced under the long-term operation under DC condition, resulting in complete insulation failure, such as electric treeing or water treeing [91]. There are inevitable defects and weak points in the preparation of insulating materials [92]. Also, there are many kinds of micro defects affecting the electrical properties of dielectrics, including the inherent defects introduced during material processing and molding and the aging defects caused by electrical and thermal stress during the operation of power equipment.

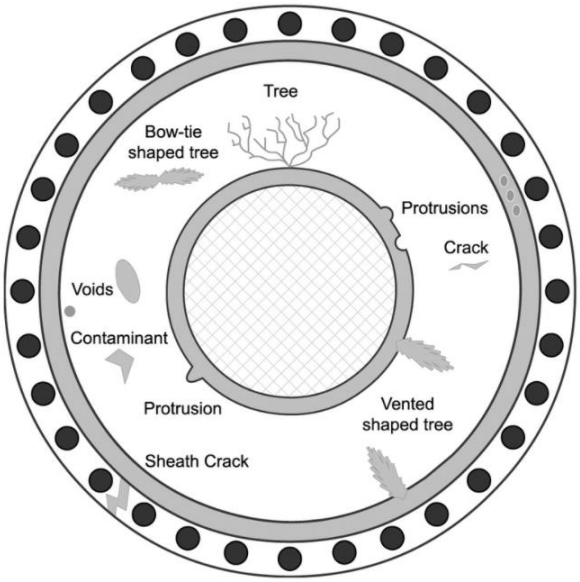

Figure 2.6 Some typical defects of polymeric insulation layer in the cable [93]

The working temperature of DC cable during normal operation is generally 50-70 ℃. In case of emergency, the working temperature may reach 130 ℃ (insulating material near the conductor side), and the electric field may reach 40 kV/mm. However, extruded PP cable can be estimated to work above 90 ℃ due to its high melting point and excellent performance. During the long-term operation of cable insulation, aging and deterioration will gradually occur under the combined action of electrical, thermal and other factors, resulting in the reduction of mechanical and electrical properties, and finally lead to insulation failure. Also, under the effect of ultraviolet, high temperature, and stress, hydrogen on the tertiary carbon atom of PP molecular chain can react with oxygen, resulting in molecular chain fracture and insulating degradation. Therefore, it is important to evaluate the aging properties of PP insulation materials.

The long-term performance of PP composites should be evaluated by thermal-oxidation aging and electro-thermal aging under 110℃ in the chapter 7 and the chapter 8 in the thesis.

2.3 Conclusion

This chapter describes the contents related to literature reading. From the concept of nanodielectric proposed by T. J. Lewis in 1984 to the models of various nanodielectric theories, this chapter describes the improvement of nanotechnology on the nanofillers and the development of nanodielectrics theorem on the electrical properties of polymer nanocomposites in the past few decades. Most scholars believe that the interface between nano filler and polymer plays an important role in the polymer modification. However, the interface related theories more reflect the influence of the compatibility between nanofillers and the polymer matrix on the electrical properties of polymer nanocomposites, and the existing theoretical models are still insufficient. In the first chapter of this paper, it is mentioned that the surface treatment of nanofillers with coupling agent is essentially the introduction of chemical groups. Finally, the improvement of the electrical properties of polymer nanocomposites actually comes not only from the nanofillers themselves, but also from the chemical groups on the coupling agent. In view of the need to analyze chemical groups, this thesis considers that the DFT method is important to analyze the introduction of deep traps by chemical groups. The influence of the introduction of polar chemical groups on the trap distribution of polymers can be more fully obtained by using Gaussian software.

3. Methodologies to measure the properties of polymeric insulating materials

3.1 Field-emission scanning electron microscope

The FE-SEM technique can be used to observe the dispersion of nanofillers in the polymers. The FE-SEM can be roughly divided into two parts: mirror body and power circuit system. The mirror body is composed of an electron optical system including electron gun, scanning coil, et al., a sample chamber, a detector and a vacuum pumping system [94].

The vacuum system is very important in electron optical instruments because electron beams can only be generated and manipulated under vacuum. For SEM, the vacuum degree is usually required to be better than $10^{-3} \sim 10^{-4}$ Pa. Any decrease in vacuum will increase the electron beam scattering, shorten the filament life of the electron gun, produce a false secondary electron effect, accelerate the pollution of hydrocarbon on the lens aperture and sample surface, and seriously affect the imaging quality. Therefore, the quality of the vacuum system is one of the reference indexes to measure the quality of SEM.

The function of electron gun is to produce the electron light source, and its performance determines the quality of SEM. The resolution of SEM images is generally limited by the brightness of electron gun. According to Langmuir equation, the electron density can be emitted by the cathode material, which can determine the brightness of observed samples [95].

The process of SEM operation is shown in Figure 3.1 [96]. The electron beam emitted by a three-pole electron gun (usually 50 μm) , under the action of accelerating voltage (2 ~ 30 kV), three electromagnetic lenses (or two electromagnetic lenses) converge to form an electron probe as small as 5 nm. Under the action of the scanning coil on the upper part of the final lens, the electron probe makes grating scanning on

the sample surface (the number of grating lines depends on the line scanning and frame scanning speed). Due to the interaction between high-energy electrons and matter, various information is generated on the sample, such as secondary electrons, back reflected electrons, Auger electrons, X-rays, cathodoluminescence, absorbed electrons and transmitted electrons. Because the intensity and distribution of various information obtained from the sample are related to the surface morphology, composition, crystal orientation, and some physical properties of the surface state (such as electrical properties, magnetic properties, etc.), by receiving and processing these information, we can obtain the scanning electron image characterizing the sample morphology.

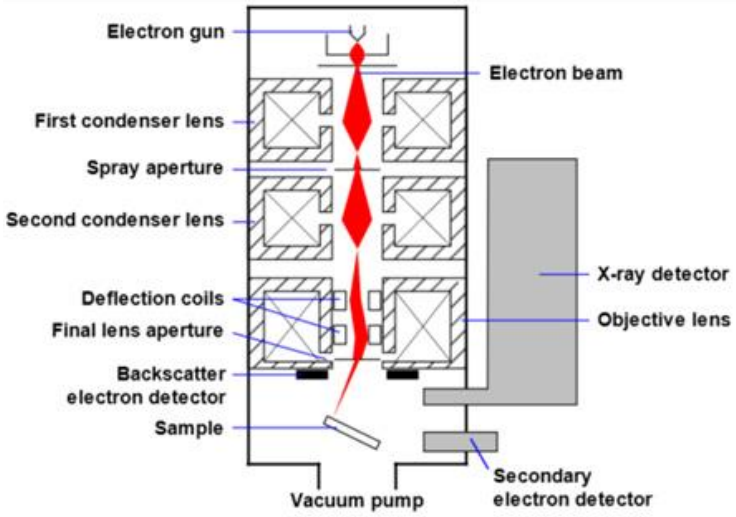

Figure 3.1 The basic process of SEM operation [96]

In the thesis, the morphology of PP and its nanocomposites and the dispersion of nano fillers were analyzed by SEM (Hitachi 8010, Japan) shown in Figure 3.2. The brittle fracture of the sample was carried out in liquid nitrogen. The cross section of brittle fracture was observed under electron microscope after gold sputtering in the vacuum condition. The electron acceleration voltage was 10 kV.

Figure 3.2 The diagram of FE-SEM (Hitachi 8010, Japan)

3.2 Polarized optical microscopy

The polymeric crystals under micron size can be observed by the POM due to the crystal birefringence effect and the polarized light characteristics [97]. The structure of POM is shown in Figure 3.3 [98]. The polarizer in the POM only allows the vibration light in the polarization direction to pass through and absorbs the vibration light in this direction at the same time. Therefore, natural light will become polarized light with a certain vibration direction after passing through the polarizer in POM.

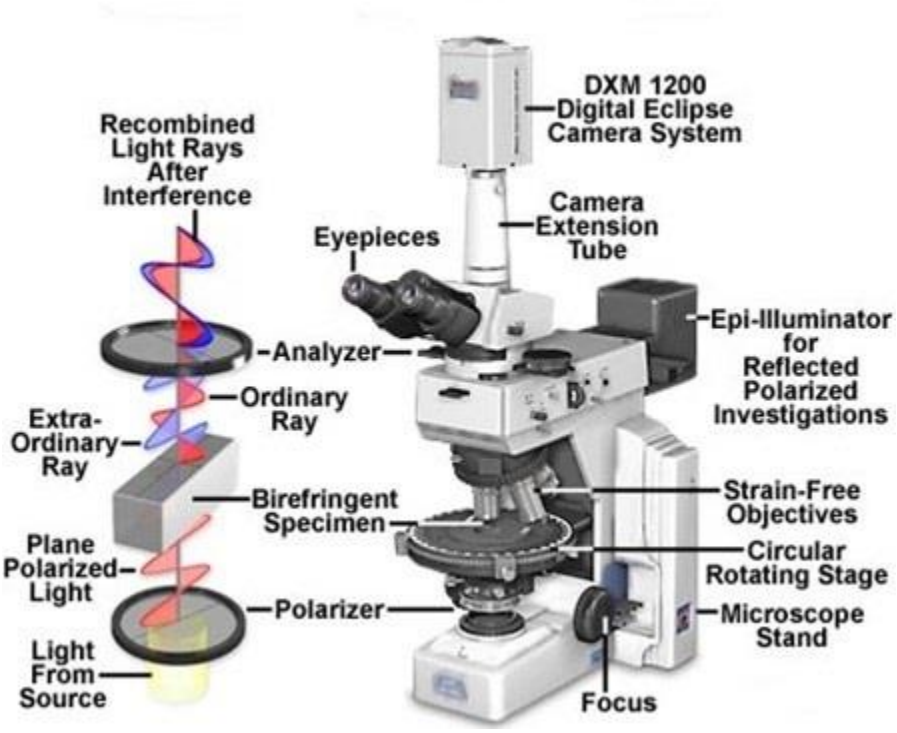

Figure 3.3 The structure of POM [100]

When a beam of polarized light passes through the spherulite, that is, birefringence occurs with different refractive indices in the direction parallel to and perpendicular to the molecular chain, and it is divided into two beams of polarized light whose electric vectors are perpendicular to each other. This means that two beams are parallel and perpendicular to the radius of the spherulite respectively. Due to the different refractive index of the two directions, the speed of the two beams passing through the sample is unequal, which will inevitably produce a certain phase difference and interfere. Part of the light passing through the spherulite can pass through the polarizing mirror orthogonal to the polarizing mirror, and the light in the other part cannot pass through. Finally, a bright and dark area is formed, showing the unique black cross extinction pattern of the spherulite [97]. Therefore, the spherulites of PP and its nanocomposites could be observed by POM (Nikon Eclipse microscope LV1100NPOL, Japan) shown in Figure 3.4.

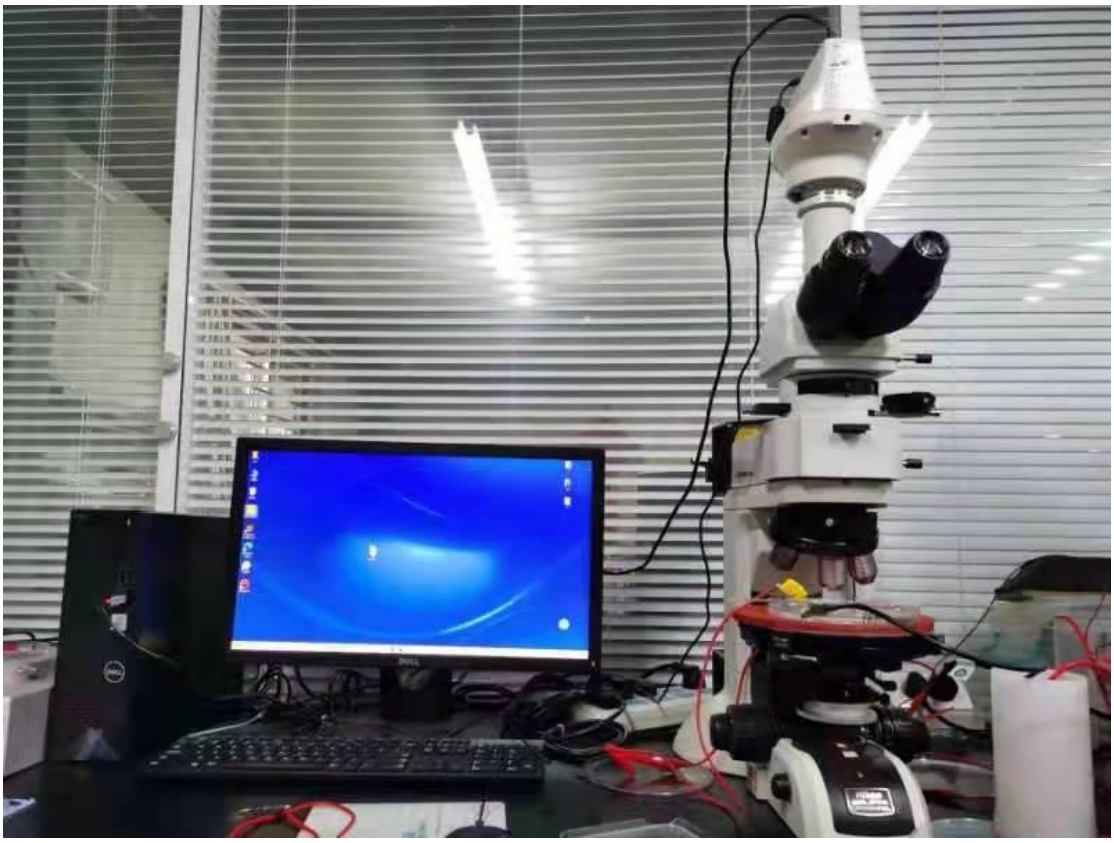

Figure 3.4 The diagram of POM ((Nikon Eclipse microscope LV1100NPOL, Japan)

3.3 Thermogravimetric analysis

The thermal stability of materials and the fraction of volatile components can be measured by the thermogravimetric analysis through monitoring the weight change of samples when heated at a constant rate. Therefore, it can be used to analyse the thermal stability of nanofillers and PP under the manufacturing process and operational conditions. In the thesis, TGA results of nanofillers and PP was carried out on TA Q500 instrument shown in Figure 3.5. It was heated from room temperature to 800 ℃ at a heating rate of 10 ℃ / min in a nitrogen atmosphere to avoid the oxidation of samples under oxygen atmosphere.

Figure 3.5 The diagram of TGA device (TA Q500)

3.4 Dielectric Spectroscopy Measurement

There are two important factors to evaluate the dielectric properties of PP, including the permittivity and dissipation factor [99-100]. The dielectric constant of nanocomposites can be calculated by the equation and the model below.

$$I = j\omega\varepsilon C_0 U ----(2)$$

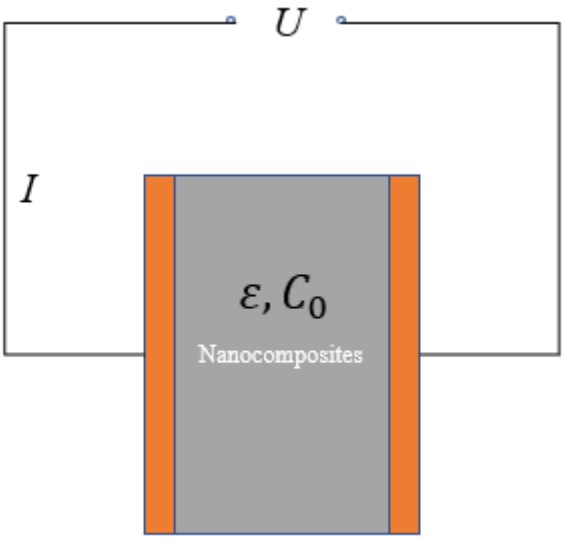

Figure. 3.6 The circuit model for the calculation of dielectric constant

Where: ε is the permittivity of nanocomposites. C_0 is the capacitance between two electrodes. ω is the angular frequency of AC power source. U is the value of AC voltage, and I is the value of AC current. Because under HVDC conditions, there is not dielectric loss occurring during the cable operation, the dissipation factor is not considered in the thesis. it reflects structural and other properties of the system.

The sample holder of dielectric spectroscopy has been shown in the figure below [103]. The electrodes are made of copper and the broadband dielectric spectrometer (Novolcontrol, Germany) with Alpha-A high performance frequency analyzer was used to measure the dielectric constant of PP and its nanocomposites.

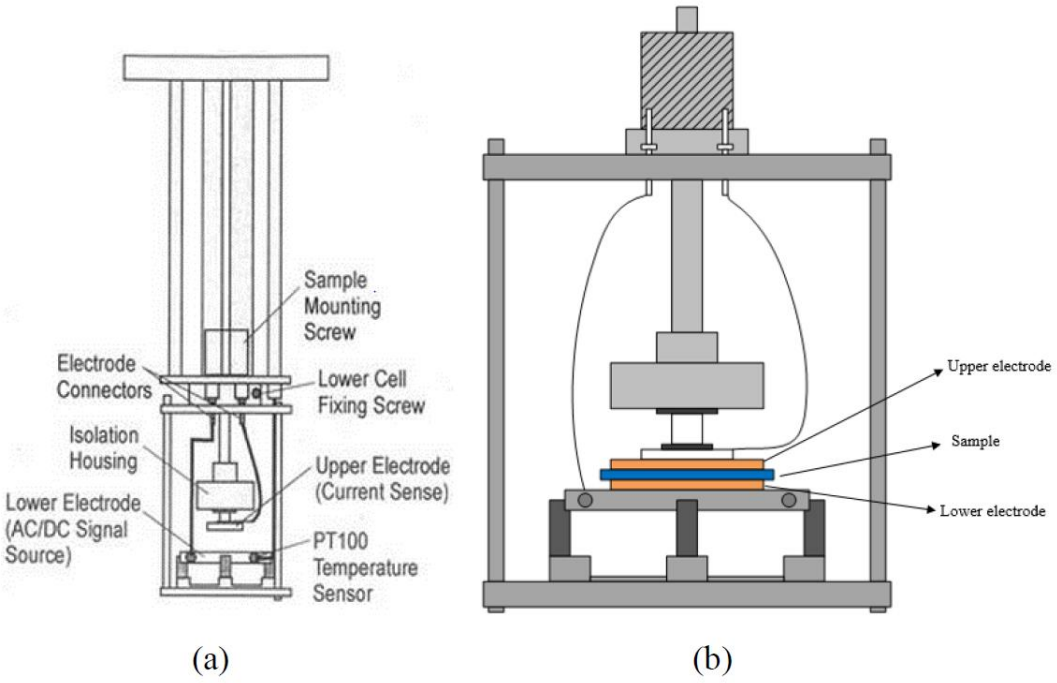

Figure 3.7 The sample holder for dielectric spectroscopy [101]

3.5 Fourier transform infrared spectroscopy

The analysis of Fourier Transform Infrared Spectroscopy is a method to identify a substance and determine its chemical composition, structure or relative content according to its spectrum [102]. According to the analysis principle, spectral technology is mainly divided into infrared absorption spectrum, emission spectrum and scattering spectrum; Infrared absorption spectrum belongs to molecular spectrum, including infrared emission spectrum and infrared absorption spectrum. The commonly used is infrared absorption spectrum.

From Figure 3.8, there are three kinds of energy level transitions in the diatomic molecule [103]. The diatomic molecule absorbs a photon with an energy of hv from the lower energy level and can transition to the higher energy level. The whole motion process satisfies the law of energy conservation E(high) - E(low) = hv. The smaller difference between energy levels, the lower the frequency and longer the wavelength of the light absorbed by the molecule.

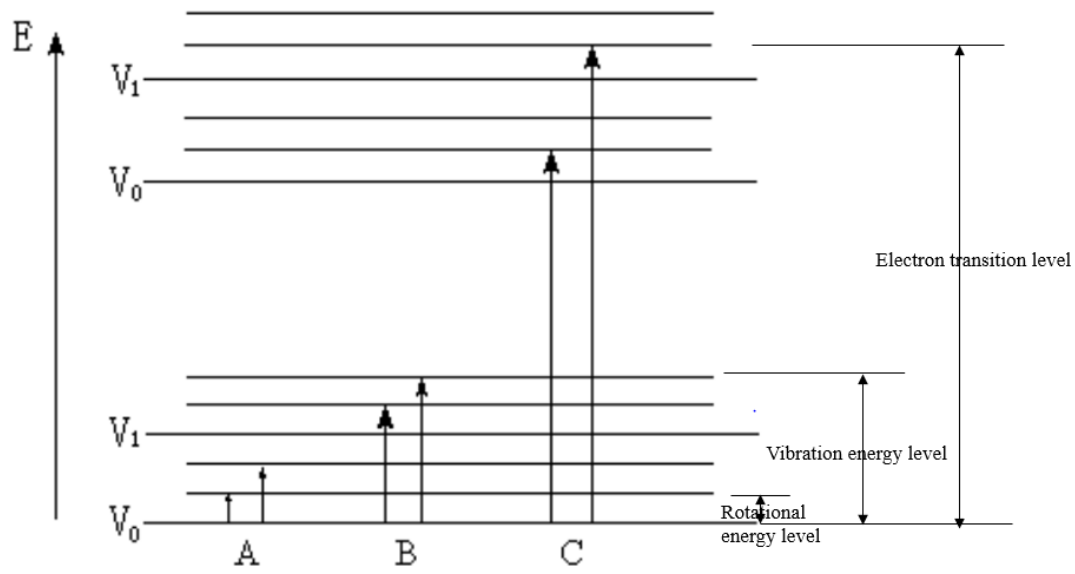

Figure 3.8 Schematic diagram of three energy level transitions of diatomic molecules

The molecular vibrational energy is greater than the rotational energy. When the vibrational energy level transition occurs, it is inevitably accompanied by the rotational energy level transition. Therefore, it is impossible to measure the pure vibrational spectrum, but only the molecular vibrational, rotational spectrum, which is called an infrared absorption spectrum. FTIR absorption spectrum is produced due to the molecular vibration and the rotational transition. The atoms constituting chemical bonds or functional groups are in a state of continuous vibration or rotation, and their vibration frequency is equivalent to that of infrared light. Therefore, when the molecule is irradiated with infrared light, the chemical bonds or functional groups in the molecule can undergo vibration absorption. Different chemical bonds or functional groups have different absorption frequencies and will be in different positions in the infrared spectrum, so as to obtain the information about what chemical bonds or functional groups are contained in the molecule.

Therefore, the technique of FTIR spectroscopy is carried out by Nicolet 6700, USA shown in Figure 3.9 to analyse the chemical group of nanofillers. unaged nanocomposites, and aged nanocomposites in the thesis.

Figure 3.9 The photo of FTIR spectroscope (Nicolet 6700, USA)

3.6 Differential scanning calorimetry

Differential scanning calorimetry (DSC) is a technique to measure the relationship between heat flow and temperature of the sample under the comparison with the reference sample. It can provide quantitative or qualitative information about heat absorption, heat release, heat capacity change and so on. The amorphous aggregates of PP formed after undercooling treatment will begin to crystallize and release crystallization heat. Therefore, there is an exothermic peak appeared on the crystallization process of the DSC curve of polymers. With the increase of temperature, the crystalline part of PP begins to melt. The compensator in the DSC device measures that the heat flow must be increased to overcome the phase change enthalpy required for melting in order to maintain the same temperature, so an endothermic peak will appear on the DSC curve. In the thesis, the DSC device (NETZSCH 200F3, USA) shown in Figure 3.10 was used to calculate the crystallinity of PP and its nanocomposites through the equation below:

$$X_c = \frac{\Delta H_m}{\Delta H_m^{\infty}} \times 100\% \quad \text{----} \quad (3)$$

where ΔH_m is the melting enthalpy which is the integral value of melting procedure from DSC curves, and ΔH_m^{∞} is the melting enthalpy for complete crystallization of pure PP with the value of 209 J/g [104]. Through the integration of heat flow on temperature for the heating process, the melting enthalpy ΔH_m.

After the DSC measurement, the effect of nanofillers addition on the crystallization, the melting point and the crystallinity of PP could be clarified.

Figure 3.10 The diagram of DSC devices (TA Q2000, USA)

3.7 Thermal stimulated depolarized current measurements

The thermally stimulated depolarized current (TSDC) method is based on the study of medium physics and can be used to study the micro molecular motion and the charge trapping characteristics of the medium [105-106]. The properties of traps, dipoles and movable ions in dielectric materials can be easily studied by TSDC curve, and the trapping density and trapping depth of dielectric materials can be measured. When the temperature is high, the charge in PP is easy to obtain energy from the outside. When the temperature is low, the charge in PP is not easy to obtain energy from the outside. If a higher thermally stimulated current is detected at low temperature, it indicates that

the depth of charge traps is shallow. On the contrary, at higher temperature, higher thermally stimulated current is detected, which indicates that the depth of charge trap is deep. Therefore, it can be used to analyse the effect of nanofillers addition on the trapping characteristics of PP.

The TSDC measurement was achieved by using a broadband dielectric spectrometer (Novocontrol GmbH Concept 40, Germany). The temperature range of TSDC system shown in Figure 3.11 is from -150 to 200 ℃. The cooling process can be achieved by the release of liquid nitrogen and the heating process can be achieved by the heating system. Firstly, the contact area of the sample between sample and test-electrodes was sputtered with gold. Secondly, the sample was polarized at 20 ℃ for 40 min at 6 kV/mm and then cooled down to -100 ℃ with a cooling rate of 10℃/min. After that, the samples were short-circuited for 5 min to remove the space charge on the surface of PP's nanocomposites.

Figure 3.11 The configuration of TSDC measurement system

3.8 DC conductivity tests

The DC volume conductivity was measured by a digital high-resolution galvanometer (6517B, Keithley) with a standard three-electrode system under different temperature and the measuring temperature is controlled by the Vacuum Oven. The experimental design is shown in Figure 3.12, including the DC power source (2290-10, Keithley), digital high-resolution galvanometer (6517B, Keithley) and the protective resistance (>100 kΩ). The range of applied voltage is between 0 to 1000 V and the upper and lower electrodes were made of 304 stainless steel. The data of conductivity could be recorded in the desktop. The vacuum oven in the test is electrostatic shielded in order to avoid the influence of electromagnetic interference from PC and mobile phone on the test result. The results of DC volume conductivity measurement showed the effect of nanofillers on the DC volume resistivity of pure PP.

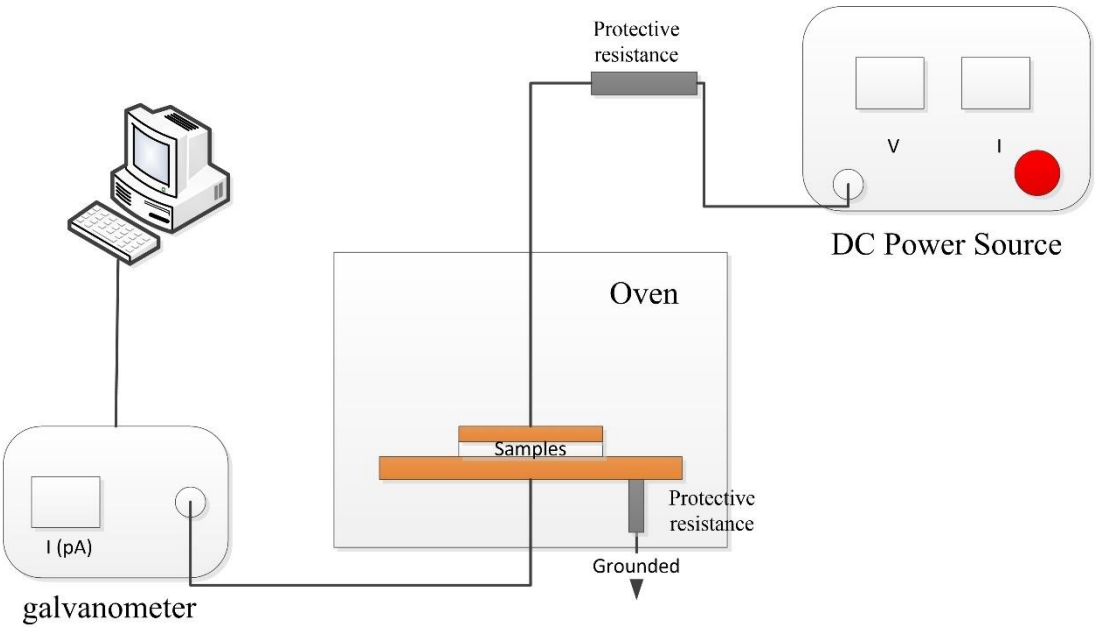

Figure 3.12 The experimental design of DC conductivity test under different temperature

3.9 DC breakdown strength tests

The high voltage DC breakdown test system has been shown in Figure 3.13. The high voltage DC breakdown test system includes ±80 kV DC high voltage power supply, voltage test system, protection resistance, two spherical electrodes and temperature controller. There is a sphere-sphere electrode configuration with a sphere diameter of 2.0 cm so that the effect of breakdown test could be controlled within 5.0 mm around the breakdown points of the axis of symmetry. The tested samples should be immersed in the silicon oil to prevent the flashover occurring during the breakdown strength test. The temperature of oil could be adjusted by the heating plate which is controlled by the temperature controller. There were 20 measuring points marked uniformly on each film and each point was aligned with the axis of the sphere-electrodes prior to each DC breakdown test. The rising rate of DC voltage applied was 1 kV/s until breakdown occurred.

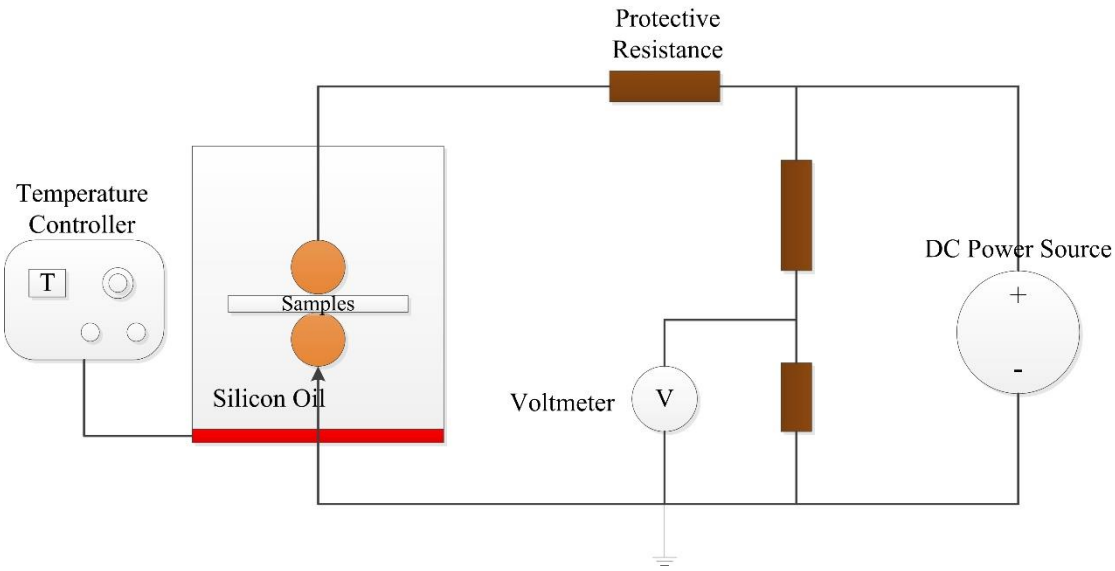

Figure 3.13 The experimental design of DC breakdown strength test

3.10 Pulse electro-acoustic measurement

The electric field of the space charge test system can only reach the maximum value of 100 kV/mm for the tested sample because the flashover will occur if the electric field

is over 100 kV/mm. The measured temperature can be adjusted by the temperature controller from 20 to 100 ℃. The principle of pulse electro-acoustic (PEA) measurement for space charge is that the charge in PP vibrates by the narrow pulse, and the high-speed vibrating charge generates an ultrasonic signal. Then the ultrasonic signal is received by the piezoelectric sensor (polyvinylidene fluoride (PVDF)) of the electrode below and converted into an electrical signal. The signal amplifier amplifies the electrical signal and transmits it to the oscilloscope and the desktop for storage.

In the PEA system for space charge measurement shown in Figure 3.14, the signal generator is Tektronix 3000C. The model of voltage amplifier is TREK MODEL30/20A which means that the maximum voltage applied by this voltage amplifier is 30 kV. Also, the rising rate of voltage is 550 V/μs. The model of pulse generator is AVTECHAVG-4B-C and its pulse width and frequency are 6 ns and 10 kHz respectively. The Lecroy WaveRunner 610Zi was adopted as the oscilloscope to show the curve of the result of measurements. The bandwidth of this oscilloscope is 1.0 GHz and the sampling frequency is 2.5 GHz. Finally, the model of signal amplifier is Metiq 1291 with the amplify ratio of 63.0 dB.

The space charge distribution in the bulk of PP's nanocomposites was measured by the PEA system under the temperature of 30, 50, 70 and 90 ℃. The pulse voltage was set to 800 V with a frequency of 1.0 kHz. A DC electric field of 60 kV/mm and 30 kV/mm was applied to the unaged samples and aged samples respectively during the testing.

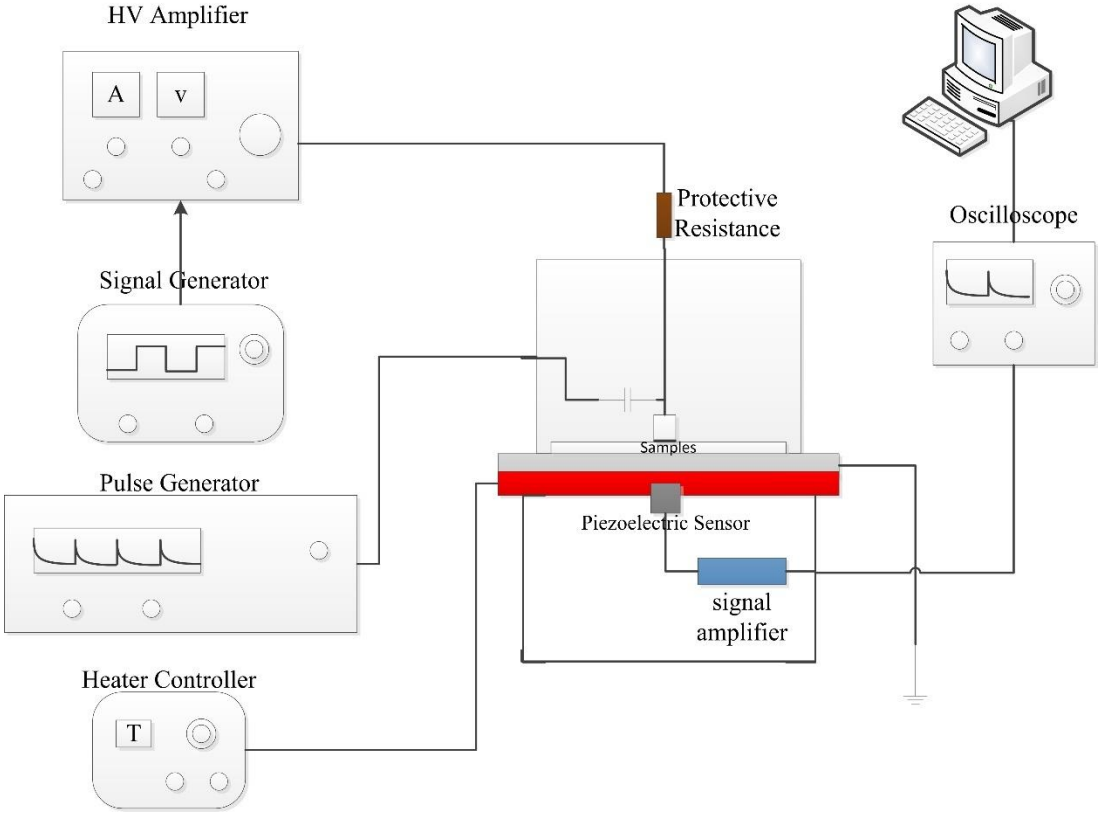

Figure 3.14 The experimental design of PEA system for space charge measurement

3.11 Tensile strength tests

The tensile strength test was carried out by electromechanical high-temperature testing machine (SANS, CMT4304) at the room temperature with the tensile rate of 10 mm/min. The shape of testing sample like a dog bone shown in Figure 3.15 [107]. The sample for tensile strength test has a thickness of 0.2 mm, a gauge distance of 16.0 mm and a width of 4.0 mm. The shape of dog bone is adopted to make the tensile force uniformly distributed on the sample. The final mechanical properties of PP and its nanocomposites were demonstrated by the breaking elongation and tensile strength, which could reveal the deformation and the hardness of samples. Tensile strength is equal to the highest tensile force divided by the cross-sectional area, and elongation at break is equal to the increased length at break divided by the gauge length.

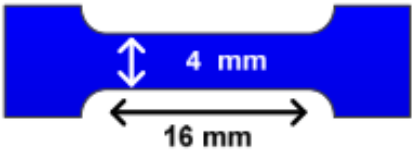

Figure 3.15 The shape of testing samples

3.12 Conclusion

The third chapter describes the experimental technology and principle used to measure the microstructure and macro properties of polypropylene and its nanocomposite insulating materials.

i. The surface of PP and its nanocomposites were scanned by FE-SEM technique to generate microstructure images. By using liquid nitrogen to break the sample, the generated cross section is sputtered with gold to enhance the scanning of electrons in the cross section. The dispersion of nanofillers in PP can be demonstrated by observing the interface diagram under electron microscope.

ii. Polarizing microscope can observe the spherulite interface of nanocomposites through the adjustment of polarizer, so as to get the effect of the addition of nano filler on the spherulite morphology of polypropylene.

iii. Thermogravimetric analysis can be used to analyze the thermal stability of polypropylene and nano fillers at different temperatures.

iv. Dielectrics can be used to evaluate the dielectric properties of nanocomposites under DC conditions.

v. Fourier infrared spectroscopy can reflect the chemical bonds and chemical groups in the matrix according to the chemical bond absorption spectra of different groups. At the same time, it can be used to characterize the surface of inorganic nano fillers after surface treatment and detect the oxidized groups of aging PP's nanocomposites to indicate the aging degree of nanocomposites.

vi. The results of differential scanning calorimetry can be used to measure the effect of nano filler on the crystallinity, crystallization process and melting point of polypropylene.

vii. Thermally stimulated depolarization current can be used to measure the charge trapping characteristics of polypropylene and its nanocomposite insulating materials.

viii. The DC volume conductivity can reflect the effect of nanofillers on the charge transport of PP.

ix. DC breakdown test is an important parameter to measure the electrical properties of polypropylene and its nanocomposites.

x. The accumulation of space charge in polypropylene and its nanocomposites and the electric field distortion can be measured by PEA method.

xi. Finally, the mechanical properties of polymers play an important role in the process of cable installation, especially the breaking elongation and tensile strength. Therefore, the mechanical test of PP and its nanocomposites is carried out by extensometer.

4. Experimental Samples

4.1 Material for this research

4.1.1 Polymeric matrix material

At present, most polymer DC cables use XLPE as the insulating medium, and its working temperature generally does not exceed 70 ℃ [108]. With the further improvement of the operating voltage and transmission capacity of high voltage DC cable, the working temperature of DC cable will also increase. Nowadays, the working temperature of XLPE cable has reached its limit of working temperature, and due to its non-recyclable characteristics, there is an urgent need to develop new DC cable insulation materials to meet the operational needs of cable at high temperature and the trend of environmental protection in the world.

PP has excellent electrical properties and excellent mechanical properties at higher temperature than XLPE [108]. It has a potential to be next generation of DC cable insulation material with environmental-friendly properties due to its thermoplastic properties. In terms of cost, PP is one of common commercial polymers with low price. In terms of the manufacture, PP does not need crosslinking process in the production process of cable extrusion, which reduces the production energy consumption and avoids the release of some pollutants. In terms of environmental protection, PP can be recycled after use so that it can satisfy with the need of low-carbon society. Therefore, in the thesis, iPP provided from Aladdin Industrial Inc., China. was selected as the matrix material to develop the new nanocomposites insulation material.

4.1.2 Nanofillers selection

In the past few decades, most of research work was focused on the inorganic nanoparticles especially for nano-MgO, nano-Al_2O_3. But due to the smaller size and the functional side group of POSS, it might have a better performance to improve the properties of PP. Therefore, in the thesis, nano-MgO, nano-Al_2O_3, octavinyl-POSS

(OvPOSS) and octaphenyl-POSS (OpPOSS) were used as nanofillers to modify PP and then to compare the electrical properties of those nanocomposites to optimize the nanocomposites manufacture. Nano-MgO, nano-Al_2O_3 and OpPOSS were purchased from Aladdin Industrial Inc., China. OvPOSS was bought from Zhengzhou Alfache Co., LTD., China. The coupling agent, γ-methacryloxypropyltrimethoxysilane (KH570) with the purity of 98.0 %, was provided by Sinopharm Chemical Reagent Co., Ltd., China. Xylene with the purity of 98.0 % was purchased from Tongguang Chemistry Co. LTD., China as an organic solvent. The specific parameters of nano filler are shown in the table below:

Table 4.1 The specific parameters of nanofillers

Nanofillers	Diameter (nm)	Relative Permittivity	Volume Resistivity (Ω. m)	Purity (%)	Density (g/cm^3)
nano-MgO	50.0±5.0	6.8	$> 10^{12}$	99.9	3.58
nano-Al_2O_3	50.0±5.0	9.4	$> 1 \times 10^{10}$	99.9	3.95
OvPOSS	1.0-1.5	3.9	none	98.0	0.93
OpPOSS	1.0-1.5	3.5	none	99.0	0.95

4.1.2.1 The structure of POSS

Due to desirable advantages, different kinds of polyhedral oligomeric silsesquioxane (POSS) have attracted much attention in electrical applications [55, 109-111]. Some reports reveal that the good dispersion of POSS in PP under higher contents and the AC breakdown strength of PP can be enhanced by the addition of POSS [112-113]. From the paper [114], the structure of POSS has a nano-silica cage structure in the nanometer scale and organic-side groups. The classification of POSS is determined by the side-groups. In contrast with some kinds of POSS that are in the liquid state, the OvPOSS and the OpPOSS are semi-crystalline solid at room temperature. The main cage of POSS can perform a similar role

to traditional nano-silica to improve the electrical performance and the side groups of OvPOSS can not only increase the compatibility between POSS and polymers due to their structural similarity but also introduce the polar group to improve the trapping characteristics of polymers. The structure of OvPOSS and OpPOSS have been shown in Figure 4.1 and Figure 4.2 [115-116]. Each single OvPOSS and OpPOSS molecular chain has a length of about 1.5 nm. This means that, for the same volume of contents of the nanofiller, POSS nanofillers have more interfacial areas with the polymeric chain when compared with those of nano-MgO and nano-Al_2O_3. Additionally, the densities of OvPOSS and OpPOSS are around 0.93 g/cm^3, which is much lower than inorganic nanofillers. Therefore, the volume contents of OvPOSS and OpPOSS would be higher than that of inorganic nanofillers under the same weight content in the matrix materials.

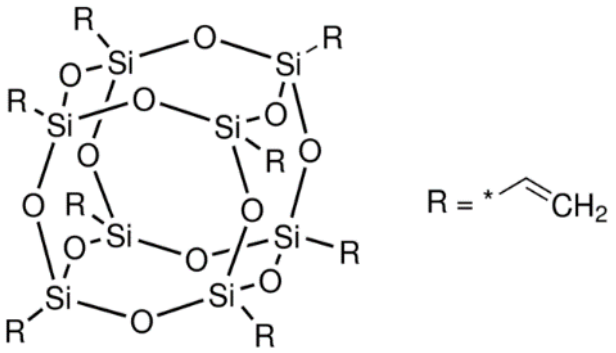

Figure 4.1 The chemical structure of OvPOSS molecular.

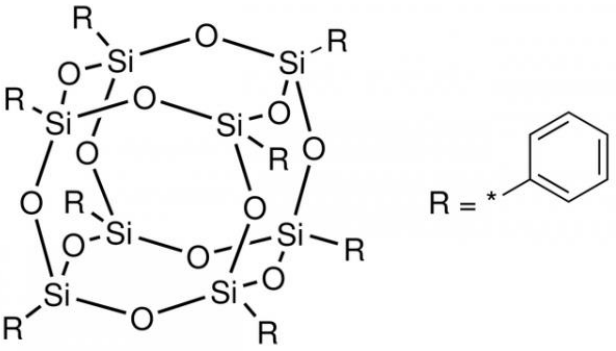

Figure 4.2 The chemical structure of OpPOSS molecular.

4.1.2.2 The surface treatment of inorganic nanofillers

KH570 is selected for surface treatment of nano-MgO and nano-Al_2O_3, purchased from Sinopharm Chemical Reagent Co., Ltd., China., with the purity of 98.0 %, the molecular weight of 248.35 g/mol, the boiling point of 195 °C and the density of 1.045 g/ml. The molecular structure of KH570 is shown in Figure 4.3.

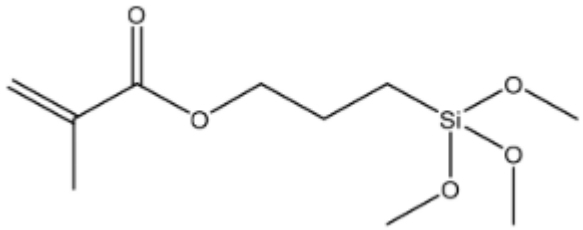

Figure 4.3 The chemical structure of γ-methacryloxypropyltrimethoxysilane (KH570)

The process of surface treatment of nano-MgO and nano-Al_2O_3 are shown in Figure 4.4. The methoxy group on KH570 molecule reacts with the hydroxyl group on the surface of nanofillers to produce water and surface treated nanofillers, so KH570 molecule is coated on the surface of nanoparticles. The similar structure of KH570 and PP can improve the compatibility between nanofillers and the molecular chain of PP and promote the nanofillers to be better dispersed in PP [117].

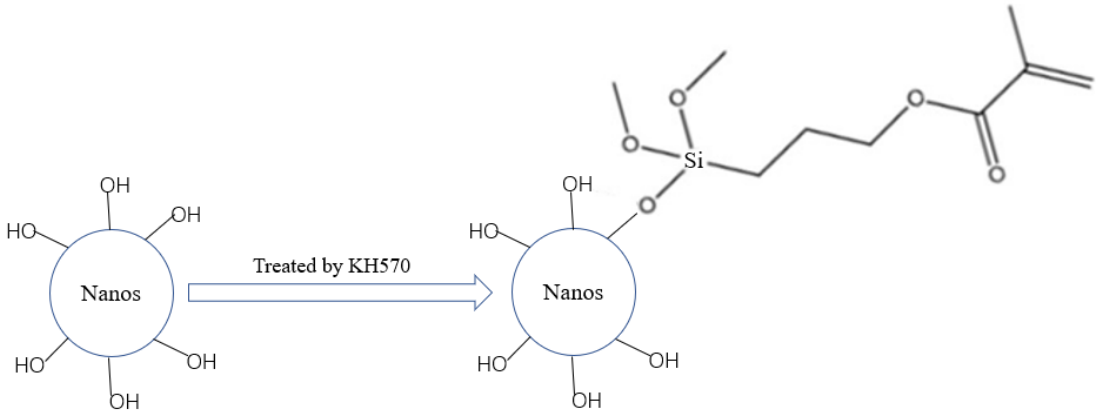

Figure 4.4 The process of surface treatment of nano-MgO and nano-Al_2O_3

The surface treatment process of nanofillers including nano-MgO and nano-Al_2O_3 is described as follows and shown in figure 4.5:

i. The nanofillers were dried at 120 ° C for 8 h.

ii. 5g of nano filler was added to a beaker containing 200ml of xylene, and the nano filler was well dispersed in xylene solution after ultrasonic treatment for 30 minutes.

iii. The nanofiller/xylene solution and 20ml KH570 were poured into a three-mouth flask in an oil pot and stirred under 110℃ at 500 rpm for 12 hours to ensure that KH570 could fully react with the hydroxyl group on the surface of the nanofiller.

iv. The stirred solution was centrifuged at 6000 rpm for 6 minutes to collect the nanofiller and remove the unreacted KH570.

v. The collected nanofiller was cleaned by twice with xylene to remove the residual KH570 on the surface of the nanofiller.

vi. The resulting nanofiller was placed in a vacuum oven and dried at 90 ° C for 24 hours.

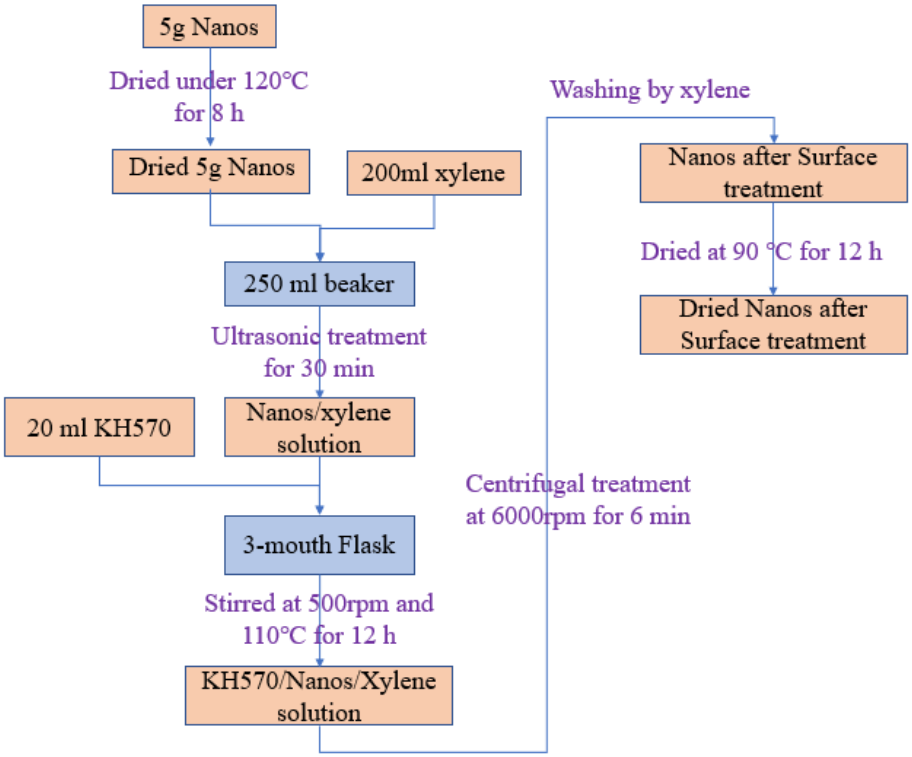

Figure 4.5 The process of surface treatment of nano-MgO and nano-Al_2O_3

4.1.3 Fourier transform infrared spectrum of nanofillers

The surface of nanofillers is characterized by FTIR spectrum. The test mode is reflection mode, the test resolution is 2 cm^{-1} and the average value is calculated after 16 tests. The test results are subject to baseline calibration after deducting the atmospheric background. The results of nano-MgO and nano-Al_2O_3 are shown in Figure 4.6 to confirm that the surface modification of nano-MgO and nano-Al_2O_3. New absorption peaks appeared at 2960, 2920, 2850, 1720 and 1150 cm^{-1} of the surface treated nano-MgO and nano-Al_2O_3, corresponding to the infrared absorption peaks of stretching vibration of -CH_2-, -CH_3, C = O and C-O respectively, indicating that the surface of the nanofillers has successfully modified by the coupling agent.

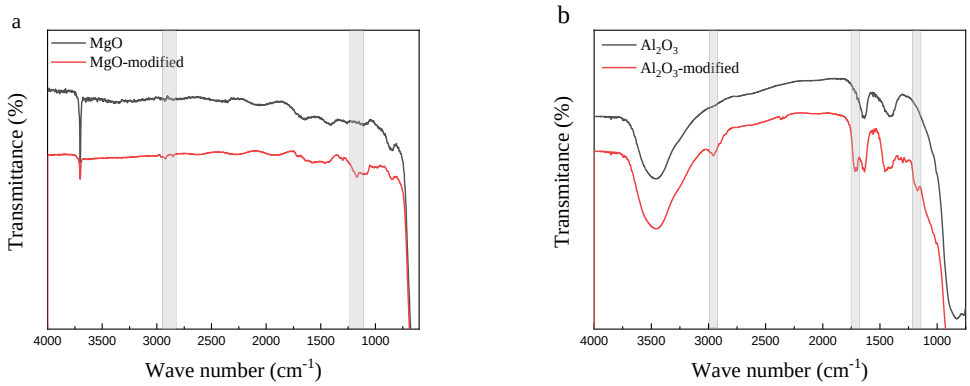

Figure 4.6 The FTIR spectrum singular of nanofillers

4.1.4 Raw materials and research ideas

The above are the raw materials for preparing nanocomposite insulating materials selected in the experiment. As described in the Chapter 2 of the thesis, nanocomposite technology based on inorganic nanoparticles can be used as an effective means to improve the electrical properties of polymeric insulating materials and has achieved good results in a variety of polymers. Although it has become a consensus that inorganic nanoparticles improve the electrical properties of polymers, the compatibility between inorganic nanoparticles and matrix is still not good enough, especially the agglomeration is easy to occur in the production process and causes electrical defects in the insulation layer of cable. It is found that the ultra-fine nanofillers represented by POSS can improve the electrical properties of PP. Because its density is close to PP, it is relatively difficult to settle and agglomerate in PP after full stirring. In the structure of POSS, the side-group of POSS can increase the compatibility between POSS and polymers and the cage of POSS can perform as the nano-silica to improve the electrical properties of polymers. However, it is still unclear how POSS affects the electrical properties of PP. In the thesis, the effects of typical inorganic nanoparticles, including nano-MgO, nano-Al_2O_3 and two kinds of ultra-fine nanofillers including octavinyl-POSS (OvPOSS) and octaphenyl-POSS (OpPOSS) on the electrical properties of PP

are compared, the optimized nanocomposite insulation material is obtained, and its mechanism is analyzed.

4.2 Sample preparation

The matrix material, iPP with a density of 0.92 g/cm^3 and a melt flow rate of 0.6 g/10 min is adopted to manufacture nanocomposites insulation material. Differing from the actual cable melting extrusion process, the research in the thesis is to establish the potential of nanofillers as a dielectrically active filler agnostic of the route of incorporation. Therefore, the solution blending method is used in the nanocomposites' manufacture in order to achieve better dispersion of nanofillers in PP.

Before preparing nanocomposites, PP and four kinds of nanofillers including nano-MgO, nano-Al_2O_3, OvPOSS and OpPOSS were put into a vacuum oven and dried at 90 ℃ and 0.1 kPa for 24 hours. Then, xylene was used to dissolve the PP pellets and the required contents of different nanofillers are shown in Table 4.2.

Table 4.2 the required contents of different nanofillers for nanocomposites

Sample	MgO (phr)	Al_2O_3 (phr)	OvPOSS (phr)	OpPOSS (phr)
Pure PP	0	0	0	0
MgO/PP-0.5	0.5	0	0	0
MgO/PP-1.0	1.0	0	0	0
MgO/PP-2.0	2.0	0	0	0
MgO/PP-3.0	3.0	0	0	0
Al_2O_3/PP-0.5	0	0.5	0	0
Al_2O_3/PP-1.0	0	1.0	0	0
Al_2O_3/PP-2.0	0	2.0	0	0

Al_2O_3/PP-3.0	0	3.0	0	0
OvPOSS/PP-0.5	0	0	0.5	0
OvPOSS/PP-1.0	0	0	1.0	0
OvPOSS/PP-2.0	0	0	2.0	0
OpPOSS/PP-0.5	0	0	0	0.5
OpPOSS/PP-1.0	0	0	0	1.0
OpPOSS/PP-2.0	0	0	0	2.0
OpPOSS/PP-3.0	0	0	0	3.0

Finally, the manufacturing process of PP's nanocomposites through the solution blending method is described as below and shown in Figure 4.7.

The manufacturing process of nanocomposites:

i. 50 g PP pellets were dissolved by 400 ml xylene in the three-mouth flask under the temperature of 120℃ in 30 min.

ii. The mixing platform consists of the experimental stirrer, the three-mouth flask and the heating platform. The different contents of nanofillers shown in Table 4.2 were added into the mixture of PP and xylene.

iii. The mixed solution was stirred by the blender under the temperature of 120℃ and the rotor speed of 500 rpm for 12 h.

iv. The mixed solution was dried in a blast drying oven at 120 ℃ for 12 h to produce the powder of nanocomposites.

v. Film samples with different thickness were manufactured by using compression moulding at a temperature of 200℃ and the pressure of 15 MPa for a duration of 12 min.

vi. The film samples were cooled to room temperature under the pressure of 10 MPa for 15 min. The thicknesses of samples were nominally 100 and 200 μm.

vii. The samples were put into a vacuum oven (0.01 Pa) at 8800℃ for 24 h and cooled down to room temperature.

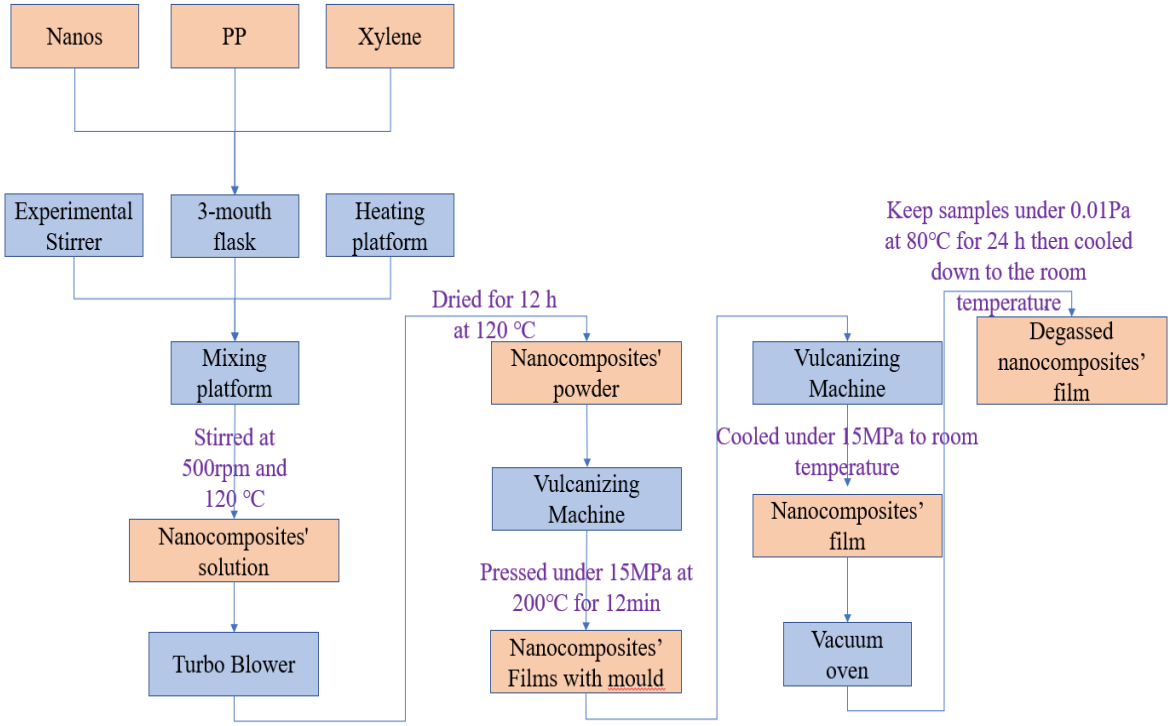

Figure 4.7 The manufacturing process of nanocomposites film

4.3 Physical characterization of samples

4.3.1 The observation of crystal spherulites of samples

To explain the effect of nano filler on the spherulite morphology of PP, the spherulite structure of PP and its nanocomposites was observed directly by polarizing microscope. The steps are as follows.

i. A 100 μm sample with an area of 3 mm × 3 mm was placed between two glass slides, and then placed on a hot table (Linkam).

ii. Raising the temperature to 200 °C at a heating rate of 50 °C/min and keeping the sample at 200℃ for 15 min to remove the thermal history

iii. The temperature was reduced to 130 °C at a cooling rate of 15 °C/min, so that the molten sample could be formed as single layer of crystal spherulites for observation.

iv. The samples were placed under a polarized optical microscope for observation. The observed results are shown in the following four figures.

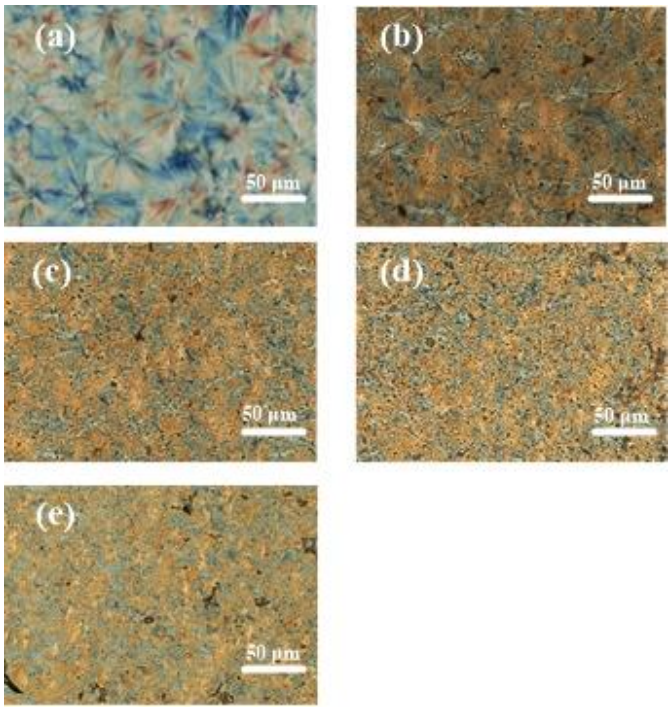

Figure 4.8 The POM Observation of PP and OvPOSS/PP nanocomposites samples. (a) PP, (b) 0.5 phr MgO/PP, (c) 1.0 phr MgO/PP, (d) 2.0 phr MgO/PP, (e) 3.0 phr MgO/PP

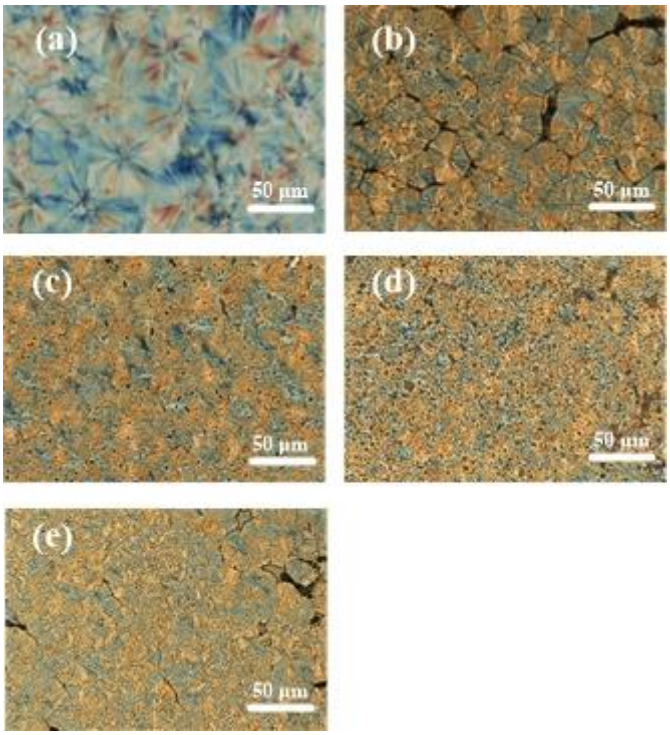

Figure 4.9 The POM Observation of PP and OvPOSS/PP nanocomposites samples. (a) PP, (b) 0.5 phr Al_2O_3/PP, (c) 1.0 phr Al_2O_3/PP, (d) 2.0 phr Al_2O_3/PP (e) 3.0 phr Al_2O_3/PP

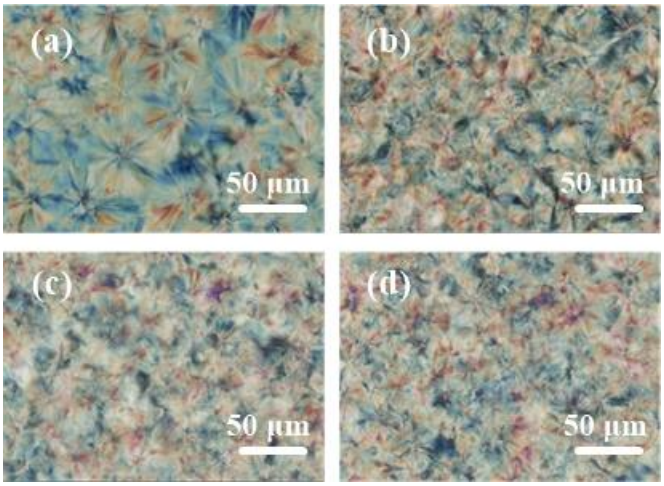

Figure 4.10 The POM Observation of PP and OvPOSS/PP nanocomposites samples. (a) PP, (b) 0.5 phr OvPOSS/PP, (c) 1.0 phr OvPOSS/PP, (d) 2.0 phr OvPOSS/PP

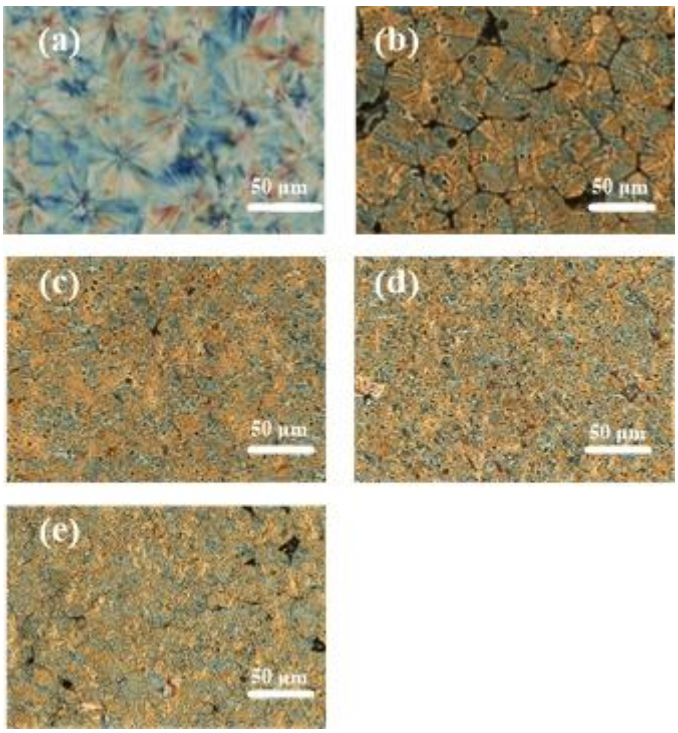

Figure 4.11 The POM Observation of PP and OpPOSS/PP nanocomposites samples. (a) PP, (b) 0.5 phr OpPOSS/PP, (c) 1.0 phr OpPOSS/PP, (d) 2.0 phr OpPOSS/PP, (e) 3.0 phr OpPOSS/PP

As shown in Figure 4.8-4.11, during the cooling process from melting to crystallization, the spherulite size of PP is about 100 μm. After adding nanofillers, the spherulite size of PP decreased obviously. With the increase of nanofillers content, the size of spherulites in PP is smaller, the number of spherulites is also increasing, and it is difficult to observe the boundary region between spherulites. The existing research results show that the electrical breakdown process of PP is more likely to occur at the boundary between spherulites and spherulites [45]. After the introduce of nanofillers, the increase of the number of spherulites shows that nanofiller could perform the role as heterogeneous nucleation in the crystallization process of PP, promote the crystallization process, and form irregular spherulites in nanocomposites. The resistance of the low-resistivity path is increased, and the length of the low resistance path is longer, making the breakdown process less likely to occur. Therefore, the

addition of nanofillers can induce the irregular crystallization in the nanocomposites of PP to reduce physical defects so that the electrical properties of PP could be further improved in some extents.

However, even though the improvement of crystallization behavior of PP has been improved, the agglomeration problem caused by the high content of nanofillers would degrade the electrical properties. This problem will be discussed in the next parts.

4.3.2 The observation by scanning electron microscope

The micro-morphology of the nanocomposites of PP and the dispersion of nanofillers were analyzed by FE-SEM. The sample was brittle broken in liquid nitrogen, and the brittle section was observed under electron microscope after the gold sputtering process under the vacuum condition. The electron acceleration voltage was 12.0 kV and the magnification of SEM is 10000. Because the dispersion of nanofillers in the nanocomposites of PP has a great impact on the improvement of electrical properties of PP, it is necessary to observe the dispersion state of nanofillers in PP.

Through the observation of SEM for the nanocomposites of PP, the dispersion of different nanofillers in PP is shown in the following 4 figures. For the addition of inorganic nanofillers in PP, including nano-MgO and nano- Al_2O_3, when the content of inorganic nanofillers increased to 3.0 phr, large agglomerates with the particle size of more than 300 nm appeared in both MgO/PP and Al_2O_3/PP nanocomposites. When the added content is less than 2.0 phr, the distribution of nanofillers is more dispersed and uniform, and there is no agglomeration of more than 300 microns. For the nanofillers of two kinds of POSS, the agglomerates of more than 300 nm appear in the nanocomposites when the content of OvPOSS and OpPOSS is 2.0 phr, and the dispersion of OvPOSS and OpPOSS nanofillers in PP is more uniform in the nanocomposites when the content is 1.0 phr or less. While under the comparison between OvPOSS and OpPOSS nanofillers, the OvPOSS nanofiller shows the better compatibility with the molecular chain of PP than that of OpPOSS.

Considering the volume content of nanofillers, compared with other nanofillers, OvPOSS has the smallest agglomerates in the nanocomposites of PP, followed by OpPOSS nanofiller, nano-MgO and nano-Al_2O_3, which indicates that POSS nanofillers have the better compatibility with the molecule of PP than nano-MgO and nano-Al_2O_3.

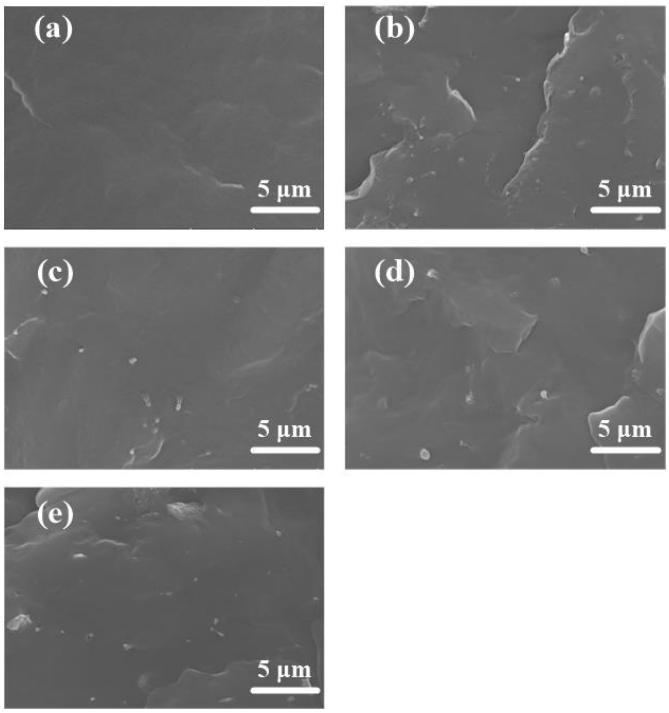

Figure 4.12 ×10000 SEM photograph of PP and MgO/PP nanocomposites sample. (a) PP, (b) 0.5 phr MgO/PP, (c) 1.0 phr MgO/PP, (d) 2.0 phr MgO/PP, (e) 3.0 phr MgO/PP

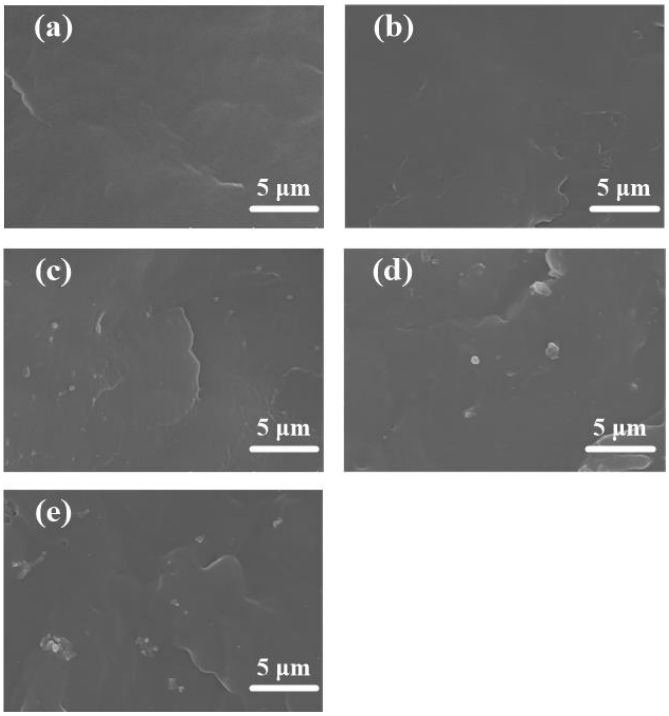

Figure 4.13 ×10000 SEM photograph of PP and Al_2O_3/PP nanocomposites sample. (a) PP, (b) 0.5 phr Al_2O_3/PP, (c) 1.0 phr Al_2O_3/PP, (d) 2.0 phr Al_2O_3/PP, (e) 3.0 phr Al_2O_3/PP

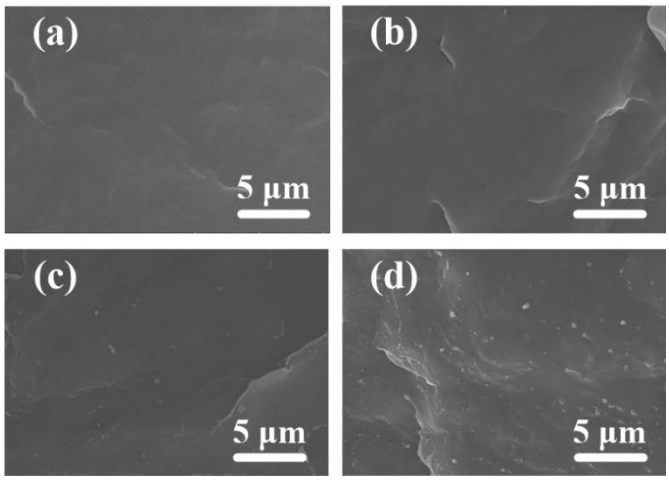

Figure 4.14 ×10000 SEM photograph of PP and OvPOSS/PP nanocomposites sample. (a) PP, (b) 0.5 phr OvPOSS/PP, (c) 1.0 phr OvPOSS/PP (d) 2.0 phr OvPOSS/PP

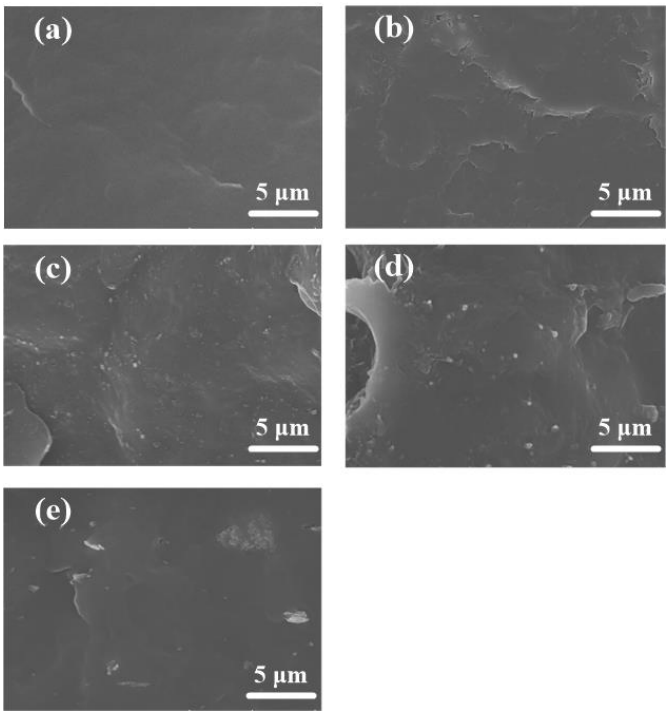

Figure 4.15 ×10000 SEM photograph of PP and OpPOSS/PP nanocomposites sample. (a) PP, (b) 0.5 phr OpPOSS/PP, (c) 1.0 phr OpPOSS/PP, (d) 2.0 phr OpPOSS/PP, (e) 3.0 phr OpPOSS/PP

4.3.3 The results of differential scanning calorimeter measurements

In this section, the crystallization behavior of PP and its nanocomposites was studied by DSC technique. This section will focus on the analysis of the effects of the addition of nano filler on the melting point (T_m), the melting enthalpy (ΔH), the crystallization temperature (T_c) and the crystallinity (X_C) of PP and its nanocomposites. There are 3 cycles for temperature control during the DSC measurement and the procedure of DSC measurement is mentioned as below:

i. Taking about 7 mg of PP or its nanocomposites and placing them in a container.

ii. Placing the sample in the DSC instrument, keeping it at 20 ℃ for 5 min.

iii. Raising the temperature to 200 ℃ with the heating rate of 5 ℃/min and maintaining it at 200 ° C for 5 min to remove the thermal history of the sample.

iv. Cooling down to 20 ℃ at the cooling rate of 5 ℃/min and recording the crystallization process of the sample.

v. Raise the temperature to 200 ℃ at the heating rate of 5 ℃/min and record the melting process of the sample.

The DSC melting curves and the crystallizing curves of PP and its nanocomposites are shown in the following figures. The crystallinity of samples could be calculated by the equation (2) which was mentioned in the Chapter 2. Table 4.3 has summarized the parameters of DSC measurement including the melting point, the melting enthalpy, the crystallization temperature and the crystallinity of PP and its nanocomposites.

For the crystallinity of PP's nanocomposites, it can be seen from the figures and the table below that the melting temperature of PP's nanocomposites with four nanofillers is basically maintained at about 165 ℃, and the crystallinity is between 36 % and 39 %. When the mass fraction of inorganic nanofillers is 2.0 phr or less, the crystallinities of MgO/PP and Al_2O_3/PP nanocomposites reach the highest to 37.9 % and 37.8 % respectively. When the mass fraction of inorganic nanofiller reaches 3%, the crystallinities decrease slightly to 37.6 % and 37.4 % compared with 2.0 phr nanocomposites for MgO/PP and Al_2O_3/PP nanocomposites. For the crystallization temperature of nanocomposites were kept stable around 116 ℃ under the introduction of those 4 kinds of nanofillers.

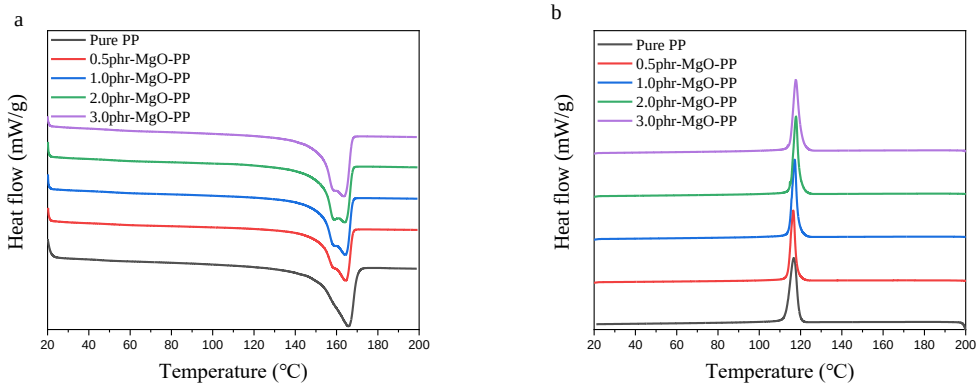

Figure 4.16 (a). DSC melting curves and (b). Crystallizing curves of MgO/PP nanocomposites with different contents.

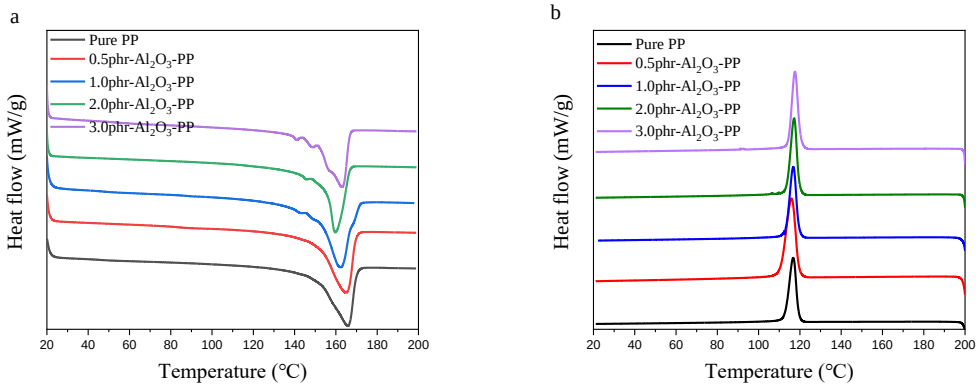

Figure 4.17 (a). DSC melting curves and (b). Crystallizing curves of Al_2O_3/PP nanocomposites with different contents.

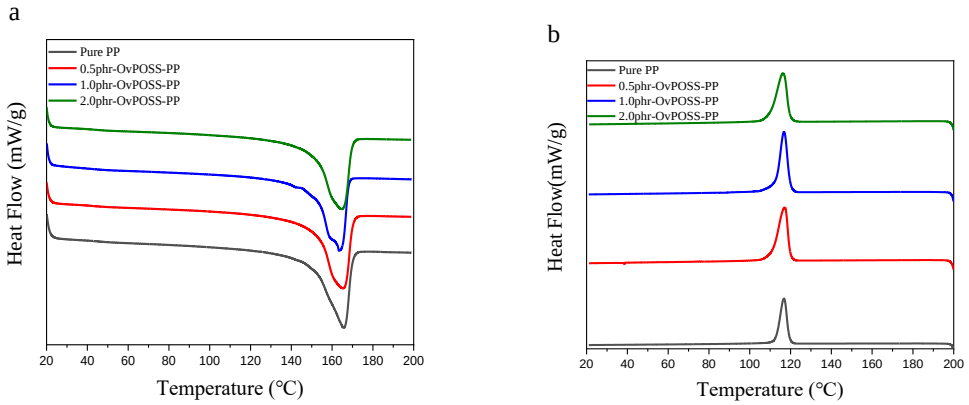

Figure 4.18 (a). DSC melting curves and (b). Crystallizing curves of OvPOSS/PP nanocomposites with different contents.

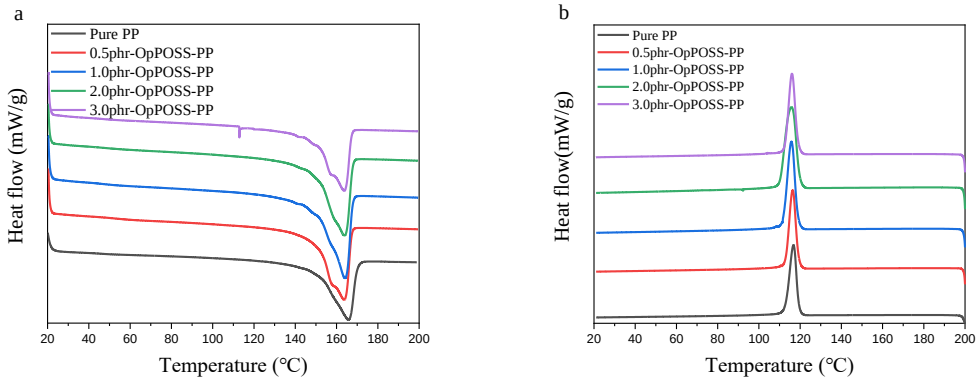

Figure 4.19 (a). DSC melting curves and (b). Crystallizing curves of OpPOSS/PP nanocomposites with different contents.

Table 4.3 Parameters from DSC measurement of PP's nanocomposites with different contents.

Samples	Melting point T_m(℃)	Melting enthalpy ΔH (J/g)	Crystallization temperature Tc (℃)	Crystallinity X_C (%)
Pure PP	165.8	75.8	116.8	36.3
MgO/PP-0.5	164.5	78.4	116.5	37.5
MgO/PP-1.0	164.5	79.6	117.1	38.1
MgO/PP-2.0	163.9	80.4	117.9	38.5
MgO/PP-3.0	163.8	80.3	117.7	38.4
Al_2O_3/PP-0.5	164.9	77.6	116.0	37.1
Al_2O_3/PP-1.0	162.2	78.2	116.8	37.4
Al_2O_3/PP-2.0	159.3	72.3	117.1	34.6
Al_2O_3/PP-3.0	162.9	70.5	117.5	33.7
OvPOSS/PP-0.5	164.3	80.6	117.0	38.6
OvPOSS/PP-1.0	163.4	81.0	116.8	38.8
OvPOSS/PP-2.0	164.7	81.0	116.3	38.7

OpPOSS/PP-0.5	163.5	80.7	116.2	38.6
OpPOSS/PP-1.0	164.4	81.1	115.6	38.8
OpPOSS/PP-2.0	163.7	81.4	115.6	38.9
OpPOSS/PP-3.0	163.1	76.1	115.9	36.4

Through the above analysis, it can be concluded that the crystallinity of PP could be increased by adding these four nanofillers. Combined with the observation results of polarizing microscope, it is more strongly explained that the four nanofillers play the role of heterogeneous nucleation in the crystallization process of PP. By reducing the size of spherulites, the arrangement of spherulites is much denser than pure PP, so as to increase the crystallinity of PP. Combined with the observation of SEM, when the content of nanofillers further increases, the large agglomerates of nanofillers will slightly reduce its heterogeneous nucleation effect during the crystallization procedure. Therefore, the crystallinity of nanocomposites with high content of nanofillers would be slightly lower than that of PP and nanocomposites with lower content of nanofillers. Additionally, there are some obvious ripples in Al_2O_3/PP nanocomposites with the content of 3.0 phr, which means that the phase separation between Al_2O_3 and PP occurred in the 3.0 phr Al_2O_3/PP nanocomposites. Finally, higher crystallinity means larger crystalline regions and smaller amorphous regions. As indicated in [45], electrical breakdown is more likely to occur in amorphous regions than in crystalline regions. Therefore, it is pointed that suitable content of nanofillers can increase the crystallinity of PP then the electrical performance of PP would be also improved.

4.3.4 The thermal stability of nanocomposites

In this section, TGA technique is used to analyze the thermal stability of nanofillers and nanocomposites, and the analyzing results are used to judge whether the materials

will degrade during the production of nanocomposites. All nanofillers and PP were selected for TGA measurement. The test temperature is from 30 to 800 ℃ with the increasing rate of 10 ℃/min. The TGA measurement was carried out in the atmosphere of nitrogen to prevent the nanofillers and nanocomposites from being degraded by the oxidation of oxygen.

In the research paper of our group, Zhou Y, et al. pointed that the weight loss of nano-MgO with and without the surface treatment by KH570 were reduced at the beginning of TGA measurements from 30 to 240 ℃ which is mainly related to the loss of water desorption and the weight loss of MgO-KH570 from 240 to 800 ℃ is mainly caused by the degradation of organic groups grafted on the surface of nano-MgO [81]. For the nano-Al_2O_3, the rate of weight loss is increased when the temperature reaches around 180℃, which means that the organic groups grafted on the surface of nano-Al_2O_3 starts to be degraded [82]. Therefore, the organic group from KH570 on the surface of nano-Al_2O_3 would be degraded during the manufacture of Al_2O_3/PP nanocomposites' film samples. For PP, OvPOSS and OpPOSS, the weight of them could be kept stable below the temperature of 200 ℃, which means that the OvPOSS/PP and OpPOSS/PP could be stable during the manufacturing process.

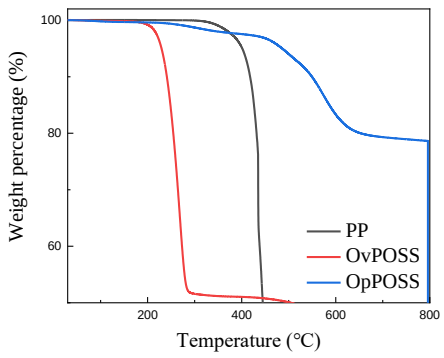

Figure 20. The results of TGA measurements for PP and OvPOSS, OpPOSS

4.3.5 The results of tensile strength tests

5 samples with the thickness between 200 and 240 μm were selected for the tensile strength test and figure 4.23 shows the stress tensile curve of PP and its nanocomposites at room temperature (30 ℃). Two sides of the dog-bone samples are stretched with a speed of 10 mm/min during the tests. and all samples show elastic deformation before sharp yield point. When the stress modulus reaches the tensile modulus of the sample, the sample begins to undergo plastic deformation. At this time, the stress on the material surface turns white, and breaking point will occur after the large deformation. When the sample is broken, the tensile length at breaking point divided by the original length of the sample is the maximum breaking elongation of the sample. Table 4.4 summarizes the mechanical parameters of PP and its nanocomposites. It can be seen that the tensile strength and the breaking elongation of nanocomposites decrease with the increase of nanofillers' content. This is because nanofillers with high content are easy to agglomerate, resulting in stress defects and reducing the tensile strength and elongation at break of the samples. Because the OvPOSS and OpPOSS nanofillers have a small particle size and better compatibility with the matrix, the decline of mechanical properties of OvPOSS/PP and OpPOSS/PP nanocomposites is lower than that of MgO/PP and Al_2O_3/PP.

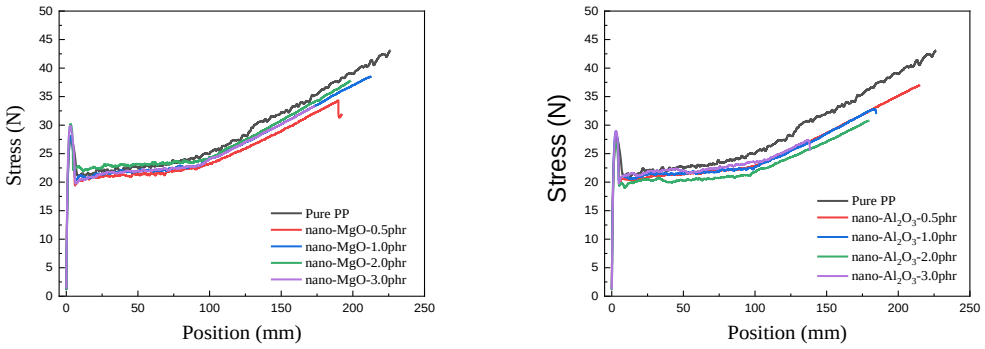

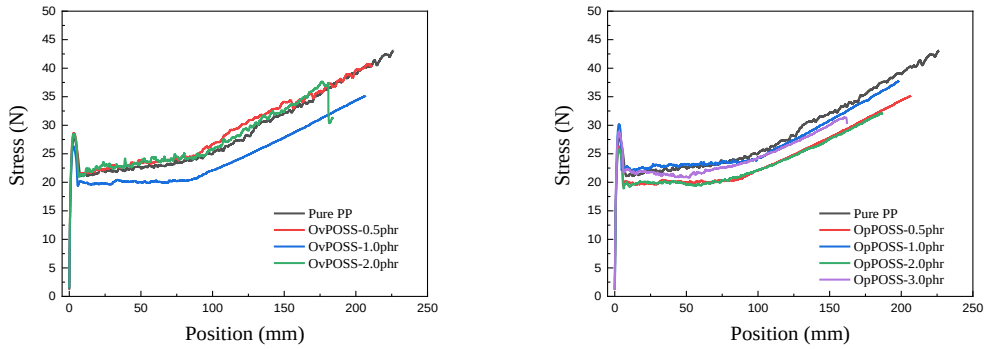

Figure 4.21 Tensile strength test curve of MgO/PP, Al_2O_3/PP, nano-OvPOSS/PP and nano-OpPOSS/PP nanocomposites

Table 4.4 The mechanical parameter of PP and it's nanocomposites

Samples	Tensile strength (MPa)	Breaking elongation (%)
Pure PP	46.2±2.0	1256.2±103.1
MgO/PP-0.5	39.3±1.9	1068.3±98.7
MgO/PP-1.0	45.0±1.6	1181.3±84.6
MgO/PP-2.0	43.5±1.7	1102.5±86.4
MgO/PP-3.0	36.8±1.2	961.8±75.8
Al_2O_3/PP-0.5	45.1±2.1	1194.1±108.1
Al_2O_3/PP-1.0	39.5±1.8	1025.4±104.1
Al_2O_3/PP-2.0	39.5±1.7	997.5±93.1
Al_2O_3/PP-3.0	35.9±0.9	768.4±63.1
OvPOSS/PP-0.5	46.4±2.4	1174.6±114.6
OvPOSS/PP-1.0	43.9±2.0	1148.9±95.9
OvPOSS/PP-2.0	37.2±2.1	1021.7±91.6
OpPOSS/PP-0.5	43.3±1.8	1207±87.3
OpPOSS/PP-1.0	43.5±1.8	1102.5±92.1
OpPOSS/PP-2.0	42.3±1.9	1039.0±93.5
OpPOSS/PP-3.0	36.5±1.2	900.7±53.9

4.4 Conclusion

This chapter has introduced how to prepare PP's nanocomposite insulation materials with four kinds of nanofillers including nano-MgO, nano-Al_2O_3, OvPOSS and OpPOSS. The effects of different kinds of nanofillers on the micro morphology, crystal morphology, crystal behavior, thermal stability and mechanical properties of PP's nanocomposite insulation materials at different contents were summarized, and the ways of how nanofillers affect the electrical properties of PP in terms of microstructure were obtained. The specific summary is as follows:

i. By solution method, magnesium oxide and alumina can be uniformly dispersed in PP at a mass fraction of 2.0 phr, and OvPOSS and OpPOSS can be uniformly dispersed at a mass fraction of 1.0 phr. When the content of the above nano fillers continues to increase, there will be more than 300 nm aggregates of nanofillers in the nanocomposites, which will slightly reduce the heterogeneous nucleation effect of the nanofillers on PP.

ii. Under the uniform dispersion of nanofillers, the crystallinity of nanocomposites would be higher than that of pure PP. In the crystallization process of PP, nanofillers could reduce the spherulite size of PP, increase the number of crystal spherulites, form irregular spherulites, and make the boundary between spherulites more difficult to be observed under the polarized optical microscope. This phenomena indicated that the low resistance path of PP is extended with the reduction of spherulites and the resistivity of the low resistance path would be also increased with the reduction of the boundary region between spherulites. Finally, the electrical properties of PP were also improved with the introduction of nanofillers.

iii. In terms of thermal stability of nanofillers and nanocomposites, the results of TGA showed that those nanofillers will not degrade below the temperature of

200 ℃, and those nanofillers will not degrade and not accelerate the degradation of the matrix material in the preparation of PP's nanocomposites.

iv. In terms of mechanical properties of PP's nanocomposites, with the increase of nanofillers content, the tensile strength and the breaking elongation of nanocomposites would be decreased. Due to agglomerates of nanofillers, the stress defects would be introduced into the nanocomposites, which would reduce the tensile strength and the breaking elongation of the samples. Compared with the OvPOSS and OpPOSS/PP nanocomposites, the breaking elongation of the MgO/PP and Al_2O_3/PP nanocomposites would be more decreased. The reason is that the size of the aggregates of nano-MgO and nano-Al_2O_3 is large, which makes the nanocomposites bear non-uniform stress when stretched on both sides. Therefore, local cracking reduces the elongation at break of the nanocomposites.

5. Electrical properties of polypropylene's nanocomposites under the room temperature

5.1 Materials

Although PP has better electrical properties than XLPE and LDPE, especially under high operational temperatures. In order to improve the electrical properties of PP to a greater extent, it is necessary to solve the problems of space charge accumulation in PP. Nanocomposite dielectrics have become an effective method to improve the electrical properties of polymeric insulating materials. As described in Chapter 2, many literatures and reports show that the addition of nanofillers can improve DC electrical properties including DC breakdown strength, DC conductivity, space charge characteristics etc., in a variety of polymer systems, especially for MgO and Al_2O_3. Compared with inorganic nanofillers, POSS has the characteristics of both inorganic nanofillers and functional groups because of its special structure. In the aspect of PP's nanocomposites, the comparison between POSS and inorganic nanofillers and the improvement of electrical properties of PP by POSS are still worthy of research. Compared with traditional inorganic nano fillers, the research on POSS/PP nanocomposites can also provide better ideas for the design of a new generation of polymeric DC cable insulation materials in the future.

In this chapter, the electrical properties of PP and its nanocomposites containing four different nanofillers prepared by solution method, including nano-MgO, nano-Al_2O_3, OvPOSS and OpPOSS would be measured under the room temperature. The regulation and influence of the type and content of nanofillers on the electrical properties of PP at room temperature would be analysed, and the macro electrical properties and micro morphology characteristics would be further studied. Then, the effects of different kinds and different contents of nano fillers on the improvement of electrical properties of PP are compared, including dielectric properties, DC volume conductivity, space charge characteristics and DC breakdown strength.

Combined with the results of the micromorphology analysis in the chapter 4 and thermal stimulation current measurement in this chapter, the improvement of electrical properties of PP nanocomposites is explained. Then, considering the electrical performance parameters of nanocomposites at 30 ℃, the types and contents of nanofillers will be optimized. Then, the microstructures of OvPOSS and OpPOSS were built and the electrostatic potential was calculated by using GaussianView09 according to DFT . After that, the DOS in OvPOSS and OpPOSS was used to get the further analysis of the electrical performance test of optimized PP's nanocomposites at different temperatures.

5.2 The dielectric properties

The dielectric properties of PP and its nanocomposites were measured at room temperature by broadband dielectric spectrometer. The thickness of the sample is controlled between 100 and 120 μm, and the upper and lower surfaces of the sample is sputtered with a gold layer with a diameter of 2.0 cm to ensure good contact between the two electrodes and the sample. The electric field in the test is 10 V/mm and the test frequency range is 0.1 Hz to 10 MHz.

The dielectric spectra of the four nanocomposites under the wide range of frequency are shown in Figure 5.1. Because PP is a non-polar polymer, electrons cannot move freely in the bulk of PP, the polarization time of PP is very short, and the polarization process is determined by the electron displacement of each atom in the molecule of PP. Therefore, the dielectric properties of PP will be stable under the AC conditions with different frequency.

For the nanocomposites of MgO/PP and Al_2O_3/PP, their relative permittivity basically remains between 2.4 and 2.55 in all frequencies. Compared with OvPOSS/PP and OpPOSS/PP nanocomposites, the more increase of the relative permittivity of the nanocomposites may be the polarization effect caused by the high

relative permittivity of nano-MgO and nano-Al_2O_3, which promotes the interfacial polarization between the inorganic nanofillers and PP. For the nanocomposites of OvPOSS/PP and Al_2O_3/PP, the relative permittivity of OvPOSS/PP and OpPOSS/PP are around 2.43 and 2.48 respectively, which are slightly higher than that of PP. The increasing dielectric constant of nanocomposites might be caused by the interface between POSS and PP, which means that OpPOSS can also introduce the interfacial effect into PP with a suitable content.

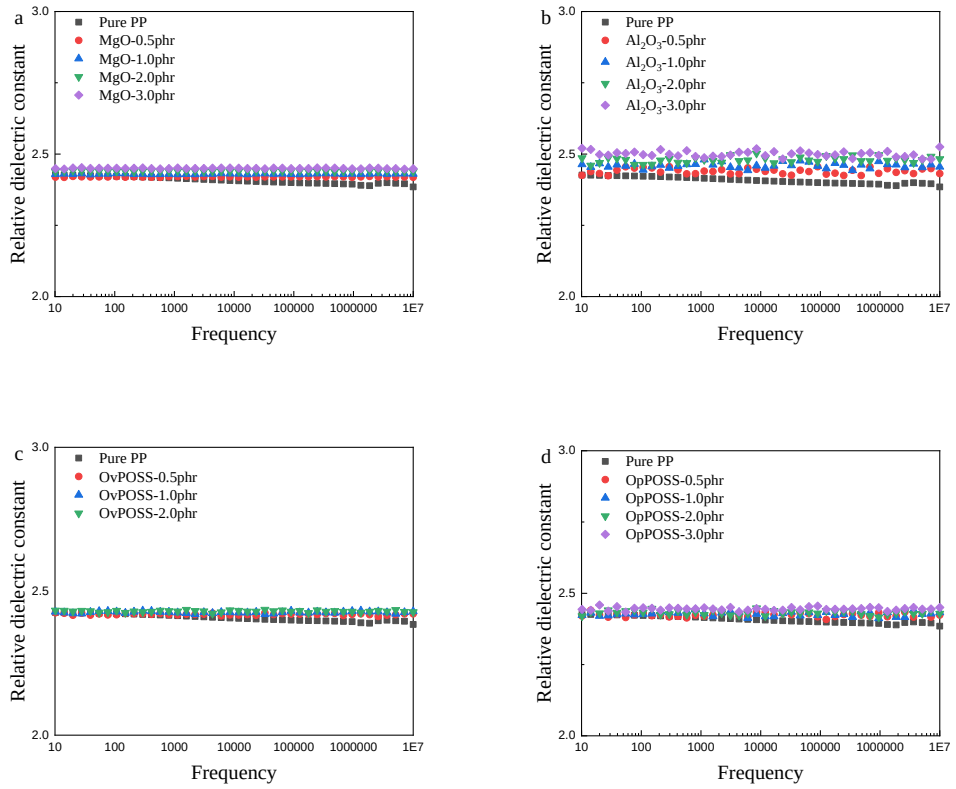

Figure 5.1 The dielectrics spectrums of MgO/PP, Al_2O_3/PP, OvPOSS/PP and OpPOSS/PP nanocomposites

5.3 The results of thermal stimulated depolarized current measurements

In order to detect the effect of the addition of nanocomposites on the trapping characteristics of PP, the trapping characteristics of PP and its nanocomposites were characterized by TSDC measurements. The TSDC test process is described as below:

i. Samples with a thickness of 100 μm were selected for TSDC measurement. A gold electrode with a diameter of 2.0 cm was sprayed on the upper and lower surfaces of the sample.

ii. The samples were short-circuited at 60 ℃ for 4.0 hours to remove the residual charge in the sample in the oven.

iii. At 20 ° C, the samples were polarized for 40 minutes under a DC electric field of 6 kV/mm to inject charge into the samples.

iv. The temperature of the samples was rapidly reduced to -100 ℃ with a coolling rate of 10 ℃/min then the samples were short-circuited for 5 min to remove the surface charge of the sample.

v. The temperature of the samples was raised from - 100 ℃ to 130 ℃ at a heating rate of 5 ℃/min, and the galvanometer measured the thermally stimulated depolarized current caused by the de-trapping process of captured charges during the heating process

5 samples from each group were selected for space charge test and only one typical result from each group of samples was selected as the basis for data analysis.

The TSDC curves of PP and its nanocomposites have been given in Figure 5.2. In PP and its nanocomposites, the TSDC curves have a thermal stimulation current peak at -5 ℃, which is due to the transition point of PP from glass state to high elastic state at glass temperature. The TSDC curve of PP shows a peak of thermally stimulated current

at 64 ℃, but the peak value is smaller than the corresponding peaks in the nanocomposites due to the low density of deep traps. In the TSDC curve of MgO/PP nanocomposites, the thermal stimulation current peak of 1.07 pA is located at 86 ℃ and the peak is much higher than PP, indicating that the trap depth and density of deep traps in MgO/PP nanocomposites are much higher than PP. The TSDC curve of Al_2O_3/PP nanocomposites shows a thermally stimulated current peak of 0.75 pA around 52 ℃, which is also higher than PP but lower than MgO/PP nanocomposites, indicating that the addition of nano-Al_2O_3 can also introduce a certain degree of deep traps, but the trapping level of Al_2O_3/PP nanocomposites is lower than MgO/PP nanocomposites. Compared with those inorganic nanofillers, the TSDC curves of OvPOSS/PP nanocomposites show a thermally stimulated depolarized current peak of 1.26 pA at 96 ℃, while the TSDC curves of OpPOSS/PP nanocomposites show a thermally stimulated depolarized current peak of 1.79 pA and 0.95 pA at 98 ℃ and 128 ℃ respectively. This indicated that POSS can introduce most deep traps with the high density into PP, especially for the addition of OpPOSS nanofillers.

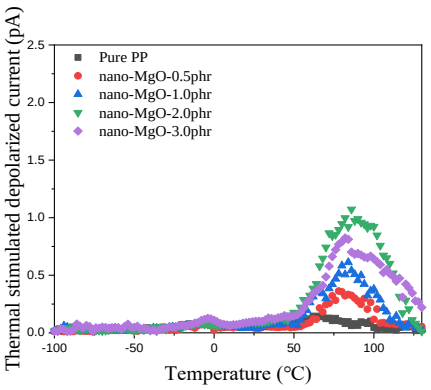

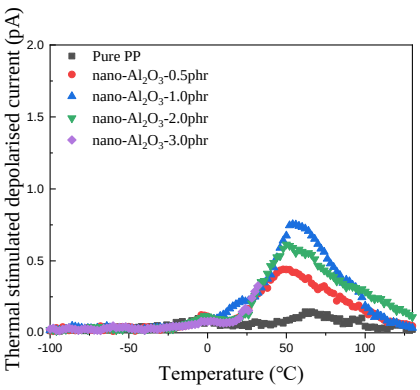

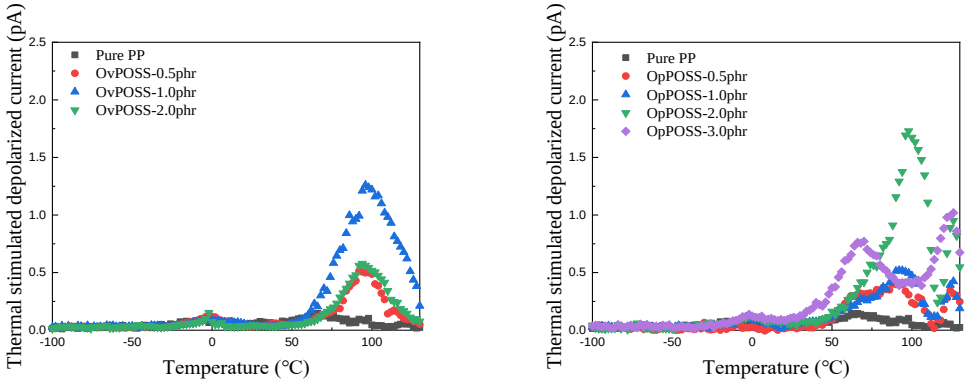

Figure 5.2 The thermal stimulated depolarized current in MgO/PP, Al_2O_3/PP, OvPOSS/PP and OpPOSS/PP nanocomposites

5.4 The conductivity tests

The DC conductivity of PP and its nanocomposites was measured by three electrode method and the experimental design is shown in Figure 3.12. The procedure of DC conductivity measurement has been listed below [81]:

i. Before the sample measurement, each sample was short-circuited for 10 min to remove the surface charge of samples and the temperature of the oven was adjusted to 30℃.

ii. 5 samples with the thickness between 100 and 125 μm were sputtered by the gold to make sure the better contact between electrodes and samples. The diameter of these area sputtered by gold is 2.0 cm

iii. Then, these samples were tested under the range of DC electric field from 5.0 kV/mm to 80 kV/mm with a step of 5.0 kV/mm.

iv. The duration of each step was set to 600 s.

v. Finally, the DC conductive current would be determined by the stable value after 180 s in the duration of each step.

5 samples from each group were selected for space charge test and only one typical result from each group of samples was selected as the basis for data analysis.

The DC conductive current under different electric field was determined by more stable value and the error was controlled within 0.5 pA in each polarized step. Because the conductivities of PP and its nanocomposites is stable, the difference between the conductivity result in the same group is small and then it can be ignored. Therefore, only one result in each group is used to explain the results of conductivity tests. Figure 5.3 show the DC conductive current of PP and its nanocomposites under the DC voltage level from 5 to 80 kV/mm. In the result of DC conductive current measurement, PP has the highest DC conductivity current. All nanofillers could inhibit the increase of DC conductive current of PP under the increase of electric field, which means that the volume resistivity of PP could be increased by the addition of nanofillers. The DC volume resistivity of PP and its nanocomposites under 80 kV/mm have been calculated in Figure 5.3. When the electric field is 80 kV/mm, 1.0 phr OvPOSS and 2.0 phr OpPOSS can improve the volume resistivity of PP to the highest value of 3.47×10^{15} Ω·m and 5.61×10^{15} Ω·m respectively. While for inorganic nanofillers including nano-MgO and nano-Al_2O_3, 2.0 phr nano-MgO and 1.0 phr nano-Al_2O_3 can increase the resistivity of PP to 4.02×10^{15} Ω·m and 2.31×10^{15} Ω·m respectively. Overall, POSS has a better performance in improving the bulk resistivity of PP than inorganic nanofillers.

Each group of nanofillers has the most appropriate content to improve the volume resistivity of PP. With the increase of nanofillers' content, the volume resistivity of nanocomposites will be increased and then decreased. From the observation of SEM, large agglomerates of nanofillers under high contents could limit the increase of PP resistivity by the nanocomposites techniques.

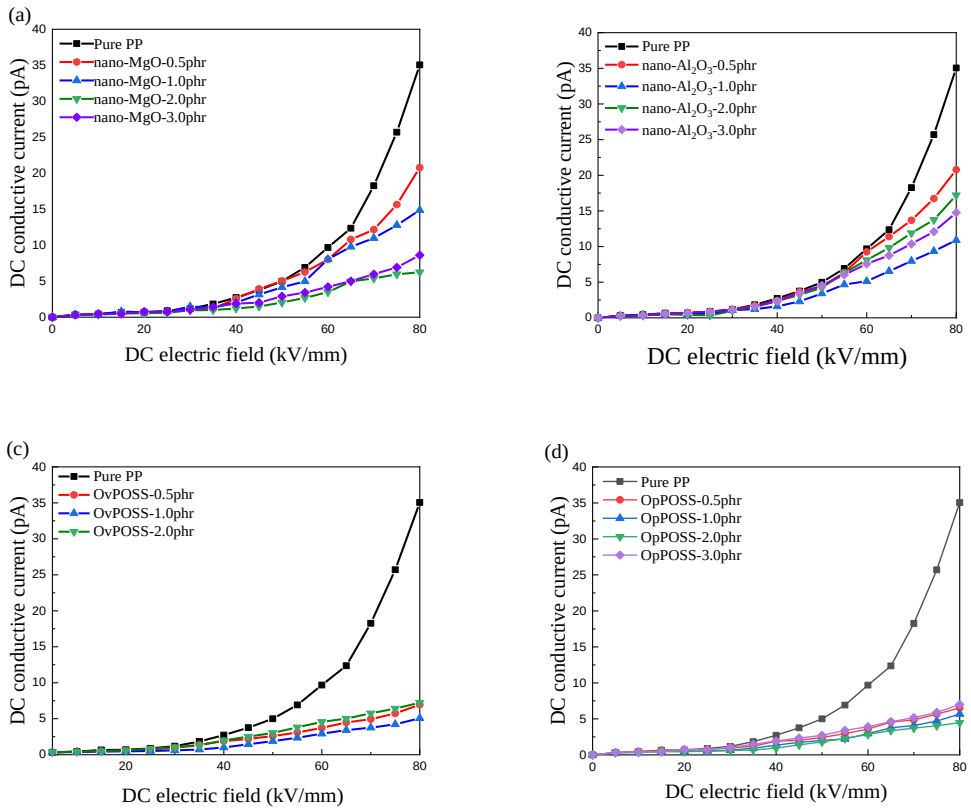

Figure 5.3 DC leakage current for PP and its nanocomposites under DC electric field from 0 to 80 kV/mm at 30℃.

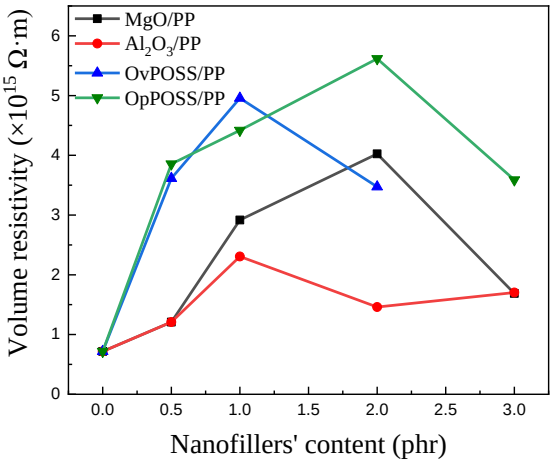

Figure 5.4 DC volume resistivity of PP and its nanocomposites under the DC electric field of 80 kV/mm

Combined with the measurement results of thermal stimulated depolarized current and SEM observation, the relatively uniform distribution of nanofillers could improve the trapping characteristics of PP by introducing a large number of deep traps due to the interfacial effect [82]. Under the applied DC electric field, the mobile charges would be captured by those deep traps in the nanocomposites then form the potential barriers. This phenomena further inhibits the injection of homocharges from the electrodes, and then improves the volume resistivity of PP. However, with the increasing content of nanofillers, the agglomeration problem will inevitably occur. The agglomeration of nanofillers would not only reduce the interface area, but also introduce some shallow traps, which would reduce the improvement of the resistivity of PP by the nanofillers addition.

5.5 The DC breakdown strength tests

The DC breakdown strength of PP and its nanocomposites is measured by the experimental design shown in Fig. 3.13. The procedure of DC breakdown strength measurement has been listed below:

i. Taking 5 samples with a thickness between 100 and 130 μm and an area 16 cm×16 cm, marking 20 points on the sample and measuring the thickness of each point.

ii. Heating the silicone oil through the heating plate, adjusting the temperature to 30 ℃, and waiting until the silicone oil temperature was stable.

iii. Immersing the sample in silicone oil to avoid the flashover occurring in the DC breakdown test and placing it between two spheres-electrodes.

iv. Adjusting the rising rate of DC voltage to 1.0 kV/s and start the DC breakdown test.

v. Finally, recording the breakdown voltage for every point after the DC breakdown of the sample and calculating the breakdown strength by dividing the breakdown voltage by the thickness.

For the analysis of result, only one reliable data set was selected to analyse the breakdown strength of each sample and those data can be reproduced by other researchers.

The DC breakdown strength of PP and its nanocomposites could be described by the Weibull distribution which can be used to analyse the breakdown strength data of polymer insulation materials . The equation of the Weibull distribution was given below [118]:

$$P = 1 - \exp[-(\frac{E}{E_0})^{\beta}] \_ \_ \_ \_ (4)$$

Where P is the DC breakdown probability for the Weibull distribution, E is the measured value of breakdown strength, E_0 is the critical value of DC breakdown strength at 63.2 % cumulative probability of DC breakdown at which log(-ln(1-P)) = 0 and β is the shape factor of Weibull distribution which indicates the distribution of the experimental data points of DC breakdown strength. The critical value of DC breakdown strength is a key parameter to evaluate the DC breakdown characteristics. The characteristics Weibull breakdown strength of PP and its nanocomposites is shown in Figure 5.5 and the critical values of breakdown strength, and the shape factors are listed in Table 3.

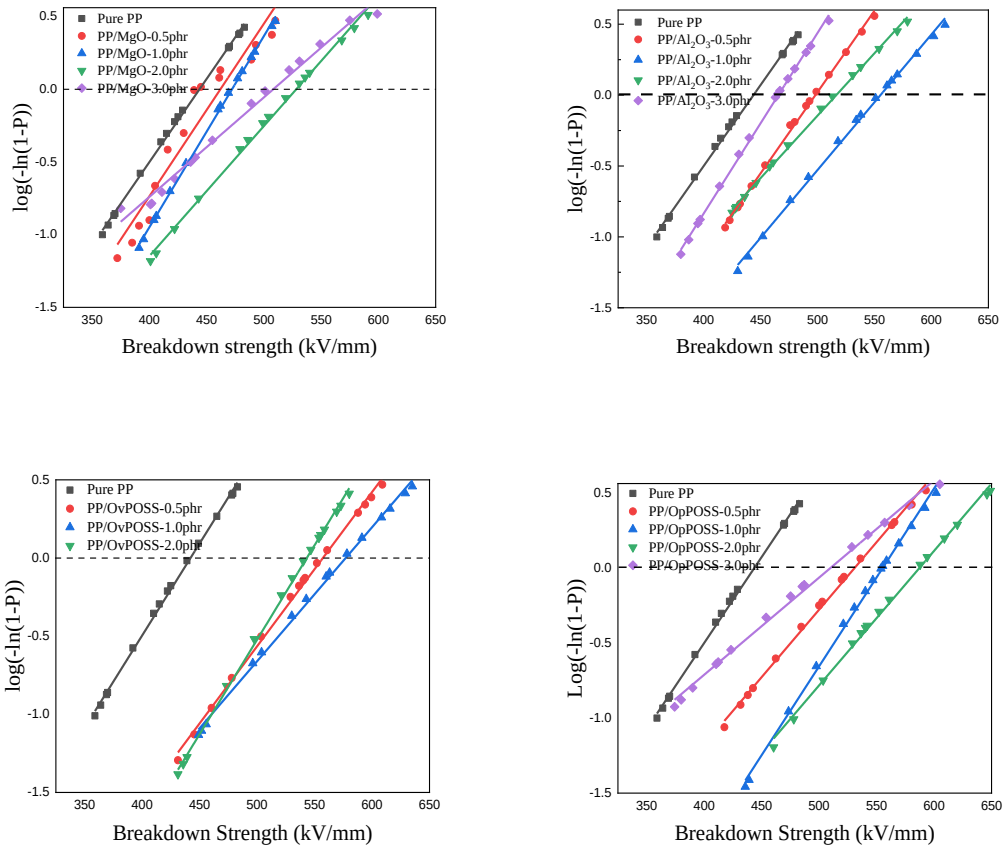

Figure 5.5 The DC breakdown strength of PP and its nanocomposites in the Weibull distribution

Table 5.1 The parameters of DC breakdown strength of PP and its nanocomposites

Samples	Critical value E_0 (kV/mm)	Shaping factor β	Improvement (%)
Pure PP	440.1	11.1	0
MgO/PP-0.5	474.8	11.6	8.0
MgO/PP-1.0	491.1	14.1	11.6
MgO/PP-2.0	560.5	10.8	27.5
MgO/PP-3.0	522.4	8.4	18.9

Al_2O_3/PP-0.5	497.3	12.6	13.0
Al_2O_3/PP-1.0	553.4	11.3	25.7
Al_2O_3/PP-2.0	513.8	10.0	16.8
Al_2O_3/PP-3.0	464.2	12.9	5.5
OvPOSS/PP-0.5	554.9	11.8	26.3
OvPOSS/PP-1.0	574.7	10.6	30.6
OvPOSS/PP-2.0	542.2	13.9	23.2
OpPOSS/PP-0.5	527.6	9.3	20.0
OpPOSS/PP-1.0	554.4	13.9	25.9
OpPOSS/PP-2.0	585.9	11.1	33.2
OpPOSS/PP-3.0	505.1	7.1	14.8

As shown in the figure and table, all four nanofillers can be used to improve the DC breakdown strength of PP. OvPOSS and OpPOSS could increase the DC breakdown strength of PP from 440.1 kV/mm to 574.7 kV/mm and 585.9 kV/mm respectively, while nano-MgO and nano-Al_2O_3 can increase the DC breakdown strength of PP to 560.5 kV/mm and 553.4 kV/mm respectively. Compared with pure PP, the breakdown strength of OvPOSS/PP, OpPOSS/PP, MgO/PP and Al_2O_3/PP nanocomposites were increased by 30.1 %, 37.5 %, 27.5 % and 25.7 % respectively.

The improvement of the breakdown performance of PP's nanocomposites can be explained in the following aspects. First, from the test results of thermally stimulated depolarization current, the significant improvement of breakdown strength of four nanocomposites of PP is related to the improvement of charge trap caused by the addition of four nanofillers. By introducing many deep traps, the nanofillers captures the injected space charges to forming a potential barrier, which would inhibits the

injection of homocharges from the electrodes and reduce the generation of hot electrons. Finally, the electric field distortion caused by the space charge accumulation would be suppressed in PP's nanocomposites, so as to improve the DC breakdown strength of PP. Secondly, in terms of the spherulite structure of PP, the addition of nanofillers greatly reduces the boundary area between spherulites and increases the length of conductive path, further reducing the defects between spherulites in PP. Finally, in terms of crystallinity, the addition of nanofillers also increases the crystallinity of PP and makes the arrangement of spherulites denser, which greatly improves the DC breakdown strength of PP.

However, it can be seen from the results of SEM in Figure 4.12-4.15 that with the increasing content of nanofillers, nanofillers will agglomerate in PP's nanocomposites. The agglomeration of large size nanofillers not only reduces the interface effect between nanofillers and PP, but also introduces physical defects into the matrix. Because the size of agglomeration is random, defects are also randomly distributed in matrix material PP. Compared with magnesium oxide and alumina, due to the low density of POSS itself (about one-third of nano-MgO), higher volume of POSS will be introduced under the same mass fraction with nano-MgO and nano-Al_2O_3, which means more agglomeration. Therefore, at the same high mass fraction, the dispersion of DC breakdown strength of POSS/PP nanocomposites is larger, that is, the shaping factor of the breakdown strength data is higher than MgO/PP and Al_2O_3/PP nanocomposites.

In sum, by comparing the improvement of DC breakdown strength of PP by the addition of four nanofillers, it can be found that OvPOSS and OpPOSS could achieve the higher improvement of DC breakdown strength of PP than nano-MgO and nano-Al_2O_3.

5.6 The space charge characteristics

5.6.1 The space charge measurement and the electric field distortion

The space charge characteristics of PP and its nanocomposites are carried out by the pulse electro-acoustic (PEA) system as shown in Figure 3.14. In the space charge measurement, the thickness of film samples was controlled between 220 to 250 μm. The film should be short-circuited before the space charge measurement to avoid the influence of the surface charge on the detection of space charge. Due to the good space charge characteristics of PP, it is difficult to measure the space charge accumulation in the bulk of film samples under the electric field level of DC cable operation in the HVDC system. Therefore, the DC electric strength of 60 kV/mm is selected to detect the space charge of thin film samples at room temperature. Then, the steps of space charge measurements for PP and its nanocomposites are set as follows:

i. The contact surface between the sample and the electrode was covered with an appropriate amount of silicone oil to eliminate the air gap between the electrode and the sample.

ii. The upper surface of the sample was closely contacted with the upper electrode through a semi-conductive layer, and the lower surface of the sample was directly contacted with the lower electrode. The upper electrode was connected to the high-voltage DC power source, and the lower electrode was grounded.

iii. The temperature of PEA system was set to 30 ℃.

iv. The DC electric field of the sample was set to 60 kV/mm and the high-voltage pulse source was turned on. The pulse width of the high-voltage pulse source was set to 6 ns, the frequency was set to 800 Hz, and the pulse voltage amplitude was set to 800 V. Warming-up the PEA system and waiting for its stable operation of the PEA system.

v. After the PEA system works stably, start the collection of PEA signal during sample polarization, and the polarization process is 40 minutes. The DC electric field of the sample was set to 60 kV/mm and the space charge measurement was started. In the space charge measurement, the sampling frequency of the oscilloscope is adjusted to 5000 Hz, so that the oscilloscope can average 5000 waveforms within 1.0 second to reduce the error from the white noise, in order to accurately detect the dynamic space charge movement process under the high DC electric field.

vi. After the polarization process was completed, the depolarization process of the sample is started, and the space charge dissipation characteristics of the depolarization process are detected. The duration of depolarization of samples was 20 min.

5 samples from each group were used for space charge test, and only one result from each group of samples was selected as the basis for data analysis.

According to the distribution of space charge in the bulk of film sample, the electric field in the sample at the position of x could be calculated by the following equation.

$$E(x) = \frac{1}{\varepsilon_r \varepsilon_0} \int_0^d \rho(x) dx \quad ---------(3)$$

and the electric field distortion could be obtained through the formula below:

$$\Delta E = \left| \frac{E_{max} - E_{av}}{E_{av}} \right| \times 100\% \quad ------(4)$$

where: in terms of local electric field, $\rho(x)$ is the charge density distribution, $\varepsilon_r \varepsilon_0$ is the dielectric constant of the sample, $E(x)$ is the local electric field in the thickness of x and d is the thickness of the film samples. In the electric field distortion, E_{max} is the maximum value of the electric field and E_{av} is the average value of the electric field within the sample, equal to the applied electric field.

The space charge formation and electric field distribution of PP and its nanocomposites at 30 ℃ is shown in Figure 5.6 -5.9. It can be seen from the figure that in pure PP, there is an obvious homocharges injection near the cathode from the time of 400 seconds. With the increase of polarization time, the homocharges injected from the cathode is increasing, and the injection depth is also increased. In this process, there is no obvious homocharges injection from the anode, but the peak of positive charges accumulated at the anode is slightly higher due to the inductive effect by the injection of negative charges from the cathode. Therefore, with the increase of injected charges at the cathode and the increase of injection depth, the charge peak at the cathode gradually decreases and the positive charge peak at the anode increases. With the increase of polarization time, the injection of homocharges from the cathode, not only weakens the electric field near the cathode, but also leads to the increase of local electric fields near the anode, resulting in obvious electric field distortion in pure PP. In 2000 seconds, the maximum electric field in pure PP has reached 68.2 kV/mm, and the electric field distortion reaches 13.7 %. Space charge injection will lead to the distortion of local electric fields. Therefore, the breakdown strength will be reduced due to the distortion of the electric field caused by space charge accumulation under DC conditions.

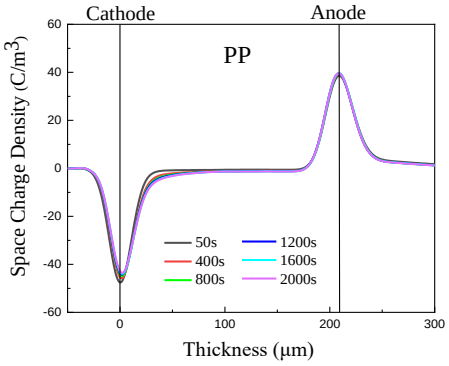
Cathode
Anode
PP
Space Charge Density (C/m3)
Thickness (μm)
50s
400s
800s
1200s
1600s
2000s

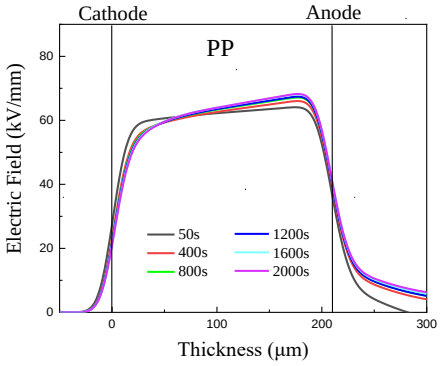
Cathode
Anode
PP
Electric Field (kV/mm)
Thickness (μm)
50s
400s
800s
1200s
1600s
2000s

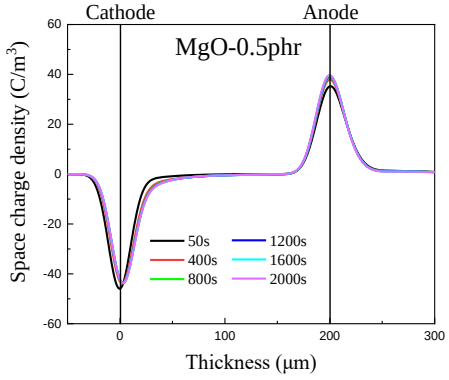
Cathode
Anode
MgO-0.5phr
Space charge density (C/m3)
Thickness (μm)
50s
400s
800s
1200s
1600s
2000s

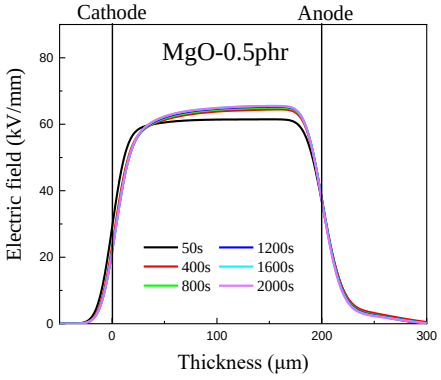
Cathode
Anode
MgO-0.5phr
Electric field (kV/mm)
Thickness (μm)
50s
400s
800s
1200s
1600s
2000s

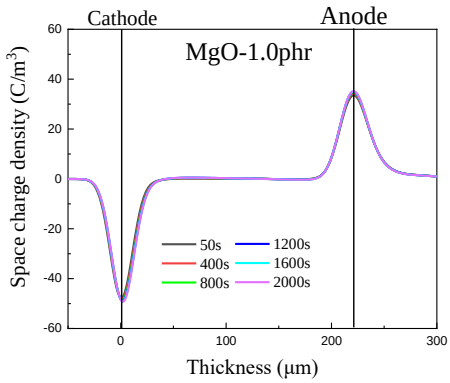
Cathode
Anode
MgO-1.0phr
Space charge density (C/m3)
Thickness (μm)
50s
400s
800s
1200s
1600s
2000s

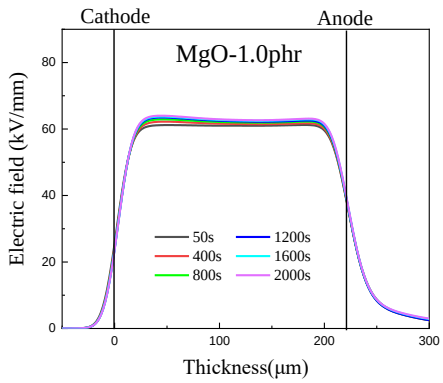
Cathode
Anode
MgO-1.0phr
Electric field (kV/mm)
Thickness(μm)
50s
400s
800s
1200s
1600s
2000s

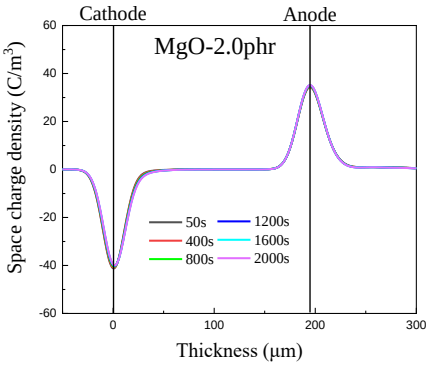
Cathode
Anode
MgO-2.0phr
Space charge density (C/m3)
Thickness (μm)
50s
400s
800s
1200s
1600s
2000s

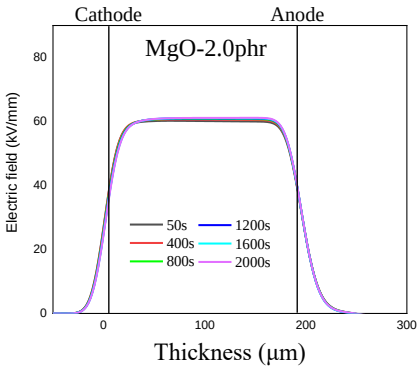
Cathode
Anode
MgO-2.0phr
Electric field (kV/mm)
Thickness (μm)
50s
400s
800s
1200s
1600s
2000s

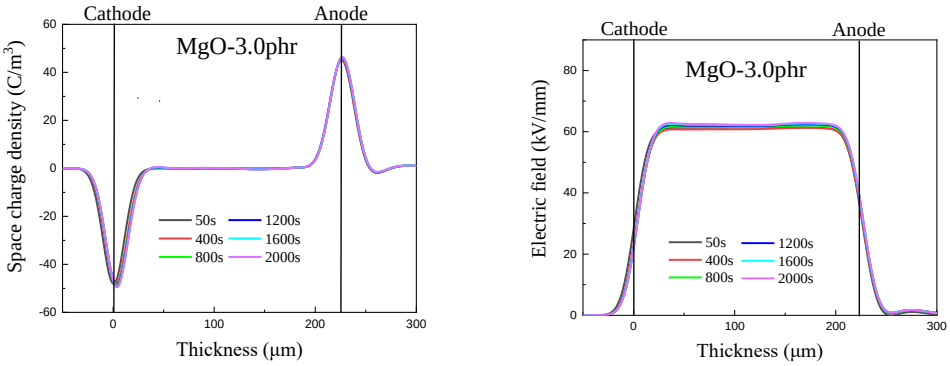

Figure 5.6 The space charge formation and the electric field distribution in the MgO/PP nanocomposites under the DC electric field of 60 kV/mm

In terms of those inorganic nanofillers including nano-MgO and nano-Al_2O_3. As shown in Figure 5.6, the space charge characteristics of PP are improved after adding nano-MgO. In the MgO/PP nanocomposites with the content of 1.0 phr, 2.0 phr and 3.0 phr, the space charge injection is greatly reduced, and there is almost no obvious space charge injection. In terms of electric field distortion, the degree of electric field distortion caused by space charge accumulation is greatly reduced. In the MgO/PP nanocomposites with the content of 0.5 phr, 1.0 phr and 2.0 phr, the maximum electric fields are 65.5 kV/mm, 63.9 kV/mm and 61.6 kV/mm, respectively. When the content of MgO is 3.0 phr, the maximum internal electric field of the MgO/PP nanocomposites increases to 63.9 kV/mm. This is due to the introduction of physical defects caused by the agglomeration of nano-MgO and the reduction of interfacial area between nano-MgO and PP which reduces the interface effect.

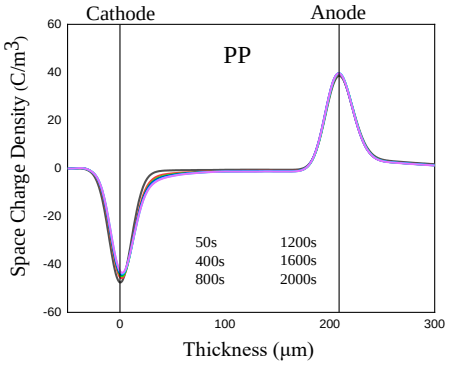
Cathode
Anode
PP
Space Charge Density (C/m3)
Thickness (μm)
50s
400s
800s
1200s
1600s
2000s

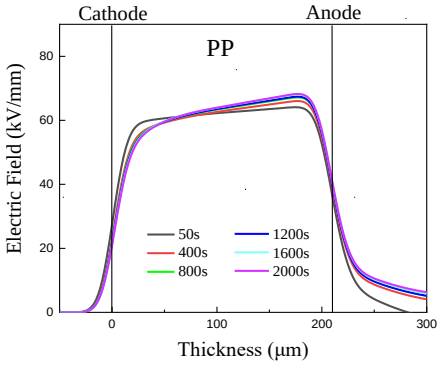
Cathode
Anode
PP
Electric Field (kV/mm)
Thickness (μm)
50s
400s
800s
1200s
1600s
2000s

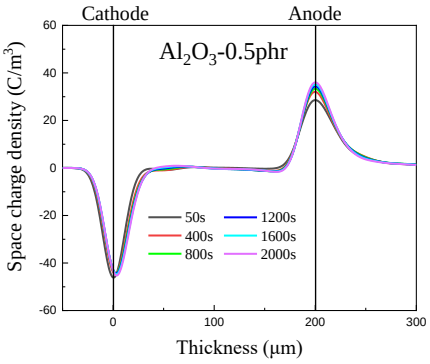
Cathode
Anode
Al2O3-0.5phr
Space charge density (C/m3)
Thickness (μm)
50s
400s
800s
1200s
1600s
2000s

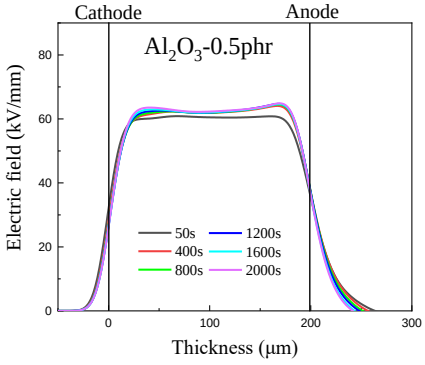
Cathode
Anode
Al2O3-0.5phr
Electric field (kV/mm)
Thickness (μm)
50s
400s
800s
1200s
1600s
2000s

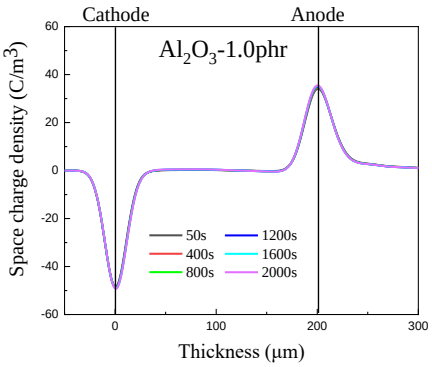
Cathode
Anode
Al2O3-1.0phr
Space charge density (C/m3)
Thickness (μm)
50s
400s
800s
1200s
1600s
2000s

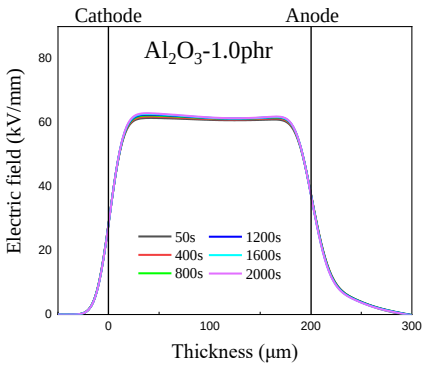
Cathode
Anode
Al2O3-1.0phr
Electric field (kV/mm)
Thickness (μm)
50s
400s
800s
1200s
1600s
2000s

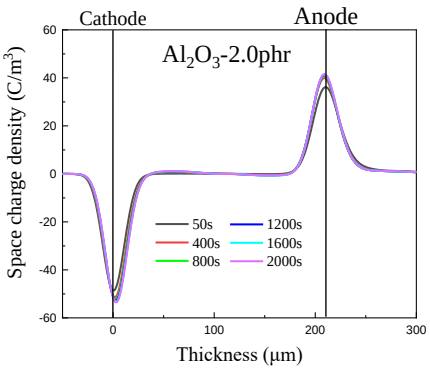
Cathode
Anode
Al2O3-2.0phr
Space charge density (C/m3)
Thickness (μm)
50s
400s
800s
1200s
1600s
2000s

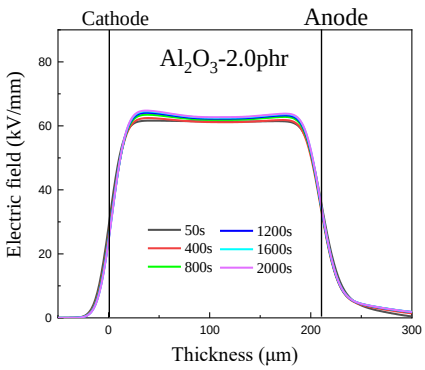
Cathode
Anode
Al2O3-2.0phr
Electric field (kV/mm)
Thickness (μm)
50s
400s
800s
1200s
1600s
2000s

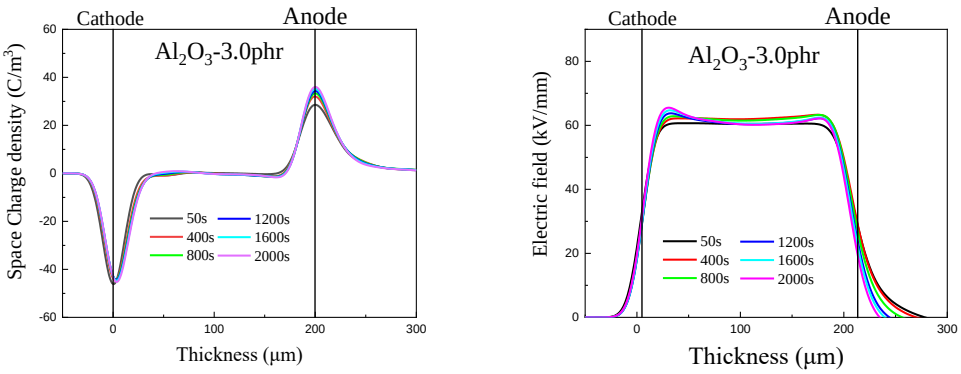

Figure 5.7 The space charge formation and the electric field distribution in the Al_2O_3/PP nanocomposites under the DC electric field of 60 kV/mm

Figure 5.7 shows the regulation of space charge formation and electric field distribution of PP by different content of nano-Al_2O_3. Although the effect of adding alumina is not as good as nano-MgO, the addition of nano-Al_2O_3 also helps to reduce the space charge injection and space charge accumulation of PP, and the electric field distortion of PP is also reduced. Although the electric field of Al_2O_3/PP nanocomposites decreased from 68.2 kV/mm to 64.7 kV/mm, 62.9 kV/mm and 64.8 kV/mm by the addition of 0.5 phr, 1.0 phr and 2.0 phr nano-Al_2O_3 respectively. When the content of nano-Al_2O_3 increased to 3.0 phr, there began to be obvious space charge injection in Al_2O_3/PP nanocomposites. Many charges are injected into the nanocomposites from the cathode and anode, which increases the maximum local electric field to 65.5 kV/mm, still slightly lower than the maximum local electric field of pure PP.

According to the results of thermal stimulation depolarized current measurement, the addition of 1.0 phr nano-Al_2O_3 could introduce highest deep traps into pure PP to improve the trapping characteristics. However, because the trap density of deep traps in 1.0 phr Al_2O_3/PP nanocomposites is much lower than that of 2.0 phr MgO/PP nanocomposites, the enhancement of trapping characteristics by the addition of nano-Al_2O_3 is not better than the addition of nano-MgO. The measurement results of the

space charge formation coincide with the measurement results of thermal stimulation depolarized current measurement.

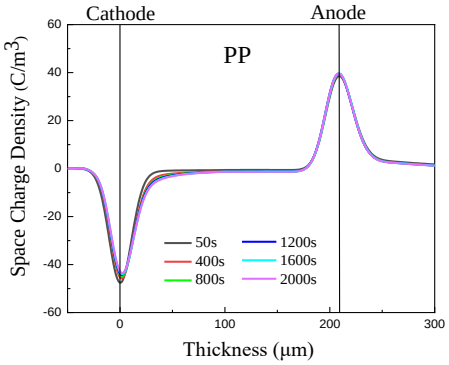

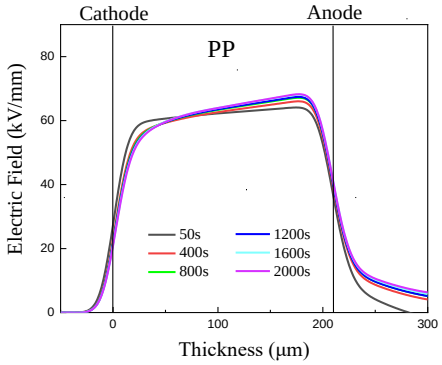

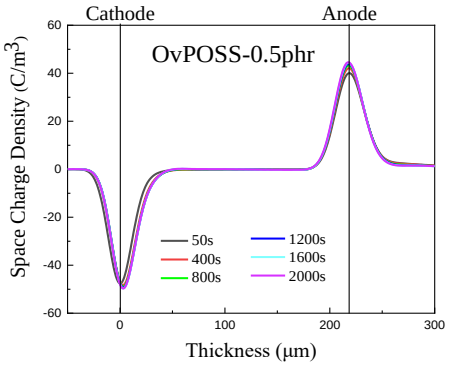

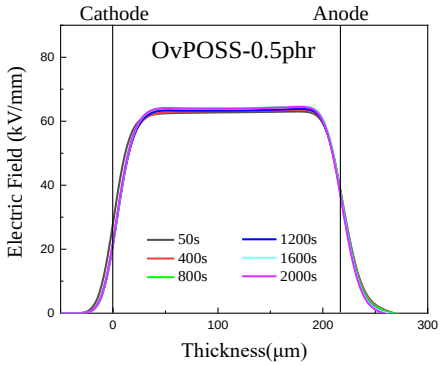

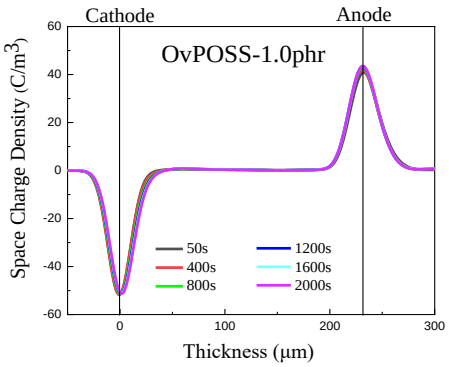

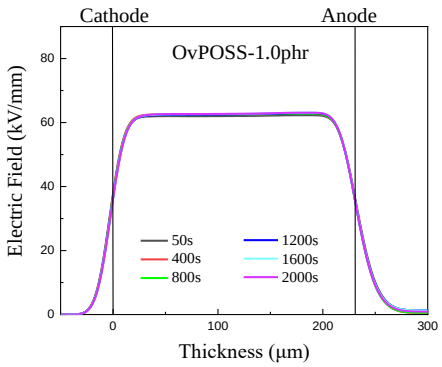

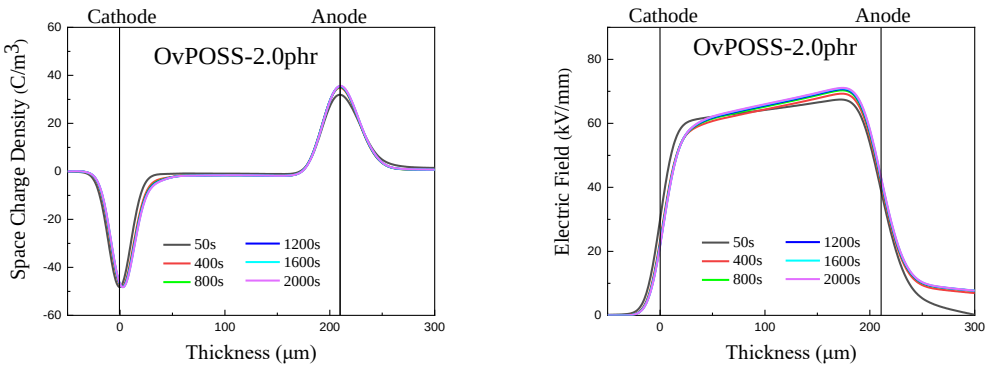

Figure 5.8 The space charge formation and the electric field distribution in the OvPOSS/PP nanocomposite under the DC electric field of 60 kV/mm

Compared with pure PP, it is found that less charges are injected from the cathode and anode in the OvPOSS/PP nanocomposites with the content of 0.5 and 1.0 phr. This case means that the addition of OvPOSS nanofiller can capture the charges near the electrodes, which increase the potential barrier between the surface of nanocomposite film and the electrodes so that the space charge injected from the cathode and anode are suppressed. However, some space charges flow into the bulk of OvPOSS/PP nanocomposites with 0.5 and 2.0 phr. This is because there is not enough interfacial effect between pure PP and OvPOSS nanofiller to capture the space charges under low content and the appearance of physical defects by agglomeration of OvPOSS nanofiller under high content. Space charge accumulation in the film sample with 2.0 phr OvPOSS nanofiller is worse than pure PP. After the addition of OvPOSS, the electric field distortions are reduced to 7.4 % and 5.1 % with the contents of 0.5 and 1.0 phr respectively. However, the electric field distortion increases to 18.3 % when the contents of OvPOSS raises to 2.0 phr. The OvPOSS/PP nanocomposites with 1.0 phr OvPOSS have the lowest distortion of electric field than pure PP.

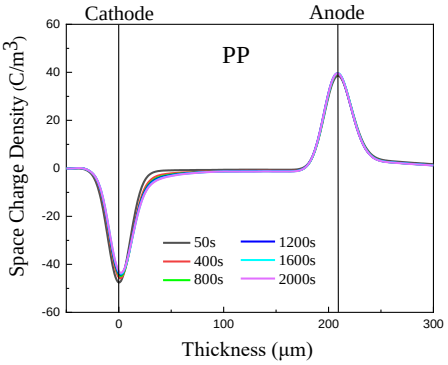
Cathode
Anode
PP
Space Charge Density (C/m3)
50s
400s
800s
1200s
1600s
2000s
Thickness (μm)

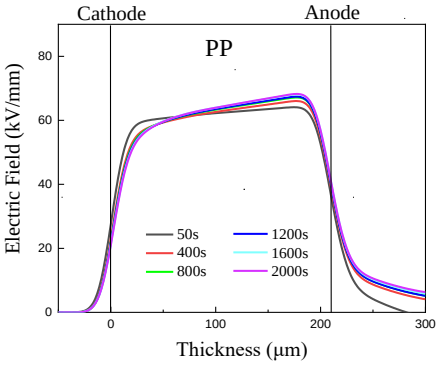
Cathode
Anode
PP
Electric Field (kV/mm)
50s
400s
800s
1200s
1600s
2000s
Thickness (μm)

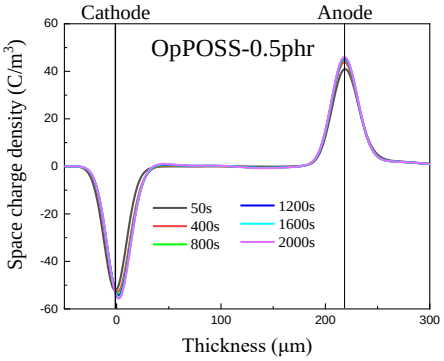
Cathode
Anode
OpPOSS-0.5phr
Space charge density (C/m3)
50s
400s
800s
1200s
1600s
2000s
Thickness (μm)

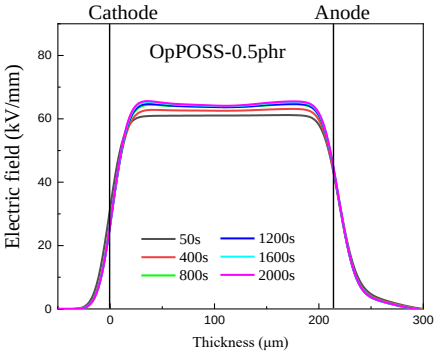
Cathode
Anode
OpPOSS-0.5phr
Electric field (kV/mm)
50s
400s
800s
1200s
1600s
2000s
Thickness (μm)

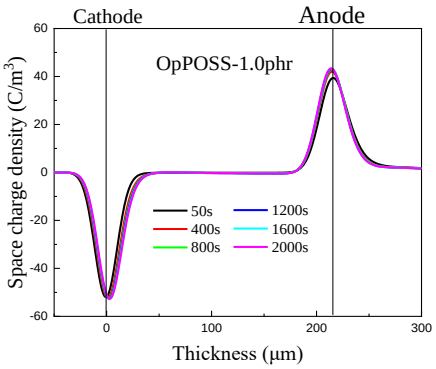
Cathode
Anode
OpPOSS-1.0phr
Space charge density (C/m3)
50s
400s
800s
1200s
1600s
2000s
Thickness (μm)

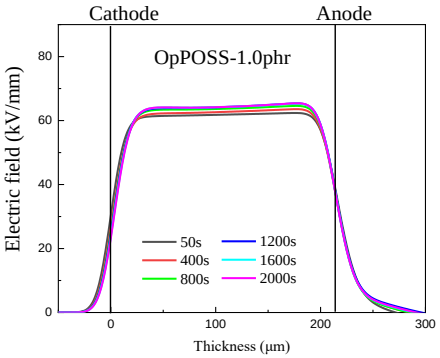
Cathode
Anode
OpPOSS-1.0phr
Electric field (kV/mm)
50s
400s
800s
1200s
1600s
2000s
Thickness (μm)

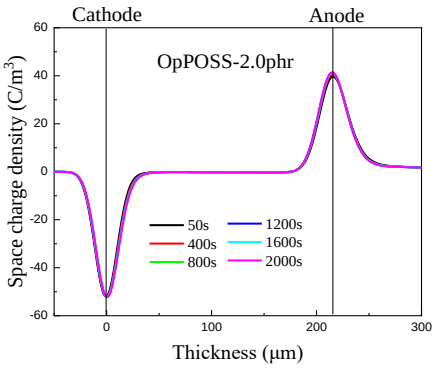
Cathode
Anode
OpPOSS-2.0phr
Space charge density (C/m3)
50s
400s
800s
1200s
1600s
2000s
Thickness (μm)

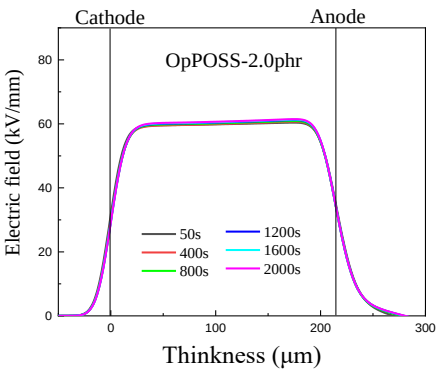
Cathode
Anode
OpPOSS-2.0phr
Electric field (kV/mm)
50s
400s
800s
1200s
1600s
2000s
Thinkness (μm)

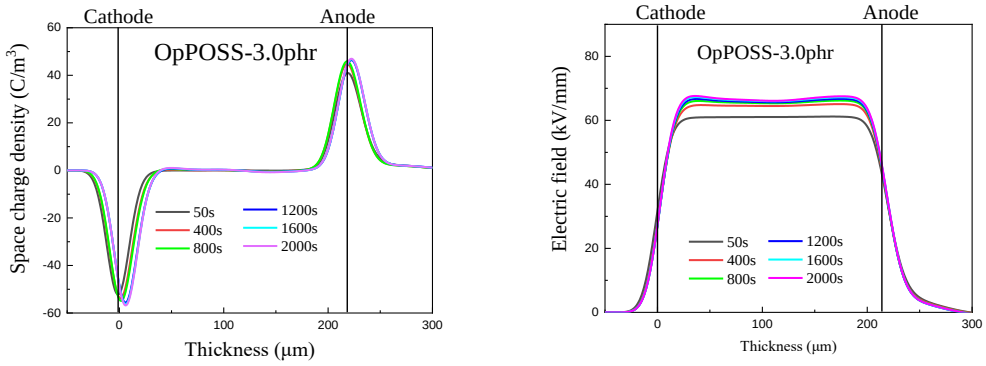

Figure 5.9 The space charge formation and the electric field distribution in the OpPOSS/PP nanocomposites under the DC electric field of 60 kV/mm

For OpPOSS/PP nanocomposites, the addition of 2.0 phr OpPOSS nanofillers could achieve the best space charge distribution and the best electric field distribution in the OpPOSS/PP nanocomposites. At this time, the space charge was hardly injected from the cathode and anode and the maximum electric field was reduced from 68.3 kV/mm to 61.5 kV/mm. When the content of OpPOSS increased to 3.0 phr, the space charge accumulation and electric field distortion in OpPOSS/PP nanocomposites increased under the comparison with OpPOSS/PP nanocomposites with the content of 2.0 phr. The electric field distortion was increased from 2.5 % to 12.7 %.

5.6.2 The mechanism of the suppression of space charge accumulation and the electric field distortion by the nanofillers addition

As a result of the space charge measurement by the PEA system, the addition of nano-MgO, nano-Al_2O_3, OvPOSS and OpPOSS could be used to suppress the space charge accumulation and reduce the electric field distortion in PP. The thermal stimulated depolarized current measurements show the addition of those nanofillers could increase the trapping level and the density of deep traps, which indicates the mechanism of nanodielectrics about the suppression of space charge accumulation. This mechanism is like the Schottky emission [119].

Due to the Schottky emission process shown in Figure 5.10, the injected charges from the electrodes to the insulation layer should overcome the potential barrier which is calculated by the formula below:

$$\phi' = \phi - \frac{e^2 T}{16\pi\varepsilon x} - e|E|x \quad (5)$$

Where: ϕ is the potential barrier with the unit of eV for the injection of charges without the applied electric field. $\frac{e^2 T}{16\pi\varepsilon x}$ is related to the thermionic emission which has the positive correlation with temperature. ε is the permittivity which is equation to $\varepsilon_0\ \varepsilon_r$. x is the position in samples $|E|x$ is the electric potential from the surface between metal and polymeric insulating layer to the position x, and e is the electron quantity ($1.6 \times 10^{-19} C$). Therefore, $e|E|x$ is the energy which provided by the applied voltage.

As the result of space charge measurement shown, the injected charges are mainly negative and come from the cathode. With the addition of nanofillers, the trapping level of nanocomposites would be increased. The injected charges from the cathode would be captured by these traps and form a potential barrier to reduce the effect of the external voltage between the new potential barrier and the cathode. Then, the electric field of the cathode is equivalent to $|E - \Delta E|$. Finally, the potential barrier of Schottky emission effect would be calculated by the equation below:

$$\phi'' = \phi - \frac{e^2 T}{16\pi\varepsilon x} - e|E|x + |\Delta E|x = \phi' + |\Delta E|x'' \quad (6)$$

Where: x' is the position of potential barrier formed by trapped charges.

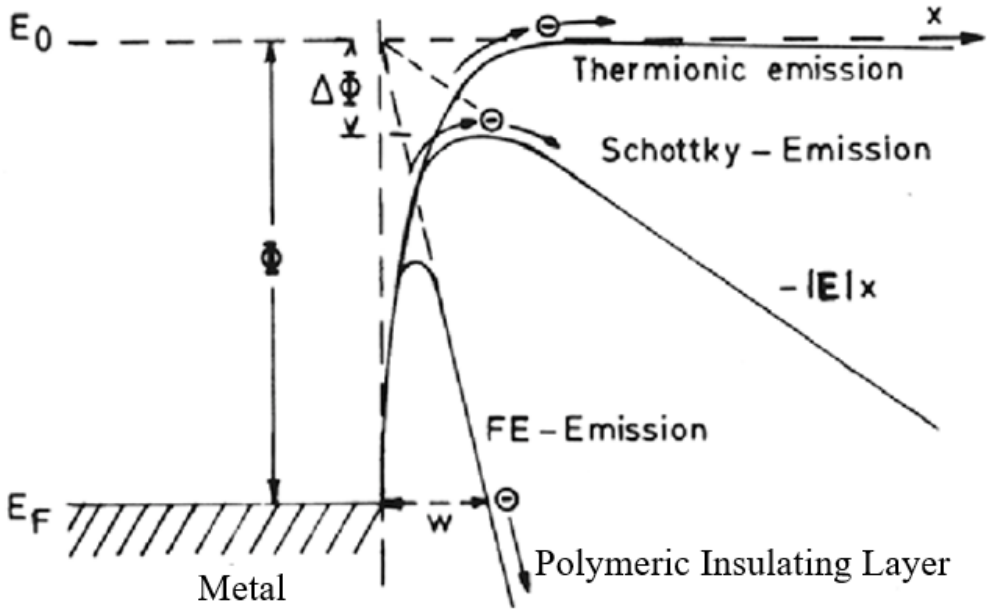

Figure 5.10 The schematic diagram of Schottky emission process

That is why the space charge accumulation can be suppressed by the addition of nanofillers due to the Schottky-emission effect.

5.7 The comparison between nanocomposites

In this section, three parameters, including the conductivity under the DC voltage of 80 kV/mm, the DC breakdown strength and the distortion of the electric field, of four nanocomposites will be compared in order to get the optimization of nanocomposites. These three parameters of nanocomposites have been shown in Table 5.2 below.

Table 5.2 Main electrical properties of PP and PP's nanocomposites

Samples	Volume Resistivity ($\times 10^{15}$ Ω·m)	DC breakdown strength (kV/mm)	The distortion of electric field (%)
Pure PP	0.7	440.1	13.7
2.0 phr MgO/PP	4.0	560.5	2.7
1.0 phr Al_2O_3/PP	2.3	553.4	5.5
1.0 phr OvPOSS/PP	5.0	574.7	5.1
2.0 phr OpPOSS/PP	5.6	585.9	2.5

The comparison result shows the higher improvement of PP's electrical performance by the addition of OvPOSS and OpPOSS than nano-MgO and nano-Al_2O_3. Obviously, OpPOSS/PP has the best electrical performance in terms of those parameters. Even though the space charge characteristics of MgO/PP nanocomposites are better than OvPOSS/PP nanocomposites, the volume resistivity under 80 kV/mm and the breakdown strength of OvPOSS/PP is still higher than MgO/PP. Therefore, the electrical performance of OvPOSS/PP is better than MgO/PP.

Finally, the optimizations of nanocomposites at room temperature (30 ℃) are 1.0 phr OvPOSS/PP and 2.0 phr OpPOSS/PP nanocomposites. Next part is to analyse the difference between OvPOSS and OpPOSS in terms of electrostatic potential and DOS.

5.8 The analysis of POSS characteristics by GaussianView.

5.8.1 The calculation procedure of electrostatic potential and the relationship between energy level and density of state in pure PP, OvPOSS and OpPOSS

From the above parts, it can be concluded that PP's nanocomposites with OvPOSS and OpPOSS have the best electrical properties at room temperature. This is due to the unique structure of OvPOSS and OpPOSS, which can introduce polar groups into PP at low concentration. It can improve the trapping characteristics of PP to improve the electrical properties of PP. It can be seen from the dielectric spectrum in Figure 5.1 that when the content of POSS reaches 1.0 phr, the dielectric constant will increase slightly compared with 0.5 phr, which means that an interface is formed between the small agglomerates of POSS and PP. The small agglomerate of POSS could still introduces the interfacial effect and improves the electrical properties of PP. An insight as to why OvPOSS and OpPOSS PP nanocomposites are better than those formed with MgO and Al_2O_3 can be gained by calculating the electrostatic potentials and density of states of the materials. Gaussian software is a useful tool for analyzing chemical molecules. It can be used to analyze molecules by density universal function calculation, including atomic charge and electrostatic potential, vibration frequency, infrared and Raman spectrum, nuclear magnetic properties, etc. It consists of Gaussian and GaussianView. Gaussian can be used to generate the calculating result as a output file and GaussianView can read the output file from Gaussian to achieve the visualization of data results. In the process of using Gaussian software to analyze molecular electrostatic potential, it is difficult to draw and optimize the molecular structure diagram, such as the setting of chemical bond angle and chemical bond length. Also, Gauss software would take a long time to calculate the electrostatic potential of PP, OvPOSS and OpPOSS. In this part, DFT method with the B3LYP hybrid functional and the 6–31 G (d) basis function in Gaussian software are selected to obtain 3D electrostatic potential

distribution, electronic energy level and density of state (DOS). All quantum mechanics (QM) computations were done using program Gaussian 16 [120]. DOS was using Multiwfn 3.8 [121].

Here is the procedure of calculation for PP, OvPOSS and OpPOSS:

i. The initial structures of isotactic PP with long chain (5 monomers), OvPOSS and OpPOSS were established by GaussView09 and then optimized with a small group by Gaussian, and then optimized with the final group.

ii. After optimization, using the formchk command (input) to generate the corresponding fchk file (output).

iii. Use GaussView to read fchk file and make an electrostatic potential diagram.

iv. Using multiwfn 3.8 to read the fchk file, then producing the DOS spectrum according to the prompt, and guide the corresponding data.

5.8.2 The electrostatic potential of PP, OvPOSS and OpPOSS

The structures of PP chain, OvPOSS and OpPOSS in GaussianView09 have been shown in Figure 5.11.

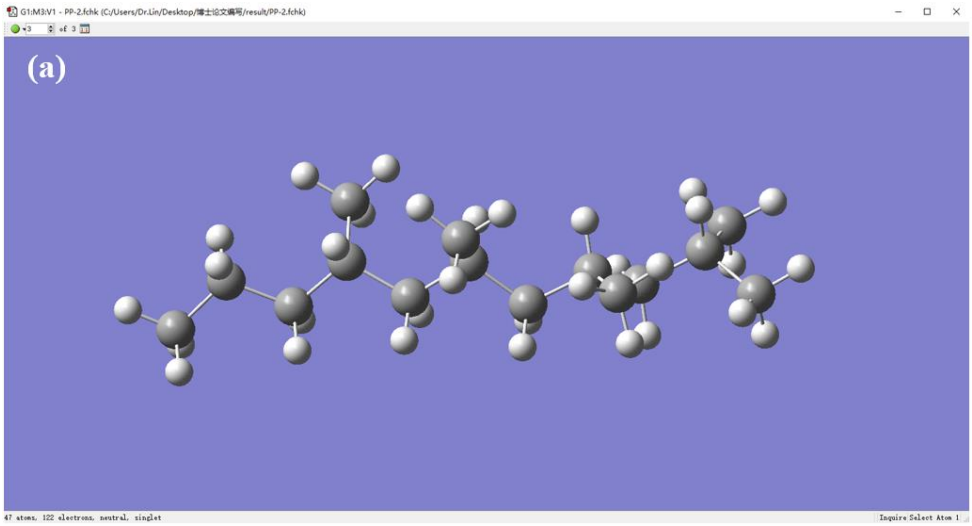

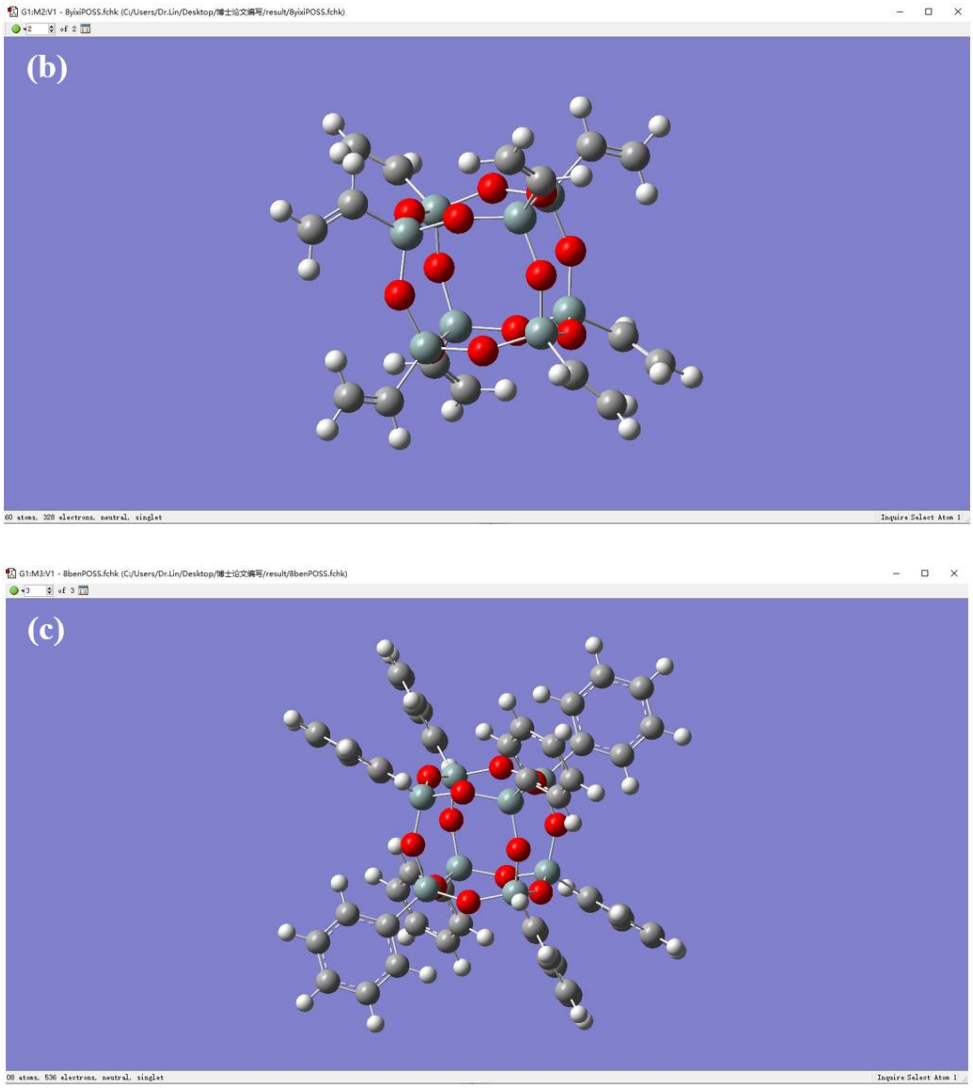

Figure 5.11 The structures of (a) PP chain, (b) OvPOSS and (c) OpPOSS in GaussianView09

Then after the calculation of electrostatic potential, the results are shown in Figure 5.12.

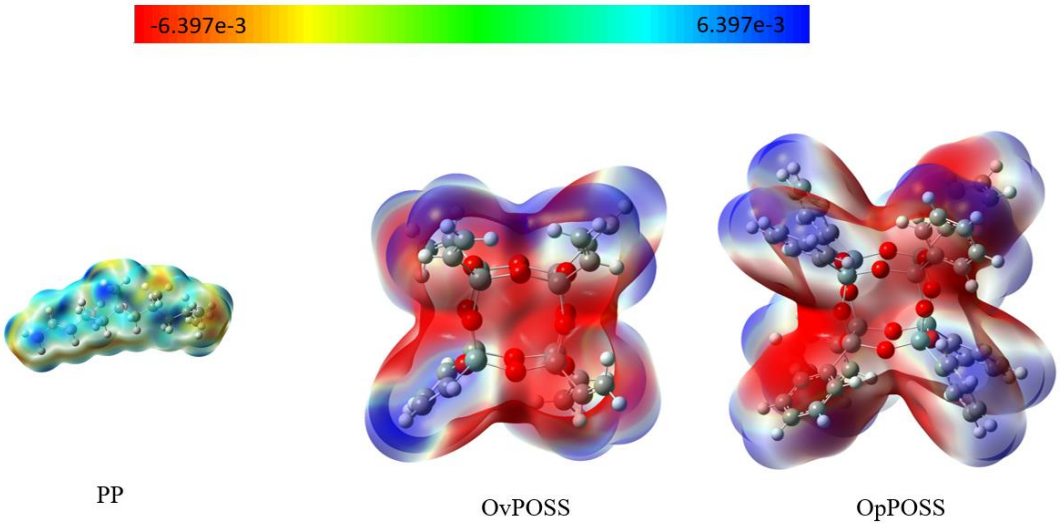

Figure 5.12 The electrostatic potential of PP, OvPOSS and OpPOSS by GaussianView09

In Figure 5.12, the electrostatic potential value of the red regions is negative, indicating that for these regions it is easier to give or repel electrons, or more nucleophilic than other regions. The positive electrostatic potential in the blue region indicates that this region will attract electrons and is more electrophilic than other regions.

On the molecular chain of PP, the electronegativity of carbon atom (2.50) is stronger than that of hydrogen atom (2.10), resulting in electron shift between hydrocarbon bonds. Therefore, the carbon in the main chain and the hydrogen in the side chain of PP are negatively and positively charged respectively. After POSS introduces chemical group, the electrostatic potential of side group would become positive under the strong negativity of oxygen atom (3.50). Hence, it would be easier for the side group to capture electrons and form deep traps for negative charges. While the oxygen atom in the main cage skeleton is negatively charged, which forms deep traps for positive charges in PP's nanocomposites.

Also, for the OvPOSS, 8 side groups are vinyl, and the chemical bond of C = C in vinyl is formed by SP2 hybridization. Under the induction effect of oxygen atom shown in Figure 5.13 [122], the electrons of the vinyl group, especially in the chemical bond of C = C would trend to silicon atom and the electrons of the silicon atom would trend to an oxygen atom. Therefore, even under the singular molecular dispersion of OvPOSS, it could still introduce deep traps into PP.

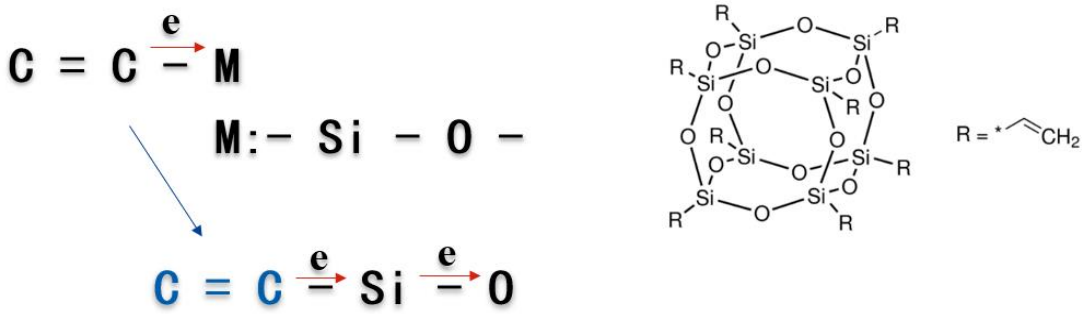

Figure 5.13 The induction effect on the vinyl group by the oxygen atom

Finally, for the OpPOSS, 8 side groups are phenyl groups, which are formed by SP2 hybridization of 6 carbon atoms. According to the conjugated structure and the resonance effect of the phenyl ring, the chemical bonds of C = C are distributed on 6 carbon atoms. Under the induction effect on phenyl groups by the oxygen atom shown in Figure 5.14 [122-123], the electrons of phenyl group would trend to silicon atom and the electrons of the silicon atom would trend to an oxygen atom. Then, the phenyl group could be positively charged. Also, the phenyl group has a conjugated carbon double bond (C = C), so a trap position can be generated by the inherent (permanent) dipole moment, which generates a potential well to capture the charge carrier in the polymer [124-125].

Due to these good advantages, the addition of OvPOSS and OpPOSS can introduce deeper traps than nano-MgO and nano-Al_2O_3 in PP.

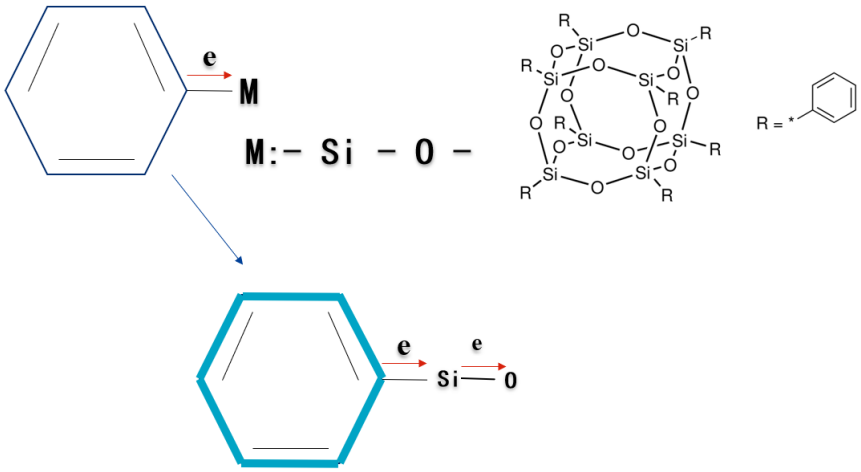

Figure 5.14 The induction effect on the phenyl group by the oxygen atom

5.8.2 The relationship between energy level and density of state in PP, OvPOSS and OpPOSS

The relationships between energy level and DOS in PP, OvPOSS and OpPOSS have been shown in Figure 5.15. In pure PP, the energy level of lowest unoccupied molecular orbital and highest occupied molecular orbital are 2.19 eV and -7.56 eV. Therefore, the energy gap is equal to 9.75 eV. Secondly, in the OvPOSS molecule, the energy level of lowest unoccupied orbital and highest occupied orbital are -0.38 eV and -7.34 eV respectively, so that the energy gap of OvPOSS molecule is 6.96 eV. Finally, in the OpPOSS molecule, the lowest unoccupied orbital is -0.56 eV and the highest occupied orbital is -6.66 eV. Hence the energy gap of OpPOSS is -7.22 eV. From the DOS schematics, the new hole traps and the new electron traps could be introduced by the OvPOSS and the OpPOSS nanofillers by the highest occupied molecular orbital and the lowest unoccupied molecular orbital. As the result of space charge measurements shown, the main moving charges are the negative charges (electrons) from the cathode. For the pure PP, because the lowest unoccupied molecular orbital is higher than 0 eV, it is difficult to provide the electrical traps to capture the electrons by itself.

Since high energy level of traps for the moving electrons is introduced into the nanocomposites, it would be easier to capture the injected charges and build the potential barrier by the captured charges. Then, the production of hot electrons would be reduced. Finally, the electrical properties of PP would be enhanced.

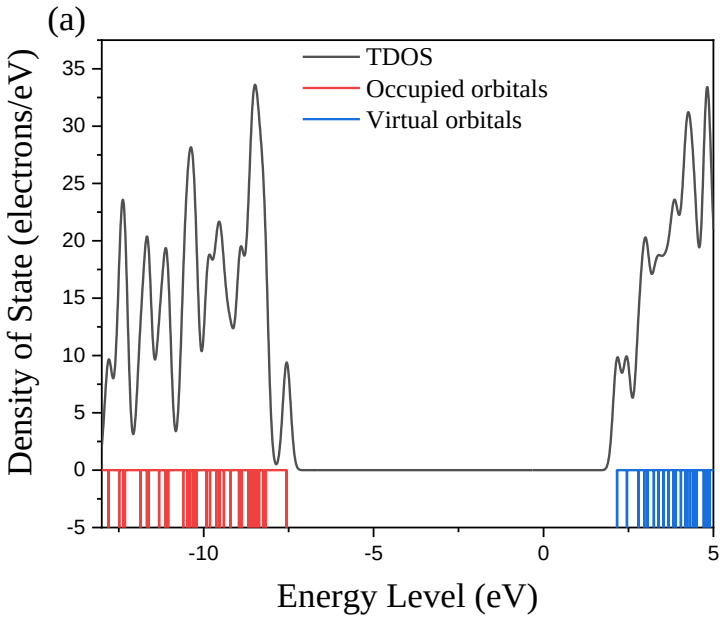

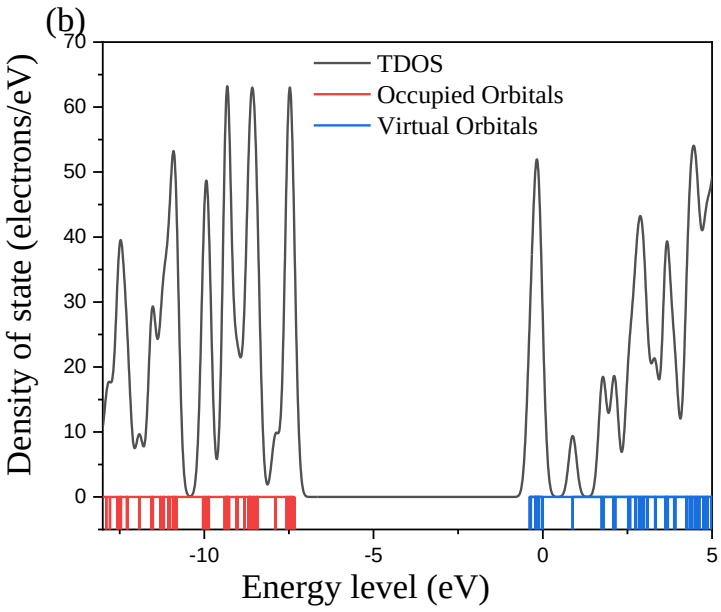

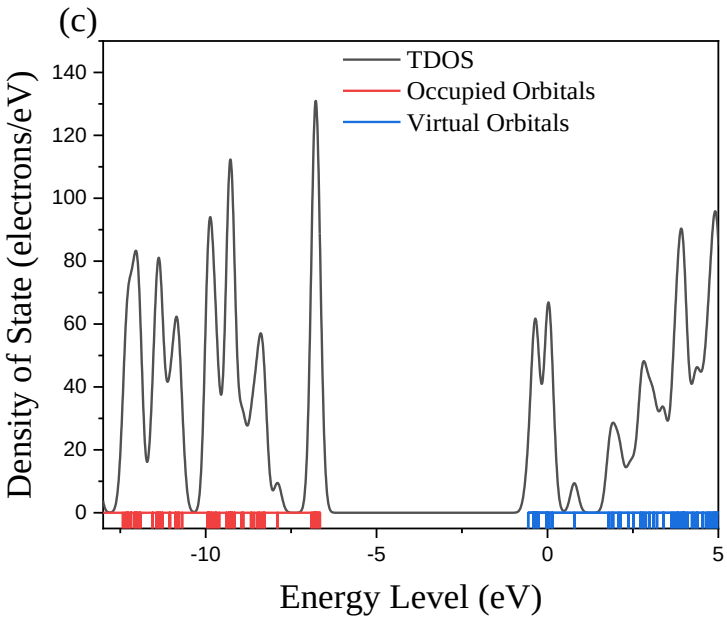

Figure 5.15 The relationship between density of state and energy level in (a) Pure PP, (b) OvPOSS and (c) OpPOSS

Therefore, from the analysis of electrostatic potential and the DOS spectrum of OvPOSS and OpPOSS, it could be found that the OvPOSS and OpPOSS nanofillers have not only the much smaller size than nano-MgO and nano- Al_2O_3, but also the more superior characteristics given by the special structure and the side groups of POSS. Additionally the Conjugated structure of phenyl group can still enhance the trapping characteristics of OpPOSS [126]. That is why the OvPOSS/PP and OpPOSS/PP nanocomposites has better electrical performance than MgO/PP and Al_2O_3/PP nanocomposites under HVDC conditions.

5.9 Conclusion

In this chapter, PP and PP's nanocomposites with different contents of nano-MgO, nano-Al_2O_3, OvPOSS and OpPOSS nanofillers were investigated. The effects of different nanoparticles on the microstructure morphology, crystallization behavior to improve the electrical properties of PP's nanocomposites have been further discussed. By comparing the electrical properties of the four nanocomposites at 30 ℃, including

conductive current, electric field distortion and DC breakdown strength, the formula about the type and content of nanofillers was optimized. The improvement of the electrical properties of PP by the four nanofillers was deeply analyzed through chemical structure analysis, microstructure analysis, and trap depth analysis by TSDC measurement. Additionally, the more superior characteristics of OvPOSS and OpPOSS than nano-Al_2O_3 and nano-MgO have been found. The main conclusions of this chapter are listed as follows:

i. Among PP and its four nanocomposites prepared by solution method, the results of dielectric spectrum indicate that the dielectric constant of nanocomposites also increase slightly with the addition of nanofillers. The slight increase of dielectric constant is not only due to the dielectric properties of nanofillers, but also due to the formation of interface between nanofillers and the molecular chains of PP.

ii. Combined with the observation of the microstructure morphology in the chapter 4 and compared with pure PP, the electrical properties of PP's nanocomposites are improved when the nano fillers are uniformly dispersed. With the addition of nanofillers, the DC volume conductivity of PP is decreased under high DC electric field, while the DC breakdown strength is increased. The introduction of nanofillers also inhibits the injection of homocharges from the cathode, greatly reduces the distorted electric field in the bulk of PP and improves the space charge characteristics of PP. However, the addition of high content of nanofillers will reduce the enhancement of electrical properties of PP due to the influence of agglomeration.

iii. The mechanism of nanofillers tuning the electrical properties of PP was analyzed, which is based on the introduction of deep traps by the addition of nanofillers.

iv. The DC bulk conductance, DC breakdown strength and electric field distortion coefficient of four nanocomposites were compared. It was found that the

addition of OvPOSS and OpPOSS had the best performance in improving the electrical properties of PP, especially for OpPOSS. Compared with pure PP, OpPOSS can reduce the bulk conductivity to a minimum of about one eighth of PP. The addition of 2.0 phr OpPOSS can increase the breakdown strength of PP from 440 kV/mm to 586 kV/mm, achieving the increase of 33.2 % in breakdown strength. In terms of space charge characteristics, the addition of 2.0 phr OpPOSS reduces the electric field distortion of PP from 13.4 % to 2.5 % by inhibiting the injection of charge from the cathode and the anode.

v. Combined with the content of Chapter 4, the DSC measurement results show that the nanofillers play the role of heterogeneous nucleating agent in the crystallization process of PP and improves the crystallinity of PP. POM observation shows that the spherulite size of PP is greatly reduced with the addition of nanofillers, and the boundary between spherulites is more difficult to observe. Generally, the boundary between spherulites is the weak point where PP is prone to breakdown. Therefore, the reduction of spherulite boundary regions means that the internal defects of PP are decreasing, and the resistance of the low resistance path between spherulites and spherulites is increasing, which is helpful to improve the electrical properties of PP. Combined with the measurement results of TSDC, it shows that the introduction of nano filler improves the trapping characteristics of PP. The addition of nano filler will introduce high-density deep traps into PP to capture the space charge injected from the cathode and form a new potential barrier to inhibit the injection of space charge from the cathode and the electric field distortion in PP.

vi. Using the DFT method, combined with B3LYP mixed functional and 6-31G (d) basis function, the three-dimensional electrostatic potential distribution, electron energy level and DOS for PP, OvPOSS and OpPOSS are obtained through the Quantum Mechanism Computation in GaussianView09. The electrostatic

potential calculation results of PP, OvPOSS and OpPOSS show that OvPOSS and OpPOSS have the ability to introduce deep traps in the side groups (Vinyl and Phenyl) through the SP2 hybridization orbits, the induction effect and the resonance effect under the strong electronegativity of oxygen atoms. DOS spectrum shows that compared with PP, OvPOSS and OpPOSS have the unoccupied orbits to containing moving electrons, which could introduce deep traps into the bulk of PP. The electrostatic potential calculation and DOS spectrum show that OvPOSS and OpPOSS have better characteristics than inorganic nanofillers at the molecular level, so that they can improve the electrical properties of PP to a greater extent.

vii. Finally, the OvPOSS/PP and OpPOSS/PP nanocomposites will be adopted for the further research in Chapter 6.

6 Electrical properties of polypropylene's nanocomposites under high temperature

6.1 Materials

Compared with XLPE and LDPE, PP has a higher melting point, which means that PP has better mechanical properties at high temperature. The melting point of LDPE is only 110 ℃, and at 90 ℃, LDPE cannot be used as insulation material because it begins to melt. Even XLPE has the thermoset properties through the crosslinking procedure, and its working temperature is usually no more than 70 ℃. With the increase of temperature, XLPE would become too soft and to be used as insulating material for cable insulation under HVDC conditions. Usually, the temperature of the core of the DC cable during operation does not exceed 70 ℃. However, the temperature of cable core would be higher due to the higher demand for transmission capacity during cable operation. Compared with XLPE and LDPE, PP has better thermal stability due to its higher melting point, so PP's nanocomposites have the potential to become the next generation of thermoplastic polymeric insulation materials. Therefore, it is necessary to estimate the electrical performance of OvPOSS/PP and OpPOSS/PP nanocomposites under high temperature. At high temperature, it would be easier for electrons to obtain energy from the surroundings and become hot electrons. Hot electrons would bombard the molecular chain of PP, resulting in the chemical degradation of PP , then the electrical properties of PP would be reduced by the chemical degradation. Because the transport mode of space would be changed in PP, the volume conductivity under different electric fields would be increased significantly at high temperature, and the DC breakdown strength would be also decreased due to the movement of high-energy electrons. Therefore, it is necessary to re-measure the volume conductivity, DC breakdown strength and space charge characteristics of PP and its nanocomposites in order to find the effect of nanofillers on tuning electrical performance of PP at high temperature.

In this chapter, the OvPOSS/PP and OpPOSS/PP nanocomposites were selected as the experimental subjects and the contents of nanofillers have been shown in Table 6.1. The dielectric spectrum, DC conductive current, DC breakdown strength and space charge characteristics of PP and its nanocomposites were measured at different temperatures including 50, 70 and 90 ℃. From these measurement the influence of temperature on: charge transport; the development of space charge and the electrical properties of the nanocomposites could be found which will help optimization in the future. Finally, by the comparation between OvPOSS/PP and OpPOSS/PP nanocomposites in terms of the electrical measurement results, the types and contents of nanofillers in nanocomposites are further optimized for next work.

Table 6.1 The types and contents of nanocomposites in Chapter 6

Samples	OvPOSS	OpPOSS	PP
Pure PP	0	0	100
OvPOSS/PP-0.5	0.5	0	99.5
OvPOSS/PP-1.0	1.0	0	99.0
OvPOSS/PP-2.0	2.0	0	98.0
OpPOSS/PP-0.5	0	0.5	99.5
OpPOSS/PP-1.0	0	1.0	99.0
OpPOSS/PP-2.0	0	2.0	98.0
OpPOSS/PP-3.0	0	3.0	97.0

6.2 The dielectric properties

The broadband dielectric spectrometer (Novolcontrol, Germany) with Alpha-A high performance frequency analyzer was used to measure the dielectric constant of PP and its nanocomposites at the temperature of 30, 50, 70 and 90 ℃. This data is shown in

figure 6.1 with data from measurements at 30 ℃ previously reported in chapter 5. The relative permittivity of OvPOSS/PP and OpPOSS/PP nanocomposites with different contents decreased slightly with the increase of temperature. Because PP is an insulating material and there are no free moving electrons inside, its polarization mode is caused by the weak displacement of electrons in atomic orbits. The temperature change from 30 ℃ to 90 ℃ will not cause the internal electronic energy of PP from the valence band to the conduction band, so the dielectric constant of PP and its nanocomposites will not change.

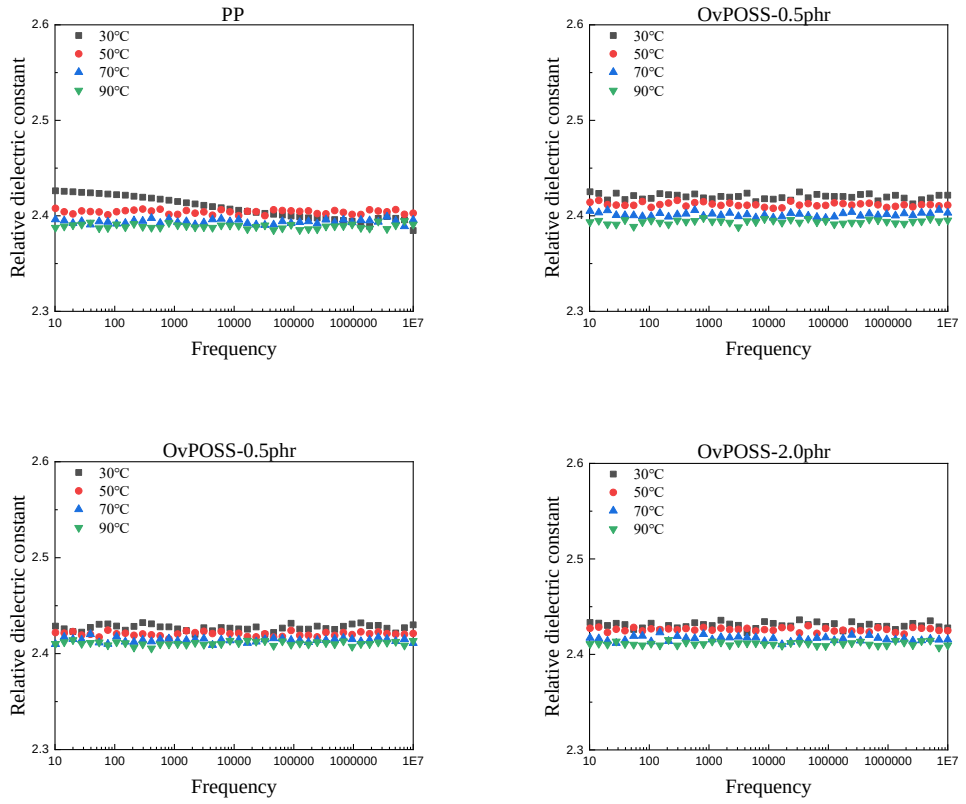

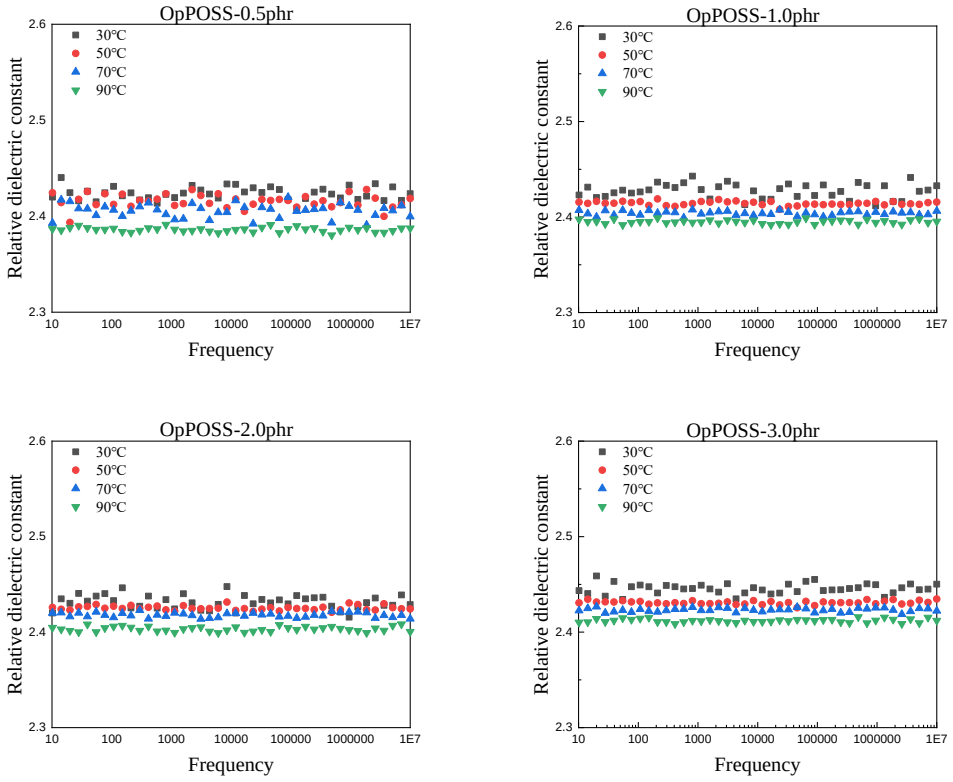

Figure 6.1 The dielectrics spectrums of PP and its nanocomposites under the temperatures of 30, 50, 70 and 90 ℃.

6.3 The DC conductivity tests

6.3.1 The experimental procedure

The DC conductivity of PP and its nanocomposites under different temperatures was measured by three-electrode method shown in Figure 3.12. Because of the need of DC conductivity with the change of temperature, the procedure is slightly different from the DC conductivity measurement in Chapter 5. The temperature under the test is set to 50, 70, and 90 ℃. The DC conductivity measurement is achieved by the experimental design in Figure 3.12 and the procedure has been described in chapter 5.

6.3.2 The results of DC conductive current under different electric field and different temperatures

Now, the DC conductive current measurement of PP and its nanocomposites under different temperatures have been shown in Figure 6.2. For pure PP, at room temperature (30℃), the DC conductive current in pure PP increases linearly with the increase of DC electric field when the DC electric field is lower than 40 kV/mm. When the DC electric field further increases, the DC conductive current in pure PP increases dramatically with the increase of the DC electric field. With the increase of temperature, in the graph of DC conductive current of PP, the linear region of DC conductive current is reduced, and the nonlinear region of DC conductive current increases. That is, the ohmic region gradually reduced and the non-ohmic region increases. The boundary electric fields between ohmic region and non-ohmic region in 30, 50, 70 and 90 ℃ are 40 kV/mm, 35 kV/mm, 30 kV/mm and 25 kV/mm respectively in pure PP.

In PP's nanocomposites with OvPOSS and OpPOSS nanofillers, the increasing trend of DC conductive current with electric field intensity is obviously inhibited. As described in Chapter 5, at room temperature (30 ℃), the addition of OvPOSS and OpPOSS nanofillers can reduce the DC conductive current of PP from 35.05 PA to 5.06 PA and 4.78 PA respectively, which means that the volume resistivity of PP is increased by 6.92 times and 7.33 times by OvPOSS and OpPOSS nanofillers respectively. With the increase of temperature, the DC conductive current of OvPOSS/PP and OpPOSS/PP nanocomposites at different electric field also increased, but it was still much lower than that of pure PP. This phenomena indicated that these two kinds of POSS could effectively improve the volume resistivity of PP at room temperature (30 ℃) and high temperatures (50 ℃ - 90 ℃), especially the OpPOSS/PP nanocomposites with 2.0 phr had the best effect. According to the analysis in Chapter 5, the space charge accumulation is closely related to the trapping characteristics of PP and its nanocomposites, and the conductivity characteristics are also closely related to the

trapping characteristics. Therefore, the bulk conductivity of PP is inhibited by the addition of OvPOSS and OpPOSS nanofillers, which indirectly indicates that the space charge will also be inhibited at high temperature.

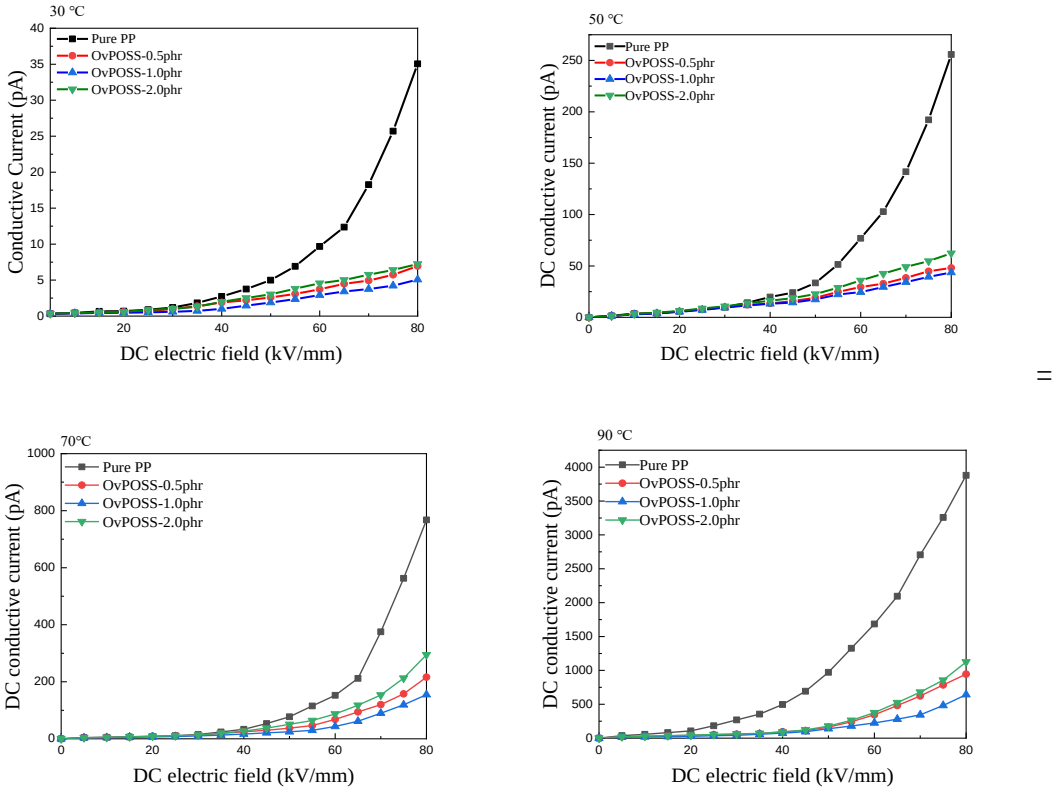

Figure 6.2 The DC conductive current of OvPOSS/PP nanocomposites under 30, 50, 70 and 90 ℃

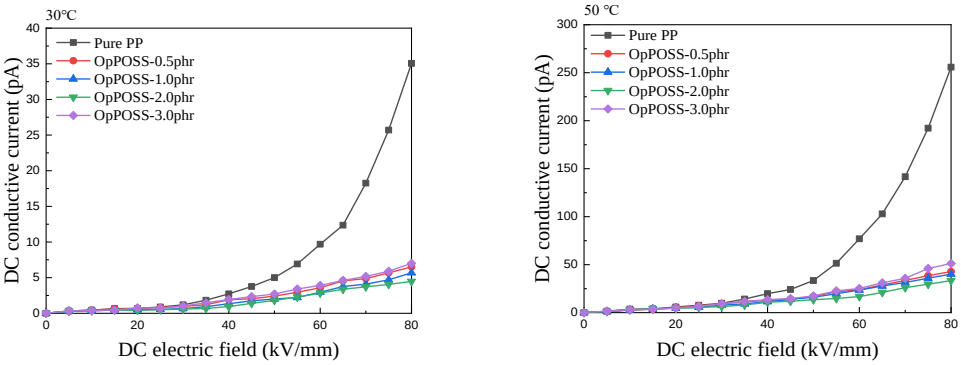

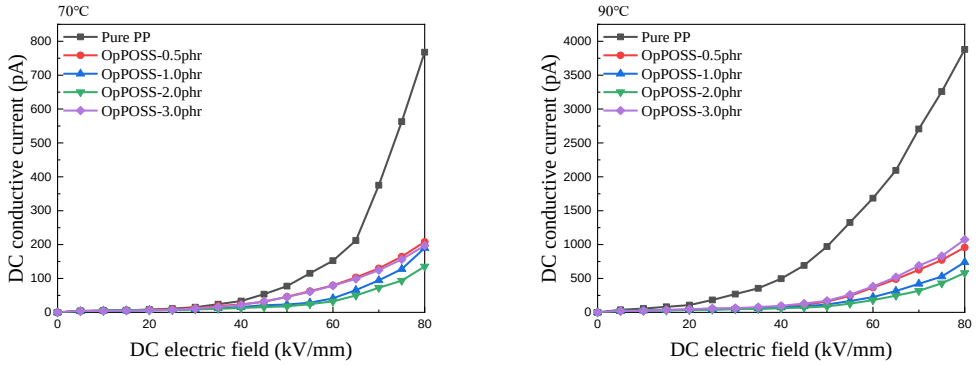

Figure 6.3 The DC conductive current of OvPOSS/PP nanocomposites under 30, 50, 70 and 90 ℃

6.3.3 The threshold electric field for PP and its nanocomposites

According to the space charge limited current theory proposed in [127], the curve of DC conductive current with the increase of electric field could be divided into three regions: ohmic region (V-I), trap-filled limited region (TF) and space charge-limited current (SCLC) region shown in Figure 6.4 [128].

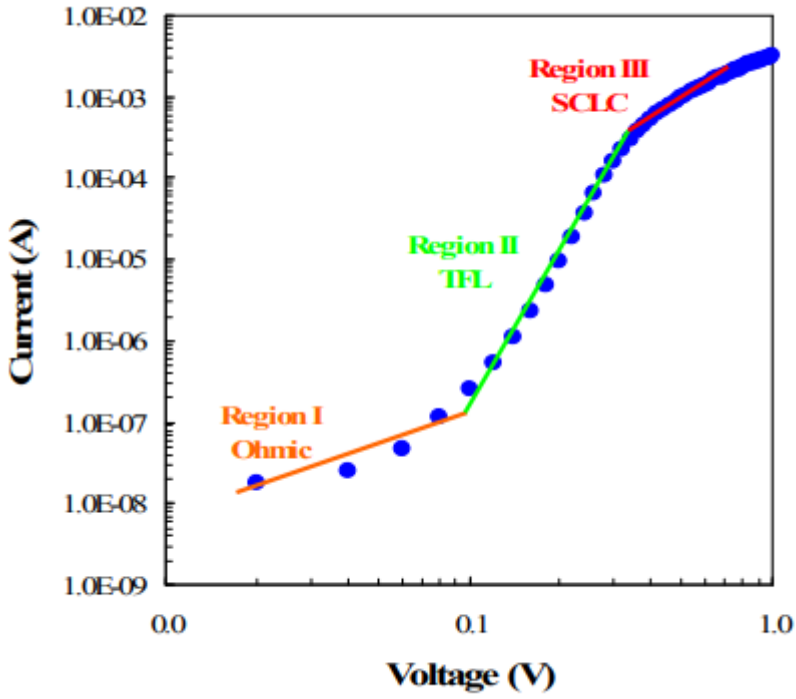

Figure 6.4 Three regions of the relationships between DC conductive current and electric field [128].

Firstly, the electric field is low in the ohmic region, and the charge density injected from the electrodes (n) is much higher the charge density produced by the thermal excitation (n_t) in the polymeric insulation material. Therefore, the density of DC conductive current could be obtained by the equation below:

$$j = ne\mu\frac{V}{d} - - - - - (7)$$

Where : j is the conductive current density, μ is the mobility of charges, V is the applied voltage and d is the thickness of polymeric insulation material.

Then, with the increasing electric field, more charges with higher density would be injected from the electrodes and some charges would be trapped by the trapping characteristics. However, in the ohmic region, only a low percentage of charges would be trapped in the bulk of the polymer and the density of charge injection from the electrodes is much higher the density of the charges produced by the thermal excitation in the polymeric insulation material.

With the increase of applied electric field, the charge injected from the electrodes also increases. When the density of injected charge captured by the deep trap (n_c) inside the polymer exceeds the charge density produced by the thermal excitation (n_t), the directional movement of the migrating charge under the applied electric field will be affected by the captured charges in traps and not affected by the charges from thermal excitation . This effect mainly comes from the trapping characteristics of polymers. Under these conditions, the density of DC conductive current inside the polymer could be transformed from the Eq. (7) to the Eq. (8) below [126]:

$$j = e^{1-l}N_c\mu\left(\frac{2l+1}{l+1}\right)^{l+1}\left(\frac{\varepsilon_0\varepsilon_r}{H_t}\frac{l}{l+1}\right)^{l}\left(\frac{V^{l+1}}{d^{2l+1}}\right) - - - (8)$$

Where N_c is the DOS in the conduction band, H_t is the total trap density, T_t is the characteristic temperature of traps distribution and l is the ratio between the characteristic temperature T_t and measuring temperature T, that is $l = {T_t}/{T}$. Because the results of DC conductive current measurement show the power law relationship between conductive current and electric field, the ratio l is larger than 1, and $T_t >$ 90℃.

Finally, with the increase of applied electric field, the effect of traps would be much less than the applied electric field. The DC conductive current would be mainly affected by the space charge accumulation inside the polymer. And the increase of DC conductive current would have a power law relationship with DC applied voltage.

Under the electric field of 80 kV/mm, the DC conductive current would be remained in the TFL region, which can be defined as trap-limited space-charge-limited region (TLSCL). The relationship between DC conductive current and a DC electric field under the logarithmic coordinates is shown in Figure 6.5 and the threshold electric fields of pure PP and different nanocomposites are shown in Table 6.2.

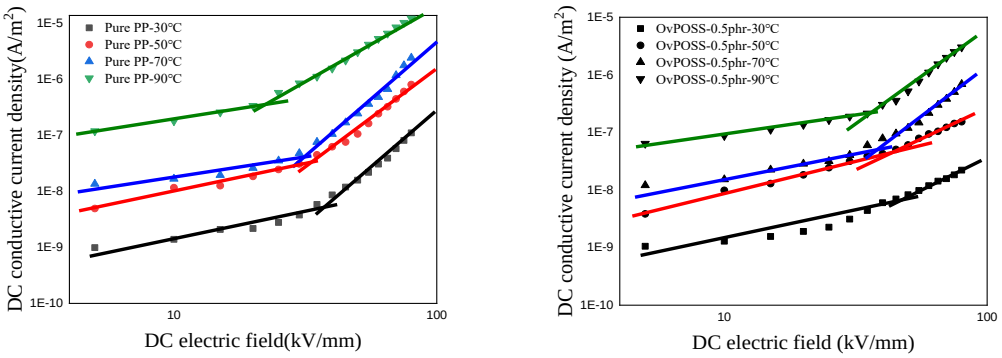

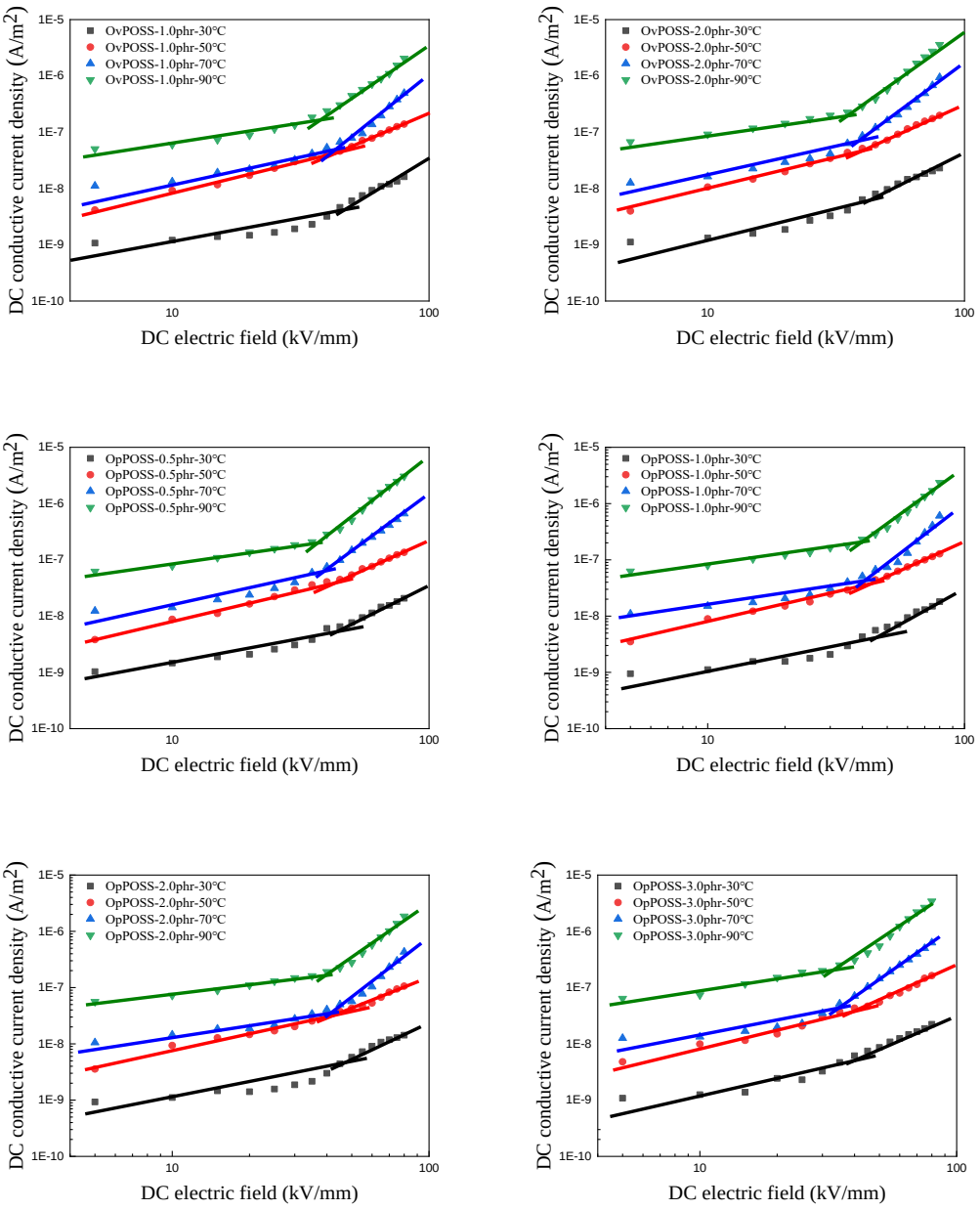

Figure 6.5 The DC conductive current of the samples in the logarithmic coordinates

Table 6.2 The threshold electric field E_c of Pure PP and its nanocomposites

Samples	30℃ E_c(kV/mm)	50℃ E_c(kV/mm)	70℃ E_c(kV/mm)	90℃ E_c(kV/mm)
Pure PP	37.2	33.5	31.7	22.3
OvPOSS-0.5phr	47.2	42.9	38.1	36.2
OvPOSS-1.0phr	47.2	43.6	42.9	38.2
OvPOSS-2.0phr	42.6	39.4	38.4	34.8
OpPOSS-0.5phr	44.0	43.1	39.1	36.9
OpPOSS-1.0phr	46.0	42.9	41.0	39.6
OpPOSS-2.0phr	47.4	42.6	41.2	39.7
OpPOSS-3.0phr	40.6	40.1	35.0	33.1

The regions of conductive current in Figure 6.4 match the ohmic region and the trap-filled limited region. The transition electric field of ohmic region and trap-filled limited region is the threshold electric field, which corresponds to the transition of conductivity mechanism from ohmic region to trap-filled limited region and represents more injected charges from electrodes would start to be trapped in the insulation materials. From Table 6.2, although the threshold electric field increases with the increase of temperature, the threshold electric field of PP increases significantly at all temperatures after the addition of OvPOSS and OpPOSS nanofillers, indicating that the introduction of OvPOSS and OpPOSS nanofillers could inhibit the injection of charge from the electrode at different temperatures.

Figure 6.6 shows the threshold electric field of nanocomposites under 50 ℃, 70 ℃ and 90 ℃. In the temperature of 50 ℃, the threshold electric fields of OvPOSS/PP-

0.5phr, OvPOSS/PP-1.0 phr, OpPOSS/PP-1.0 phr and OpPOSS/PP-2.0 phr nanocomposites are very similar. Under the temperature of 90 ℃, OpPOSS/PP-2.0 phr have the highest threshold electric field about 39.7 kV/mm and OvPOSS/PP nanocomposites could achieve the highest threshold electric field about 38.2 kV/mm with the content of 1.0 phr, which have increased the threshold electric field of pure PP by 77.6 % and 71.3%. However, higher contents of nanofillers would reduce the improvement of threshold electric field, which means that the non-uniform distribution would cause some shallow traps to reduce the deep trap effect by nanofillers. Both of results indicate that the addition of OvPOSS and OpPOSS nanofillers with appropriate contents could suppress the charge injection from electrodes within the temperature of 90 ℃.

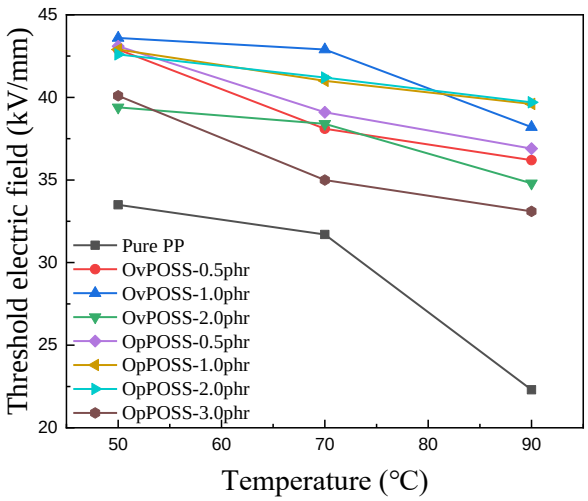

Figure 6.6 The threshold electric field E_c of Pure PP and its nanocomposites

6.4 The DC breakdown strength tests

6.4.1 The experimental procedure

The DC breakdown strength of PP and its nanocomposites under different temperatures is measured by the experimental design shown in Fig. 3.13. The procedure of DC breakdown strength measurement has been listed below:

i. The thickness of each samples was controlled between 100 and 130 μm. The samples were marked by 20 points on the surface and the thickness of each point was measured by the micrometer.

ii. The heating plate was heated to the required temperature, the silicone oil temperature was measured by the thermometer.

iii. Until the temperature of oil is stable at the required temperatures, the sample was immersed in silicone oil and placed between two spheres-electrodes.

iv. Adjusting the rising rate of DC voltage to 1.0 kV/s and start the DC breakdown test.

v. The breakdown voltage was recorded for every point after the DC breakdown of the sample and calculating the breakdown strength by dividing the breakdown voltage by the thickness.

For the result selection, only one reliable data from each group of samples is selected to analyse the breakdown strength of each sample and those data can be reproduced by other researchers.

6.4.2 The analysis of DC breakdown test

Figure 6.7 shows the Weibull distribution of DC breakdown strength of PP and its nanocomposites at 30 ℃, 50 ℃, 70 ℃ and 90 ℃. The addition of OvPOSS and OpPOSS nanofillers could improve the DC breakdown strength of PP at various temperatures. Among them, 1.0phr OvPOSS/PP and 2.0phr OpPOSS/PP nanocomposites have the highest breakdown strength at different temperatures. At 90 ℃, the DC breakdown strength of PP could be increased from 335 kV/mm to 436 kV/mm and 443 kV/mm by adding 1.0 phr of OvPOSS and 2.0 phr of OpPOSS respectively, with the increase of 30.1 % and 33.1 % respectively. This result shows

that the addition of appropriate content of OvPOSS and OpPOSS nanofillers could obviously improve the electrical performance of PP.

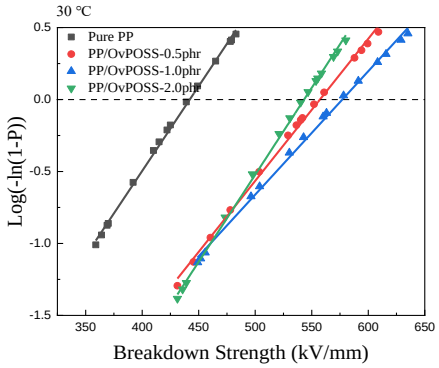

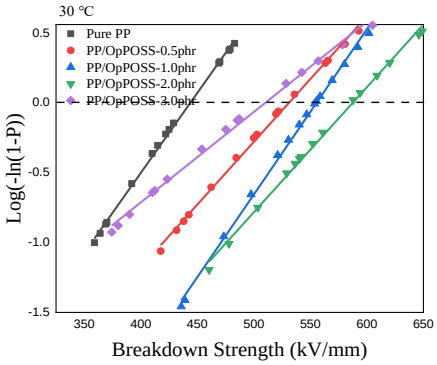

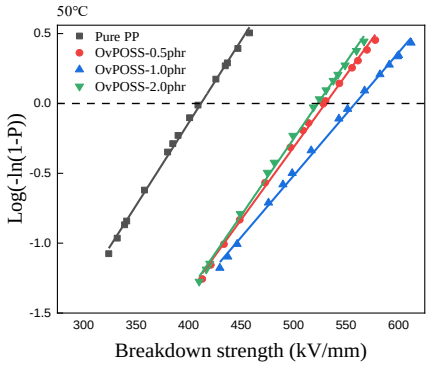

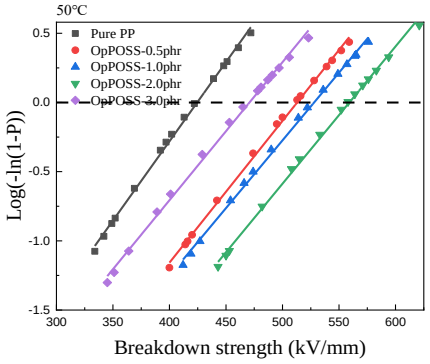

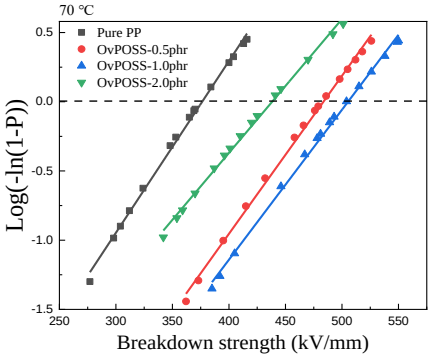

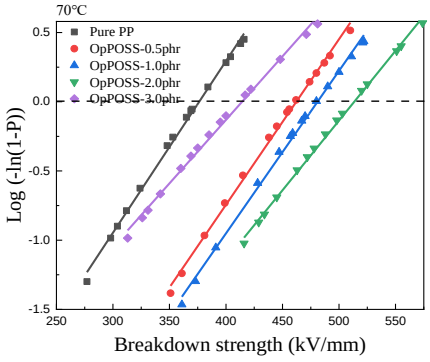

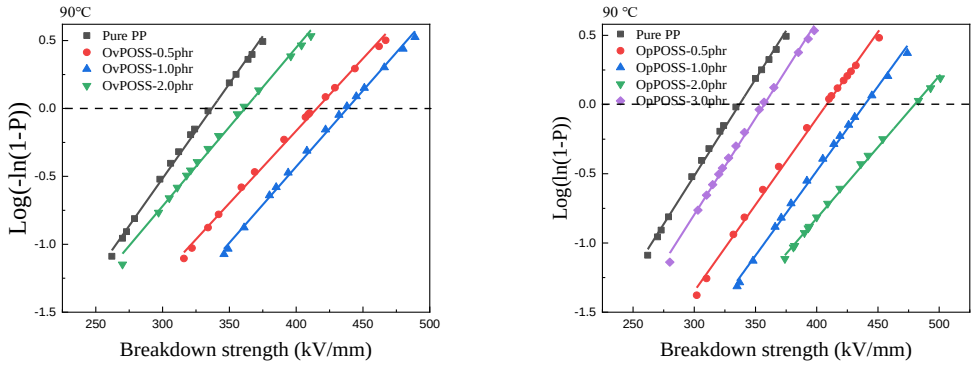

Figure 6.7 The breakdown strength of OvPOSS/PP and OpPOSS/PP nanocomposites with different contents under different temperatures

Table 6.3 shows the characteristic breakdown strength and distribution coefficient of different samples at different temperatures. It can be seen from Table 6.3 that the breakdown strength of PP and its nanocomposites decreases with the increase of temperature. The increase of external temperature leads to the increase of internal temperature of PP and its nanocomposites. The moving electrons are easy to obtain energy from the outside, so electrons could have enough energy and get out of the trap in PP, OvPOSS/PP and OpPOSS/PP nanocomposites to increase their own free path. Under the action of an electric field, hot electrons move directionally from cathode to anode, bombard the molecular chain of PP to cause the degradation of PP locally, and finally lead to the breakdown of the whole sample. The addition of OvPOSS and OpPOSS nanofillers introduces high-density deep traps into PP, which could capture moving charges, forms a new potential barrier, reduces the injection of charges from the electrode, increases the volume resistivity of PP and improves the insulation performance of PP. However, at high temperature, especially at the transition point from 70 ℃ to 90 ℃, too high temperature gives electrons more energy, making it easier for electrons to break away from the bondage of deep traps and resulting in more reduction of DC breakdown strength of PP nanocomposites at high temperature. However, although the DC breakdown strength of nanocomposites is reduced from low temperature to high temperature, the addition of OvPOSS and OpPOSS nanofillers

could still improve the spherulite structure of PP, raise the crystallinity of PP and introduce deep traps with high density. Therefore, the POSS/PP nanocomposites could have higher DC breakdown strength compared with PP at high temperatures.

Table 6.3. The critical values and shaping factors of breakdown strength in the Weibull distribution

Samples	30℃		50℃		70℃		90℃	
	E_0 (kV/m)	β	E_0 (kV/m)	β	E_0 (kV/m)	β	E_0 (kV/m)	β
Pure PP	440.1	11.1	410.0	10.5	373.9	9.9	335.1	10.2
OvPOSS-0.5phr	554.9	11.8	539.5	11.7	482.1	11.6	412.7	9.5
OvPOSS-1.0phr	573.7	10.6	556.4	10.5	503.7	11.6	436.1	11.0
OvPOSS-2.0phr	542.2	13.9	521.5	12.2	435.1	9.3	359.9	9.2
OpPOSS-0.5phr	527.6	9.3	511.1	11.2	460.2	11.7	406.4	10.8
OpPOSS-1.0phr	554.4	13.9	526.0	11.1	479.6	11.9	419.0	10.7
OpPOSS-2.0phr	585.9	11.1	557.5	11.9	551.7	11.4	447.2	10.1
OpPOSS-3.0phr	505.1	7.1	468.6	9.8	411.5	8.3	355.7	11.0

6.5 The space charge characteristics

6.5.1 The experimental setup

Because the use of pulse electro-acoustic (PEA) system to measure space charge at high temperatures will cause the damage of signal amplifier and the piezoelectric sensor (PVDF) would be expanded at high temperatures (over 70 ℃), the test temperature of

space charge is generally limited to 50 ℃. To measure the space charge characteristics of PP and its nanocomposites at high temperature, the amplifier needs to be taken out and placed in an external iron box, and the connection between the signal amplifier and PEA system is realized through copper. Also, the contact between the piezoelectric sensor and the bottom electrode should be adjusted.

In the space charge test at high temperature, the sample used is a film pattern with a thickness of 220 microns. Before the test, short circuit both ends of the sample to remove the surface charge. The samples will be tested for space charge in an electric field of 60 kV/mm and temperatures of 30 ℃, 50 ℃, 70 ℃ and 90 ℃. The polarization time is 40 min and the depolarization time is 20 min.

Before the space charge measurement, the pulse width of the high-voltage pulse source is adjusted to 6 ns, the frequency is adjusted to 10 kHz and the amplitude is adjusted to 800V. The sampling rate of the oscilloscope is adjusted to 2.5 Gs/s and the bandwidth is adjusted to 1GHz. The time resolution of PEA system is 1.0 s.

The test process is as follows:

i. Pure PP, OvPOSS/PP nanocomposites with 1.0 phr and OpPOSS/PP nanocomposites with 2.0 phr were selected as the tested samples for the space charge measurements.

ii. The contact surface between the sample and the electrode was covered with an appropriate amount of silicone oil to eliminate the air gap between the electrode and the sample.

iii. The upper surface of the sample was close contact with the upper electrode through a semi-conductive layer, and the lower surface of the sample was directly contacted with the lower electrode. The upper electrode was connected with the high-voltage DC power source, and the lower electrode was grounded.

iv. The temperature of PEA system was set to 30 ℃, 50 ℃, 70 ℃ and 90 ℃ and then waiting for 30 min until the temperature of the film sample reached the measuring temperature.

v. The DC electric field of the sample was set to 0 kV/mm and the high-voltage pulse source was turned on. Warming-up the PEA system and waiting for its stable operation of the PEA system.

vi. Finally, after the PEA system works stably, the collection of PEA signal was started during sample polarization and depolarization.

Each film sample was only allowed to be tested by once even they are not broken down. 5 samples from each group were selected for space charge test and only one typical result from each group of samples was selected as the basis for data analysis.

6.5.2 The result of PEA measurement

6.5.2.1 The space charge formation and electric field distribution in pure PP

Figure 6.8 below shows the space charge distribution and electric field distribution in the bulk of PP at different temperatures. At 30 ℃, pure PP has obvious negative charge injection near the cathode, and the homocharges injection depth near the cathode increases with the increase of polarization time. Due to the induction effect of cathode injection charge, the positive charge peak near the anode increases slightly, but there is no obvious positive charge injection. At 50 ℃, the homocharges injection near the cathode increases slightly, but there is an obvious space charge injection near the anode. In addition, there is no injection and accumulation of heterocharges in the whole pure pp. when the temperature rises to 70 ℃, heterocharges begin to appear in pure PP and gradually accumulates near the cathode with the increase of polarization time, while there is not obvious heterocharges near the anode, but the injection depth of positive charge increases. When the temperature rises to 90 ℃, pure PP shows obvious

heterocharges injection near the cathode and increases with the increase of polarization time. There is not heterocharges accumulated near the anode of pure PP, but the injection depth of positive charges increases with the increase of polarization time under the temperature of 90 ℃.

When the temperature is 30 ℃, there is only homocharges injection from the cathode in pure PP and the charges injection is mainly injected electrons. When the temperature rises to 50 ℃ and above, heterocharges begin to appear near the cathode in the bulk of pure PP, and the positive charge injection depth at the anode also increases with the increase of temperature. Part of the heterocharge is due to the ionization of impurities in pure PP under the high temperatures and high electric fields, resulting in positive ion and electrons. Because the large size of ion products is not conducive to the movement in pure PP, they will accumulate locally. While the size of electron is much smaller than ion, so it is easier for electron to move in the film samples. There is an academic paper showing that the ionization of impurities will have an adverse impact on the electrical properties of polymers, especially the space charge characteristics, and then reduce the electrical properties of polymers [130]. Another part of the heterocharges is due to the directional movement of holes and electrons in the medium to the opposite electrode under the action of an electric field and accumulation at the electrode. At 50 ℃ and 70 ℃, the heterocharges of pure PP mainly comes from the hole and electron injection and movement. When the temperature rises to 90 ℃, the ionization of impurities might increase the heterocharges near the cathode in pure PP. The increase of temperature and polarizing time also promotes the directional movement of holes and electrons in pure PP. Moreover, the extraction of interfacial charge is limited by the interfacial barrier, which eventually leads to the accumulation of heterocharge more obvious with the increase of polarization time.

The electric field distribution at different temperatures is also shown in the Figure 6.8. It could be seen that with the increase of temperature, the electric field distortion

in pure PP is also increased due to the more and more serious accumulation of space charge, especially for the heterocharge injection and accumulation near cathode. It could be seen that the deep traps in PP are not sufficient to capture the space charges and to form the potential barrier to space charges from electrodes. Then, more positive charges accumulated near the cathode so that the electric field near cathode is increased and the electric field near the anode is reduced. Finally, the maximum electric field distortion coefficients of pure PP at 30, 50, 70 and 90 ℃ are 13.9 %, 12.0 %, 14.5 % and 24.3 %, respectively.

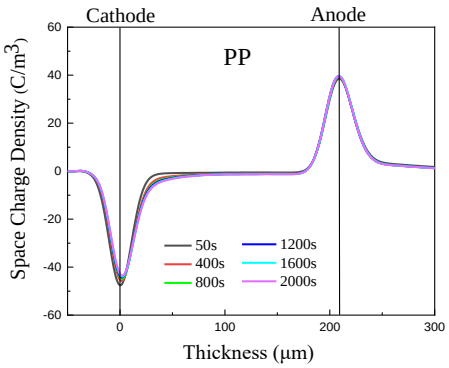

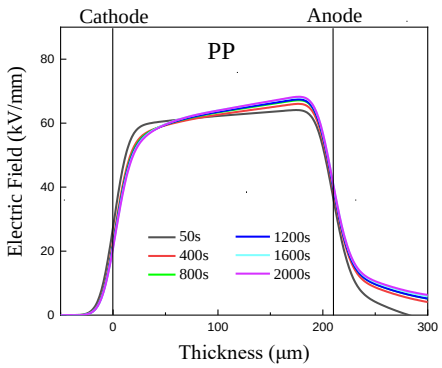

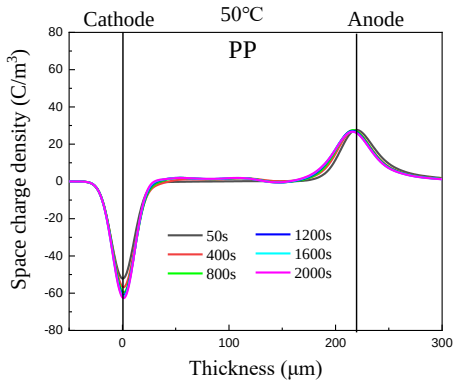

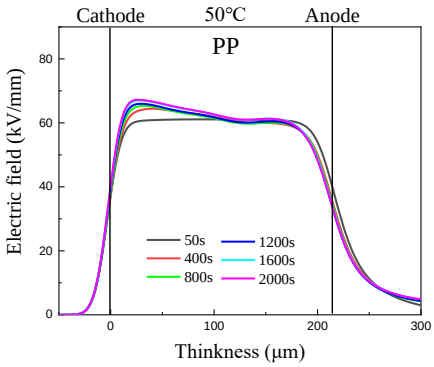

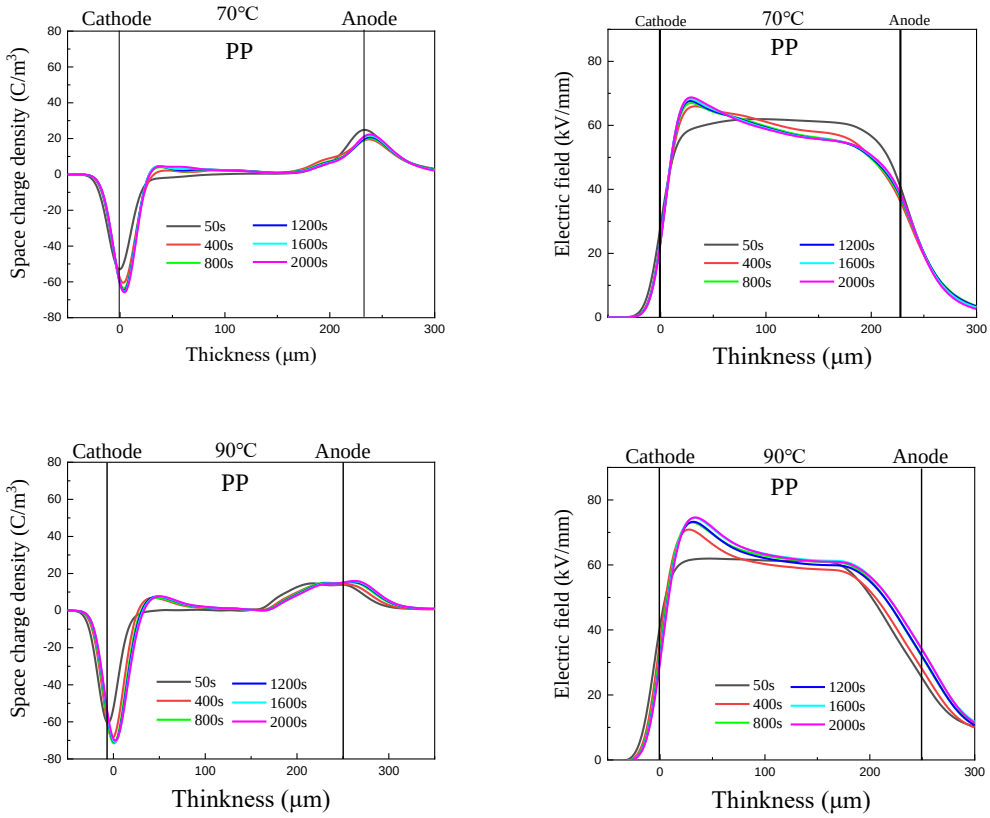

Figure 6.8. The space charge distribution and electric field distribution in the bulk of Pure PP under different temperatures

6.5.2.2 The space charge accumulation and electric field distribution in OvPOSS/PP nanocomposites

Figure 6.9 shows the space charge distribution and electric field distribution of OvPOSS/PP nanocomposites. When the temperature is 30 ℃, the space charge accumulation in OvPOSS/PP nanocomposites is inhibited, the electric field distortion is also reduced, and there is no obvious space charge injection. However, as the temperature increases to 50 ℃, the amount of negative charge injected from the cathode and the injection depth increase, while the depth of positive charge injected at the anode increases slightly, which leads to the increase of local electric field distortion coefficient in OvPOSS/PP nanocomposites. At this time, there is no obvious accumulation of heterocharges at the electrode. When the temperature rises to 70 ℃, the peak of

heterocharges appears at the cathode, resulting in the increase of local electric field at the cathode. The injection depth of positive charge at the anode is also increasing. When the temperature is 90 ℃, the accumulation of heteropolar charges in OvPOSS/PP nanocomposites increases significantly with the increase of polarization time. The charges at the anode and cathode induce higher charge peaks due to the accumulation of heterocharges, resulting in greater local electric field distortion.

As a result, the maximum electric field distortion coefficients of 1.0 phr OvPOSS/PP nanocomposites at 30 ℃, 50 ℃, 70 ℃ and 90 ℃ are 5.1 %, 10.3 %, 10.3 % and 19.6 % respectively. Compared with pure PP, the space charge accumulation and electric field distortion have been suppressed by the addition of OvPOSS nanofiller.

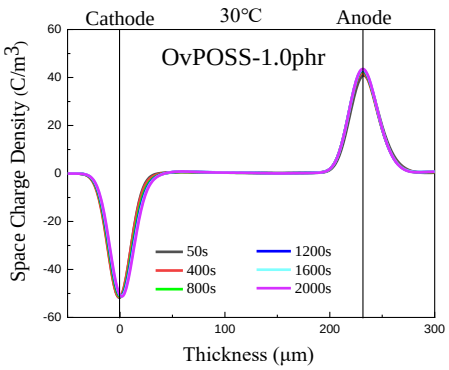

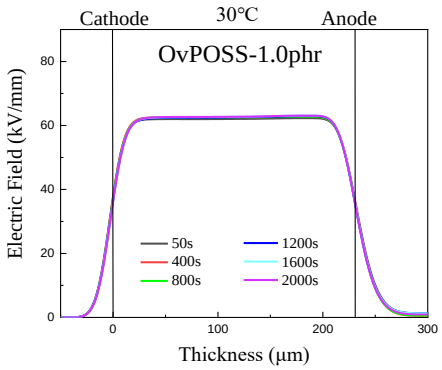

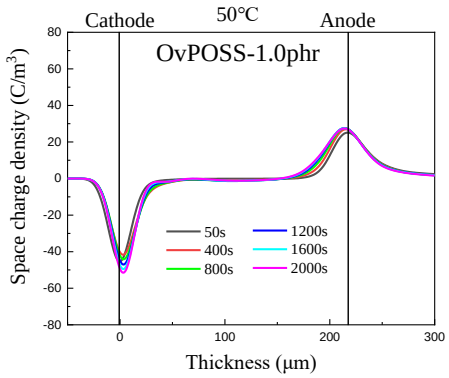

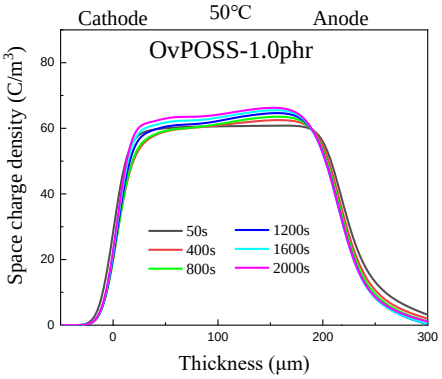

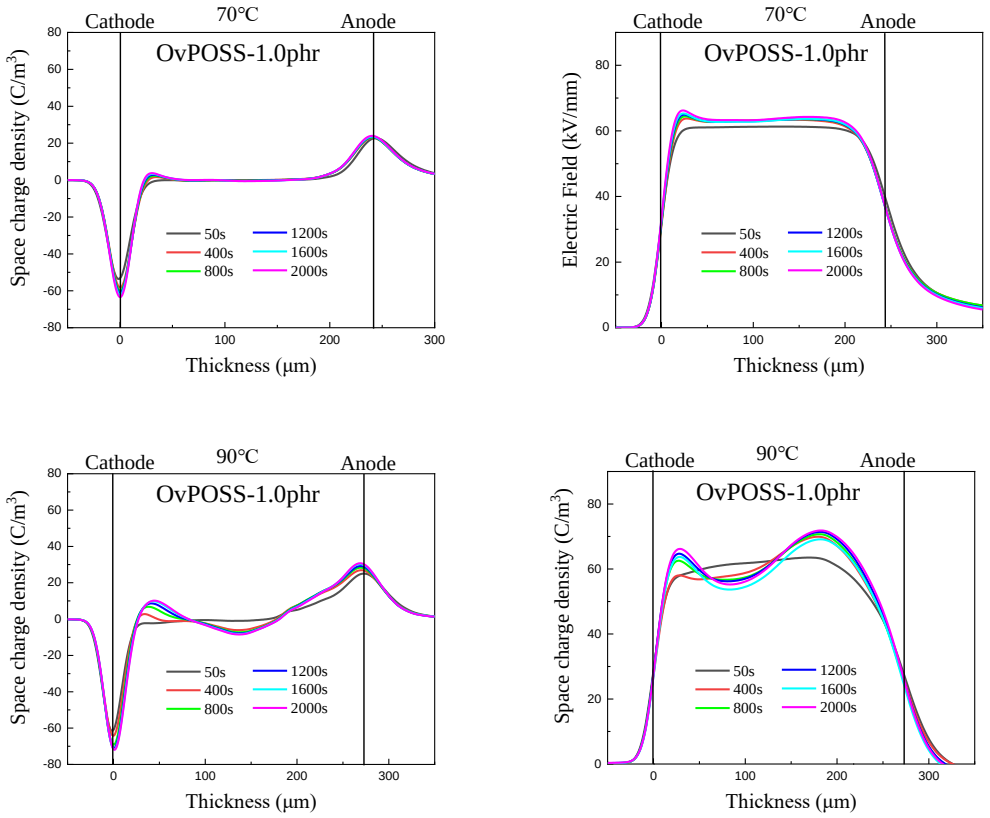

Figure 6.9 The space charge distribution and electric field distribution in the bulk of OvPOSS/PP nanocomposites under different temperatures

6.5.2.3 The space charge accumulation and electric field distribution in OpPOSS/PP nanocomposites

Figure 6.10 shows the space charge distribution and electric field distribution in OpPOSS/PP nanocomposites at different temperatures. 2.0 phr OpPOSS/PP nanocomposites has better space charge characteristics were obtained than pure PP and OvPOSS/PP nanocomposites. When the temperature is 30 ℃, there is almost no space charge injection into OpPOSS/PP nanocomposites. However, with the increase of polarization time, two peaks of charge accumulation near the electrodes increase slightly in the bulk of OpPOSS/PP nanocomposites. When the temperature rises to 50 ℃, the charge peak at the cathode increases slightly and the injection depth of homocharges near the anode increases. At this time, there is almost no heterocharges

injection in OpPOSS/PP nanocomposites. At the temperature of 70 ℃, the cathode of OpPOSS/PP nanocomposites has an obvious heterocharges accumulation, which increases continuously in the polarization process, and the injection depth of homocharges near the anode increases with the increase of polarization time. When the temperature rises to 90 ℃, there is a higher accumulation of heterocharge peaks near the cathode, and there is an obvious accumulation of positive and negative charges between 100 μm and 200 μm. Compared with the results in 30 ℃, 50 ℃ and 70 ℃, the homocharges injection near the anode is increased significantly at 90 ℃. Although the injection of heterocharges increases the local electric field distortion in OpPOSS/PP nanocomposites, the space charge characteristics of OpPOSS/PP nanocomposites are better than those of pure PP. In sum, with the increase of temperature, the improvement of space charge characteristics of PP by the addition of OpPOSS and OvPOSS would be reduced.

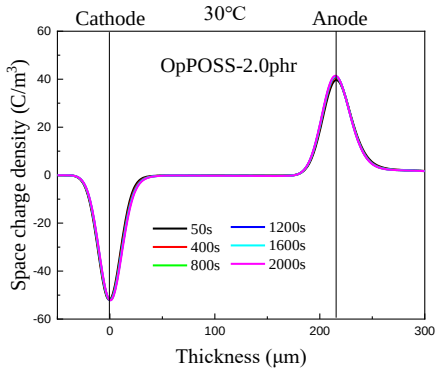

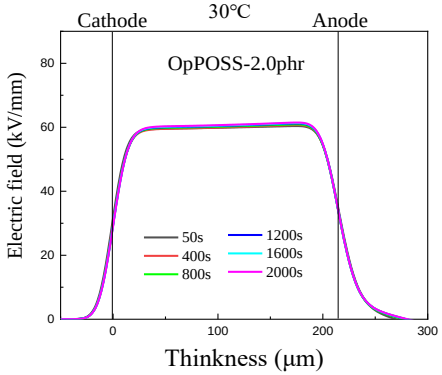

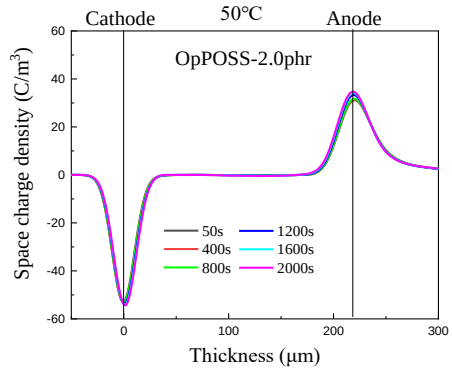

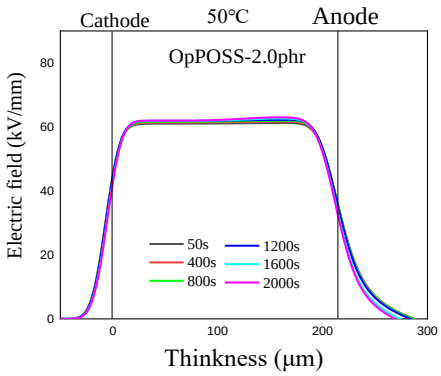

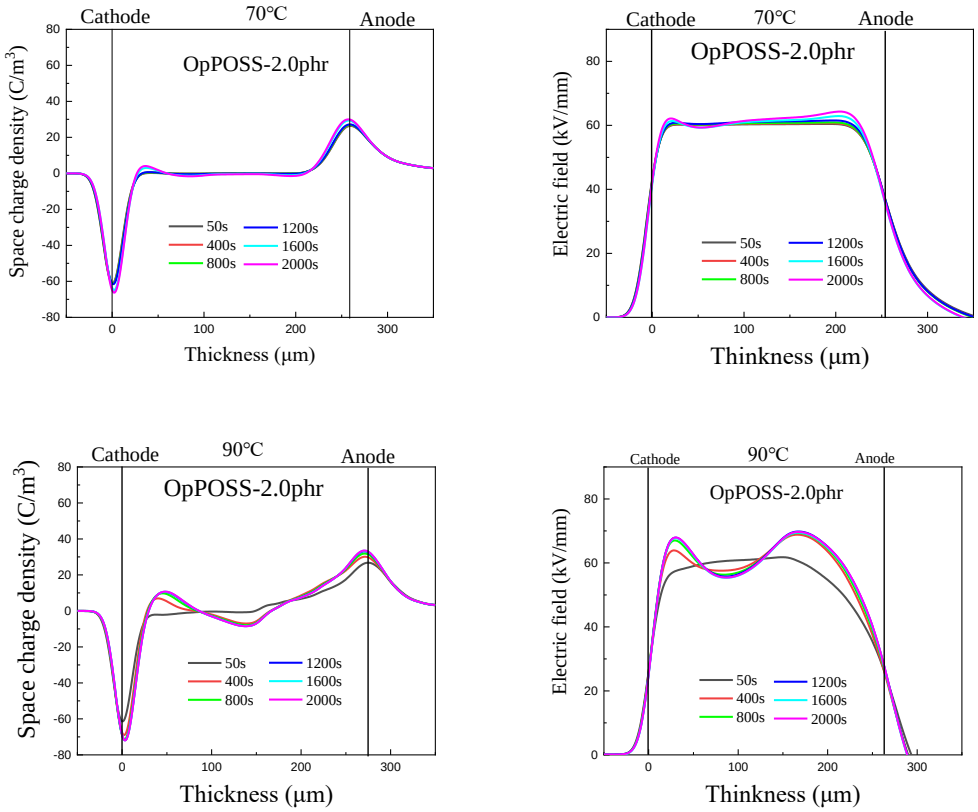

Figure 6.10 The space charge distribution and electric field distribution in the bulk of OpPOSS/PP nanocomposites under different temperatures

6.5.3 The mechanism of the electrical improvement of PP by OvPOSS and OPPOSS

As described in Chapter 4 , it can be seen from the observation results of POM and the test results of DSC that OvPOSS and OpPOSS nanofillers play the role of heterogeneous nucleating agent in the crystallization of PP, which can reduce the spherulite size of PP and increase the spherulite number of PP and the crystallinity of PP. Therefore, the electrical properties of PP are improved from the physical level. From the measurement results of thermal stimulation current, it could be seen that the addition of OvPOSS and OpPOSS nanofillers could introduce high-density deep traps in pure PP to capture the space charge injected from the electrode and generate a new potential barrier near the cathode to suppress the accumulation of space charge. In the

process of rising temperature, space charge can obtain more and more energy from the outside, resulting in the space charge escaping from the trap.

Through method 2 in [129], the measurement results of thermal stimulation depolarized current are transformed into the relationship between trap depth and trapping level density. Figure 6.11 shows the relationship between trap energy level and density according to TSDC test results. The TSDC peaks of pure PP are - 4 ℃ and 64 ℃, the corresponding trap energy levels are 0.75 eV and 0.92 eV, and the corresponding trap densities are 0.18×10^{17}/eV·m^3 and 0.45×10^{17}/eV·m^3, respectively. OvPOSS/PP nanocomposites with 1.0 phr OvPOSS has the best trapping characteristics in all contents. The TSDC peak of OpPOSS/PP nanocomposites appears at 96 ℃ and the peak value is 1.26 pA. The corresponding trap energy level is 1.01 eV and the trapping level density is 4.21×10^{17}/eV·m^3. OpPOSS/PP nanocomposites with the content of 2.0 phr has the best trapping characteristics among all OpPOSS/PP nanocomposites. The addition of 2.0 phr OpPOSS makes the two TSDC peaks of PP appear at 100 ℃ and 114 ℃ respectively, the corresponding trap energy levels are 1.02 eV and 1.1 eV, and the trapping level densities are 5.8×10^{17}/eV·m^3 and 3.4×10^{17}/eV·m^3, respectively.

Since the addition of 1.0 phr OvPOSS and 2.0 phr OpPOSS could introduce deep traps with the high energy level and maximum density, the electrical properties of PP, including conductivity, DC breakdown strength and space charge characteristics, could be improved. The influence of nanofillers on the trapping characteristics of PP is mainly reflected in the following aspects. Firstly, the heterogeneous nucleation of nanofiller could improve the crystallization behavior of PP and increase the crystallinity of PP. Secondly, the interface between nanofillers and PP would affect the trap energy level distribution. Thirdly, the electrostatic potential of chemical groups on the surface of nanofillers would affect the trap distribution of PP. Therefore, in the process of charge

transport, firstly, the charge would be captured by the deep trap in the interface region. Secondly, the moving charge would be captured by the groups on the nanofillers.

When the temperature is low, the charge injected at the electrode in PP nanocomposites would be captured by deep traps to form a new potential barrier, which inhibits the homocharges injection from electrodes. Therefore, there are no injection and accumulation of heterocharges. With the increase of temperature, more charges trapped by the deep trap obtains higher energy from the surroundings and have more opportunity to becomes a high-energy electron. This kind of electron has higher energy and it is easier for them to escape from the bondage of the deep trap. Therefore, with the increase of temperature, the improvement of the electrical properties of PP by the addition of OvPOSS and OpPOSS would be reduced. However, in actual cable operation, the electric field will be much lower than the threshold electric field. When the applied field is lower than the threshold electric field, only few charges would be trapped in the polymers and the electric field distortion would be low. In sum, even the temperature rise, the electrical properties of OvPOSS/PP and OpPOSS/PP nanocomposites will also be better than pure PP.

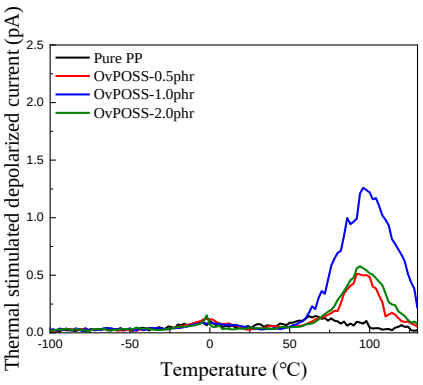

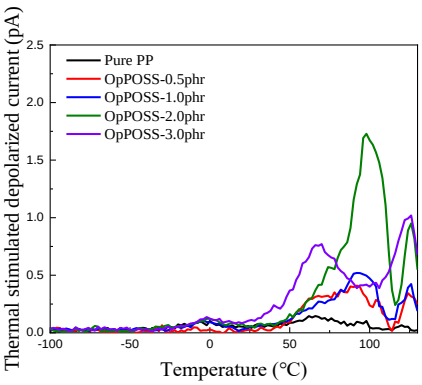

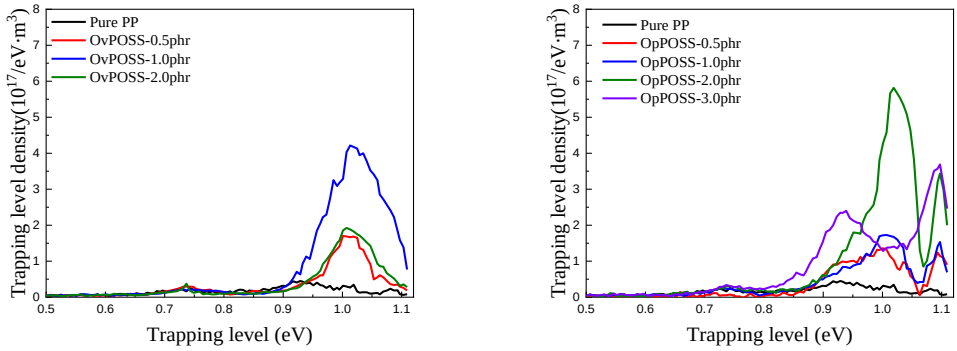

Figure 6.11 The trapping characteristics of PP and POSS/PP nanocomposites under different contents. TSDC measurement results and the trapping characteristics

6.6 The comparison between OvPOSS and OpPOSS

In this section, three parameters, including the high-electric-field (80 kV/mm) conductivity, the DC breakdown strength and the distortion of the electric field, of two nanocomposites under 90 ℃ will be compared in order to get the nanocomposite with the best electrical performance under HVDC conditions. These three parameters of nanocomposites have been shown in Table 6.4 below.

Table 6.4 Main electrical properties of PP, 1.0 phr OvPOSS/PP and 2.0 phr OpPOSS/PP at the temperature of 90℃

Samples	DC volume resistivity at 80 kV/mm (×10^{17} Ω·m)	DC breakdown strength (kV/mm)	The distortion of electric field (%)
Pure PP	0.65	335.2	24.3
1.0 phr OvPOSS/PP	3.91	436.1	19.6
2.0 phr OpPOSS/PP	4.32	442.8	16.2

The comparison result shows the best improvement of PP's electrical performance has been achieved by the addition of 2.0 phr OpPOSS nanofillers. Therefore, the

optimization of nanocomposites for the electrical performance at high temperature is 2.0 phr OpPOSS/PP nanocomposites. In chapter 7 and chapter 8, the aging characteristics of 2.0 phr OpPOSS/PP nanocomposites will be measured.

6.7 Conclusion

This chapter studies the electrical properties of two kinds of PP nanocomposites from 30 to 90 ℃, including OvPOSS/PP and OpPOSS/PP nanocomposites. The conductivity mechanism, DC breakdown strength and space charge characteristics of nanocomposites at different temperatures and high electric fields were investigated. Combined with the analysis of Chapter 4 and Chapter 5, through the influence of the addition of OvPOSS and OpPOSS nanofillers on the modification of spherulite structure and trapping characteristics of PP. This chapter explains how OvPOSS and OpPOSS could affects the high-temperature electrical properties of PP and provides the further optimization of PP's nanocomposites to tuning the electrical properties of PP under high temperatures and DC high voltage. Finally, the main conclusions of this chapter are as follows:

i. Because PP is a non-polar polymer, under the influence of external electric field, PP realizes its own polarization process through the shift of electrons in atoms. Therefore, the temperature change from 30 ℃ to 90 ℃ is not enough to change the dielectric constant of PP and its nanocomposites, which also shows that the interface between nanofillers and PP is not damaged by high temperatures.

ii. The addition of OvPOSS and OpPOSS nanofillers can obviously inhibit the DC conductive current of PP at high temperature. At 90 ℃ and 80 kV/mm DC electric field, OvPOSS and OpPOSS could reduce the DC conductivity, current of pure PP from the 3879.2 PA to 642.1 pa and 581.2 pa respectively, which means that the bulk resistance of pure PP is increased to 6.2 times and 6.7 times respectively.

iii. The conductivity characteristics of PP and its nanocomposites accord with the theoretical model of space charge limited current. When the temperature increases from 30 ℃ to 90 ℃, the threshold electric field of space charge injection of pure PP decreases from 37.2 kV/mm to 22.3 kV/mm. The addition of OvPOSS and OpPOSS nanofillers could increase the threshold electric field of pure PP. The threshold electric fields of OvPOSS/PP nanocomposites with a content of 1.0 phr were 47.2 kV/mm and 38.2 kV/mm at 30 ℃ and 90 ℃, respectively, which increased by 26.9 % and 71.3 % compared with pure PP, respectively. While the threshold electric fields of OpPOSS/PP nanocomposites with a content of 2.0 phr were 47.4 kV/mm and 39.7 kV/mm at 30 ℃ and 90 ℃ respectively, which increased by 27.4 % and 78.0 % compared with pure PP.

iv. At 90 ℃, the addition of OvPOSS and OpPOSS nanofillers can increase the DC breakdown strength of pure PP from 335.2 kV/mm to 436.1 kV/mm and 442.8 kV/mm, respectively, which means that the DC breakdown strength of PP is increased by 30.1 % and 32.2 % respectively.

v. The space charge accumulation in PP mainly comes from the charge injection from the electrode, especially from the cathode. When the temperature is low, the accumulation of space charge is mainly caused by the accumulation of homocharges. At higher temperature, the appearance of heterocharges would also aggravate the distortion of the electric field. The heterocharges mainly comes from the directional movement of the charge injected at the two poles under the action of an electric field, and secondly from the ionization of impurities under high temperature and high electric field. The addition of OvPOSS and OpPOSS nanofillers could suppress the electric field distortion in the bulk of PP under high temperatures and high electric field.

vi. Compared with pure PP, nanocomposites have higher electrical properties at high temperature, including lower DC conductivity, higher DC breakdown

strength and better space charge characteristics. First, the spherulite morphology and crystallinity of PP were improved by the addition of OvPOSS and OpPOSS nanofillers, so the free path of charge transport was reduced. Second, the addition of OvPOSS and OpPOSS nanofillers could introduce high-density deep traps into PP to capture the charge injected at the electrode to build a new potential barrier. The new potential barrier will produce an electric field opposite to the electric field at the electrode and inhibit the injection of homocharges. Therefore, both OvPOSS/PP and OpPOSS/PP have better space charge characteristics at different temperatures. Even under higher temperatures, the addition of OvPOSS and OpPOSS can still achieved better electrical properties in PP.

vii. By comparing the electrical properties of OvPOSS/PP and OpPOSS/PP at high temperature, it could be found that OpPOSS/PP nanocomposites with a content of 2.0 phr have the highest electrical properties.

7 The thermal-oxidation aging process of polypropylene's nanocomposites

7.1 Materials

Although the results before this chapter have shown that the addition of OpPOSS nanofiller could introduce deep traps into the bulk of PP, which can improve the electrical properties of PP at different temperatures. However, different from XLPE and LDPE, due to the existence of tertiary carbon, the hydrogen on the tertiary carbon atom of PP molecular chain is easy to react with oxygen at high temperature without the antioxidant, causing molecular chain fracture and material embrittlement, which reduces the electrical properties of PP [131]. Although the outer layer of the cable has a sheath to protect the insulating layer, the oxidation of PP molecular chain at high temperature will still occur when the sheath is damaged under external physical and chemical stress. Therefore, for PP and OpPOSS/PP nanocomposites with a content of 2.0 phr, whether the physical and chemical structure can be stable for a long time at high temperature has a great impact on their electrical and mechanical properties, but it is still unclear about the electrical performance of thermal oxidation aged PP and its nanocomposites. Hence, it is necessary to analyze the electrical and mechanical properties of PP and OpPOSS/PP nanocomposites under long-term high temperature conditions.

In this chapter, 100 μm and 200 μm films of pure PP and OpPOSS/PP nanocomposites with a content of 2.0 phr were prepared. The thermal oxygen aging process of PP and its nanocomposites was designed. FTIR was used to observe the formation of new chemical bonds during thermal oxygen aging. The mechanical and electrical properties of the samples were characterized by tensile strength tests, conductivity test, DC breakdown test and space charge test. Finally, the effects of OpPOSS nanofiller on the mechanical and electrical properties of aging samples by thermal-oxidation aging process were studied.

7.2 The experimental setup of thermal-oxidation aging process

In order to explore the mechanical and electrical properties of PP and its nanocomposites, this chapter would carry out thermal-oxidation aging process of PP and its nanocomposites at the temperature of 110 ℃.

The thicknesses of thermal-oxidation aged samples are 100 μm and 200 μm. 200 μm aged samples were used for the SEM observation and the tensile strength tests. The aging samples with the thickness of 100 μm were characterized by FTIR spectroscopy, DC breakdown test and DC conductivity test. The thermal-oxidation aging process was design as the Figure 7.1. Firstly, the sample will be placed in a vacuum oven at 60 ℃ for degassing treatment for 2 hours to remove the moisture on the material surface. Then, the samples were placed in a blast drying oven at 110 ℃ and taken out every 5 days. The surface of aged sample was wiped with alcohol to remove the impurities on the surface, and the aged samples were tested. PP and its OpPOSS/PP nanocomposites were labeled as PP-TA-0d, PP-TA-5d, PP-TA-0d, PP-TA-10d, PP-TA-15d, PP-TA-20d, PP-TA-25d, PP-TA-30d, OpPOSS-2.0phr-TA-0d, OpPOSS-2.0phr-TA-5d, OpPOSS-2.0phr-TA-10d, OpPOSS-2.0phr-TA-15d, OpPOSS-2.0phr-TA-20d, OpPOSS-2.0phr-TA-25d and OpPOSS-2.0phr-TA-30d,respectively.`

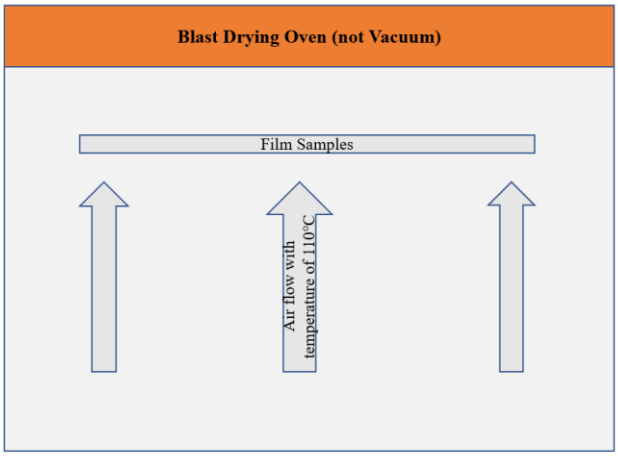

Figure 7.1 Schematic diagram of thermal-oxidation aging in the blast drying oven

7.3 The characterization of aged samples

7.3.1 Fourier transform infrared spectroscopy

The FTIR technique could be used to confirm the existence of the chemical group by the stretching vibration of the atoms in the group along the valence bond direction. Therefore, FTIR spectra could be used to detect whether the carbon atoms on PP molecular chains react with oxygen during the thermal-oxidation aging process.

The FTIR spectrum of PP and its nanocomposites before and after thermal-oxidation aging process are shown in Figure 7.4. In the unaged samples, the vibration peaks mainly exist at 2955, 2922, 2873, 2842, 1460, 1378 and 1167 cm^{-1}. The corresponding vibration forms of these peaks are shown in Table 7.1. After 5 days of thermal-oxidation aging process, new reflection peaks appeared at around 1720cm^{-1} in both composites, indicating that carbonyl groups were generated inside the materials [130]. The generation of carbonyl group indicates that the thermal oxygen aging reaction has taken place in the material, and its main process is shown in equation (11). Under the action of heat and oxygen, the molecular chain segment RH in PP is cracked to produce alkyl radicals R · and H·. The alkyl radical R · is very easy to react with oxygen in the air to produce alkyl peroxy radical ROO· and alkyl radical R·. The alkane peroxy radical ROO· has strong oxidizability and could capture the hydrogen atom in the molecular segment of PP to produce ROOH. The decomposition of ROOH produces alkoxy radical RO· and hydroxyl radical ·OH. In chain disproportionation of alkoxy radical RO· can form carbonyl, so the wavenumber of carbonyl can reflect the degree of thermal oxygen aging in the sample to a certain extent. Therefore, the infrared peak of carbonyl was also increasing with the increasing time of thermal-oxidation aging process. However, due to low resolution of FTIR spectroscopy could not be used to quantifies the products of thermal oxygen aging, but could be used to detect whether the oxidation reaction of PP occurs.

$$RH \xrightarrow{Break} R\bullet + \bullet H$$
$$R\bullet + O_2 \rightarrow ROO\bullet + \bullet R$$
$$ROO\bullet + RH \rightarrow ROOH + \bullet R \quad ----(11)$$
$$ROOH \rightarrow RO\bullet + \bullet OH$$

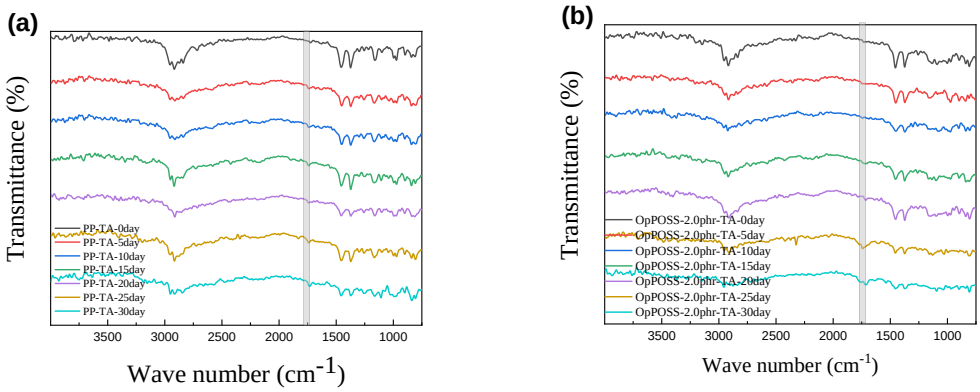

Figure 7.2 The FTIR spectrum of PP and OpPOSS/PP nanocomposites after the thermal-oxidation aging process

Table 7.1 Peaks of chemical groups in PP [132]

Wavenumber (cm^{-1})	Chemical groups
2955	CH_3 asymmetric stretching vibrations
2922	Main chain CH_2asymmetric stretching vibration
2873	CH_3symmetric stretching vibrations
2843	Main chainCH_2symmetric stretching vibration
1460	CH_3 asymmetric deformation vibrations or CH_2 scissor vibrations
1378	CH_3 symmetric deformation vibrations
1167	C-C asymmetric stretching, CH_3 asymmetric rocking and C-H wagging vibrations
998	CH_3 asymmetric rocking vibrations
974	CH_3 asymmetric rocking and C–C asymmetric stretching vibrations
901	CH_3 asymmetric rocking and C–C asymmetric and symmetric stretching vibrations
844	CH_2 rocking vibrations

810	CH_2 rocking vibrations

Table 7.2 New Peaks of chemical groups in aged PP

Wavenumber (cm^{-1})	Chemical groups
3300-3650	OH stretching vibrations
1738	The presence of carbonyl (C=O)

7.3.2 The results of tensile strength tests

The mechanical properties of PP at room temperature are an important parameter to measure the aging degree of PP. Due to aging, the molecular chain in PP will break, which will affect the mechanical properties of PP, especially the elongation at break. By comparing the mechanical properties of PP and its nanocomposites with different aging days, the influence of the aging process on the mechanical properties of PP and its nanocomposites was measured. The mechanical test process is described in Chapter 3.

Figure 7.3 is the stress-strain curve of PP and its nanocomposites after thermal-oxidation aging process at room temperature. The tensile process of all samples is the same as that of um-aged samples. All samples show elastic deformation before the deformation yield point. After the material yields, it begins to undergo plastic deformation, the deformed part turns white, and finally breaks.

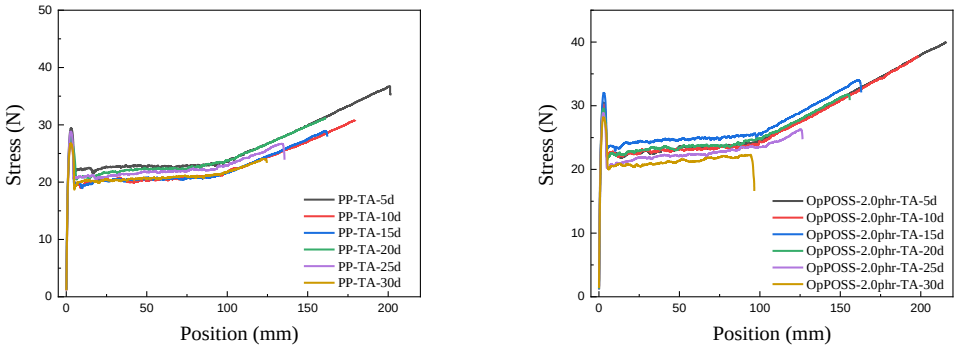

Figure 7.3. The mechanical property curves of PP and OpPOSS/PP nanocomposites after different days.

Figure 7.4 summarizes the mechanical property parameters of the samples after thermal-oxidation aging process, including tensile strength and elongation at break. With the increase of aging time, the tensile modulus and elongation at break of PP and OpPOSS/PP nanocomposites decreased. After 30 days of thermal-oxidation aging process, the tensile strength and elongation at break of PP were reduced to 33.4 MPa and 622.1 % respectively, while the tensile strength and elongation at break of OpPOSS/PP nanocomposites were only 32.6 MPa and 543.6 % respectively. In the longterm use of cable insulation, the degradation of mechanical properties wound damage the structure of insulating layer in the cable, cause electrical defects, and further reduce the insulation performance of the cable.

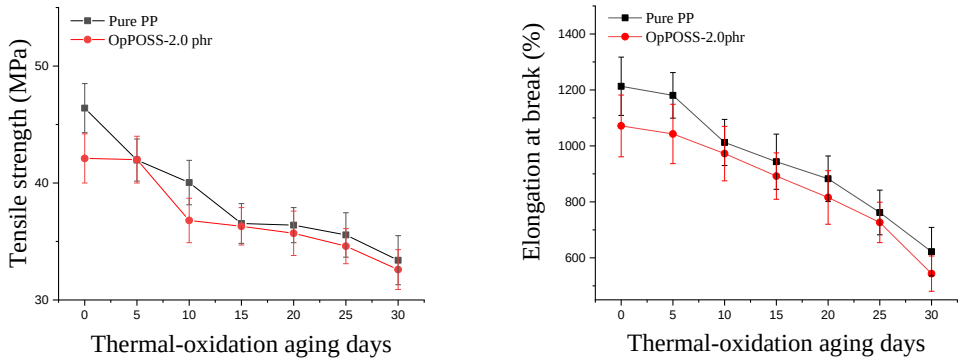

Figure 7.4 The parameters of aged PP and its nanocomposites for the tensile strength tests

7.3.3 DC breakdown strength tests

The DC breakdown test of aged PP and its nanocomposites will be carried out in the DC breakdown system shown in Figure 3.13. The temperature is set to 30 ℃ the thickness of the sample is controlled between 100 μm and 125 μm, and the DC voltage is linearly increased at the rising rate of 1 kV/s until the sample was broken down. Each sample was broken down at 20 points, and the experimental data are processed by Weibull distribution. Before the test, the temperature of DC breakdown test was raised

to 30 ℃, then the sample was placed between two spherical electrodes and the system should wait for 30 minutes until the internal temperature of the sample reach the test temperature. The DC breakdown strength of PP and OpPOSS/PP nanocomposites after the thermal-oxidation aging process in Weibull distribution are shown in Figure 7.5 and the parameters of breakdown strength are shown in Figure 7.6.

According to Figure 7.5 and Figure 7.6, with the increase of thermal-oxidation aging time, the DC breakdown strength of PP decreased continuously, and the degree of decline accelerated with the increase of aging time, especially for the aging time of 20 days. When the thermal-oxidation aging time was 30 days, the DC breakdown strength of PP decreased from 440.1 kV/mm to 318.9 kV/mm, with a decrease of 27.5 %. The DC breakdown strength of OpPOSS/PP nanocomposites is also decreased with the thermal-oxidation aging process. When the thermal-oxidation aging time is 30 days, the DC breakdown strength of OpPOSS/PP nanocomposites is decreased from 585.9 kV/mm to 335.3 kV/mm, with a decrease of 42.8 %. With the increase of thermal-oxidation aging time, the effect of OpPOSS addition on the DC breakdown strength of PP is decreased and the difference between the characteristic value E_0 of PP and OpPOSS/PP nanocomposites is reduced from 146.2 kV/mm to 16 kV/mm.

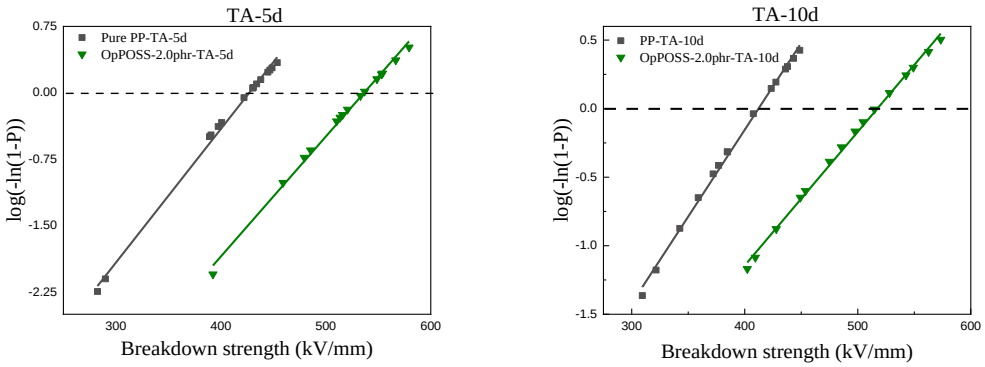

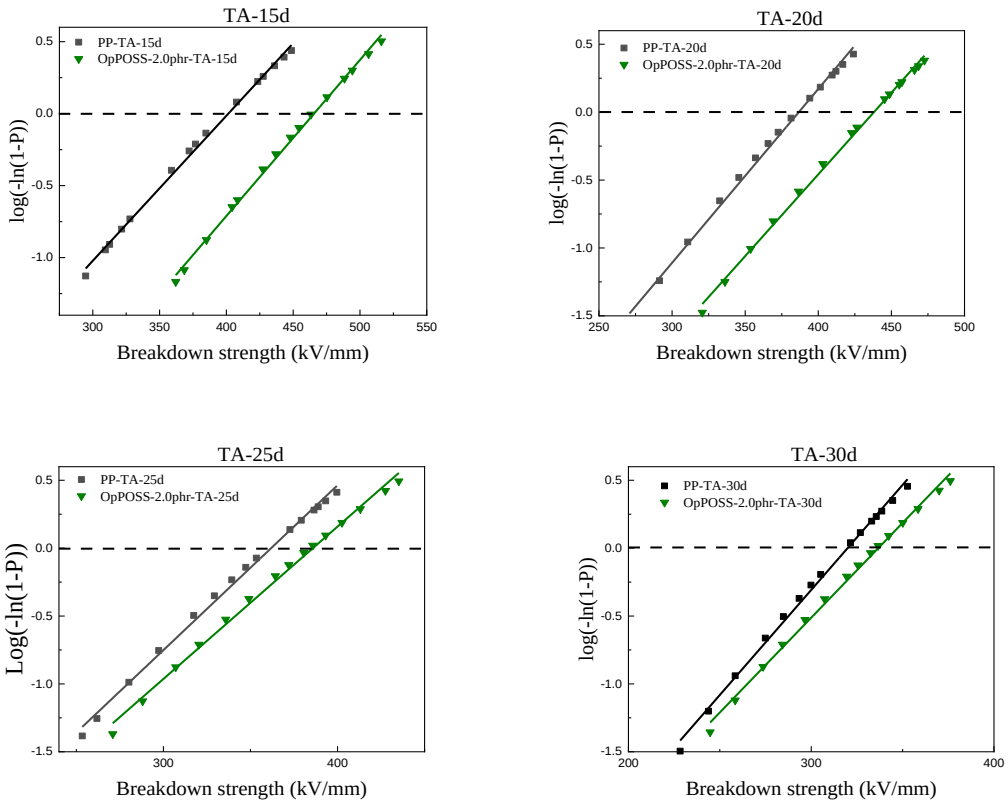

Figure 7.5 The DC breakdown strength of thermal-oxidation aged samples

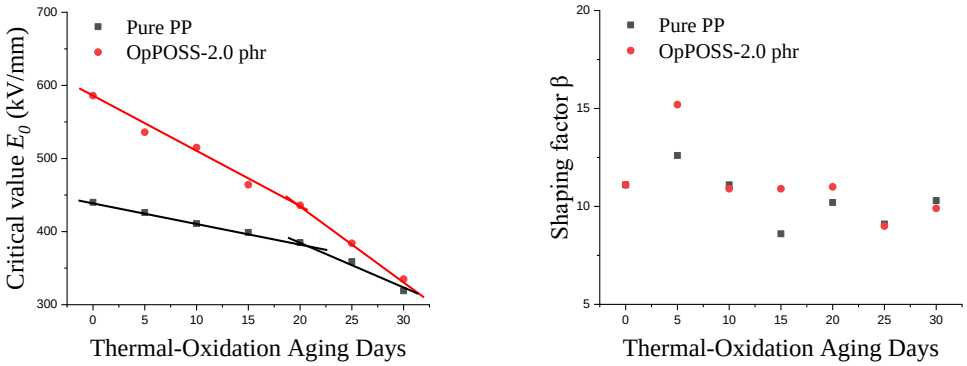

Figure 7.6 The Weibull parameters of breakdown strength of thermal-oxidation aged samples

7.3.4 DC conductivity measurements

The DC conductivity test system is shown in Figure 3.12 in Chapter 3. Aged samples with a thickness of 100 μm to 125 μm were selected for the conductivity tests. The test temperature was adjusted to 30 ℃. Before the test, the system should wait for 30

minutes until the internal temperature of the sample reaches the test temperature. The test electric field is from 5 kV/mm to 80 kV/mm with the increasing step of 5 kV/mm. The duration of each step was 600 s. The remaining operating procedures are described in the conductivity test in Chapter 5.

As figure 7.7 shown, the DC conductive current of PP and OpPOSS/PP nanocomposites under different electric fields increases with the increase of thermal-oxidation aging time, which means that the resistivity decreases with the increase of aging time. With the increase of thermal-oxidation aging time, the DC conductive current of PP and OpPOSS/PP nanocomposites under different electric fields increases, which means that the resistivity decreases with the increase of aging time. From 5 days to 15 days, the DC conductive current of aged samples increased slowly, and the resistivity of OpPOSS/PP was still higher than that of PP. When the aging time reaches 20 days, the DC conductance current of the aged samples increases significantly, and the inhibitory effect of OpPOSS on the DC conductivity of PP was decreased. When the aging time is 30 days, the conductivity of OpPOSS/PP increases to 75.4 % of that of PP, which is due to the long-term aging process, which damages the coupling between OpPOSS and PP. At the same time, as shown in Figure 7.8 and Figure 7.9, the threshold electric fields of PP and OpPOSS/PP were reduced to 33.3 kV/mm and 35.3 kV/mm respectively after 5-days aging time then increased to 42.0 kV/mm and 44.5 kV/mm from 5 days to 15 days.After 15 days, the threshold electric fields of PP and OpPOSS/PP were continued reduced to 27.9 kV/mm and 26.7 kV/mm.

In the beginning of thermal-oxidation aging process, thermal oxidation aging mainly occurs on the surface of PP. With the increase of thermal-oxidation aging time, the surface of PP would be damaged and small cracks would appear. The oxidation reaction at the crack would increase the damage depth in PP, resulting in the continuous decline of the electrical properties of PP. This is why the electrical performance of PP did not reduce much in before 15 days, but after 15 days, the electrical performance of PP is

decreased with the accelerating rate. In the process of oxidation reaction, the cracks caused by oxidation reaction would damage the coupling between PP and OpPOSS, resulting in the decline of OpPOSS' effect to regulate the electrical properties of PP.

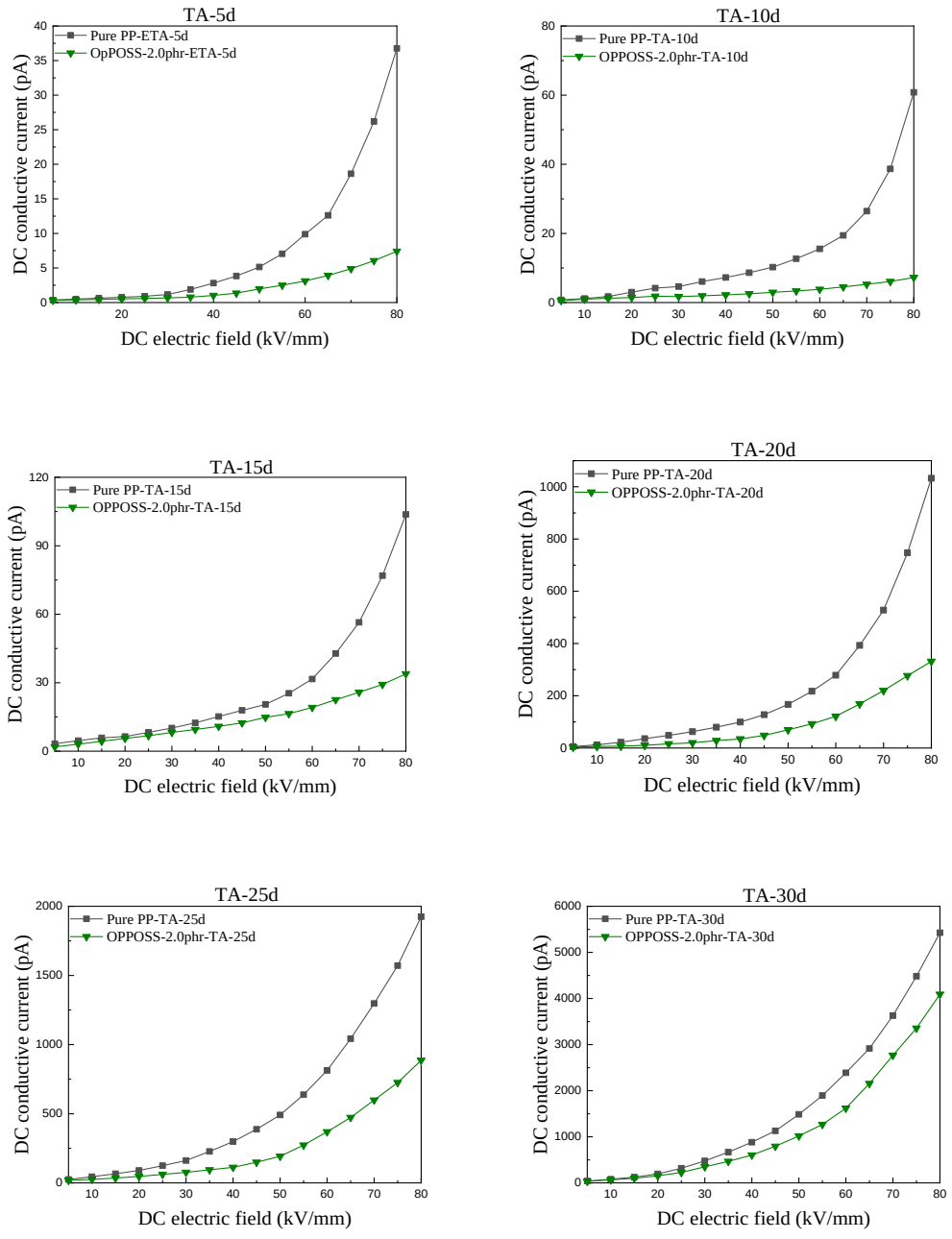

Figure 7.7 The DC conductivity of thermal-oxidation aged samples

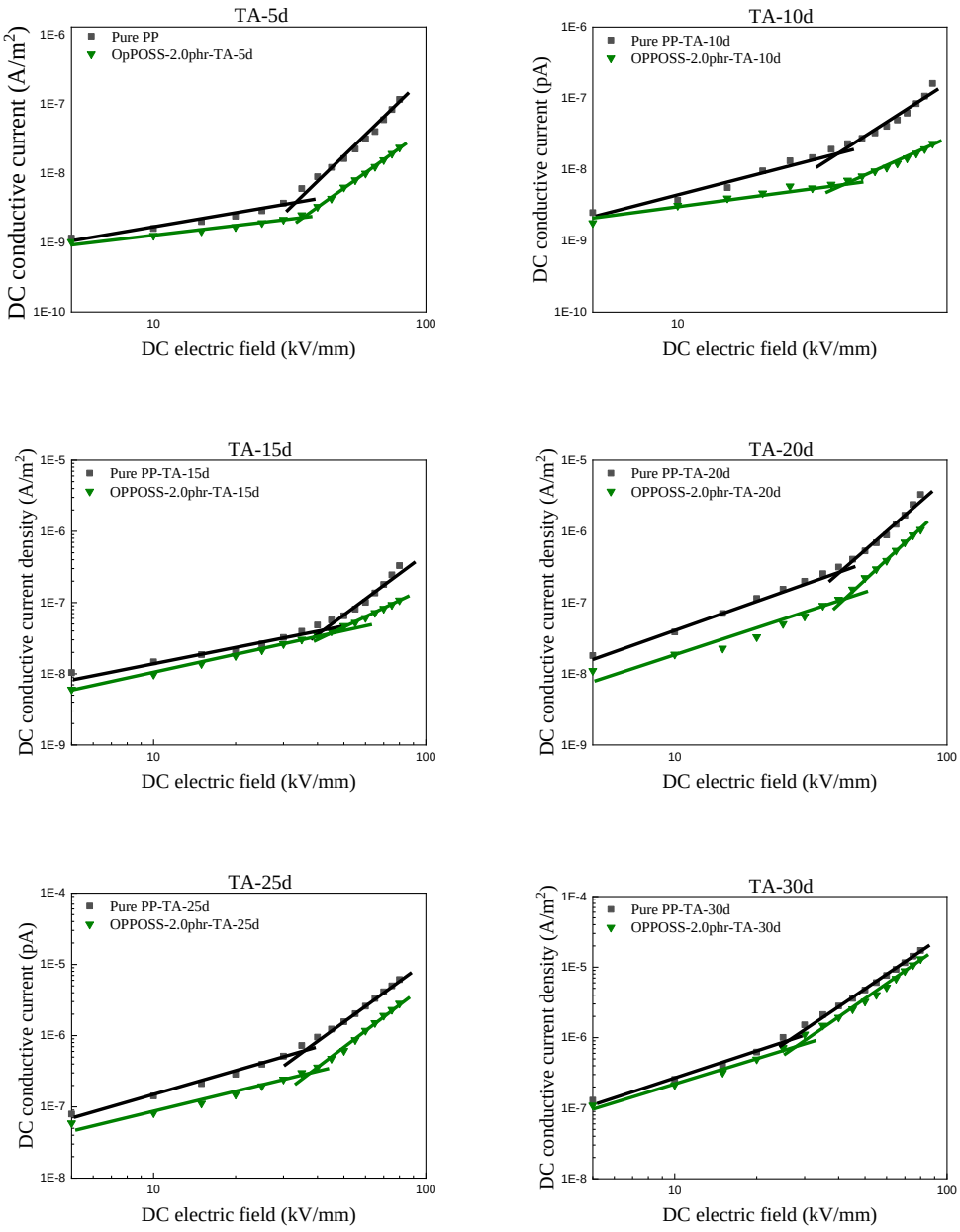

Figure 7.8 The DC conductive current density of thermal-oxidation aged samples in the logarithmic coordinates

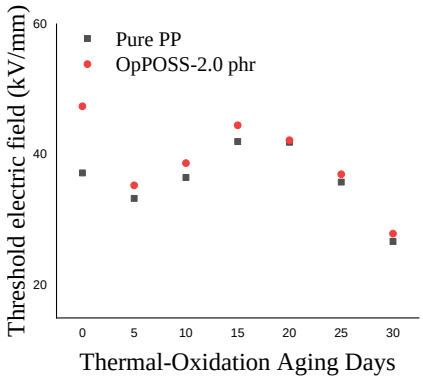

Figure 7.9 The threshold electric field of thermal-oxidation aged samples

7.3.5 Space charge measurements

The space charge test system is shown in Figure 3.14 in Chapter 3. Aged samples with a thickness of 180 μm to 250 μm were selected to the space charge measurement. In the space charge measurement, the electric field is set at 40 kV/mm and the test temperature is adjusted to 30 ℃. The other parameters and experimental procedure were the same as the space charge measurement in chapter 5. The space charge formation and the electric field distribution in PP and OpPOSS/PP nanocomposites after the thermal-oxidation aging process are shown in Figure 7.10 and Figure 7.11.

When the aging days are 5 days, there is a slight accumulation of heterocharges at the anode of PP, and the local electric field at the anode increases to 42.7 kV/mm. With the increase of aging time, the accumulation of heterocharges near the PP anode increases gradually, and the electric field at the anode also increases gradually. When the aging days are 5 days, there is a slight accumulation of heterocharges at the anode of PP, and the local electric field at the anode increases to 42.7 kV/mm. On the whole, with the increase of aging time, the accumulation of heterocharges near the anode of PP increases gradually, and the electric field also increases gradually. There is only slight homocharges injection near the cathode, and the electric field near the cathode decreases slightly. However, there is no obvious space charge accumulation in OpPOSS/PP nanocomposites, and the electric field distortion is less than 3 %,

indicating that although the sample aging is obvious, the addition of OpPOSS can still improve the space charge characteristics of PP under low electric field.

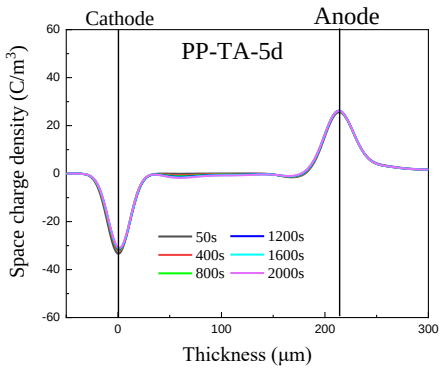

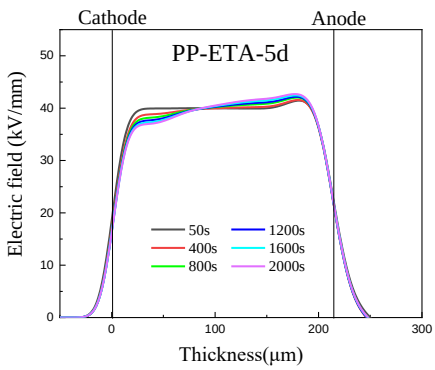

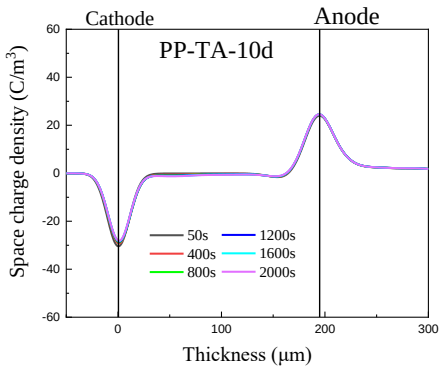

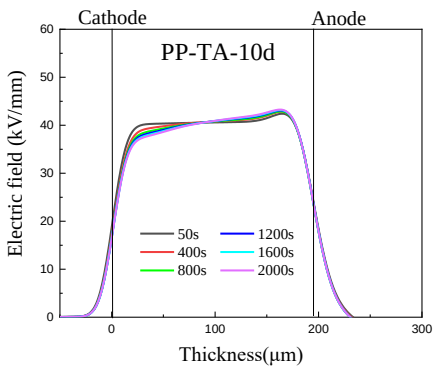

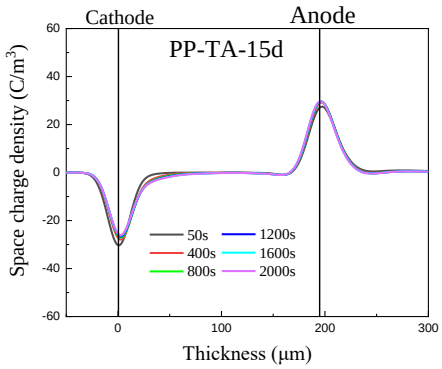

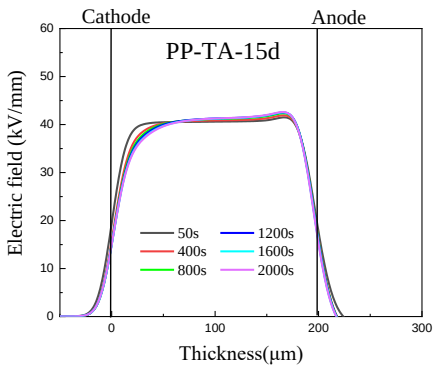

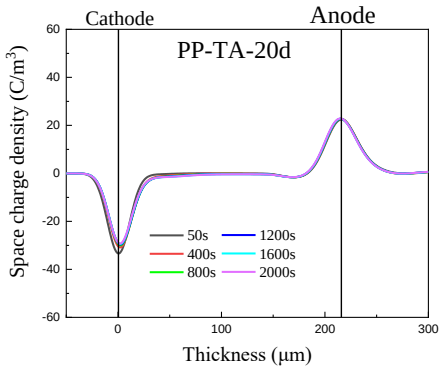
Cathode
Anode
PP-TA-20d
Space charge density (C/m3)
Thickness (μm)
50s
400s
800s
1200s
1600s
2000s

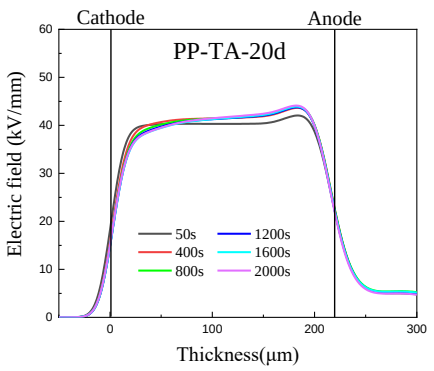
Cathode
Anode
PP-TA-20d
Electric field (kV/mm)
Thickness(μm)
50s
400s
800s
1200s
1600s
2000s

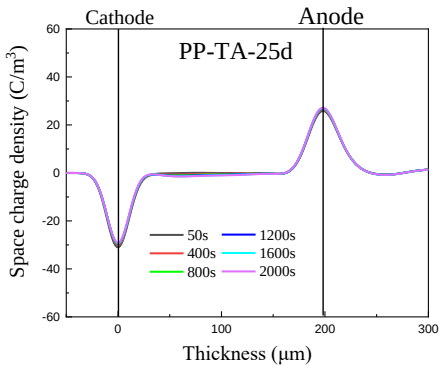
Cathode
Anode
PP-TA-25d
Space charge density (C/m3)
Thickness (μm)
50s
400s
800s
1200s
1600s
2000s

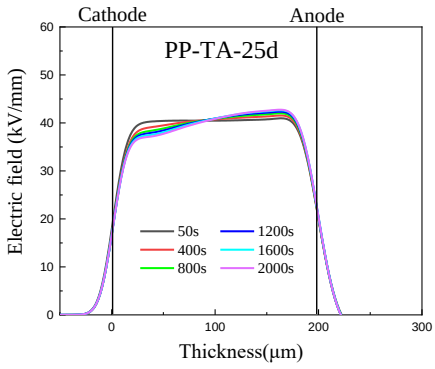
Cathode
Anode
PP-TA-25d
Electric field (kV/mm)
Thickness(μm)
50s
400s
800s
1200s
1600s
2000s

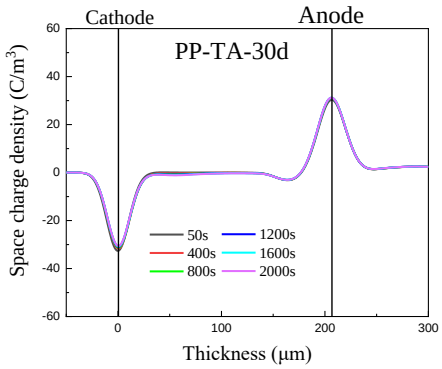
Cathode
Anode
PP-TA-30d
Space charge density (C/m3)
Thickness (μm)
50s
400s
800s
1200s
1600s
2000s

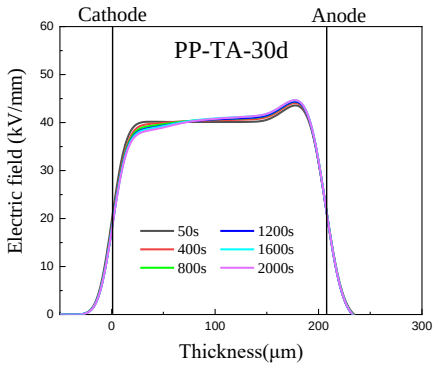
Cathode
Anode
PP-TA-30d
Electric field (kV/mm)
Thickness(μm)
50s
400s
800s
1200s
1600s
2000s

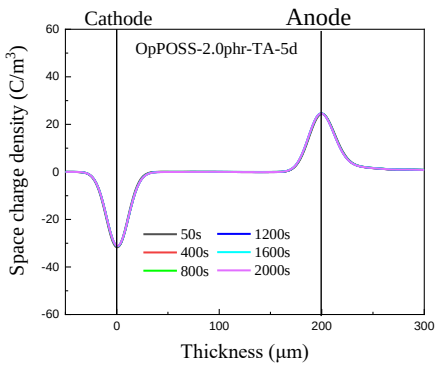
Cathode
Anode
OpPOSS-2.0phr-TA-5d
Space charge density (C/m3)
Thickness (μm)
50s
400s
800s
1200s
1600s
2000s

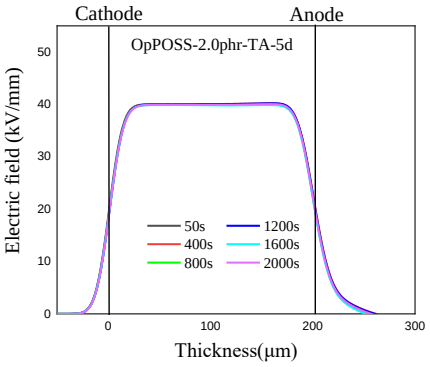
Cathode
Anode
OpPOSS-2.0phr-TA-5d
Electric field (kV/mm)
Thickness(μm)
50s
400s
800s
1200s
1600s
2000s

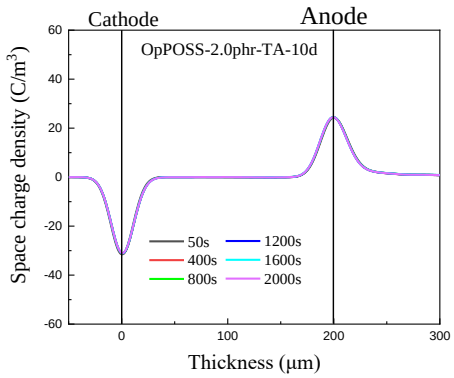
Cathode
Anode
OpPOSS-2.0phr-TA-10d
Space charge density (C/m3)
Thickness (μm)
50s
400s
800s
1200s
1600s
2000s

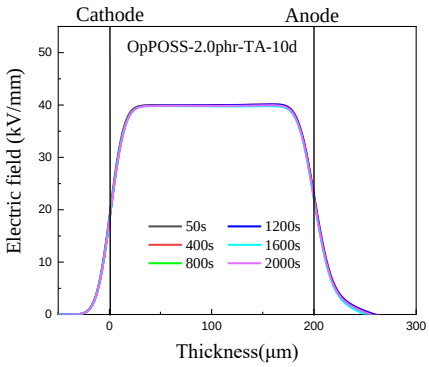
Cathode
Anode
OpPOSS-2.0phr-TA-10d
Electric field (kV/mm)
Thickness(μm)
50s
400s
800s
1200s
1600s
2000s

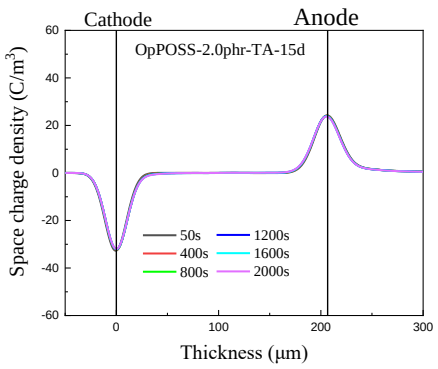
Cathode
Anode
OpPOSS-2.0phr-TA-15d
Space charge density (C/m3)
Thickness (μm)
50s
400s
800s
1200s
1600s
2000s

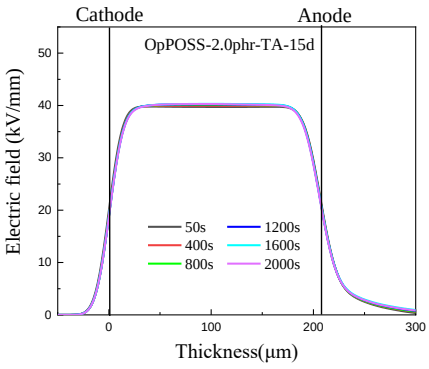
Cathode
Anode
OpPOSS-2.0phr-TA-15d
Electric field (kV/mm)
Thickness(μm)
50s
400s
800s
1200s
1600s
2000s

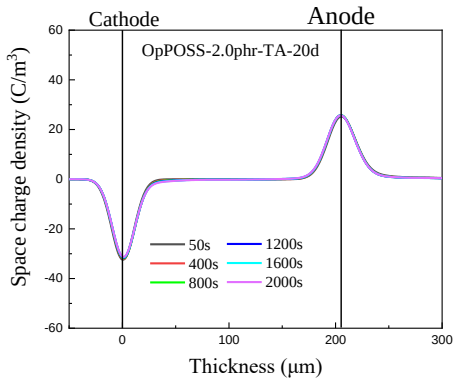
Cathode
Anode
OpPOSS-2.0phr-TA-20d
Space charge density (C/m3)
Thickness (μm)
50s
400s
800s
1200s
1600s
2000s

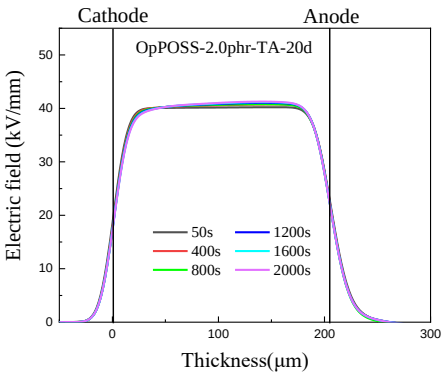
Cathode
Anode
OpPOSS-2.0phr-TA-20d
Electric field (kV/mm)
Thickness(μm)
50s
400s
800s
1200s
1600s
2000s

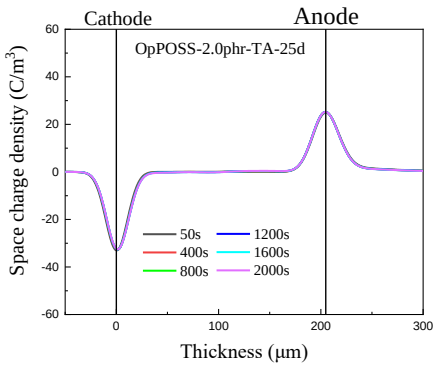
Cathode
Anode
OpPOSS-2.0phr-TA-25d
Space charge density (C/m3)
Thickness (μm)
50s
400s
800s
1200s
1600s
2000s

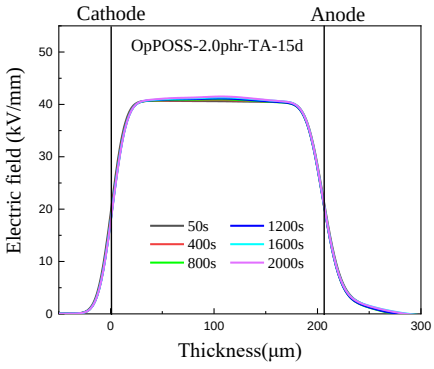
Cathode
Anode
OpPOSS-2.0phr-TA-15d
Electric field (kV/mm)
Thickness(μm)
50s
400s
800s
1200s
1600s
2000s

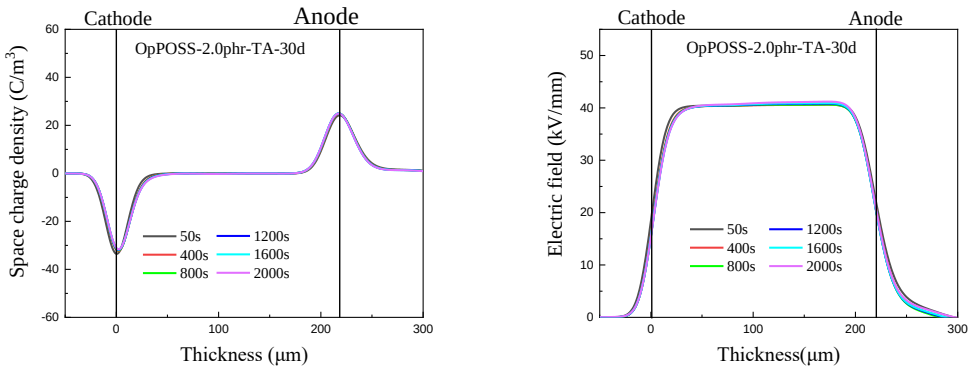

Figure 7.10 The space charge formation and the electric field distribution of thermal-oxidation aged samples

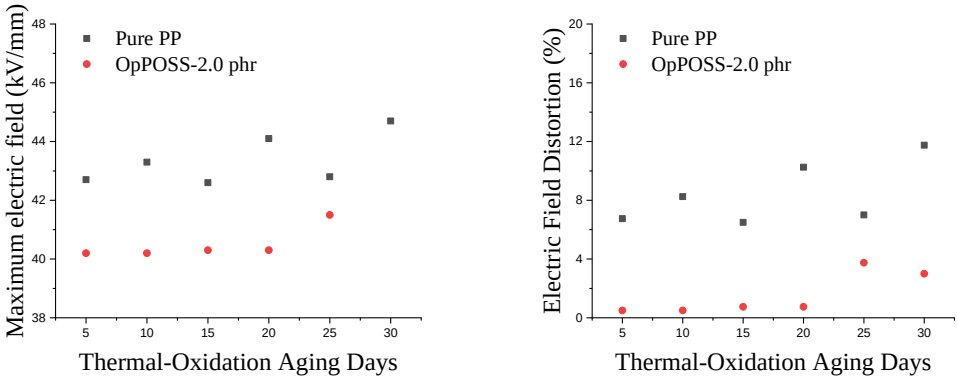

Figure 7.11 The maximum electric field distortion of thermal-oxidation aged samples

7.4 Conclusion

In this chapter, because OpPOSS/PP nanocomposites has the best electrical performance in all tested samples in previous chapters, PP and OpPOSS/PP nanocomposites with a content of 2.0 phr are selected as aged samples for the thermal-oxidation aging treatment and the thermal oxidation aging experimental process was designed. After the thermal-oxidation aging process, the microstructure morphology, FTIR spectrum , mechanical and electrical properties of PP and OpPOSS/PP nanocomposites before and after aging process were compared. The thermal oxygen aging process of the samples and the effect of the thermal-oxidation aging on the electrical properties of PP and OpPOSS/PP nanocomposites were further analyzed. Then, the mechanical and electrical properties of PP and OpPOSS/PP nanocomposites

after the aging process were compared to study the effect of OpPOSS addition on the electrical properties of thermal-oxidation aged samples. The main conclusions of this chapter are as follows:

i. Many papers reveal that there is a negative correlation between conductivity and trap level [38,43,58,67]. More deep traps mean lower the conductivity. The more shallow-traps mean the higher the conductivity. Therefore, thermal-oxidation aging weakens the trapping characteristics of PP and OpPOSS/PP nanocomposites. With the increase of thermal-oxidation aging time, the density of deep traps decreases gradually, while the density of shallow traps increases. Therefore, with the increase of aging time, the conductivity and the electric field distortion caused by space charge accumulation would be increased in the aged samples.

ii. After the thermal-oxidation aging process, the DC breakdown strength of aged samples decreased. In the thermal-oxidation aging process, the molecular chain fracture, the increase of cracks and the weakening of trapping characteristics in PP and OpPOSS/PP nanocomposites would produce the defects in the bulk of aged samples then lead to the decrease of DC breakdown strength.

iii. Compared with pure PP, the electrical properties of OpPOSS/PP nanocomposites are still high, indicating that the addition of OpPOSS still improves the electrical properties of aged PP. However, the addition of OpPOSS could not delay the aging process of the sample, and with the increase of aging time. With the extension of aging time, the spherulite structure of PP might be destroyed with the fracture of molecular chains, and the improvement of electrical properties of PP by OpPOSS is more reduced.

8 The electro-thermal aging process of polypropylene's nanocomposites

8.1 Materials

In the previous chapter, after the thermal-oxidation aging process of PP and OpPOSS/PP nanocomposites, it could be seen that with the increase of aging time, the molecular chains in PP and its nanocomposites begin to decompose due to the FTIR spectrum, and the mechanical and electrical properties are gradually decreased. The addition of OpPOSS could not delay the process of thermal oxygen aging, and the improvement of electrical properties of PP is becoming weaker and weaker with the increase of aging time. Although the thermal-oxidation aging characteristics of PP and OpPOSS/PP nanocomposites have been evaluated, it is more important to evaluate the operation state of PP and OpPOSS/PP nanocomposites at high temperature.

In this chapter, the long-term performance of PP and OpPOSS/PP nanocomposites would be evaluated by electro-thermal aging process. 100 μm and 200 μm films of PP and OpPOSS/PP nanocomposites with a content of 2.0 phr were prepared. The electro-thermal aging process of PP and OpPOSS/PP nanocomposites was designed. The microstructure and morphology of the samples were characterized by SEM to confirm the effect of electro-thermal aging process on the microstructure and morphology of pure PP and its nanocomposites. FTIR was used to observe the formation of new chemical bonds during thermal oxygen aging. The mechanical and electrical properties of the samples were characterized by tensile strength tests, conductivity tests, DC breakdown tests and space charge measurements. Finally, the effects of OpPOSS nanofillers on the mechanical and electrical properties of electro-thermal aging samples were studied.

8.2 The experimental setup of aging process

Generally, the operational temperature of DC cable would not exceed 70 ℃, and the electric field would not exceed 15 kV/mm. Also, Antioxidants are usually added into the insulating layer of DC cables to delay the aging process of the insulation material. In this chapter, the temperature of electro-thermal aging process was adjusted to 110 ℃, and the electric field was set to 30 kV/mm without the addition of antioxidants in order to accelerate the aging process of PP and OpPOSS/PP nanocomposites.

The thicknesses of electro-thermal aged samples are 100 μm and 200 μm. 200 μm aged samples were used for the SEM observation, the tensile strength test and the space charge measurement. The aged samples with the thickness of 100 μm were characterized by FTIR spectroscopy, DC breakdown test, TSDC measurement and DC conductivity test. The electro-thermal aging process of PP and OpPOSS/PP nanocomposites was carried out in the vacuum oven shown as the Figure 8.1.

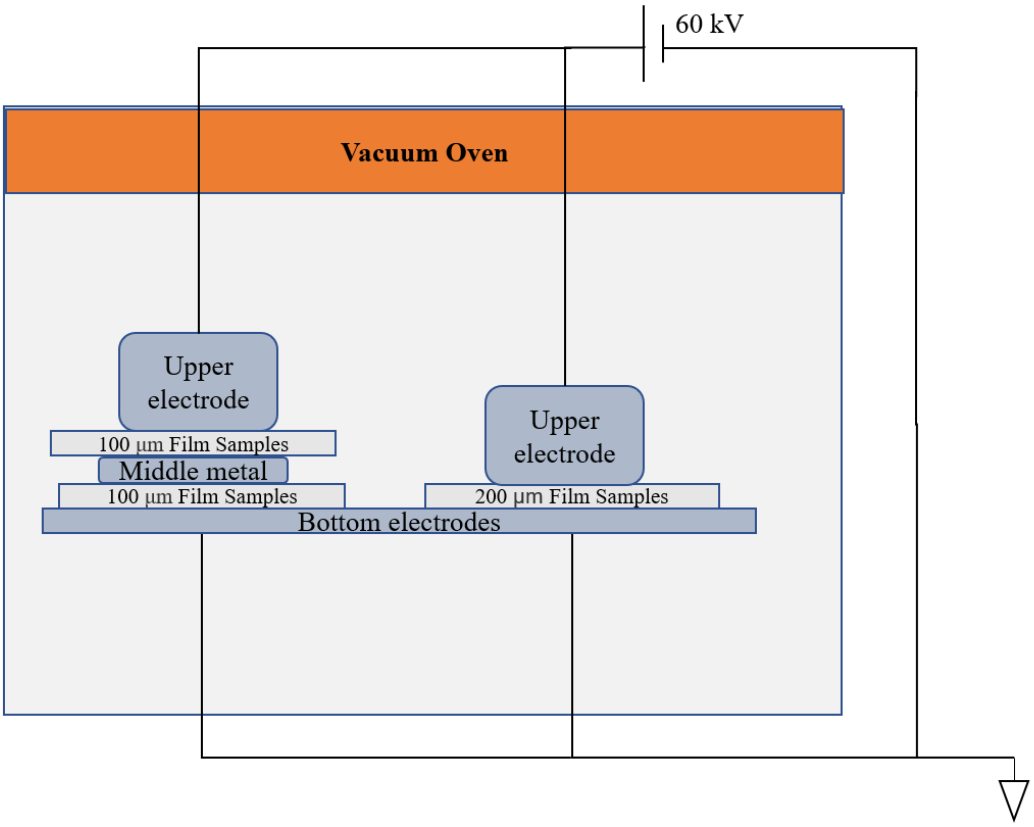

Figure 8.1 The experimental design of electro-thermal aging process for PP and OpPOSS/PP nanocomposites

Figure 8.2 The picture of electro-thermal aging process for PP and OpPOSS/PP nanocomposites

The high voltage DC source provided 60 kV DC voltage. The upper electrode block, the middle metal sheet and the lower electrode are all made of 304 steel plates. There are arc chamfers on the upper electrode and the middle metal sheet, so that the electric field distribution on the contact surface between the metal and the sample was more uniform. Before the electro-thermal aging process, the sample will be placed in a vacuum oven at 60 ℃ for degassing treatment for 2 hours to remove the moisture on

the material surface. The 200 μm sample is placed between the upper electrode and the bottom electrode metal plate. After the metal sheet was placed between two 100 μm samples to build the sandwich structure which would be placed between the upper and bottom electrodes as shown in Figure 8.1. Therefore, the applied electric field in each sample was about 30 kV/mm. There was not air flow in the vacuum oven. Those samples were taken out every 5 days. The surface of aged sample was wiped with alcohol to remove the impurities on the surface, and the aged samples were tested and measured for their characteristics. PP and its OpPOSS/PP nanocomposites were labeled as PP-ETA-0d, PP-ETA -5d, PP-ETA -0d, PP-ETA -10d, PP-ETA-15d, PP-ETA -20d, PP-ETA-25d, PP-ETA-30d, OpPOSS-2.0phr-ETA-0d, OpPOSS-2.0phr-ETA-5d, OpPOSS-2.0phr-ETA-10d, OpPOSS-2.0phr-ETA-15d, OpPOSS-2.0phr-ETA-20d, OpPOSS-2.0phr-ETA-25d and OpPOSS-2.0phr-ETA-30d, respectively.

8.3 The characterization of aged samples

8.3.1 The results of scanning electron microscope

As shown in Figure 8,3, cracks of different degrees appear on the surface of the aged samples after electro-thermal aging process. The surface microstructure and the OpPOSS nanofillers distribution of PP and 2.0 phr OpPOSS/PP nanocomposites after the treatment of electro-thermal aging process by different days were observed by SEM technique shown in Figure 8.3. The surface roughness of PP increased with the increase of electro-thermal aging time. Especially when the electro-thermal aging time reaches 15 days, obvious cavities begin to appear, and the deterioration of PP surface begins to become more serious with the increase of time. Although the cracks on the surface of OpPOSS/PP nanocomposites become more serious with the increase of electro-thermal aging time, the surface roughness and deterioration degree are lower than that of PP. Because PP and OpPOSS/PP nanocomposites are aged under normal temperature and pressure in a vacuum oven, and the upper and lower surfaces of the samples are covered by electrodes, the damage of the samples mainly comes from electrical damage. It can

be seen from Chapter 6 that the addition of OpPOSS can greatly improve the trapping characteristics of PP, and the introduction of high-density deep traps hinders the transport of charge in PP. Therefore, in the process of electro-thermal aging, the electrical damage of PP decreases by the addition of OpPOSS.

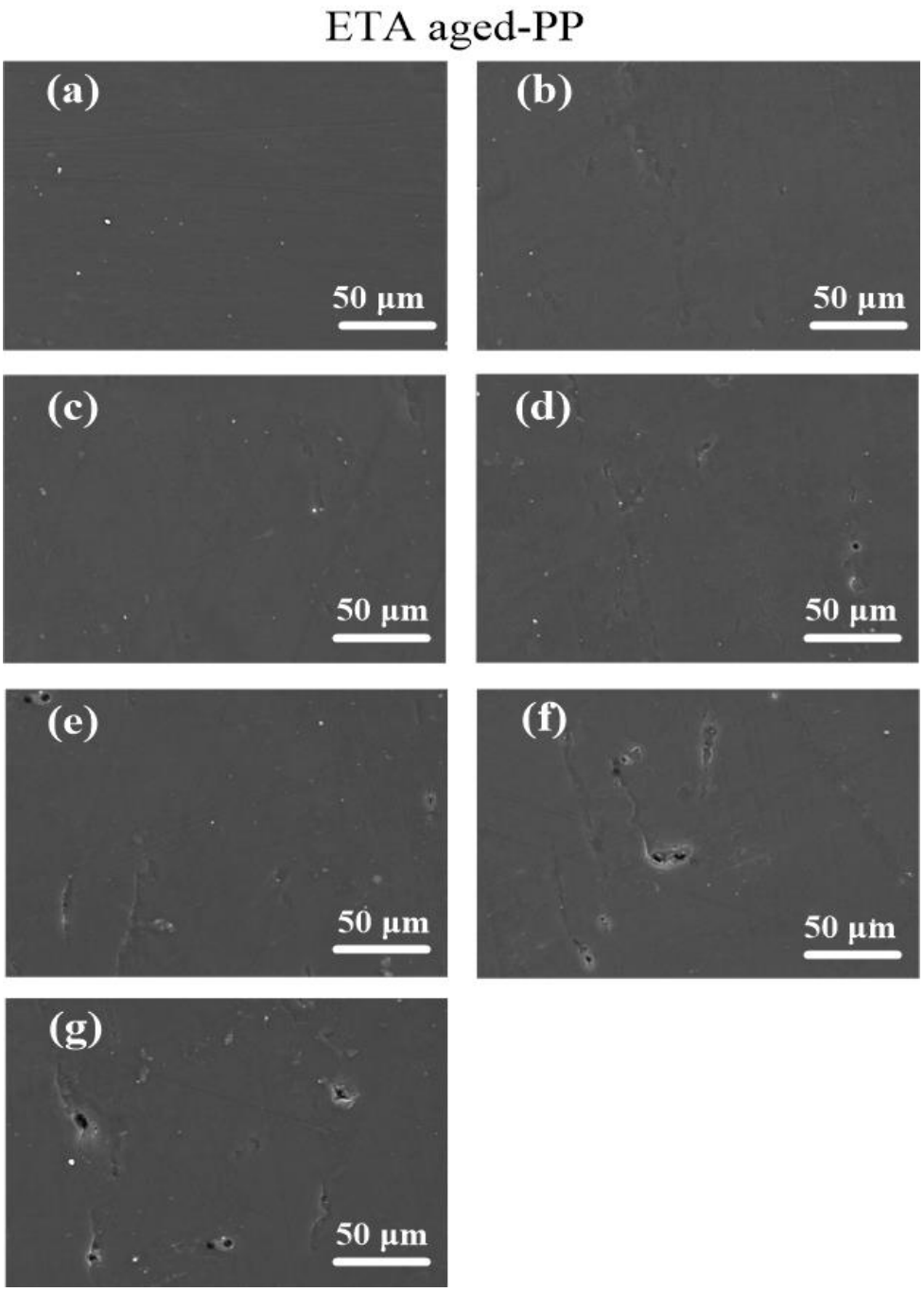

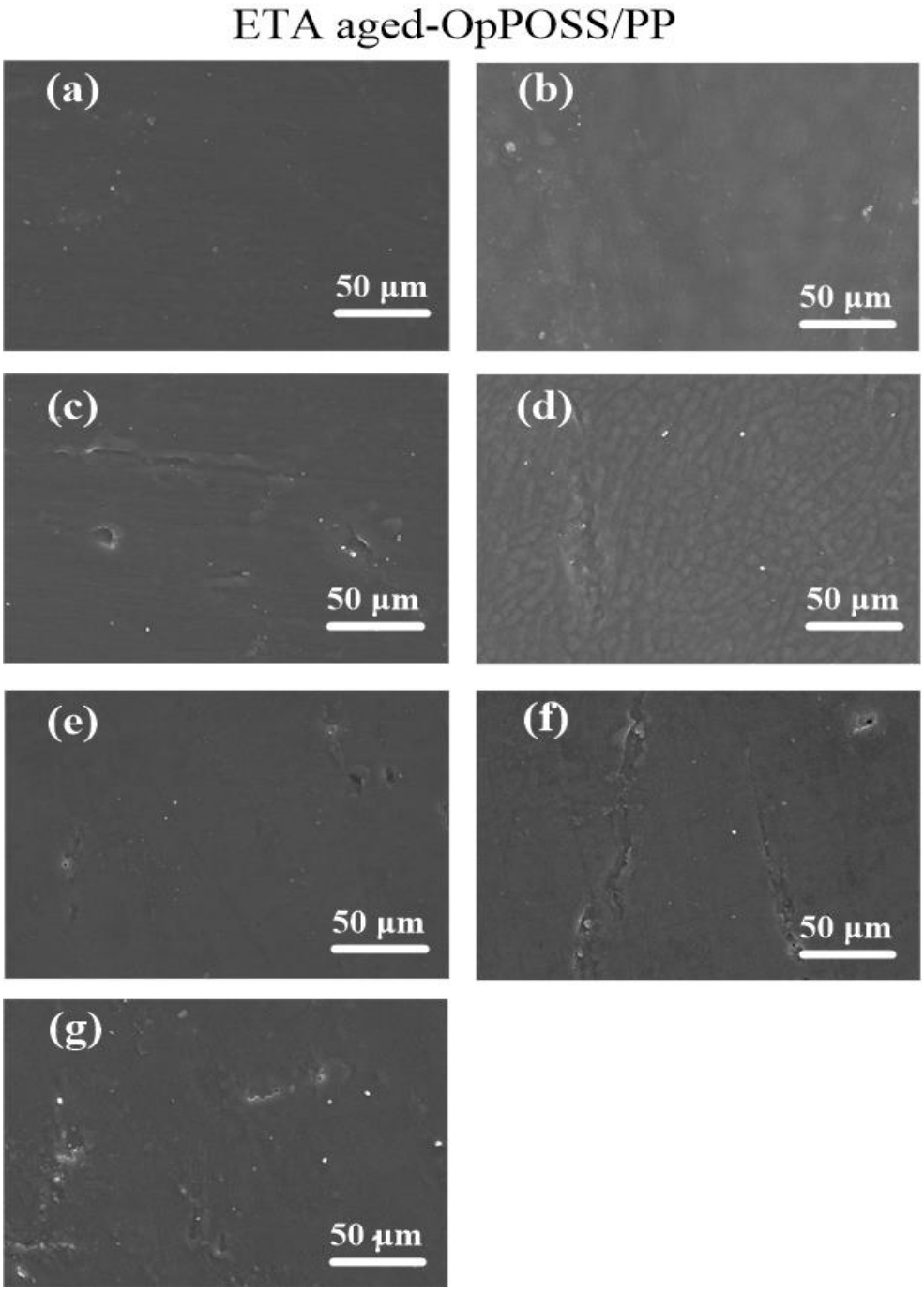

Figure 8.3. The surface microstructure of aged samples at different days(a) ETA-0day (b) ETA-5day (c) ETA-10day (d) ETA-15day (e) ETA-20day (f) ETA-25day and (g) ETA-30day

8.3.2 Fourier transform infrared spectroscopy

The FTIR spectrum of PP and its nanocomposites before and after thermal-oxidation aging process are shown in Figure 8.4. The FTIR spectrum of PP and its nanocomposites before and after thermal-oxidation aging process are shown in Figure 7.4. In the unaged samples, the vibration peaks mainly exist at 2955, 2922, 2873, 2842, 1460, 1378 and 1167 cm^{-1}. According to Table 7.1, after 5 days of electro-thermal aging process, a slight reflection peaks appeared at 1720cm^{-1} in PP and OpPOSS/PP nanocomposites, which means that the carbonyl groups were produced in the bulk of the samples and the reaction between oxygen and the molecular chains of PP still occurred. The chain reaction of free radicals shown by Eq. (11) also occurred in the samples. Although the oxygen content in the electro-thermal aging process is not as high as that in the thermal oxygen aging process, more electrons would obtain energy and might become hot electrons to bombard the molecular chain of PP under the electric field of 30 kV/mm and the high temperature of 110 ℃. After the molecular chain of PP broken, it was easy to react with residual oxygen in the oven, which eventually leads to the oxidation and degradation of PP. Therefore, the carbonyl group would be produced.

Since the addition of OpPOSS nanofillers could introduce high-density deep traps, more charges will be bound by deep traps. Compared with pure PP, the conductive current of OpPOSS/PP nanocomposites will be much smaller at the same electric field, so OpPOSS/PP would receive less electrical damage than pure PP. Because the electrical damage of molecular chain would be reduced, the production of carbonyl group would be reduced in OpPOSS/PP nanocomposites.

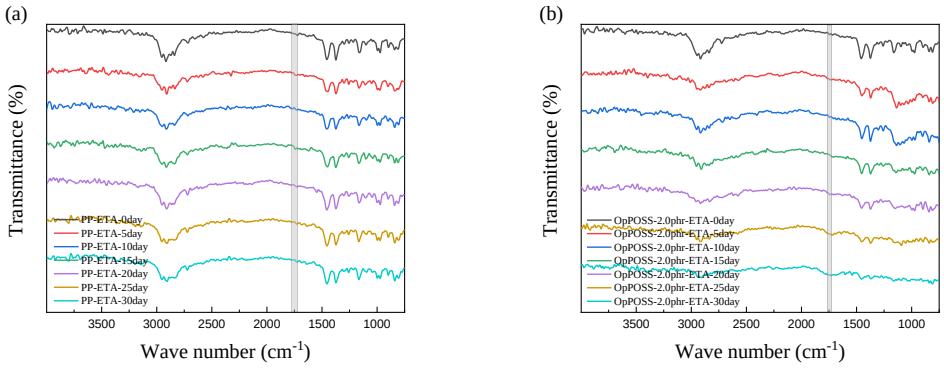

Figure 8.4 The FTIR spectrum of PP and OpPOSS/PP nanocomposites after the electro-thermal aging process

8.3.3 The results of tensile strength tests

The following Figure 8.5 shows the mechanical property curves of PP and OpPOSS/PP nanocomposites treated by the electro-thermal aging process for 0, 5, 10, 15, 20, 25 and 30 days.

The following Figure 8.5 shows the mechanical property curves of PP and OpPOSS/PP nanocomposites treated by the electro-thermal aging process for 0, 5, 10, 15, 20, 25 and 30 days. Figure 8.5 is the stress-strain curve of PP and its nanocomposites after electro-thermal aging process at room temperature. The tensile process of all samples is the same as that of un-aged samples and ETA-aged samples.

Figure 8.6 summarizes the mechanical property parameters of the samples after electro-thermal aging process, including tensile strength and elongation at break. With the increase of aging time, the tensile modulus and elongation at break of aged PP and aged OpPOSS/PP nanocomposites decreased. After 30 days of electro-thermal aging process, the elongation at break of aged PP was reduced to 741.6 % from 1213.1 %, while the elongation at break of aged OpPOSS/PP nanocomposites were reduced to 856.4 % from 1071.5 %. In the electro-thermal aging process, the degradation of mechanical properties was less than the thermal-oxidation aged samples because the

contact area between the sample and oxygen is much less in the electro-thermal aging process than the thermal-oxidation aging process.

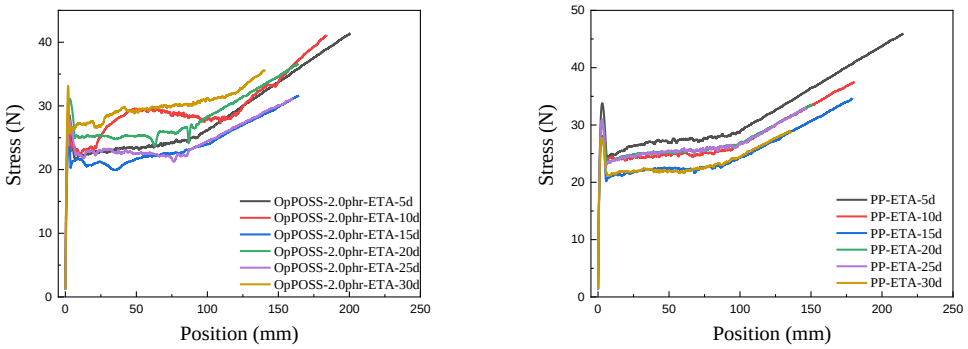

Figure 8.5. The mechanical property curves of PP and OpPOSS/PP nanocomposites after different days.

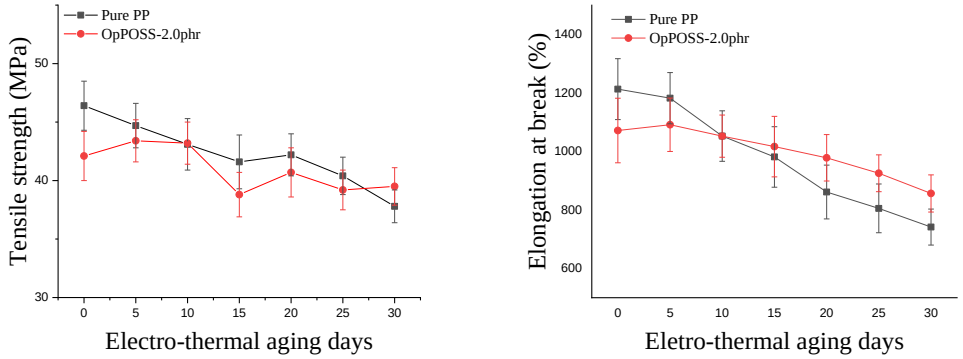

Figure 8.6 The parameters of aged PP and its nanocomposites for the tensile strength tests

8.3.4 DC Breakdown strength tests

The experimental procedure of DC breakdown test was carried out as last chapter and the data of DC breakdown strength would be demonstrated by the Weibull distribution. The DC breakdown strength of PP and OpPOSS/PP nanocomposites after the electro-thermal aging process in Weibull distribution are shown in Figure 8.7 and the parameters of breakdown test results are shown in Figure 8.8.

With the increase of electro-thermal aging time, the DC breakdown strength of PP is decreased continuously. When the electro-thermal aging time was 30 days, the DC

breakdown strength of PP decreased from 440.1 kV/mm to 330.9 kV/mm, with a decrease of 24.8 %. While the DC breakdown strength of OpPOSS/PP nanocomposites decreased from 585.9 kV/mm to 401.2 kV/mm, with a decrease of 31.6 %. With the electro-thermal aging process, the effect of OpPOSS on the DC breakdown strength of PP decreased. But compared with the thermal-oxidation aged samples, the degrading rate of electro-thermal aged samples is slower. The OpPOSS/PP can still improve the breakdown strength of PP from 331 kV/mm to 401 kV/mm by the increasing rate of 21.1 %. Combined with FTIR spectrum analysis, there is still the free radical chain reaction in the electro-thermal aging process destroys, so the chemical structure of PP would be still degraded significantly, which would reduce the electrical properties of PP, and degrades the coupling between OpPOSS and PP. But the addition of OpPOSS could still greatly improve the breakdown strength of PP.

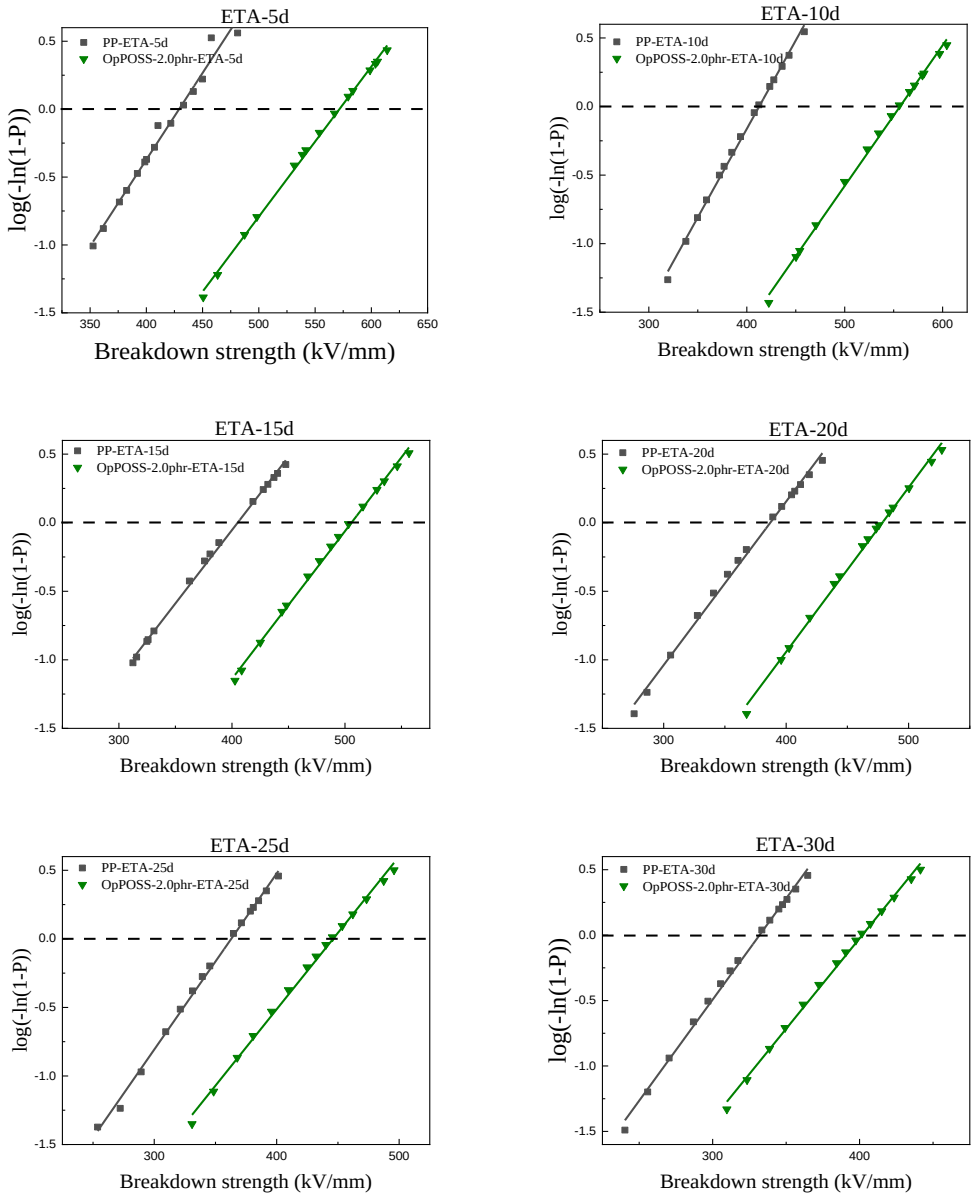

Figure 8.7 The DC breakdown strength of electro-thermal aged samples

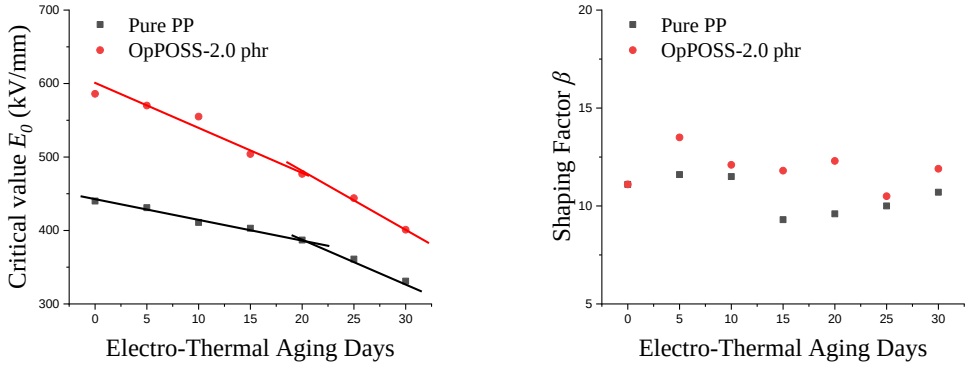

Figure 8.8 The Weibull parameters of breakdown strength of electro-thermal aged samples

8.3.5 DC conductivity testes

The experimental procedure of DC conductive test was carried out as chapter 7. As shown in Figure 8.9, the DC conductive current of PP and OpPOSS/PP nanocomposites under different electric fields is increased in the electro-thermal aging process, which means that the resistivity is decreased with the increase of aging time. When the electro-thermal aging time was 30 days, the conductivity of OpPOSS/PP is reduced to 22.6 % of that of pure PP. Compared with the samples aged by thermal-oxidation aging process, the suppression of DC conductive current of PP by the addition of OpPOSS is more obvious in the process of electro-thermal aging. The addition of OpPOSS improves the trap distribution of PP and introduces a large number of deep traps with the trapping level of 1.1 eV. Although OpPOSS nanocomposites would be degraded by the electro-thermal aging, the deep trap introduced by OpPOSS could still capture the homocharges injection from the electrode and further inhibit the charge transport in PP. Therefore, the electrical damage of PP in the process of electro-thermal aging is reduced and the coupling between OpPOSS and PP is protected.

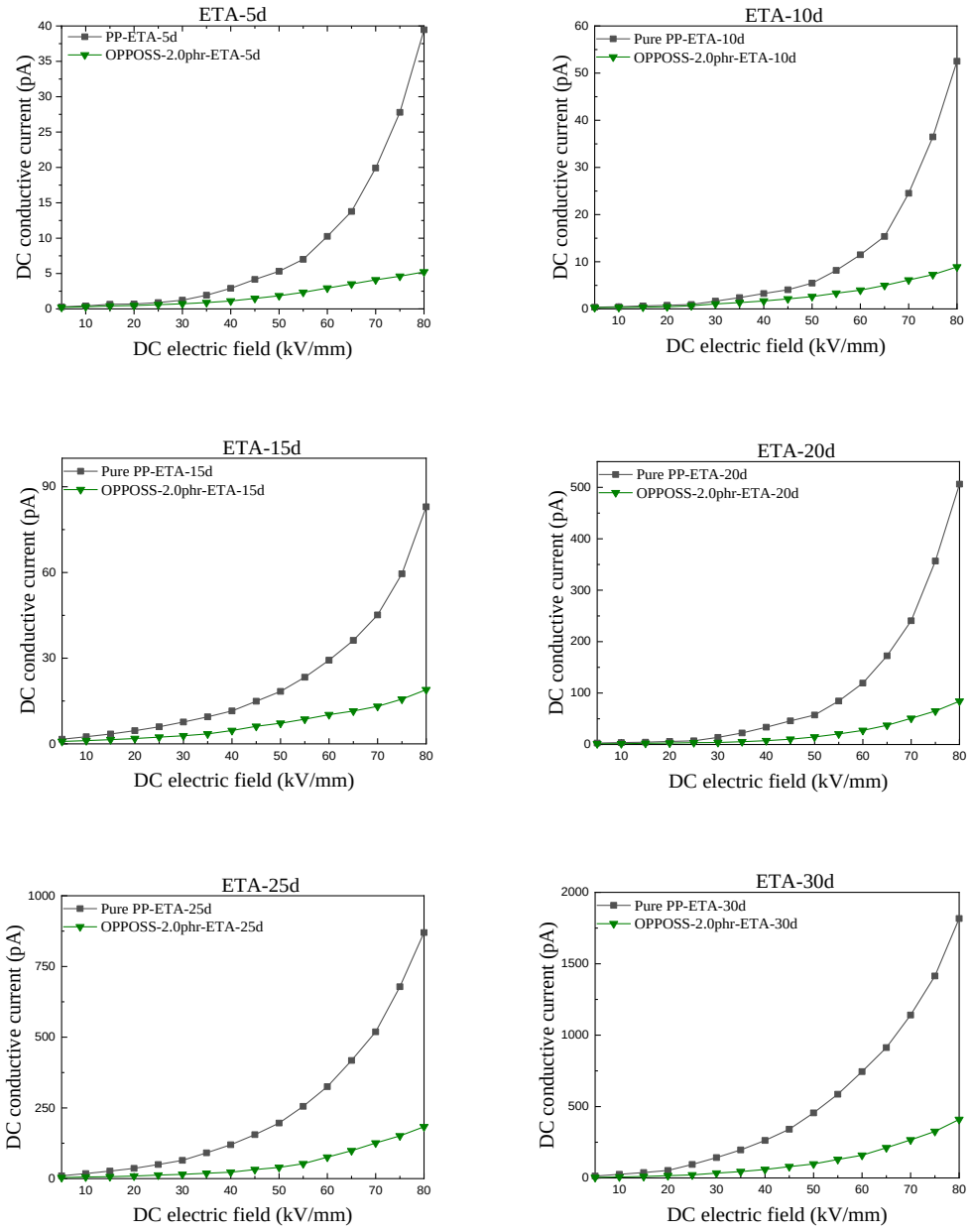

Figure 8.9 The DC conductivity of electro-thermal aged samples

At the same time, as shown in Figure 8.10 and Figure8.11, the effect of OpPOSS addition on the threshold electric field of PP continues to be reduced in the electro-thermal aging process. But the threshold electric field of PP is still increased by the addition of OpPOSS.

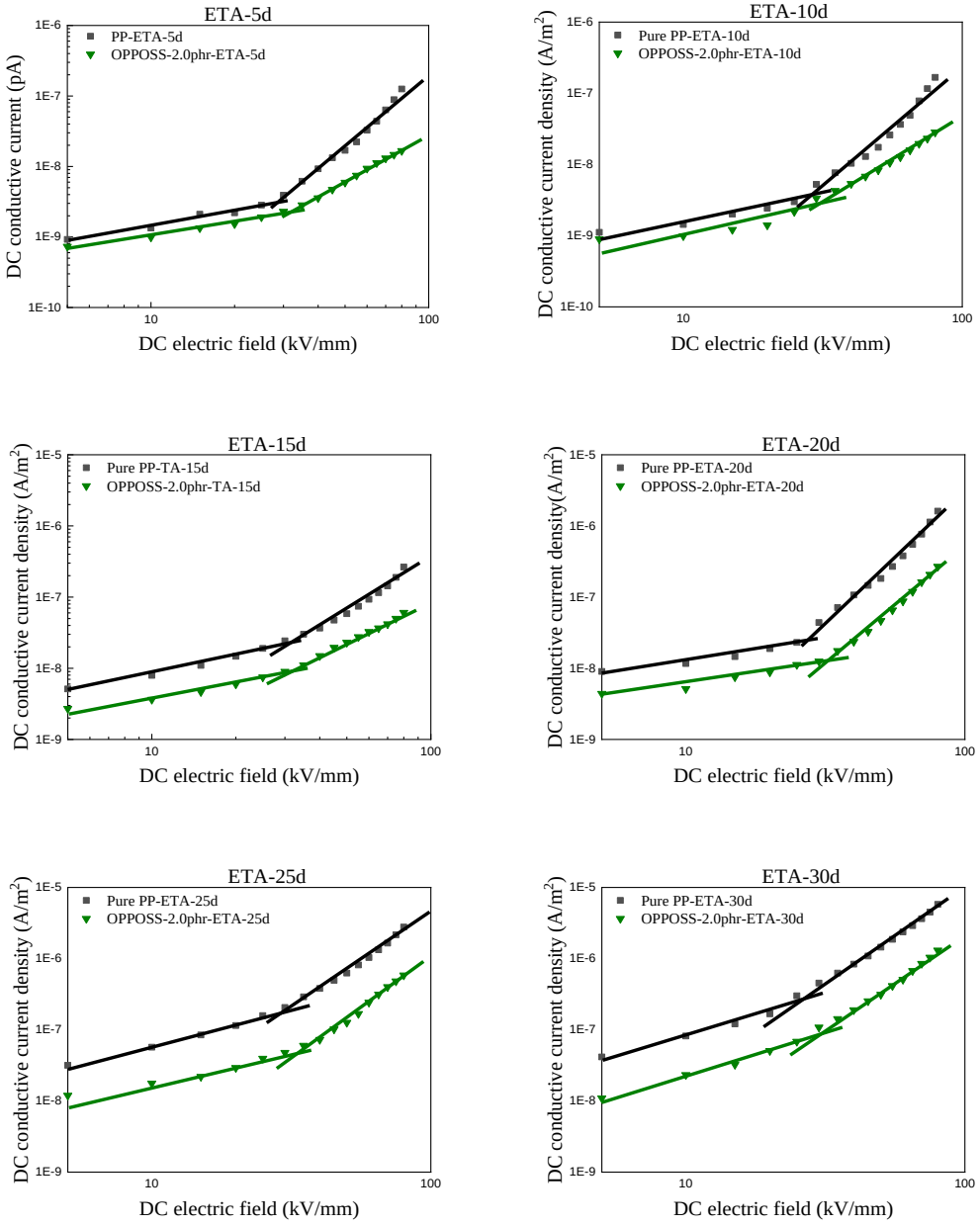

Figure 8.10 The DC conductive current density of electro-thermal aged samples in the logarithmic coordinates

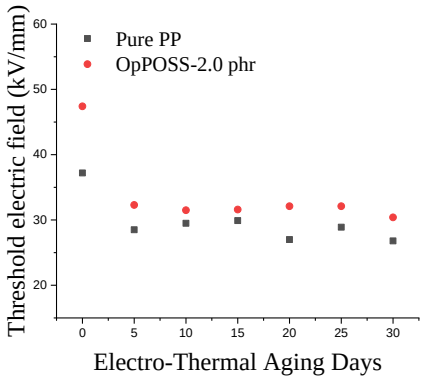

Figure 8.11 The threshold electric field of electro-thermal aged samples

8.3.6 Space charge measurements

The experimental procedure of space charge measurement was carried out as the aged samples treated by the thermal-oxidation aging process. The space charge formation and the electric field distribution in PP and OpPOSS/PP nanocomposites after the electro-thermal aging process are shown in Figure 8.12 and Figure 8.13.

In the ETA aged samples, the electric field distortion of PP treated at different times was much higher than that of OpPOSS/PP nanocomposites. When the electric field is 40 kV/mm, the injection depth of homocharges near the cathode and the accumulation of homocharges injection from the cathode in PP are much higher than those in OpPOSS/PP nanocomposites. There is almost not the charge injection in OpPOSS/PP nanocomposites under 40 kV/mm. This is because with the increase of electro-thermal aging time, the decrease of the threshold electric field of PP is higher than that of OpPOSS/PP nanocomposites, which also shows that the adverse effect of electro-thermal aging process on the electrical properties of PP is more obvious. Due to the introduction of a large number of 1.1 eV deep traps by the addition of OpPOSS, the generation of hot electrons in OpPOSS/PP nanocomposites was inhibited by deep traps. Therefore, the electrical damage of OpPOSS/PP nanocomposites during electrothermal aging is less than that of pure PP. Therefore, as shown in table 8.4, the electric field distortion of OpPOSS/PP after electro-thermal aging is less than that of PP.

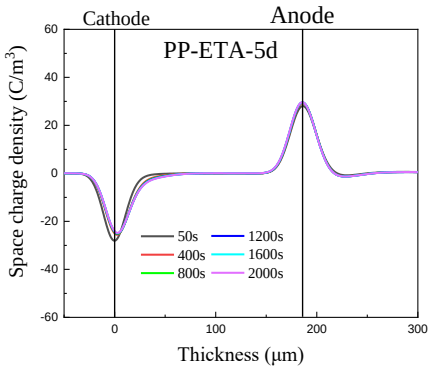
Cathode
Anode
PP-ETA-5d
Space charge density (C/m3)
Thickness (μm)
50s
400s
800s
1200s
1600s
2000s

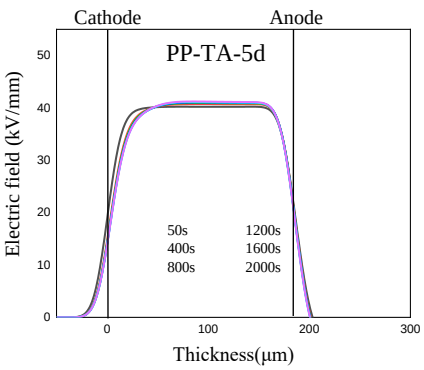
Cathode
Anode
PP-TA-5d
Electric field (kV/mm)
Thickness(μm)
50s
400s
800s
1200s
1600s
2000s

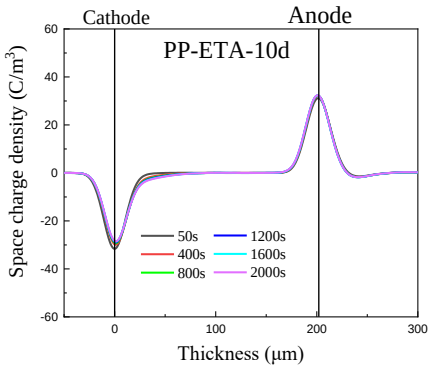
Cathode
Anode
PP-ETA-10d
Space charge density (C/m3)
Thickness (μm)
50s
400s
800s
1200s
1600s
2000s

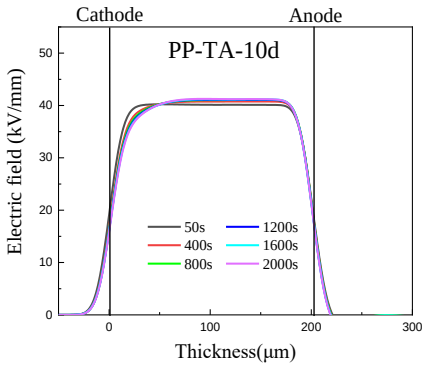
Cathode
Anode
PP-TA-10d
Electric field (kV/mm)
Thickness(μm)
50s
400s
800s
1200s
1600s
2000s

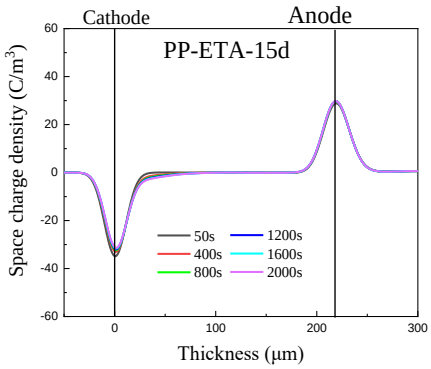
Cathode
Anode
PP-ETA-15d
Space charge density (C/m3)
Thickness (μm)
50s
400s
800s
1200s
1600s
2000s

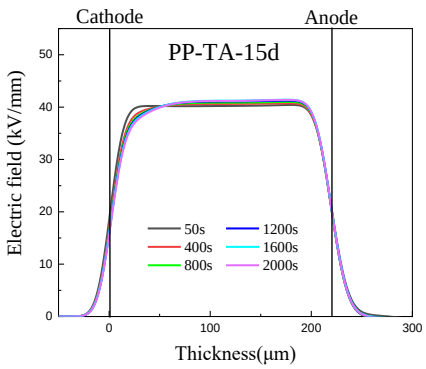
Cathode
Anode
PP-TA-15d
Electric field (kV/mm)
Thickness(μm)
50s
400s
800s
1200s
1600s
2000s

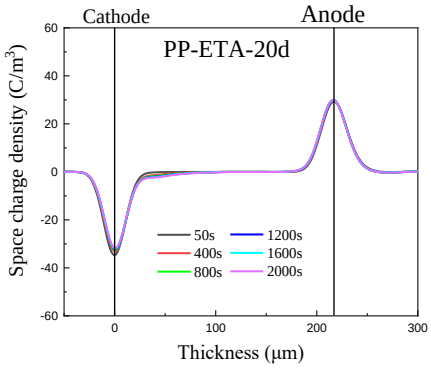
Cathode
Anode
PP-ETA-20d
Space charge density (C/m3)
Thickness (μm)
50s
400s
800s
1200s
1600s
2000s

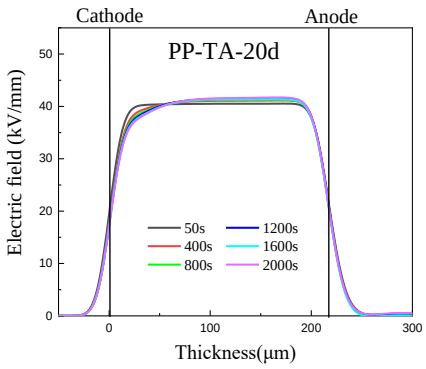
Cathode
Anode
PP-TA-20d
Electric field (kV/mm)
Thickness(μm)
50s
400s
800s
1200s
1600s
2000s

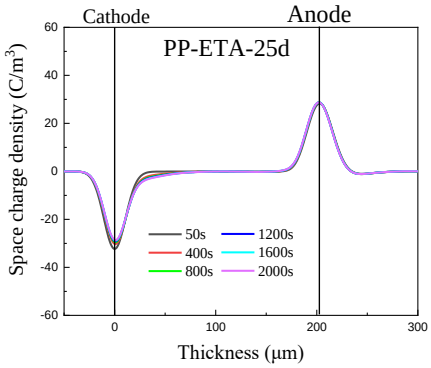
Cathode
Anode
PP-ETA-25d
Space charge density (C/m3)
Thickness (μm)
50s
400s
800s
1200s
1600s
2000s

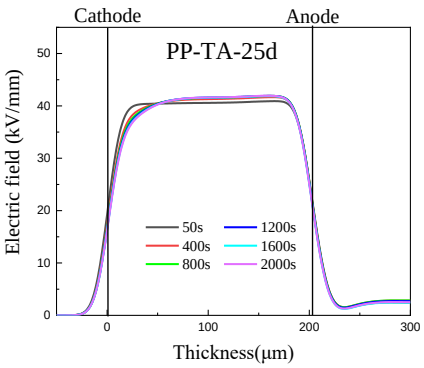
Cathode
Anode
PP-TA-25d
Electric field (kV/mm)
Thickness(μm)
50s
400s
800s
1200s
1600s
2000s

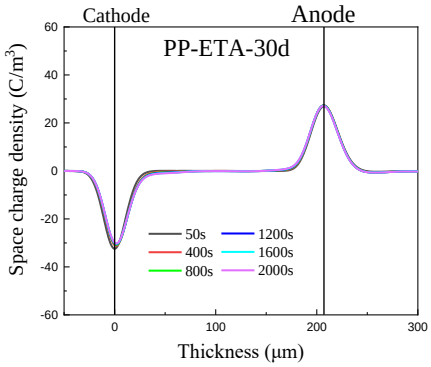
Cathode
Anode
PP-ETA-30d
Space charge density (C/m3)
Thickness (μm)
50s
400s
800s
1200s
1600s
2000s

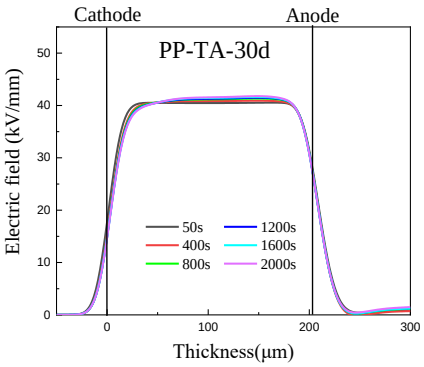
Cathode
Anode
PP-TA-30d
Electric field (kV/mm)
Thickness(μm)
50s
400s
800s
1200s
1600s
2000s

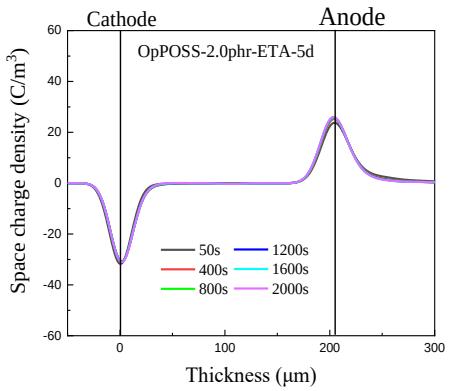
Cathode
Anode
OpPOSS-2.0phr-ETA-5d
Space charge density (C/m3)
Thickness (μm)
50s
400s
800s
1200s
1600s
2000s

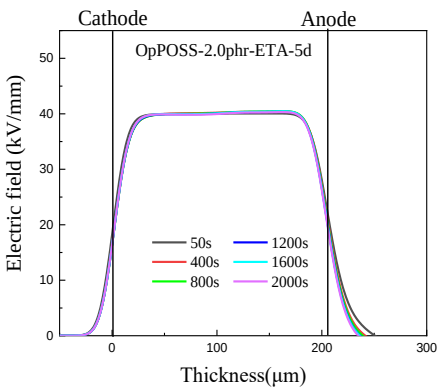
Cathode
Anode
OpPOSS-2.0phr-ETA-5d
Electric field (kV/mm)
Thickness(μm)
50s
400s
800s
1200s
1600s
2000s

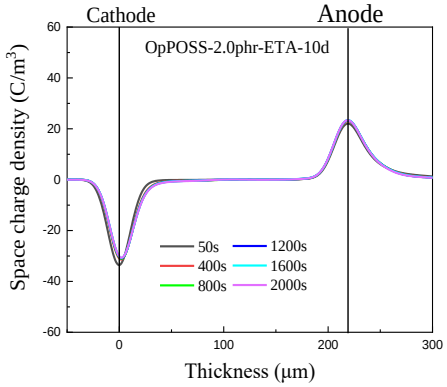
Cathode
Anode
OpPOSS-2.0phr-ETA-10d
Space charge density (C/m3)
Thickness (μm)
50s
400s
800s
1200s
1600s
2000s

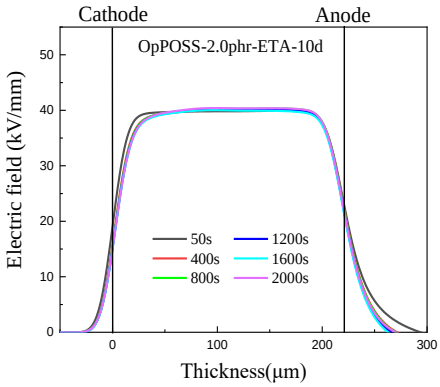
Cathode
Anode
OpPOSS-2.0phr-ETA-10d
Electric field (kV/mm)
Thickness(μm)
50s
400s
800s
1200s
1600s
2000s

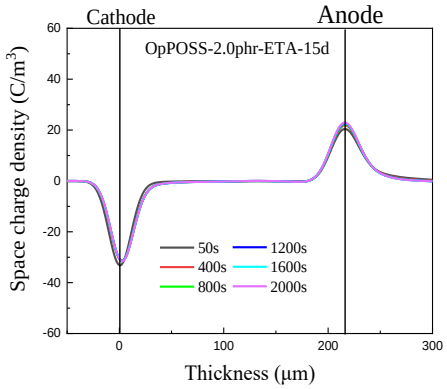
Cathode
Anode
OpPOSS-2.0phr-ETA-15d
Space charge density (C/m3)
Thickness (μm)
50s
400s
800s
1200s
1600s
2000s

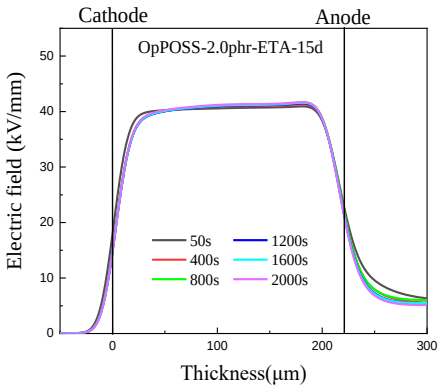
Cathode
Anode
OpPOSS-2.0phr-ETA-15d
Electric field (kV/mm)
Thickness(μm)
50s
400s
800s
1200s
1600s
2000s

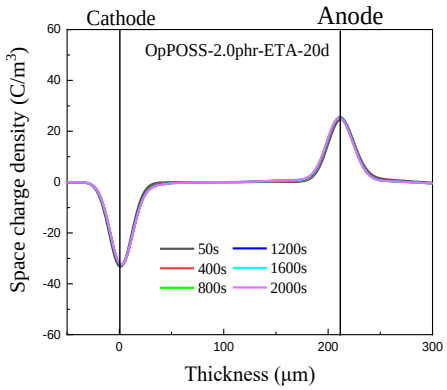
Cathode
Anode
OpPOSS-2.0phr-ETA-20d
Space charge density (C/m3)
Thickness (μm)
50s
400s
800s
1200s
1600s
2000s

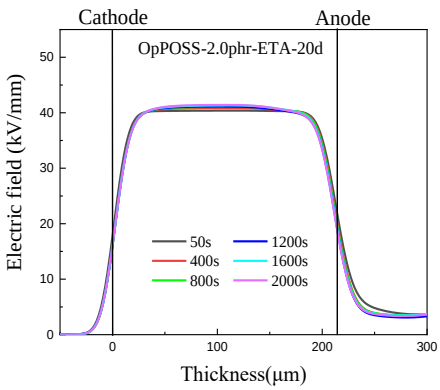
Cathode
Anode
OpPOSS-2.0phr-ETA-20d
Electric field (kV/mm)
Thickness(μm)
50s
400s
800s
1200s
1600s
2000s

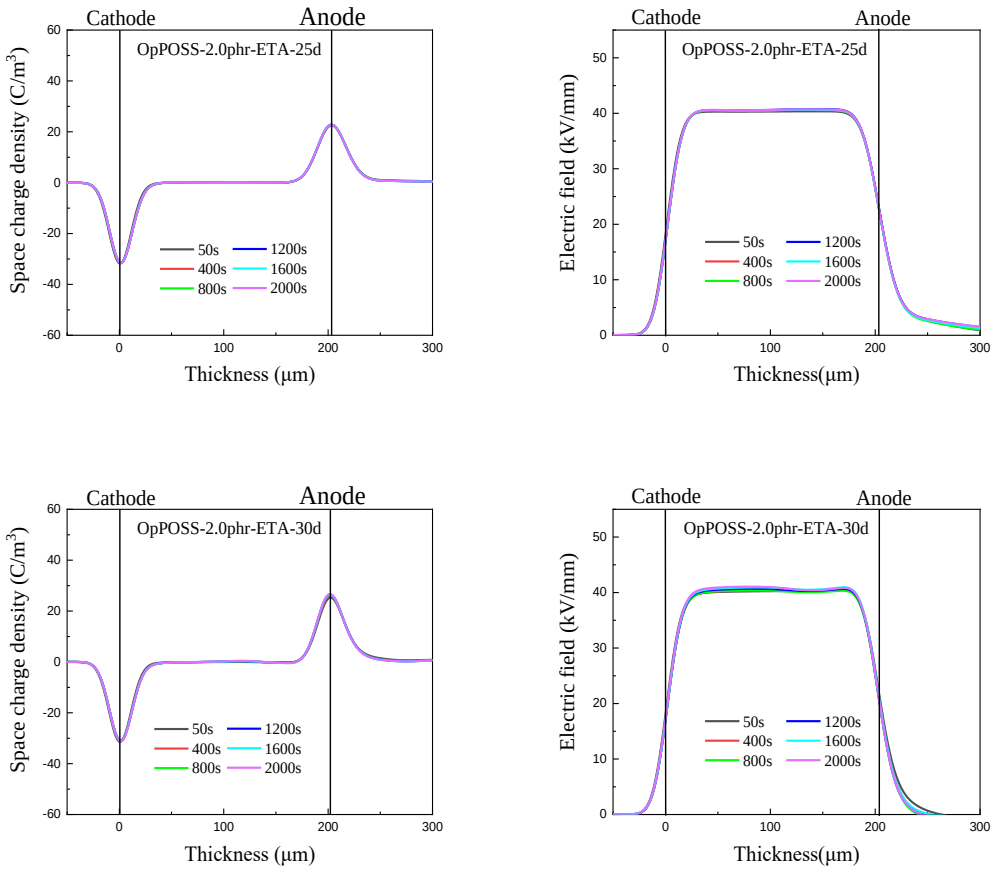

Figure 8.12 The space charge formation and electric field in the ETA aged samples under 40 kV/mm

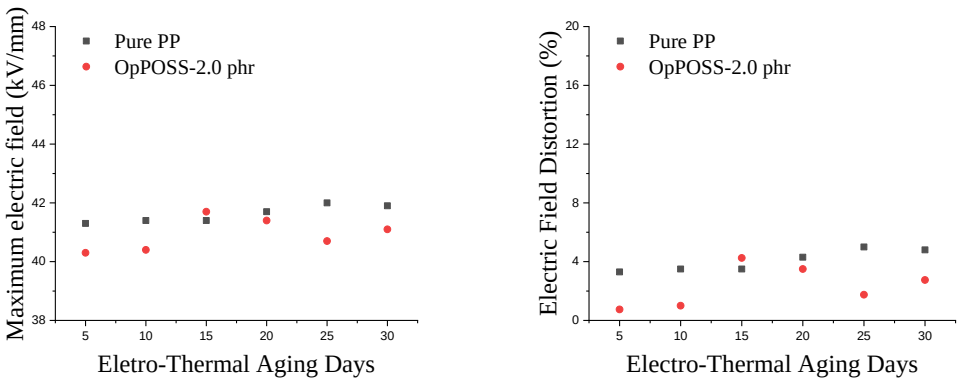

Figure 8.13 The maximum electric field distortion of electro-thermal aged samples under 40 kV/mm

8.4 The lifespan estimation of polypropylene's nanocomposites

The service life of PP and OpPOSS/PP nanocomposites will affect the feasibility of their application in HVDC cable transmission system. Therefore, a DC system is designed to predict the lifespan of PP and OpPOSS/PP nanocomposites shown in Figure 8.14, but it is not accurate. The high voltage DC power supply used in the experiment is shown in Figure 8.15. The test voltage is adjusted to 6.0 kV, the test electric field is 60 kV/mm, the temperature is set to 110 ℃, and the change of ammeter of high voltage DC power supply is recorded with the camera. Generally, due to the high resistance of PP and OpPOSS/PP nanocomposites, the current is 0 mA in the ammeter, when the sample is not broken down. Therefore, the change of number in the ammeter means that the sample is broken down. The samples were divided into two groups, one group was 8 cm × 8 cm PP film samples with a thickness of about 100 μm and another is OpPOSS/PP nanocomposite film samples with the same size as PP. The electrode is a cylindrical electrode with a diameter of 4 cm. There are 4 samples in each group for the long-term breakdown test. The breakdown time will be recorded in an hour and the average time would be used to estimate the lifespan of samples.

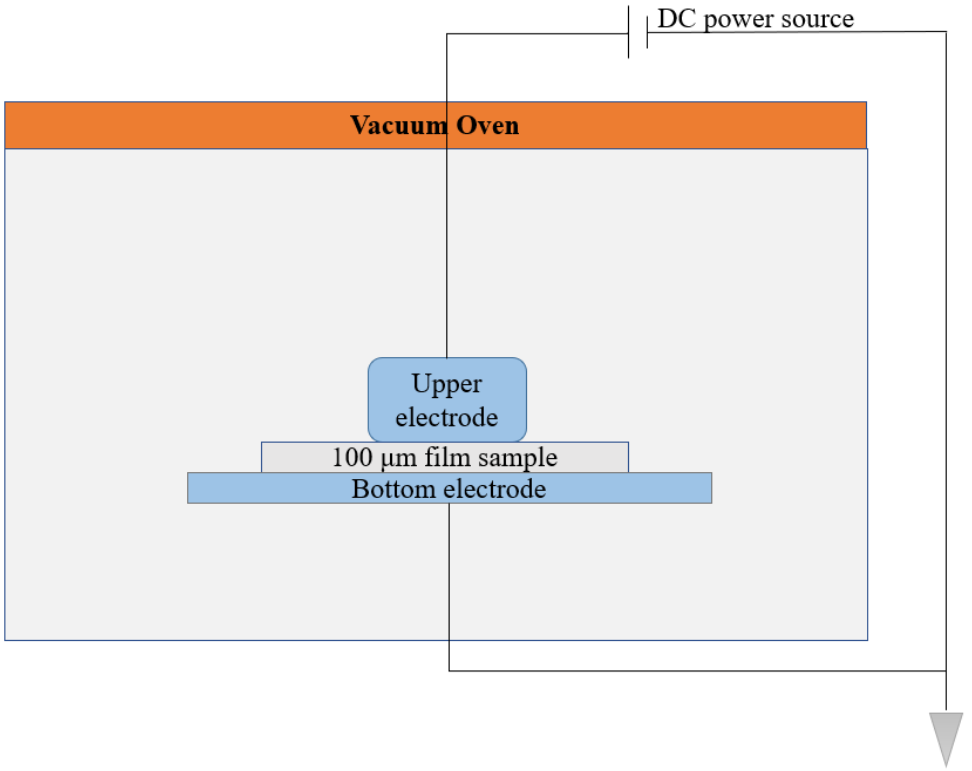

Figure 8.14 The experimental design for lifespan estimation of PP and OpPOSS/PP nanocomposites

Figure 8.15 the DC power supply in lifespan estimation of PP and OpPOSS/PP nanocomposites

The lifespan calculation method is described as follows [133]. The Weibull distribution is generally used to describe the breakdown strength of materials. Under the condition of time t and the electric field E, the breakdown probability is

$$P(t,E) = 1 - \exp\left(-C\int_0^t \left(kt^{k-1}E^{\lambda}\right)dt\right) - - - - - (13)$$

Where:

k is a shaping factor, λ is the distribution factor and C is the constant about the temperature.

When the electric field is stable, Eq.(13) can be rewritten as

$$P(t,E) = 1 - \exp\left(-Ct^k E^\lambda\right) - - - - - - - - (14)$$

Therefore,

$$t^k E^\lambda = c - - - - - - (15)$$

where c is a constant

Set $n = \lambda/k$, then

$$t = \frac{c}{E^n} - - - - - - - - (16)$$

Therefore, the lifespan becomes shorter with the increase of E^n [133].

Usually, the electric field of DC insulation materials would be lower than 15 kV/mm, so the lifespan of PP and OpPOSS/PP is assumed as t_0.

Then,

$$\frac{t}{t_0} = (\frac{E_0}{E})^n - - - - - - (17)$$

Normally the operational temperature would be lower than 70℃ and the lifespan would become half when the increasing temperature is 6-8℃. Assuming that the lifespan of insulation materials becomes half when the increasing temperature is 10 ℃ to make the calculation easier. In this part, the value of n is set to 9 and the lifespan of PP and OpPOSS/PP nanocomposites would be estimated for the conditions including 15 kV/mm and 110℃.

So

$$t_0 = t(\frac{E}{E_0})^9 = t \times 4^8 = 262144t - - - - - (18)$$

The breakdown time of PP and 2.0 phr OpPOSS/PP have been shown in Table 8.5. Therefore, when $n = 8$

For PP, the lifespan under 110℃ and 15 kV/mm is

$$t_0 = 1048576 \times \frac{4.21}{365 \times 24} = 126\ year$$

For 2.0 phr OpPOSS/PP nanocomposites, the lifespan under 110℃ and 15 kV/mm is

$$t_0 = 1048576 \times \frac{7.7}{365 \times 24} = 230.36\ year$$

Table 8.2 The breakdown time of sample under 60 kV/mm

Samples	PP	2.0 phr OpPOSS/PP
Breakdown time (h)	4.21	7.7

8.5 Conclusion

In this chapter, PP and OpPOSS/PP nanocomposites with a content of 2.0 phr were selected as aged samples for the electro-thermal aging treatment and the thermal oxidation aging experimental process was designed. After the thermal-oxidation aging process, the microstructure morphology, FTIR spectrum, mechanical and electrical properties of PP and OpPOSS/PP nanocomposites before and after aging process were compared. How the electro-thermal aging on the electrical properties of PP and OpPOSS/PP nanocomposites were further analyzed. Then, the mechanical and electrical properties of PP and OpPOSS/PP nanocomposites after the aging process were compared to study the effect of OpPOSS addition on the electrical properties of electro-thermal aged samples. The main conclusions of this chapter are as follows:

i. From the SEM detection, the surface of the aged samples became rough and cracked, but these issues were not serious as aged samples treated by the thermal-oxidation aging process. Also, the dispersion of OpPOSS nanofiller in PP would not be affected by the electro-thermal aging process.

ii. The results of conductivity test indicate that the density of deep traps was decreased, and the density of shallow traps was increased in OpPOSS/PP nanocomposites with the increase of electrothermal aging time, especially after

10 days. Because of the worse trapping characteristics of OpPOSS/PP, the DC breakdown strength, the DC conductivity and the space charge characteristics in aged samples are much worse than unaged samples.

iii. After the electro-thermal aging process, the DC breakdown strength of aged samples was reduced but still higher than the aged samples treated by the thermal-oxidation aging process, which means that the degradation of PP in the electro-thermal aging process was slower than the thermal-oxidation aging process. But the electro-thermal aging process would produce the defects in the bulk of aged samples, then lead to the decrease of DC breakdown strength.

iv. From the electrical performance test results, it could be seen that the electrical properties of aged OpPOSS/PP nanocomposites are still higher than that of aged pure PP. The results of conductivity test show that despite the decrease of deep trap density, the aged OpPOSS/PP nanocomposites still have better trapping characteristics than pure PP. The addition of OpPOSS nanofillers introduces high-density deep traps in PP, hinders the charge transport in PP and reduces the electrical damage caused by hot electrons bombarding molecular chains. Therefore, the space charge characteristics of OpPOSS/PP nanocomposites are better than those of pure PP. In the process of electrothermal aging, charge transport and electrothermal aging occur at the same time. Under high temperature and high electric field, there are a large amount of negative charges and positive charges combining together in pure PP and OpPOSS/PP nanocomposites. The recombination of charges will produce additional energy, resulting in the accelerated degradation of PP molecular chain. The degradation of the PP molecular chain increases deep traps and reduces shallow traps, resulting in more electron and hole recombination, and finally PP molecular chain will be further degraded.

v. The service life of PP and nanocomposites was evaluated by inverse power law at 110 ℃ and 60 kV/mm According to the calculation, the service life of OpPOSS/PP nanocomposites has far exceeded that of XLPE at 90 ℃ and 15 kV/mm [134].

9 Conclusions and future work

9.1 Conclusions

PP is one of the commercial thermoplastics with low manufacturing cost. Due to its good thermal performance and excellent electrical performance, PP DC cable insulation material has become one of the hotspots in the development of HVDC insulation materials. In this paper, PP nanocomposites with excellent electrical properties were prepared by the solution method with iPP as matrix material and MgO, Al_2O_3, OvPOSS and OpPOSS as nanofillers. Through a series of experiments, the electrical properties of PP and its nanocomposites at different temperatures were studied, and the physical mechanism of nano filler regulating the electrical properties of PP was systematically described. The electrical properties of four nanocomposites were compared. It was found that PP nanocomposites with OvPOSS and OpPOSS as nanofillers had higher electrical properties than traditional inorganic nanofillers, and the preparation method of nanocomposites was optimized. It provides a new idea for the development of thermoplastic insulation materials and has important engineering value. The main conclusions are as follows:

i. The ratio of PP nanocomposites was optimized by comparing the effects of MgO, Al_2O_3, OvPOSS and OpPOSS on the electrical properties of PP and the OpPOSS with 2.0 phr is the best one to manufacture the nanocomposites with highest electrical performance. The physical properties of PP and its nanocomposites were studied in detail, including FTIR spectrum, micro morphology and DSC test. In the nanocomposites of PP prepared by solution method, MgO, Al_2O_3, OvPOSS and OpPOSS can be uniformly dispersed at the contents of 2.0, 1.0, 1.0 and 2.0 phr respectively. When the content continues to increase, aggregates larger than 500 microns would appear in the matrix, which would reduce the electrical properties. Also, the addition of nanofillers could affect the crystallinity of PP during the crystallization of PP. As a heterogeneous

nucleating agent, the addition of nanofillers could make the size and the number of spherulites of PP decreased and increased respectively. Finally, the boundary area between spherulites and spherulites could be decreased by the addition of nanofillers, thus improving the electrical performance. According to the electrical performance test, the addition of OpPOSS achieved the highest electrical performance of PP. At the temperature of 30℃, the DC breakdown strength and DC volume resistivity under 80 kV/mm of OpPOSS/PP nanocomposites were increased from 440.1 kV/mm and 0.7×10^{15} Ω·m and to 585.9 kV/mm and 5.6×10^{15} Ω·m, respectively through the addition of 2.0 phr OpPOSS. Under the DC electric field of 60 kV/mm, the electric field distortion was reduced from 13.7% to 2.5% by adding 2.0 phr OpPOSS. From the results of TSDC tests, it showed that OpPOSS and OvPOSS could introduce the deepest traps with high density, especially for OpPOSS. Combined with the results of thermal stimulation current tests and electrical performance tests, the reasons why the electrical properties of OvPOSS/PP and OpPOSS/PP nanocomposites are better than those of MgO/PP and Al_2O_3/PP nanocomposites could be attributed to the introduction of deeper traps with high density.

ii. Through the analysis methods of GaussianView09 and Multifwn, the differences in microstructure between OvPOSS and OpPOSS and the mechanism of introducing deep traps are analyzed. According to the calculation results of DOS, the lowest unoccupied orbital of OpPOSS molecule is -0.56 eV which is lower than OvPOSS (-0.38 eV). Because the lowest unoccupied orbital contributes to the electron trap, the results indicates that a singular molecule of OpPOSS can introduce a deeper trap depth than that of OvPOSS.

iii. The electrical properties of OvPOSS/PP and OpPOSS/PP nanocomposites at different temperatures were obtained and the effects of temperature on the electrical properties of the two nanocomposites were revealed, including the characteristics of DC breakdown strength, DC conductivity, and space charge

accumulation. The inhibition effect of deep trap on charge injection at different temperatures is proposed, and the physical mechanism of OvPOSS and OpPOSS improving the electrical properties of PP at high temperature is explained. Based on Tian Fuqiang's analysis method [131], the addition of OvPOSS can introduce the trapping level of 1.02 eV with the density of 5.8×10^{17}/eV·m^3 and OpPOSS could introduce the trapping level of 1.10 eV with the density of 3.7×10^{17}/eV·m^3 to the bulk of PP. Both of OvPOSS/PP and OpPOSS/PP nanocomposites could achieve the better trapping characteristics than pure PP. Therefore, under the temperature of 90℃, the breakdown strength of PP was increased from 335.1 kV/mm to 436.1 kV/mm and 442.8 kV/mm by OvPOSS and OpPOSS respectively. Also, the electric field distortion of PP was reduced from 24.3 % to 19.6 % and 16.2 % by the addition of OvPOSS and OpPOSS respectively under the electric field of 60 kV/mm and the temperature of 90 ℃.

iv. The electro-thermal aging mechanism of insulating materials was confirmed by the electrical and physical properties of PP and OpPOSS/PP under thermal-oxidation aging and electro-thermal aging process. Because the coupling of OpPOSS and the molecular chain of PP was destroyed during thermal-oxidation aging process, the influence of OpPOSS addition on the electrical properties of PP was reduced with the increase of aging time. For the electro-thermal aging process, due to introduction of the deep traps, the charge transport in PP was suppressed and the electrical damage caused by the hot electrons would be reduced during the electrothermal aging process. Therefore, it was found that after 30 days electro-thermal aging process, the DC breakdown strength of PP still could be increased from 330.9 kV/mm to 401.2 kV/mm and the electric field distortion of PP at the DC electric field of 15 kV/mm could be reduced from 4.8 % to 2.5 % by the effect of OpPOSS addition. Through the inverse power relationship between the service life of insulating materials and electric field, the service life of PP and OpPOSS/PP nanocomposites at 110 ℃ and 15

kV/mm is theoretically estimated to ~230 years, which is much higher than that of XLPE.

9.2 Future work

In this thesis, the potential of nanocomposites system to be used in DC cable insulation is investigated by solution method, especially for OvPOSS and OpPOSS. It is found that the electrical properties of PP can be significantly improved by introducing polar chemical groups to produce deep traps. However, for the industrial manufacture of extruded polymeric nanocomposites HVDC cable, the research for nanocomposite system of PP is still insufficient so that the mechanism of nanocomposites still needs to be further explored to provide a theoretical basis for the regulation of electrical properties of polymer insulating materials, especially for the industrial cable insulation, not only film samples. Therefore, the future work of polymeric nanocomposites insulation materials can be focused on further studies and investigations which will address the following aspects:

i. At present, the interface generated by the coupling of nanofillers and polymer is considered to have an important impact on the electrical properties of nanocomposites. How to accurately observe and design the interface effect to regulate the electrical properties of nanocomposites has become a very important topic. Through more accurate experimental instruments and facilities, such as atomic force microscope, nano-infrared, electrostatic force microscope, etc., the effect of nanofillers addition on polymers' properties can be further explained by microcosmic methods.

ii. At present, how to ensure the uniform dispersion of nanofillers in polymers in the production process of nanocomposites needs to be established .

iii. The long-term operational characteristics of polymeric nanocomposites insulation materials require further investigation . How to restrain the aging process of whole cable insulation is also a very important topic. The practical

applications of extruded polymeric nanocomposites cables still needs to be tested.

10 References

[1] H. Maheshwari, U. Chandra and K. Jain, “A review from greenhouse effect to carbon footprint”, Poluttion Research, 37(4), pp. 1033-1038, 2018.

[2] H. Orton, “Power Cable Technology Review”, High Voltage, 41(4), pp. 1057-1067, 2015.

[3] T. L. Hanley, R. P. Burford, R. J. Fleming, et al., “A general review of polymeric insulation for use in HVDC cables”, IEEE Electrical Insulation Magazine, 19(1), pp 13-24, 2003.

[4] https://www.rfwireless-world.com/Terminology/Advantages-and-Disadvantages-of-Underground-and-Overhead-transmission.html

[5] https://mechatrofice.com/electrical/overhead-vs-underground

[6] J. W. Feltes, B. D. Gemmell and D. Retzmann, “From smart grid to super grid: Solutions with HVDC and FACTS for grid access of renewable energy sources”, 2011 IEEE power and energy society general meeting, 2011.

[7] M. Claus, D. Retzmann, D. Sörangr, et al., " Solutions for Smart and Super Grids with HVDC and FACTS", 17th Conference of the Electric Power Supply Industry, 2008.

[8] A. Krontiris and P. Sandeberg, “HVDC technology for offshore wind is maturing”, ABB Power Grids, Sweden, 2018

[9] D. Yoon, H. Song, G. Jang, et al., “Smart Operation of HVDC Systems for Large Penetration of Wind Energy Resources,” IEEE Transactions on Smart Grid, 4(1), pp. 359-366, 2013.

[10] Mazzanti G . “Issues and Challenges for HVDC Extruded Cable Systems”. Energies, 14(15), pp 4504-4538, 2021.

[11] T. Gemma, “Wind energy in the UK: June 2021”, office for National Statistics, 2021.

[12] T. Nathalie, “UK wind power overtakes coal for first time”, in The Guardian, 2017.

[13] W. Grant and S. Iain, “Winds of change: Britain now generates twice as much electricity from wind as coal,” in the Conversation, 2018.

[14] https://www.great.gov.uk/international/content/investment/sectors/offshore-wind/?utm_source=google&utm_medium=paidsearch&utm_campaign=ditinvestme

ntatlashpopaidsearch&utm_content=DSA&gclid=EAIaIQobChMIk6uv2Ii59QIVA1dgCh0TBAKoEAAYASAAEgKtFfD_BwE

[15] Y. Zhou, S. Peng, J. Hu et al., "Polymeric insulation materials for HVDC cables: Development, challenges and future perspective", IEEE Transactions on Dielectrics and Electrical Insulation, 24(3), pp. 1308-1318, 2017.

[16] B. Zhao, R. Zeng, Z. Yu, et al., "A More Prospective Look at IGCT: Uncovering a Promising Choice for DC Grids", IEEE Industrial Electronics Magazine, 12(3), pp 6-18, 2018.

[17] European Commission, "A Clean Planet for all—A European Strategic Long-Term Vision for a Prosperous, Modern, Competitive and Climate Neutral Economy", 2018.

[18] A. Kalair, N. Abas and N. Khan, "Comparative study of HVAC and HVDC transmission systems", Renewable & Sustainable Energy Reviews, 59, pp 1653-1675, 2016.

[19] A. Alassi, S. Banales and O. Ellabban, "HVDC Transmission: Technology Review, Market Trends and Future Outlook", Renewable and Sustainable Energy Reviews, 112, pp 530-554, 2019.

[20] X. Huang, J. Zhang J and P. Jiang, "Thermoplastic Insulation Materials for Power Cables: History and Progress", Gaodianya Jishu/High Voltage Engineering, 44(5), pp 1377-1398, 2018

[21]https://www.entsoe.eu/Technopedia/techsheets/hvdc-mass-impregnated-mi-cables

[22]https://circuitglobe.com/oil-filled-cables.html

[23]https://szhuaxia.en.made-in-china.com/productimage/NOdJyYCGrihn-2f1j00dSjGVUDsAhoR/China-76-132-145-kV-High-Voltage-Oil-filled-Outdoor-Power-Cable-Terminations-Composite-for-Copper-Laminated-XLPE-Cable-240-1600sq-mm.html

[24] Paul. B, "East-West Interconnector will move Ireland closer to heart of European electricity sector", Commission for Energy Regulation, 2009.

[25] A. Stan, S. Costinas and G. Ion, "Overview and Assessment of HVDC Current Applications and Future Trends", Energies, 15(3), pp 1193-2218, 2022.

[26] U. Wijk, J. Lindgren, J. Winther, et al., "Dolwin 1-further achievements in HVDC Offshore connections", EWEA Conference, Frankfurt, 2013.

[27] Siemens AG, "Fact Sheet BorWin2 HVDC Platform", 2015

[28] Magnus. D, “Nordic Grid Master Plan”, 2008.

[29] https://www.tennet.eu/our-grid/offshore-projects-germany/sylwin1/

[30] https://www.power-technology.com/projects/nemo-link-interconnector/

[31] https://www.hitachienergy.com/case-studies/ifa2

[32] G. Chen, H. Miao, Z. Xu, et al, “Review of high voltage direct current cables”, CSEE Journal of Power and Energy Systems, 1(2), pp 9-21, 2015.

[33] N. Hirai, R. Minami, T. Tanaka, et al., “Chemical Group in Crosslinking Byproducts Responsible for Charge Trapping in Polyethylene”, IEEE Transactions on Dielectrics & Electrical Insulation, 10(2), 320-330, 2003.

[34] M. Fairhurst, A. Gowadia, G. Stevens, et al., “Integrated Development and Assessment of New Thermoplastic high voltage power cable system”, CIGRE paper, B1-215, 2012.

[35] http://www.differencebetween.com/difference-between-hdpe-and-vs-ldpe/

[36] Q. Wu, S. Chen and H. Liu, “Effect of surface chemistry of polyethyleneimine-grafted polypropylene fiber on its CO2 adsorption”, RSC ADVANCES, 4(52), pp 27176-27183, 2014.

[37] http://www.essentialchemicalindustry.org/polymers/polypropene.html [Accessed: 11/02/2022]

[38] X. Lin, W. H. Siew, J. Liggat, et al., “Octavinyl polyhedral oligomeric silsesquioxane on tailoring the DC electrical characteristics of polypropylene”, IET High Voltage. 1(2) pp1– 11, 2022.

[39] 刘丛吉, 杨佳明, 陈俊岐, 不同密度聚乙烯直流介电性能研究. 绝缘材料, 2017, 50(2):5.

[40] M. Ikeda and Y. Shimizu, “Electrical insulating resin material, electrical insulating material, and electric wire and cable using the same”, US. Patent No. 6479590. 2002.

[41] S. H. Lee, J. Park, J. H. Han and K. S. Suh, “Space charge and electrical conduction in maleic anhydride-grafted polyethylene”, IEEE Transactions on Dielectrics & Electrical Insulation, 2(6), pp 1132 – 1139, 1995.

[42] Yoshifuji. N and Niwa. T, “Development of the new polymer insulating materials for HVDC cable”, IEEE Transactions on Power Delivery, 7(3), pp 1053-1059, 1992.

[43] Y. Zhou, J. Hu, B. Dang, and J. He, “Mechanism of highly improved electrical properties in polypropylene by chemical modification of grafting maleic anhydride”, Journal of Physics D Applied Physics, 49(41), pp 415301, 2016.

[44] J. Zha, Y. Wu, S. Wang, et al., “Improvement of space charge suppression of polypropylene for potential application in HVDC cables”, IEEE Transactions on Dielectrics and Electrical Insulation2016, 23(4), pp 2337-2343, 2016.

[45] B. Ceres and J. Schultz, “Dependence of electrical breakdown on spherulite size in isotactic polypropylene”, Journal of Applied Polymer Science, 29(12), pp 4183–4197, 1984.

[46] H. Zhao, L. Honglei, J. Yang, et al., “Effect of Crystalline Characteristics on Space Charge and DC Breakdown Strength of Polypropylene”, Polymer Materials Science & Engineering, 12(11), pp 1746, 2019.

[47] L. Zhang, Y. Zhang, Y. Zhou, et al., “Crystalline modification and its effects on dielectric breakdown strength and space charge behavior in isotactic polypropylene”, Polymers, 10(4), pp 406, 2018.

[48] Y. Zhou, B. Dang, H. Wang, et al., “Polypropylene-based ternary nanocomposites for recyclable high-voltage direct-current cable insulation”, Composites Science and Technology, 165, pp 168-174, 2018.

[49]Y. Wu, J. Zha, W. Li, et al., “A remarkable suppression on space charge in isotatic polypropylene by inducing the β-crystal formation”, Applied Physics Letters, 115(11), pp 11, 2015.

[50] Y. Cao, P. C. Irwin, K. Younsi, “The future of nanodielectrics in the electrical power industry”, IEEE Transactions on Dielectrics & Electrical Insulation, 11(5), pp 797-807, 2004.

[51] J. Yang, H. Zhao, Q. Wu, et al., “Effect of multiple mixing on dispersion and DC electrical properties of SiO2/LDPE nanocomposites” 12th International Conference on the Properties and Applications of Dielectric Materials (ICPADM), pp 933-936 2018.

[52] L. Zhang, Y. Zhou, X, Cui, et al., “Effect of nanoparticle surface modification on breakdown and space charge behavior of XLPE/SiO2 nanocomposites”, IEEE Transactions on Dielectrics and Electrical Insulation, 21(4), pp 1554-1564, 2014.

[53] Y. Yang, Q. Li and J. He, “The Dielectric Properties of PP Nanocomposites Doped with Mesoporous Silica Nanoparticles”, IEEE Conference on Electrical Insulation and Dielectric Phenomena (CEIDP), pp 140-143, 2018.

[54] Zafar. R and Gupta. N, "Dielectric characterisation of epoxy nanocomposite with barium titanate fillers". IET Nanodielectrics, 3(2), pp 23-61, 2020.

[55] Du. B, J. Su, M. Tian, et al., "Understanding trap effects on electrical treeing phenomena in EPDM/POSS composites", Scientific Report, 8(1), pp 1-11, 2018.

[56] X. Duan, W. H. Siew, J. Liggat, et al., "Effect of Different Surface Treatment Agents on the Physical Chemistry and Electrical Properties of Polyethylene Nano-alumina Nanocomposites", IET High Voltage, 5(4), pp 397-402, 2020.

[57] S. Hu, C. Yuan, Q. Li et al., "High-Temperature Polypropylene Nanocomposite with Different Surface-Modified Nanoparticles for HVDC Cables", IEEE International Conference on High Voltage Engineering and Application (ICHVE), pp. 1-4, 2020.

[58] B. Dang, J. Hu, Y. Zhou and J. He, "Remarkably improved electrical insulating performances of lightweight polypropylene nanocomposites with fullerene", Journal of Physics D Applied Physics, 50(45), pp455303, 2017.

[59] T. Lewis, "Nanometric Dielectrics," IEEE Transactions on Dielectrics & Electrical Insulation, 1(5), pp. 812-825, 1994.

[60] J. K. Nelson, Y. Hu and J. Thiticharoenpong. "Electrical properties of TiO2/nanocomposites", IEEE Conference on Electrical Insulation and Dielectric Phenomena, pp 719-722, 2003.

[61] J.K. Nelson, J. C. Fothergill, L. A. Dissado, "Towards an understanding of nanometric dielectrics", IEEE Conference on Electrical Insulation and Dielectric Phenomena, pp 295- 298, 2002.

[62] M.N. Ajour, L. A. Dissado, J. C. Fothergill, et al., "Dielectric spectroscopy of epoxy/glass composite materials", IEEE Annual Report Conference on Electrical Insulation and Dielectric Phenomena, pp 438-441, 2002.

[63] M. Katz and R. J. Theis "New high temperature polyimide insulation for partial discharge resistance in harsh environments", IEEE Electrical Insulation Magazine, 13(4), pp 24-30, 1997.

[64] S. Zhong, Z. Dang, W. Zhou and H. Cai, "Past and future on nanodielectrics". IET Nanodielectrics, 1(1), pp 41-47, 2018.

[65] M. Wei, X. Wang and T. Andritsch, "Space Charge and Breakdown Strength Behaviour of PP/POE/MgO Nanocomposites", 2nd International Conference on Electrical Materials and Power Equipment (ICEMPE), pp 260-263, 2019.

[66] L. Ren, H. Li, D. Ai, et al., "Enhanced Energy Storage Performance with High-Temperature Stability of Polyetherimide Nanocomposites", IEEE International Conference on High Voltage Engineering and Application (ICHVE), pp. 1-4, 2020.

[67] C. Yuan, Y. Zhou, Y. Zhu, et al., "Polymer/molecular semiconductor all-organic composites for high-temperature dielectric energy storage", Nature Communications, 11(1), pp 1-8, 2020.

[68] Alapati. S, "Electrical treeing and the associated PD characteristics in LDPE nanocomposites". IEEE Transactions on Dielectrics & Electrical Insulation, 19(2), pp 697-704, 2012.

[69] Q. Gong, X. Hu, J. Zhang, et al., "Tunable nonlinear time response of nanocomposites by doping CdTeS quantum dots", CLEO/QELS: 2010 Laser Science to Photonic Applications, pp. 1-2, 2010.

[70] Y. Zhou, J. Hu, C. Xin, et al. "Thermoplastic polypropylene/aluminum nitride nanocomposites with enhanced thermal conductivity and low dielectric loss", IEEE Transactions on Dielectrics and Electrical Insulation, 23(5), pp 2768-2776, 2016.

[71] Tanaka. T and Imai. T. "Advances in nanodielectric materials over the past 50 years", IEEE Electrical Insulation Magazine, 29(1), pp 10-23, 2013.

[72] S. Li, S. Yu and Y. Feng, "Progress in and prospects for electrical insulating materials", IET High Voltage, 1(3), pp 122-129, 2016.

[73] M. G. Danikas and T. Tanaka, "Nanocomposites-a review of electrical treeing and breakdown", IEEE Electrical Insulation Magazine, 25(4), pp 19-25, 2009.

[74] Y. Zhou, S. Peng, J. Hu, et al. "Polymeric insulation materials for HVDC cables: Development, challenges and future perspective", IEEE Transactions on Dielectrics and Electrical Insulation, 24(3), pp 1308-1318, 2017.

[75] G. Montanari, "Bringing an insulation to failure: the role of space charge", IEEE Transactions on Dielectrics and Electrical Insulation, 18(2), pp 339-364, 2011.

[76] K. Kao, "New theory of electrical discharge and breakdown in low mobility condensed insulators", Journal of Applied Physics., 55, (3), pp. 752–755, 1984.

[77] Y. Murakami, M. Nemoto, S. Okuzumi, et al., "DC conduction and electrical breakdown of MgO/LDPE nanocomposite", IEEE Transactions on Dielectrics and Electrical Insulation, 15(1), pp 33-39, 2008.

[78] T. Maezawa, J. Taima, Y. Hayase, et al. “Space charge formation in LDPE/MgO Nano-composite under high electric field at high temperature”, IEEE Conference on Electrical Insulation & Dielectric Phenomena, pp 271-274, 2008.

[79] Q. Zhong, L. Lan, J. Wu, et al., “Effect of nano-filler grain size on space charge behavior in LDPE /MgO nanocomposite”, Proceedings of 2014 International Symposium on Electrical Insulating Materials, pp. 429-432, 2014.

[80] S. Peng, J. He, J. Hu, et al. “Influence of Functionalized MgO Nanoparticles on Electrical Properties of Polyethylene Nanocomposites”, IEEE Transactions on Dielectrics and Electrical Insulation, 22(3), pp 1512-1519, 2015.

[81] Y. Zhou, J. Hu, B. Dang, et al. “Effect of different nanoparticles on tuning electrical properties of polypropylene nanocomposites”, IEEE Transactions on Dielectrics and Electrical Insulation, 24(3), pp 1380-1389, 2017.

[82] T. J. Lewis, “Interfaces are the dominant feature of dielectrics at the nanometric level”, IEEE Transactions on Dielectrics and Electrical Insulation, 11(5), pp 739-753, 2004.

[83] X. Huang, L. Xie, K. Yang, et al., “Role of interface in highly filled epoxy/$BaTiO_3$ nanocomposites. Part I-correlation between nanoparticle surface chemistry and nanocomposite dielectric property”, IEEE Transactions on Dielectrics and Electrical Insulation, 21(2), pp. 467-479, 2014.

[84] F. Ali, B. Ugurlu, A. Kawamura, “Polymer nanocomposite dielectrics-the role of the interface”, IEEE Transactions on Dielectrics and Electrical Insulation, 12(4), pp 629-643, 2005.

[85] T. J. Lewis, “Interfaces: nanometric dielectrics”, Journal of Physics D: Applied Physics, 38(2), pp 202, 2005.

[86] T. Tanaka, M. Kozako, N. Fuse, et al., “Proposal of a Multi-core Model for Polymer Nanocomposite Dielectrics”, IEEE Transactions on Dielectrics and Electrical Insulation, 12(4), pp 669-681, 2005.

[87] T. Tanaka, “Dielectric Nanocomposites with Insulating Properties”, IEEE Transactions on Dielectrics and Electrical Insulation, 12(5), pp 914-928, 2005.

[88] T. Tanaka, “Interpretation of Several Key Phenomena Peculiar to Nano Dielectrics in terms of a Multi-core Model”, 2006 IEEE Conference on Electrical Insulation and Dielectric Phenomena, pp 298-301, 2006.

[89] T. Takada, “Space Charge Trapping in Electrical Potential Well caused by Permanent and Induced Dipoles for LDPE/MgO Nanocomposites”, IEEE Transactions on Dielectrics and Electrical Insulation, 15(1), pp 152-160, 2008.

[90] T. Takada, “Acoustic and Optical Methods for Measuring Electric Charge Distributions in Dielectrics”, IEEE Transactions on Dielectrics and Electrical Insulation, 6(5), pp 519-547, 1999.

[91] S. Hu, W. Wang, B. Dang, et al. “Thermal Properties and Space Charge Behavior of Thermally Aged Polypropylene/Elastomer Blends Nanocomposite”, IEEE Transactions on Dielectrics and Electrical Insulation, 27(1), pp 521-526, 2020.

[92] T. Zhou, G. Chen, R. Liao, et al., “Charge trapping and detrapping in polymeric materials: Trapping parameters”, Journal of Applied Physics, 110(4), pp 43724, 2011.

[93] S. Gutierrez, I. Sancho, L. Fontan, et al. “Effect of protrusions in HVDC cables”, IEEE Transactions on Dielectrics & Electrical Insulation”, 19(5), pp 1774-1781, 2012.

[94] https://microbenotes.com/scanning-electron-microscope-sem/

[95] G. Alfred, “Scanning Electron Microscopy”, 2011.

[96] https://www.nanoscience.com/techniques/scanning-electron-microscopy/

[97] C.Yu, Q, Xie, O.Y. Ba, et al. “Crystalline and Spherulitic Morphology of Polymers Crystallized in Confined Systems”. Crystals, 7(5), pp 147, 2017.

[98] R. Philip and D. Michael, “Introduction to Polarized Light Microscopy”, 2013

[99] J. A. Williams, “Underground Transmission Systems Reference Book”, EPRI Underground Transmission Program Electrical Systems Division, 1992.

[100] A. Haddad and D. Warne, et al., “Advances in High Voltage Engineering”. IET, 40, 2004.

[101] W. Zhao, “ Partial Discharge Ageing of Polymer Insulation under Combined AC and DC Stress at Elevated Temperatures”, PhD thesis, University of Strathclyde, UK, 2017.

[102] P. Ashok, H. Rainer, T. Mohammad, et al, “Industrial Biorefineries & White Biotechnology”, Elsevier, pp 575-605, 2015.

[103] Open Education Resource (OER) LibreTexts Project, “Physical Chemistry”, pp 614-616, 2021.

[104] Y. Zhou, B. Dang, J. Hu, et al. “Effect of Magnesium Oxide Nanoparticles on Tailoring the Properties of Polypropylene”, Proceedings of the CSEE, 36(24), pp 6619-6626 , 2016.

[105] Y. Shi, L. Zhang, J. Zhang, et al., “Thermally stimulated depolarization currents and dielectric properties of Mg0.95Ca0.05TiO3 filled HDPE composites”, Aip Advances, 7(12), pp 125315, 2017.

[106] P. Bräunlich, “Thermally Stimulated Relaxation in Solids”. Springer-Verlag, 1979.

[107] C. Cong, C. Cui, X. Meng , et al. “Structure and property of tetrafluoroethylene-propylene elastomer-OVPOSS composites”, Journal of Applied Polymer Science, 130(2), pp 1281-1288, 2017.

[108] S. Hu, Y. Zhou, C. Yuan, et al., “Surface-modification effect of MgO nanoparticles on the electrical properties of polypropylene nanocomposite”, IET High Voltage, 5(2), pp 31-37, 2020.

[109] M. Guo, M. Fréchette, É. David et al., “Polyethylene/polyhedral oligomeric silsesquioxanes composites: electrical insulation for high voltage power cables”, IEEE Transactions on Dielectrics and Electrical Insulation, 24(2), pp 798–807, 2011.

[110] Z. Xu, M. Guo, M. Fréchette, et al.: “Space charge properties of LDPE-based composites with three types of POSS”, IEEE Conference on Electrical Insulation and Dielectric Phenomena (CEIDP). Canada, Toronto, ON, pp. 679–682. 2016.

[111] T. Heid, É. David and M. Fréchette, “Modeling the thermal conductivity of epoxy/POSS and Epoxy/POSS/cBN composites”, IEEE International Conference on Dielectrics (ICD). Montpellier, France, pp. 414–417, 2016.

[112] A. Fina, D. Tabuani, A. Frache, “Polypropylene–polyhedral oligomeric silsesquioxanes (POSS) nanocomposites”, Polymer. 46(19), pp 7855–7866, 2005.

[113] M. Takala, M. Karttunen, P. Salovaara, et al., “Dielectric properties of nanostructured polypropylenepolyhedral oligomeric silsesquioxane compounds”, IEEE Transactions on Dielectrics and Electrical Insulation, 15(1), pp 40–51, 2008.

[114] I. Penso, E. A. Cechinatto, G. Machado, et al., “Preparation and characterization of polyhedral oligomeric silsesquioxane (POSS) using domestic microwave oven”, Journal of Non-Crystalline Solids. 428, pp 82–89, 2015.

[115] https://www.aladdin-e.com/zh_cn/p102212.html

[116] https://www.aladdin-e.com/zh_cn/p102340.html

[117] W. Ni, S. Wu, Q. Ren, “Preparation and characterization of silanized TiO_2 nanoparticles and their application in toner”, Industrial & engineering chemistry research, 51(40), pp 13157-13163, 2012.

[118] Electric strength of insulating materials - test methods - Part 2: additional requirements for tests using direct voltage, IEC Standard 60243-2, 2013-11-26

[119] P. Emtage, and W. Tantraporn. “Schottky emission through thin insulating films”, Physical Review Letters, 8(7), pp 267, 1962.

[120] M. J. Frisch, et al., Gaussian, Inc., Gaussian 16, Revision A.03, Wallingford CT, 2016.

[121] T. Lu and F. Chen, “Multiwfn: A Multifunctional Wavefunction Analyzer”, Journal of computational chemistry, 33(5), pp 580-592, 2012.

[122] R. Joseph, “Organic Chemistry Concepts and Applications for Medicinal Chemistry”, Academic Press (Elsevier Publishing Company), 51-65 (2014).

[123] S. Bohm, and O. Exner. "Interaction of two functional groups through the benzene ring: Theory and Experiment." Journal of Computational Chemistry, 30(7), pp 1069-1074, 2008.

[124] G. Teyssedre and C. Laurent, “Charge transport modeling in insulating polymers: from molecular to macroscopic scale”, IEEE Transactions on Dielectrics and Electrical Insulation, 12(5), pp 857–875, 2005.

[125] F. Zhou, J. Li, M. Liu, et al., “Characterizing traps distribution in LDPE and HDPE through isothermal surface potential decay method”, IEEE Transactions on Dielectrics and Electrical Insulation, 23(2), pp 1174–1182, 2016.

[126] M. Meunier, N. Quirke, A. Aslanides, “Molecular modeling of electron traps in polymer insulators: Chemical defects and impurities”. The Journal of Chemical Physics, 115(6), pp 2876-2881, 2001.

[127] S. Diaham, M. L. Locatelli, “Space-charge-limited currents in polyimide films”, Applied Physics Letters, 101(24): 242905, 2012.

[128] H. Koralay, N. TUĞLUOĞLU, K. AKGÜL, et al. “Analysis of hopping conduction and space charge limited currents in nearly ideal metal/semiconductor contacts”, Gazi University Journal of Science, 27(3), pp 901-907, 2014.

[129] F. Tian, W. Bu, L. Shi, et al., “Theory of modified thermally stimulated current and direct determination of trap level distribution”, Journal of Electrostatics, 69(1), pp 7-10, 2011.

[130] Y. Chong, G. Chen, I. L. Hosier, et al. “Heat treatment of cross-linked polyethylene and its effect on morphology and space charge evolution”, IEEE Transactions on Dielectrics and Electrical Insulation, 12(6), pp 1209-1221, 2005.

[131] J. Li, R. Yang, J. Yu, et al., “Deterioration of polypropylene/silicon dioxide nanocomposites before oxidative degradation”, Journal of applied polymer science, 113(1), pp.601-606, 2009.

[132] E. Strömberg and S. Karlsson, “The design of a test protocol to model the degradation of polyolefins during recycling and service life”, Journal of Applied Polymer Science, 112(3), pp 1835-1844, 2009.

[133] G. Montanari, G. Mazzanti and L. Simoni, “Progress in electrothermal life modeling of electrical insulation during the last decades”, IEEE Transactions on Dielectrics and Electrical Insulation , 9(5), pp 730-745, 2002.

[134] S. Abdulsalam and K. Rayan, “A study of expected lifetime of XLPE insulation cables working at elevated temperatures by applying accelerated thermal ageing”, Heliyon, 6 (1), 2020.